Mass Production Cost Estimation of Direct H₂ PEM Fuel Cell Systems for Transportation Applications: 2016 Update

January 2017

Prepared By:

Brian D. James

Jennie M. Huya-Kouadio

Cassidy Houchins

Daniel A. DeSantis

Rev. 3

STRATEGIC ANALYSIS INC

Sponsorship and Acknowledgements

Disclaimer

This report was prepared as an account of work sponsored by an agency of the United States Government. Neither the United States Government nor any agency thereof, nor any of their employees, makes any warranty, express or implied, or assumes any legal liability or responsibility for the accuracy, completeness, or usefulness of any information, apparatus, product, or process disclosed, or represents that its use would not infringe privately owned rights. Reference herein to any specific commercial product, process, or service by trade name, trademark, manufacturer, or otherwise does not necessarily constitute or imply its endorsement, recommendation, or favoring by the United States Government or any agency thereof. The views and opinions of authors expressed herein do not necessarily state or reflect those of the United States Government or any agency thereof.

Authors Contact Information

Strategic Analysis Inc. may be contacted at:

> Strategic Analysis Inc.
> 4075 Wilson Blvd, Suite 200
> Arlington VA 22203
> (703) 527-5410
> www.sainc.com

The authors may be contacted at:

> Brian D. James, BJames@sainc.com, (703) 778-7114

Revision History

Rev.1: Correction of Figure 26 and various typos throughout document.
Rev 2: Correction to Figures 36 and 54 and various typos throughout document.
Rev 3: Addition of text to Section 1.0 and various typos throughout document.

Table of Abbreviations

ANL	Argonne National Laboratory
APTA	American Public Transportation Association
atm	atmospheres
BDI	Boothroyd Dewhurst Incorporated
BOL	beginning of life
BOM	bill of materials
BOP	balance of plant
C_{air}	Air Management System Cost (Simplified Cost Model)
C_{BOP}	Additional Balance of Plant Cost (Simplified Cost Model)
CC	capital costs
CCE	catalyst coated electrode
CCM	catalyst coated membrane
CEM	integrated compressor-expander-motor unit (used for air compression and exhaust gas expansion)
C_{Fuel}	Fuel Management System Cost (Simplified Cost Model)
C_{Humid}	Humidification Management System Cost (Simplified Cost Model)
CM	compressor motor
CNG	compressed natural gas
C_{stack}	Total Fuel Cell Stack Cost (Simplified Cost Model)
$C_{thermal}$	Thermal Management System Cost (Simplified Cost Model)
DFMA®	design for manufacture and assembly
DOE	Department of Energy
DOT	Department of Transportation
DSM™	dimensionally stable membrane (Giner membrane support)
DTI	Directed Technologies Incorporated
EEC	electronic engine controller
EERE	DOE Office of Energy Efficiency and Renewable Energy
EOL	end of life
ePTFE	expanded polytetrafluoroethylene
EW	equivalent weight
FCT	EERE Fuel Cell Technologies Program
FCTT	Fuel Cell Technical Team
FCV	fuel cell vehicle
Ford	Ford Motor Company Inc.
FTA	Federal Transit Administration
FUDS	Federal Urban Driving Schedule
G&A	general and administrative
GDE	gas diffusion electrode

GDL	gas diffusion layer
GM	General Motors Inc.
H_2	hydrogen
HFPO	hexafluoropropylene oxide
HDPE	high density polyethylene
ID	inner diameter
IR/DC	infra-red/direct-current
kN	kilo-Newtons
kW	kilowatts
kW_{e_net}	kilowatts of net electric power
LCA	life cycle analysis
LCCA	life cycle cost analysis
LT	low temperature
MBRC	miles between road calls
MEA	membrane electrode assembly
mgde	miles per gallon of diesel equivalent
mpgge	miles per gallon of gasoline equivalent
mph	miles per hour
NREL	National Renewable Energy Laboratory
NSTF	nano-structured thin-film (catalysts)
OD	outer diameter
ODS	optical detection system
OPCO	over-pressure, cut-off (valve)
PDF	probability distribution function
PEM	proton exchange membrane
PET	polyethylene terephthalate
Pt	platinum
PtCoMn	platinum-cobalt-manganese
QC	quality control
Q/ΔT	heat duty divided by delta temperature
R&D	research and development
RFI	request for information
SA	Strategic Analysis, Inc.
TIM	traction inverter module
TVS	Twin Vortices Series (of Eaton Corp. compressors)
V	volt

Foreword

Energy security is fundamental to the mission of the U.S. Department of Energy (DOE) and hydrogen fuel cell vehicles have the potential to eliminate the need for oil in the transportation sector. Fuel cell vehicles[1] can operate on hydrogen, which can be produced domestically, emitting fewer greenhouse gasses and pollutants than conventional internal combustion engine (ICE), advanced ICE, hybrid, or plug-in hybrid vehicles that are tethered to petroleum fuels. Transitioning from standard ICE vehicles to hydrogen-fueled fuel cell vehicles (FCVs) could greatly reduce greenhouse gas emissions, air pollution emissions, and ambient air pollution, especially if the hydrogen fuel is derived from wind-powered electrolysis or steam reforming of natural gas.[2,3] A diverse portfolio of energy sources can be used to produce hydrogen, including nuclear, coal, natural gas, geothermal, wind, hydroelectric, solar, and biomass. Thus, fuel cell vehicles offer an environmentally clean and energy-secure pathway for transportation.

This research evaluates the cost of manufacturing transportation fuel cell systems (FCSs) based on low temperature (LT) proton exchange membrane (PEM) FCS technology. Fuel cell systems will have to be cost-competitive with conventional and advanced vehicle technologies to gain the market-share required to influence the environment and reduce petroleum use. Since the light duty vehicle sector consumes the most oil, primarily due to the vast number of vehicles it represents, the DOE has established detailed cost targets for automotive fuel cell systems and components. To help achieve these cost targets, the DOE has devoted research funding to analyze and track the cost of automotive fuel cell systems as progress is made in fuel cell technology. The purpose of these cost analyses is to identify significant cost drivers so that R&D resources can be most effectively allocated toward their reduction. The analyses are annually updated to track technical progress in terms of cost and to indicate how much a typical automotive fuel cell system would cost if produced in large quantities (up to 500,000 vehicles per year).

Bus applications represent another area where fuel cell systems have an opportunity to make a national impact on oil consumption and air quality. Consequently, beginning with year 2012, annually updated cost analyses have been conducted for PEM fuel cell passenger buses as well. Fuel cell systems for light duty automotive and buses share many similarities and indeed may even utilize identical stack hardware. Thus the analysis of bus fuel cell power plants is a logical extension of the light duty automotive power system analysis. Primary differences between the two applications include the installed power required (80 kilowatts of net electric power (kW_{e_net})[4] for automotive vs. ~160kW_{e_net} for

---

[1] Honda FCX Clarity fuel cell vehicle: http://automobiles.honda.com/fcx-clarity/; Toyota fuel cell hybrid vehicles: http://www.toyota.com/about/environment/innovation/advanced_vehicle_technology/FCHV.html

[2] Jacobson, M.Z., Colella, W.G., Golden, D.M. "Cleaning the Air and Improving Health with Hydrogen Fuel Cell Vehicles," *Science*, 308, 1901-05, June 2005.

[3] Colella, W.G., Jacobson, M.Z., Golden, D.M. "Switching to a U.S. Hydrogen Fuel Cell Vehicle Fleet: The Resultant Change in Energy Use, Emissions, and Global Warming Gases," *Journal of Power Sources*, 150, 150-181, Oct. 2005.

[4] Unless otherwise stated, all references to vehicle power and cost ($/kW) are in terms of kW net electrical (kW_{e_net}).

a 40 foot transit bus), desired power plant durability (nominally 5,000 hours lifetime for automotive vs. 25,000 hours lifetime for buses), and annual manufacturing rate (up to 500,000 systems/year for an individual top selling automobile model vs. ~4,000 systems/year for total transit bus sales in the U.S.).[5]

The capacity to produce fuel cell systems at high manufacturing rates does not yet exist, and significant investments will have to be made in manufacturing development and facilities in order to enable it. Once these investment decisions are made, it will take several years to develop and fabricate the necessary manufacturing facilities. Furthermore, the supply chain will need to develop, which requires negotiation between suppliers and system developers, with details rarely made public. For these reasons, the DOE has consciously decided not to analyze supply chain scenarios at this point, instead opting to concentrate its resources on solidifying the tangible core of the analysis, i.e. the manufacturing and materials costs.

The DOE uses these analyses as tools for R&D management and tracking technological progress in terms of cost. Consequently, non-technical variables are held constant to elucidate the effects of the technical variables. For example, the cost of platinum is typically held constant to insulate the study from unpredictable and erratic platinum price fluctuations. Sensitivity analyses are conducted to explore the effects of non-technical parameters.

To maximize the benefit of our work to the fuel cell community, Strategic Analysis Inc. (SA) strives to make each analysis as transparent as possible. The transparency of the assumptions and methodology serve to strengthen the validity of the analysis. We hope that these analyses have been and will continue to be valuable tools to the hydrogen and fuel cell R&D community.

---

[5] Total buses sold per year from American Public Transportation Association 2012 Public Transportation Fact Book, Appendix A Historical Tables, page 25, http://www.apta.com/resources/statistics/Documents/FactBook/2012-Fact-Book-Appendix-A.pdf. Note that this figure includes all types of transit buses: annual sales of 40-foot transit buses, as are of interest in this report, would be considerably lower.

Table of Contents

1 Overview

This 2016 report covers fuel cell cost analysis of both light duty vehicle (automotive) and transit bus applications for only the current year (i.e. 2016). This report is the tenth annual update of a comprehensive automotive fuel cell cost analysis[6] conducted by Strategic Analysis[7] (SA), under contract to the U.S. Department of Energy (DOE). The first report (hereafter called the "2006 cost report") estimated fuel cell system cost for three different technology levels: a "current" system that reflected 2006 technology, a system based on projected 2010 technology, and another system based on projections for 2015. The 2007 update report incorporated technology advances made in 2007 and re-appraised the projections for 2010 and 2015. Based on the earlier report, it consequently repeated the structure and much of the approach and explanatory text. The 2008-2015 reports[8,9,10,11,12,13,14,15] followed suit, and this 2016 report[16] is another annual reappraisal of the state of technology and the corresponding costs. In the 2010 report, the "current" technology and the 2010 projected technology merged, leaving only two technology levels to be examined: the current status (then 2010) and the 2015 projection. In 2012, the 2015 system projection was dropped since the time frame between the current status and 2015 was so short. Also in 2012, analysis of a fuel cell powered 40 foot transit bus was added.

---

[6] "Mass Production Cost Estimation for Direct H_2 PEM Fuel Cell Systems for Automotive Applications," Brian D. James & Jeff Kalinoski, Directed Technologies, Inc., October 2007.

[7] This project was contracted with and initiated by Directed Technologies Inc. (DTI). In July 2011, DTI was purchased by Strategic Analysis Inc. (SA) and thus SA has taken over conduct of the project.

[8] James BD, Kalinoski JA, Baum KN. Mass production cost estimation for direct H_2 PEM fuel cell systems for automotive applications: 2008 update. Arlington (VA): Directed Technologies, Inc. 2009 Mar. Contract No. GS-10F-0099J. Prepared for the US Department of Energy, Energy Efficiency and Renewably Energy Office, Hydrogen Fuel Cells & Infrastructure Technologies Program.

[9] James BD, Kalinoski JA, Baum KN. Mass production cost estimation for direct H_2 PEM fuel cell systems for automotive applications: 2009 update. Arlington (VA): Directed Technologies, Inc. 2010 Jan. Contract No. GS-10F-0099J. Prepared for the US Department of Energy, Energy Efficiency and Renewably Energy Office, Hydrogen Fuel Cells & Infrastructure Technologies Program.

[10] "Mass Production Cost Estimation for Direct H_2 PEM Fuel Cell Systems for Automotive Applications: *2010 Update*," Brian D. James, Jeffrey A. Kalinoski & Kevin N. Baum, Directed Technologies, Inc., 30 September 2010.

[11] "Mass Production Cost Estimation for Direct H_2 PEM Fuel Cell Systems for Automotive Applications: 2011 Update," Brian D. James, Kevin N. Baum & Andrew B. Spisak, Strategic Analysis, Inc., 7 September 2012.

[12] "Mass Production Cost Estimation for Direct H_2 PEM Fuel Cell Systems for Automotive Applications: 2012 Update," Brian D. James, Andrew B. Spisak, Strategic Analysis, Inc., 18 October 2012.

[13] "Mass Production Cost Estimation of Direct H_2 PEM Fuel Cell Systems for Transportation Applications: 2013 Update" Brian D. James, Jennie M. Moton & Whitney G. Colella, Strategic Analysis, Inc., January 2014.

[14] "Mass Production Cost Estimation of Direct H_2 PEM Fuel Cell Systems for Transportation Applications: 2014 Update" Brian D. James, Jennie M. Moton & Whitney G. Colella, Strategic Analysis, Inc., January 2015.

[15] "Mass Production Cost Estimation of Direct H_2 PEM Fuel Cell Systems for Transportation Applications: 2015 Update" Brian D. James, Jennie M. Huya-Kouadio, & Cassidy Houchins, Strategic Analysis, Inc., December 2015.

[16] For previous analyses, SA was funded directly by the Department of Energy's Energy Efficiency and Renewable Energy Office. For the 2010 and 2011 Annual Update report, SA was funded by the National Renewable Energy Laboratory. For the 2012, 2013, 2014, 2015, and 2016 Annual update reports, SA is funded by Department of Energy's Energy Efficiency and Renewable Energy Office.

In this multi-year project, SA estimates the material and manufacturing costs of complete 80 kW$_{e\_net}$ direct-hydrogen Proton Exchange Membrane (PEM) fuel cell systems suitable for powering light-duty automobiles and 160 kWnet systems of the same type suitable for powering 40 foot transit buses. To assess the cost benefits of mass manufacturing, six annual production rates are examined for each automotive technology level: 1,000, 10,000, 30,000, 80,000, 100,000, and 500,000 systems per year. Since total U.S. 40 foot bus sales are currently ~4,000 vehicles per year, manufacturing rates of 200, 400, 800, and 1,000 systems per year are considered for the bus cost analysis.

A Design for Manufacturing and Assembly (DFMA®) methodology is used to prepare the cost estimates. However, departing from DFMA® standard practice, a markup rate for the final system assembler to account for the business expenses of general and administrative (G&A), R&D, scrap, and profit, is not currently included in the cost estimates. However, markup is added to components and subsystems produced by lower tier suppliers and sold to the final system assembler. For the automotive application, a high degree of vertical integration is assumed for fuel cell production. This assumption is consistent with the scenario of the final system assembler (e.g. General Motors (GM) or Ford Motor Company [Ford]) producing virtually all of the fuel cell power system in-house, and only purchasing select stack or balance of plant components from vendors. Under this scenario, markup is not applied to most components (since markup is not applied to the final system assembly). In contrast, the fuel cell bus application is assumed to have a very low level of vertical integration. This assumption is consistent with the scenario where the fuel cell bus company buys the fuel cell power system from a hybrid system integrator who assembles the power system (whose components, in turn, are manufactured by subsystem suppliers and lower tier vendors). Under this scenario, markup is applied to most system components. (Indeed, multiple layers of markup are applied to most components as the components pass through several corporate entities on their way to the bus manufacturer.)

In general, the system designs do not change with production rate, but material costs, manufacturing methods, and business-operational assumptions do vary. Cost estimation at very low manufacturing rates (below 1,000 systems per year) presents particular challenges. Traditional low-cost mass-manufacturing methods are not cost-effective at low manufacturing rates due to high per-unit setup and tooling costs, and lower manufacturing line utilizations. Instead, less defined and less automated operations are typically employed. For some repeat parts within the fuel cell stack (e.g. the membrane electrode assemblies [MEAs] and bipolar plates), such a large number of pieces are needed for each system that even at low system production rates (1,000/year), hundreds of thousands of individual parts are needed annually. Thus, for these parts, mass-manufacturing cost reductions are achieved even at low system production rates. However, other fuel cell stack components (e.g. end plates and current collectors) and all FCS-specific balance of plant (BOP) equipment manufactured in-house do not benefit from this manufacturing multiplier effect, because there are fewer of these components per stack (i.e. two endplates per stack, etc.).

The 2016 system reflects the authors' best estimate of current technology and, with only a few exceptions, is not based on proprietary information. Public presentations by fuel cell companies and other researchers, private conversations with vendors and automotive OEMs, along with an extensive

review of the patent literature are used as a primary basis for modelling the design and fabrication of the technologies.

In 2015, Toyota came out with the Mirai commercial fuel cell vehicle and with it a significant amount of information on the Mirai fuel cell system. SA seized the opportunity to compare and understand the differences between what was publically provided on the Mirai and SA's baseline system. SA's cost assessment of the Mirai system appears in Section 7.3 and is based on fully-public, but incomplete, information: thus while every effort was taken to be accurate, some Mirai design details may be in error. Nonetheless, the Mirai analysis serves as an important snapshot of demonstrated, on-the-road technology. Additionally, it serves as a useful tool to compare against the SA 2016 baseline system. Because the automotive timeline from concept to production is typically 2-3 years (and most likely longer for fuel cell technologies), the Mirai should not be directly compared against the baseline 2016 system, as the Mirai represents reliable technology at the point of its design freeze (several years ago) whereas the 2016 baseline represents state of the art technology in 2016. Taken together, the analysis of these systems provides a good sense of the likely range of costs for mass-produced automotive and bus fuel cell systems and of the dependence of cost on system performance, manufacturing, and business-operational assumptions.

2 Project Approach

The overall goal of this analysis is to transparently and comprehensively estimate the manufacturing and assembly cost of PEM fuel cell power systems for light duty vehicle (i.e. automotive) and transit bus applications. The analysis is to be sufficiently in-depth to allow identification of key cost drivers. Systems are to be assessed at a variety of annual manufacturing production rates.

To accomplish these goals, a three step system approach is employed:

1) System conceptual design wherein a functional system schematic of the fuel cell power system is defined.
2) System physical design wherein a bill of materials (BOM) is created for the system. The BOM is the backbone of the cost analysis accounting system and is a listing and definition of subsystems, components, materials, fabrication and assembly processes, dimensions, and other key information.
3) Cost modeling where Design for Manufacturing and Assembly (DFMA$^®$) or other cost estimation techniques are employed to estimate the manufacturing and assembly cost of the fuel cell power system. Cost modeling is conducted at a variety of annual manufacturing rates.

Steps two and three are achieved through the use of an integrated performance and cost analysis model. The model is Excel spreadsheet-based, although outside cost and performance analysis software is occasionally used for inputs. Argonne National Laboratory models of the electrochemical performance at the fuel cell stack level are used to assess stack polarization performance.

The systems examined within this report do not reflect the designs of any one manufacturer but are intended to be representative composites of the best elements from a number of designs. The automotive system is normalized to a system output power of 80 kW$_{e\_net}$ and the bus system to 160 kW kW$_{e\_net}$. System gross power is derived from the parasitic load of the BOP components.

The project is conducted in coordination with researchers at Argonne National Laboratory (ANL) who have independent configuration and performance models for similar fuel cell systems. Those models serve as quality assurance and validation of the project's cost inputs and results. Additionally, the project is conducted in coordination with researchers at the National Renewable Energy Laboratory (NREL) who are experts in manufacturing quality control, bus fuel cell power systems, and life-cycle cost modeling. Furthermore, the assumptions and results from the project are annually briefed to the USDRIVE Fuel Cell Technology Team (FCTT) so as to receive suggestions and concurrence with assumptions. Finally, the basic approach of process-based cost estimation is to model a complex system (e.g. the fuel cell power system) as the summation of the individual manufacturing and assembly processes used to make each component of the system. Thus, a complex system is defined as a series of small steps, each with a corresponding set of (small) assumptions. These individual small assumptions often have manufacturing existence proofs which can be verified by the manufacturing practitioners. Consequently, the cost analysis is further validated by documentation of all modeling assumptions and their sources.

2.1 Integrated Performance and Cost Estimation

The fuel cell stack is the key component within the fuel cell system and its operating parameters effectively dictate all other system components. As stated, the systems are designed for a net system power. An integrated performance and cost assessment procedure is used to determine the configuration and operating parameters that lead to lowest system cost on a $/kW basis. Figure 1 lists the basic steps in the system cost estimation and optimization process and contains two embedded iterative steps. The first iterative loop seeks to achieve computational closure of system performance[17] and the second iterative loop seeks to determine the combination of stack operational parameters that leads to lowest system cost.

Step Number	Step Description
1)	Define system basic mechanical and operational configuration
2)	Select target system net power production.
3)	Select stack operating parameters (pressure, catalyst loading, cell voltage, air stoichiometry).
4)	Estimate stack power density (W/cm^2 of cell active area) for those parameters.
5)	Estimate system gross power (based on known net power target and estimation of parasitic electrical loads).
6)	Compute required total active area to achieve gross power.
7)	Compute cell active area (based on target system voltage).
8)	Compute stack hydrogen and air flows based on stack and system efficiency estimates.
9)	Compute size of stack and balance of plant components based on these flow rates, temperatures, pressures, voltages, and currents.
10)	Compute actual gross power for above conditions.
11)	Compare "estimated" gross power with computed actual gross power.
12)	Adjust gross power and repeat steps 1-9.
13)	Compute cost of power system.
14)	Vary stack operating parameters and repeat steps 3-13.

Figure 1. Basic steps within the system cost estimation and optimization process

Stack efficiency[18,19] at rated power of the automotive systems was previously set at 55%, to match past DOE targets. However, in 2013, a radiator size constraint in the form of $Q/\Delta T$ was imposed (see Section 6.3.2), and stack efficiencies were allowed to fluctuate so as to achieve minimum system cost while also satisfying radiator constraints.

---

[17] The term "computational closure" is meant to denote the end condition of an iterative solution where all parameters are internally consistent with one another.
[18] Stack efficiency is defined as voltage efficiency X H_2 utilization = Cell volts/1.253 X 100%.
[19] Multiplying this by the theoretical open circuit cell voltage (1.253 V) yields a cell voltage of 0.661 V at peak power.

The main fuel cell subsystems included in this analysis are:
- Fuel cell stacks
- Air loop
- Humidifier and water recovery loop
- High-temperature coolant loop
- Low-temperature coolant loop
- Fuel loop (but not fuel storage)
- Fuel cell system controller
- Sensors

Some vehicle electrical system components explicitly excluded from the analysis include:

- Main vehicle battery or ultra-capacitor[20]
- Electric traction motor (that drives the vehicle wheels)
- Traction inverter module (TIM) (for control of the traction motor)
- Vehicle frame, body, interior, or comfort-related features (e.g., driver's instruments, seats, and windows)

Many of the components not included in this study are significant contributors to the total fuel cell vehicle cost; however, their design and cost are not necessarily dependent on the fuel cell configuration or stack operating conditions. Thus, it is our expectation that the fuel cell system defined in this report is applicable to a variety of vehicle body types and drive configurations.

2.2 Cost Analysis Methodology

As mentioned above, the costing methodology employed in this study is the Design for Manufacture and Assembly technique (DFMA®)[21]. Ford has formally adopted the DFMA® process as a systematic means for the design and evaluation of cost optimized components and systems. These techniques are powerful and flexible enough to incorporate historical cost data and manufacturing acumen that has been accumulated by Ford since the earliest days of the company. Since fuel cell system production requires some manufacturing processes not normally found in automotive production, the formal DFMA® process and SA's manufacturing database are buttressed with budgetary and price quotations from experts and vendors in other fields. It is possible to identify low cost manufacturing processes and component designs and to accurately estimate the cost of the resulting products by combining historical knowledge with the technical understanding of the functionality of the fuel cell system and its component parts. This DFMA®-style methodology helps to evaluate capital cost as a function of annual production rate. This section explains the DFMA® cost modelling methodology further and discusses FCS stack and balance of plant (BOP) designs and performance parameters where relevant.

---

[20] Fuel cell automobiles may be either "purebreds" or "hybrids" depending on whether they have battery (or ultracapacitor) electrical energy storage or not. This analysis only addresses the cost of an 80 kW fuel cell power system and does not include the cost of any peak-power augmentation or hybridizing battery.
[21] Boothroyd, G., P. Dewhurst, and W. Knight. "Product Design for Manufacture and Assembly, Second Edition," 2002.

The cost for any component analyzed via DFMA® techniques includes direct material cost, manufacturing cost, assembly costs, and markup. Direct material costs are determined from the exact type and mass of material employed in the component. This cost is usually based upon either historical volume prices for the material or vendor price quotations. In the case of materials or devices not widely used at present, the manufacturing process must be analyzed to determine the probable high-volume price for the material or device. The manufacturing cost is based upon the required features of the part and the time it takes to generate those features in a typical machine of the appropriate type. The cycle time can be combined with the "machine rate," the hourly cost of the machine based upon amortization of capital and operating costs, and the number of parts made per cycle to yield an accurate manufacturing cost per part. Operating costs include maintenance and spare parts, any miscellaneous expenses, and utility costs (typically electricity at $0.08/kWh).

The assembly costs are based on the amount of time to complete the given operation and the cost of either manual labor or of the automatic assembly process train. The piece cost derived in this fashion is quite accurate as it is based on an exact physical manifestation of the part and the technically feasible means of producing it as well as the historically proven cost of operating the appropriate equipment and amortizing its capital cost. Normally (though not in this report), a percentage markup is applied to the material, manufacturing, and assembly cost to account for profit, general and administrative (G&A) costs, research and development (R&D) costs, and scrap costs. This percentage typically varies with production rate to reflect the efficiencies of mass production. It also changes based on the business type, on the amount of value that the manufacturer or assembler adds to the product, and on market conditions.

Cost analyses were performed for mass-manufactured systems at six production rates for the automotive FC power systems (1,000, 10,000, 30,000, 80,000, 100,000, and 500,000 systems per year) and four production rates for the bus systems (200, 400, 800, and 1,000 systems per year). System designs did not change with production rate, but material costs, manufacturing methods, and business-operational assumptions (such as markup rates) often varied. Fuel cell stack component costs were derived by combining manufacturers' quotes for materials and manufacturing with detailed DFMA®-style analysis.

For some components (e.g. the bipolar plates and the coolant and end gaskets), multiple designs or manufacturing approaches were analyzed. The options were carefully compared and contrasted, and then examined within the context of the rest of the system. The best choice for each component was included in the 2016 baseline configuration. Because of the interdependency of the various components, the selection or configuration of one component sometimes affects the selection or configuration of another. To handle these combinations, the DFMA® model was designed with switches for each option, and logic was built in that automatically adjusts variables as needed. As such, the reader should not assume that accurate system costs could be calculated by merely substituting the cost of one component for another, using only the data provided in this report. Instead, data provided on various component options should be used primarily to understand the decision process used to select the approach for the baseline configurations.

The DFMA®-style methodology proceeds through four iterative stages: (1) System Conceptual Design, (2) System Physical Design, (3) Cost Modeling, and (4) Continuous Improvement to Reduce Cost.

2.2.1 Stage 1: System Conceptual Design
In the system conceptual design stage, a main goal is to develop and verify a chemical engineering process plant model describing the FCS. The FCSs consume hydrogen gas from a compressed hydrogen storage system or other hydrogen storage media. This DFMA® modelling effort does not estimate the costs for either the hydrogen storage medium or the electric drive train. This stage delineates FCS performance criteria, including, for example, rated power, FCS volume, and FCS mass, and specifies a detailed drive train design. An Aspen HYSYS™ chemical process plant model is developed to describe mass and energy flows, and key thermodynamic parameters of different streams. This stage specifies required system components and their physical constraints, such as operating pressure, heat exchanger area, etc. Key design assumptions are developed for the PEM fuel cell vehicle (FCV) system, in some cases, based on a local optimization of available experimental performance data.

2.2.2 Stage 2: System Physical Design
The physical design stage identifies bills of materials (BOMs) for the FCS at a system and subsystem level, and, in some cases, at a component level. A BOM describes the quantity of each part used in the stack, the primary materials from which the part is formed, the feedstock material basic form (i.e. roll, coil, powder, etc.), the finished product basic form, whether a decision was made to make the part internally or buy it from an external machine shop (i.e. make or buy decision), the part thickness, and the primary formation process for the part. The system physical design stage identifies material needs, device geometry, manufacturing procedures, and assembly methods.

2.2.3 Stage 3: Cost Modeling
The cost modelling approach applied depends on whether (1) the device is a standard product that can be purchased off-the-shelf, such as a valve or a heat exchanger, or whether (2) it is a non-standard technology not yet commercially available in high volumes, such as a fuel cell stack or a membrane humidifier. Two different approaches to cost modeling pervade: (1) for standard components, costs are derived from industry price quotes and reasonable projections of these to higher or lower manufacturing volumes. (2) For non-standard components, costs are based on a detailed DFMA® analysis, which quantifies materials, manufacturing, tooling, and assembly costs for the manufacturing process train.

2.2.3.1 *Standardized Components: Projections from Industry Quotes*
For standardized materials and devices, price quotations from industry as a function of annual order quantity form the basis of financial estimates. A learning curve formula is applied to the available data gathered from industry:

$$P_Q = P_I * F_{LC}^{\left(\frac{\ln\left(\frac{Q}{Q_I}\right)}{\ln 2}\right)} \tag{1}$$

where P_Q is the price at a desired annual production quantity [Q] given the initial quotation price [P_I] at an initial quantity Q_I and a learning curve reduction factor [F_{LC}]. F_{LC} can be derived from industry data if two sets of price quotes are provided at two different annual production quantities. When industry quotation is only available at one annual production rate, a standard value is applied to the variable F_{LC}.

2.2.3.2 *Non-standard Components: DFMA® Analysis*

When non-standard materials and devices are needed, costs are estimated based on detailed DFMA® style models developed for a specific, full physical, manufacturing process train. In this approach, the estimated capital cost [C_{Est}] of manufacturing a device is quantified as the sum of materials costs [C_{Mat}], the manufacturing costs [C_{Man}], the expendable tooling costs [C_{Tool}], and the assembly costs [C_{Assy}]:

$$C_{Est} = C_{Mat} + C_{Man} + C_{Tool} + C_{Assy} \tag{2}$$

The materials cost [C_{Mat}] is derived from the amount of raw materials needed to make each part, based on the system physical design (material, geometry, and manufacturing method). The manufacturing cost [C_{Man}] is derived from a specific design of a manufacturing process train necessary to make all parts. The manufacturing cost [C_{Man}] is the product of the machine rate [R_M] and the sum of the operating and setup time:

$$C_{Man} = R_M * (T_R + T_S) \tag{3}$$

where the machine rate [R_M] is the cost per unit time of operating the machinery to make a certain quantity of parts within a specific time period, T_R is the total annual runtime, and T_S is the total annual setup time. The cost of expendable tooling [C_{Tool}] is derived from the capital cost of the tool, divided by the number of parts that the tool produced over its life. The cost of assembly [C_{Assy}] includes the cost of assembling non-standard components (such as a membrane humidifier) and also the cost of assembling both standard and non-standard components into a single system. C_{Assy} is calculated according to

$$C_{Assy} = R_{Assy} * \sum T_{Assy} \tag{4}$$

where R_{Assy} is the machine rate for the assembly train, i.e. the cost per unit time of assembling components within a certain time period and T_{Assy} is the part assembly time.

2.2.4 Stage 4: Continuous Improvement to Reduce Cost

The fourth stage of continuous improvement to reduce cost iterates on the previous three stages. This stage weighs the advantages and disadvantages of alternative materials, technologies, system conceptual design, system physical design, manufacturing methods, and assembly methods, so as to iteratively move towards lower cost designs and production methods. Feedback from industry and

research laboratories can be crucial at this stage. This stage aims to reduce estimated costs by continually improving on the three-stages above.

2.3 Vertical Integration and Markups

Vertical integration describes the extent to which a single company conducts many (or all) of the manufacturing/assembly steps from raw materials to finished product. High degrees of vertical integration can be cost efficient by decreasing transportation costs and turn-around times, and reducing nested layers of markup/profit. However, at low manufacturing rates, the advantages of vertical integration may be overcome by the negative impact of low machinery utilization or poor quality control due to inexperience/lack-of-expertise with a particular manufacturing step.

For the 2012 analysis, both the automotive and bus fuel cell power plants were cost modeled as if they were highly vertically integrated operations. However, for the 2013 to the 2016 analyses, the automotive fuel cell system retains the assumption of high vertical integration but the bus system assumes a non-vertically integrated structure. This is consistent with the much lower production rates of the bus systems (200 to 1,000 systems per year) compared to those of auto systems (1,000 to 500,000 systems per year). Figure 2 graphically contrasts these differing assumptions. Per long-standing DOE directive, markup (i.e. business cost adders for overhead, general & administrative expenses, profit, research and development expenses, etc.) are not included in the power system cost estimates for the final system integrator but are included for lower tier suppliers. Consequently, very little markup is included in the automotive fuel cell system cost because the final integrator performs the vast majority of the manufacture and assembly (i.e. the enterprise is highly vertically integrated). In contrast, bus fuel cell systems are assumed to have low vertical integration and thus incur substantial markup expense. Indeed, there are two layers of markup on most components (one for the actual manufacturing vendor and another for the hybrid system integrator).

Standard DFMA® practice, calls for a markup to be applied to a base cost to account for general and administrative (G&A) expenses, research and development (R&D), scrap, and company profit. While markup is typically applied to the total component cost (i.e. the sum of materials, manufacturing, and assembly), it is sometimes applied at different levels to materials and processing costs. The markup rate is represented as a percentage value and can vary substantially depending on business circumstances, typically ranging from as low as 10% for pass-thru components, to 100% or higher for small businesses with low sales volume.

Within this analysis, a set of standard markup rates is adopted as a function of annual system volume and markup entity. Portraying the markup rates as a function of actual sales revenue would be a better correlating parameter as many expenses represented by the markup are fixed. However, that approach is more complex and thus a correlation with annual manufacturing rate is selected for simplicity. Generic markup rates are also differentiated by the entity applying the markup. Manufacturing markup represents expenses borne by the entity actually doing the manufacturing and/or assembly procedure. Manufacturing markup is assessed at two different rates: an "in-house" rate if the manufacture is done

with machinery dedicated solely to production of that component and a "job-shop" rate if the work is sent to an outside vendor. The "in-house" rate varies with manufacturing rate because machine utilization varies directly (and dramatically) with manufacturing volume. The "job-shop" rate is held constant at 30% to represent the pooling of orders available to contract manufacturing businesses.[22] A pass-thru markup represents expenses borne by a company that buys a component from a sub-tier vendor and then passes it through to a higher tier vendor. Integrator's markup represents expenses borne by the hybrid systems integrator that sets engineering specifications, sources the components, and assembles them into a power system (but does not actually manufacture the components). More than one entity may be involved in supply of the finished product. Per DOE directive, no markup is applied for the final system assembler.
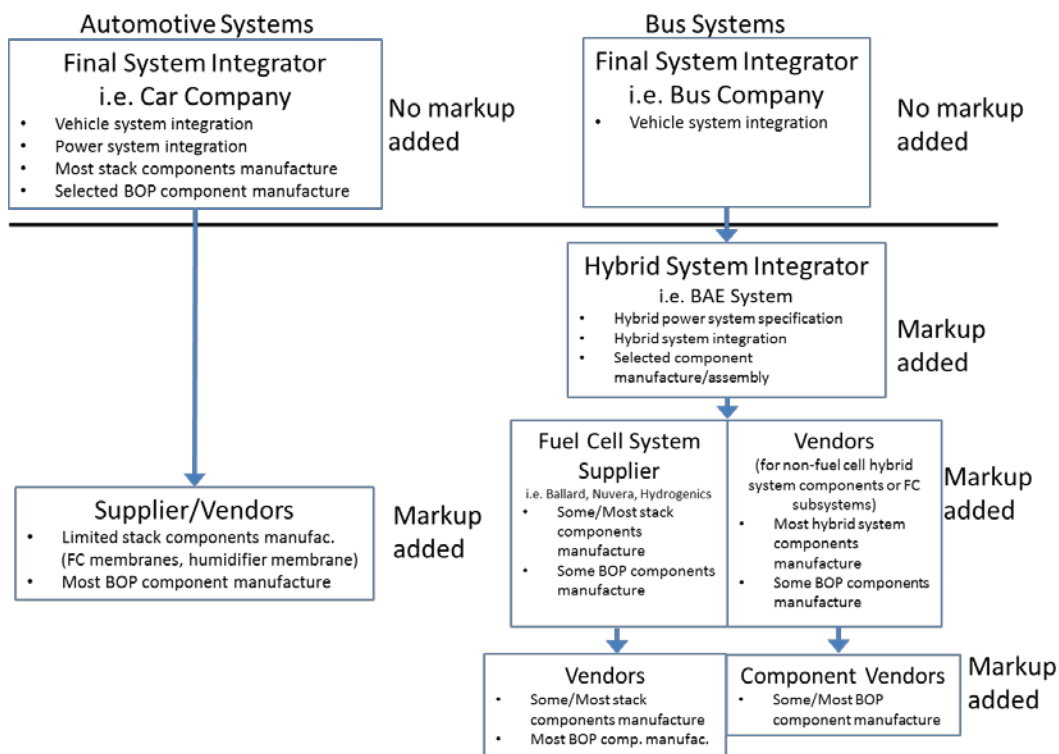
Figure 2: Comparison of bus and auto system vertical integration assumptions

Figure 3 lists the generic markup rates corresponding to each entity and production volume. When more than one markup is applied, the rates are additive. These rates are applied to each component of the automotive and bus systems as appropriate for that component's circumstances and generally apply to all components except the fuel cell membrane, catalyst, humidifier, and air compressor subsystem. Markup rates for those components are discussed individually in the component cost results below.

---

[22] The job-shop markup is not really constant as large orders will result in appreciable increases in machine utilization and thus a (potential) lowering of markup rate. However, in practice, large orders are typically produced in-house to avoid the job-shop markup entirely and increase the in-house "value added". Thus in practice, job-shop markup is approximately constant.

Business Entity	Annual System Production Rate								
	200	400	800	1000	10k	30K	80k	100k	500k
Manufacturer (in-house)	58.8%	54.3%	50.1%	48.9%	37.5%	33.0%	29.5%	28.8%	23.9%
Manufacturer (job-shop)	30%	30%	30%	30%	30%	30%	30%	30%	30%
Pass-Thru	20.2%	19.6%	19.1%	19.0%	17.3%	16.6%	16.0%	15.8%	14.9%
Integrator	20.2%	19.6%	19.1%	19.0%	17.3%	16.6%	16.0%	15.8%	14.9%

Figure 3. Generic markup rates for auto and bus cost analysis

The numeric levels of markup rates can vary substantially between companies and products and is highly influenced by the competitiveness of the market and the manufacturing and product circumstances of the company. For instance, a large established company able to re-direct existing machinery for short production runs would be expected to have much lower markup rates than a small, one-product company. Consequently, the selection of the generic markup rates in Figure 3 is somewhat subjective. However, they reflect input from informal discussions with manufacturers and are derived by postulating a power curve fit to key anchor markup rates gleaned from manufacturer discussions. For instance, a ~23% manufactures markup at 500k systems per year and a 100% markup at a few systems/year are judged to be reasonable. A power curve fit fills in the intervening manufacturing rates. Likewise, a 30% job shop markup rate is deemed reasonable based on conversations and price quotes from manufacturing shops. The pass-thru and integrator markups are numerically identical and much less than the manufacture's rate as much less "value added" work is done. Figure 4 graphically displays the generic markup rates along with the curve fit models used in the analysis.

For the automotive systems, the application of markup rates is quite simple. The vast majority of components are modeled as manufactured by the final system integrator and thus no markup is applied to those components (by DOE directive, the final assembler applies no markup). The few automotive components produced by lower tier vendors (e.g. the CEM and the PEM membrane) receive a manufacturer's markup.

For the bus systems, the application of markup rate is more complex. System production volume is much lower than for automotive systems, and thus it is most economical to have the majority of components produced by lower-tier job-shops. Consequently, the straight job-shop 30% markup is applied for job-shop manufacturing expenses. Additionally, a pass-thru markup is added for expenses of the fuel-cell-supplier/subsystem-vendor, and an integrator markup is added for expenses of the hybrid integrator. These markups are additive. Like the auto systems, no markup is applied for the final system integrator.
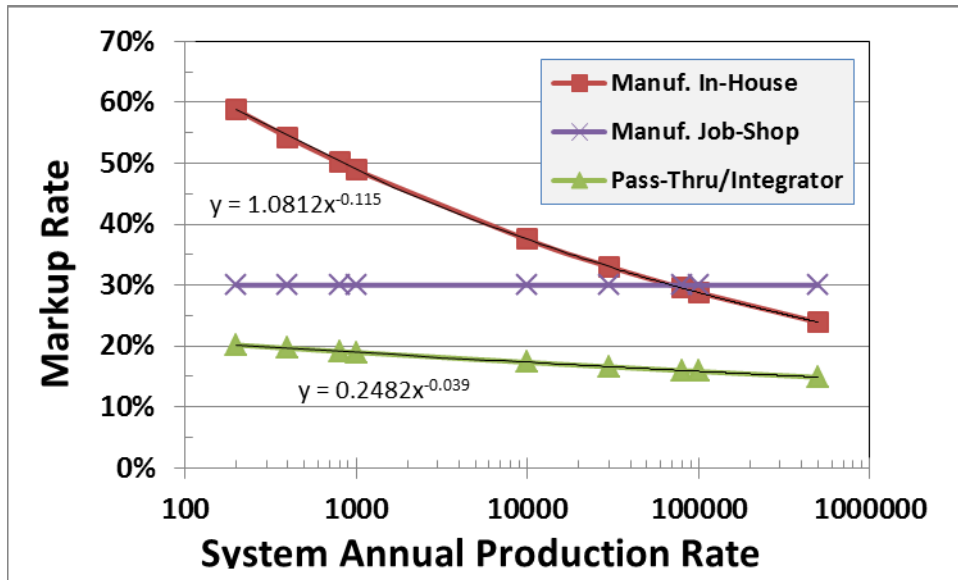
Figure 4. Graph of markup rates

Component level markup costs are reported in various sections of this report. Note that job-shop markup costs are included in the manufacturing cost line element, whereas all other markup costs (pass-thru and integrator) are included in the markup cost line element.

3 Overview of the Bus System

Fuel cell transit buses represent a growing market segment and a logical application of fuel cell technology. Fuel cell transit buses enjoy several advantages over fuel cell automobiles, particularly in the early stages of fuel cell vehicle integration, due to the availability of centralized refueling, higher bus power levels (which generally are more economical on a $/kW basis), dedicated maintenance and repair teams, high vehicle utilization, (relatively) less cost sensitivity, and purchasing decision makers that are typically local governments or quasi-government agencies who are often early adopters of environmentally clean technologies.

Transit bus fuel cell power systems are examined in this report. The transit bus market generally consists of 40' buses (the common "Metro" bus variety) and 30' buses (typically used for Suburban/Commuter[23] to rail station routes). While the 30' buses can be simply truncated versions of 40' buses, they more commonly are based on a lighter and smaller chassis (often school bus frames) than their 40' counterparts. Whereas 40' buses typically have an expected lifetime of 500k to 1M miles, 30' buses generally have a lower expected lifetime, nominally 200k miles.

There are generally three classes of fuel cell bus architecture[24]:
- hybrid electric: which typically utilize full-size fuel cells for motive power and batteries for power augmentation;
- battery dominant: which use the battery as the main power source and typically use a relatively small fuel cell system to "trickle charge" the battery and thereby extend battery range;
- plug-in: which operate primarily on the battery while there is charge, and use the fuel cell as a backup power supply or range extender.

In May 2011, the U.S. Department of Energy issued a Request for Information (RFI) seeking input[25] from industry stakeholders and researchers on performance, durability, and cost targets for fuel cell transit buses and their fuel cell power systems. A joint DOE-Department of Transportation (DOT)/Federal Transit Administration (FTA) workshop was held to discuss the responses and led to DOE publishing fuel cell bus targets for performance and cost as shown in Figure 5. While not explicitly used in this cost analysis, these proposed targets are used as a guideline for defining the bus fuel cell power plant analyzed in the cost study. In addition to the 2016 and ultimate DOE targets, the 2015 status of fuel cell bus technology is added for comparison. Values from the 2015 status are from an annual report written by NREL and the Federal Transit Administration in 2015.[26]

The cost analysis in this report is based on the assumption of a 40' transit bus. Power levels for this class of bus vary widely based primarily on terrain/route and environmental loads. Estimates of fuel cell power plant required[27] net power can be as low as 75 kW for a flat route in a mild climate to 180+ kW

---

[23] Commuter buses are typically shorter in overall length (and wheel base) to provide ease of transit through neighborhoods, a tighter turning radius, and more appropriate seating for a lower customer user base.
[24] Personal communication with Leslie Eudy, National Renewable Energy Laboratory, 25 October 2012.
[25] "Fuel Cell Transit Buses", R. Ahluwalia, , X. Wang, R. Kumar, Argonne National Laboratory, 31 January 2012.
[26] "Fuel Cell Buses in U.S. Transit Fleets: Current Status 2015", L. Eudy and M. Post, National Renewable Energy Laboratory, and C. Gikakis, Federal Transit Administration, December, 2015.
[27] Personal communication with Larry Long, Ballard Power Systems, September 2012.

for a hillier urban route in a hot climate. Accessory loads on buses are much higher than on light duty passenger cars. Electric power is needed for climate control (i.e. cabin air conditioning and heating), opening and closing the doors (which also impacts climate control), and lighting loads. In a hot climate, such as Dallas Texas, accessory loads can reach 30-60 kW, although 30-40 kW is more typical[28]. Industry experts[29] note that the trend may be toward slightly lower fuel cell power levels as future buses become more heavily hybridized and make use of high-power-density batteries (particularly lithium chemistries).

Parameter	Units	NREL 2015 Status[a]	2016 DOE Target	DOE Ultimate Target
Bus Lifetime	years/miles	0.25-4.9/7,900-117,000[b]	12/500,000	12/500,000
Power Plant Lifetime[c, d]	hours	660-20,000[b, e, f]	18,000	25,000
Bus Availability	%	40-92	85	90
Fuel Fills[g]	per day	1	1 (<10 min)	1 (<10 min)
Bus Cost[h]	$	2,100,000-2,400,000	1,000,000	600,000
Power Plant Cost[c, h]	$	N/A[i]	450,000	200,000
Road Call Frequency (Bus/Fuel-Cell System)	miles between road calls (MBRC)	1,800-6,800/9,000-104,000	3,500/15,000	4,000/20,000
Operating Time	hours per day/days per week	17-21/5-7	20/7	20/7
Scheduled and Unscheduled Maintenance Cost[j]	$/mile	0.54-1.33	0.75	0.40
Range	miles	240-340[k]	300	300
Fuel Economy	mgde[l]	5.56-7.71	8	8

a The summary of results for 2015 status represents a snapshot from NREL fuel cell bus evaluation data: data generally from August 2014–July 2015 with the exception of BC Transit, which covers April 2013 through March 2014.
b Accumulated totals for existing fleet through July 2015; these buses have not reached end of life.
c The power plant is defined as the fuel cell system and the battery system. The fuel cell system includes supporting subsystems such as the air, fuel, coolant, and control subsystems. Power electronics, electric drive, and hydrogen storage tanks are excluded.
d According to an appropriate duty cycle.
e The status for power plant hours is for the fuel cell system only; battery lifetime hours were not available.
f The highest-hour power plant was transferred from an older-generation bus that had accumulated more than 6,000 hours prior to transfer.
g Multiple sequential fuel fills should be possible without increase in fill time.
h Cost projected to a production volume of 400 systems per year. This production volume is assumed for analysis purposes only, and does not represent an anticipated level of sales.
i Capital costs for subsystems are not currently reported by the manufacturers.
j Excludes mid-life overhaul of power plant.
k Based on fuel economy and 95% tank capacity.
l Miles per gallon diesel equivalent (mgde).

Figure 5. Proposed DOE targets (From US DOE[30]) and 2015 status (From NREL and FTA[26]) for fuel cell-powered transit buses.

---

[28] Personal communication with Larry Long, Ballard Power Systems, September 2012.

[29] Personal communication with Peter Bach, Ballard Power Systems, October 2012.

[30] "Fuel Cell Bus Targets", US Department of Energy Fuel Cell Technologies Program Record, Record # 12012, March 2, 2012. http://www.hydrogen.energy.gov/pdfs/12012_fuel_cell_bus_targets.pdf

The cost analysis in this report is based on a 160 kW$_{net}$ fuel cell bus power plant. This power level is within the approximate range of existing fuel cell bus demonstration projects[31] as exemplified by the 150 kW Ballard fuel cell buses[32] used in Whistler, Canada for the 2010 winter Olympics, and the 120 kW UTC power PureMotion fuel cell bus fleets in California[33] and Connecticut. Selection of a 160 kW$_{net}$ power level is also convenient because it is twice the power of the nominal 80 kW$_{net}$ systems used for the light duty automotive analysis, thereby easily facilitating comparisons to the use of two auto power plants.

The transit bus driving schedule is expected to consist of much more frequent starts and stops, low fractional time at idle power (due to high and continuous climate control loads), and low fractional time at full power compared to light-duty automotive drive cycles.[34] While average bus speeds depend on many factors, representative average bus speeds[35] are 11-12 miles per hour (mph), with the extremes being a New York City type route (~6 mph average) and a commuter style bus route (~23 mph average). No allowance has been made in the cost analysis to reflect the impact of a particular bus driving schedule.

There are approximately 4,000 forty-foot transit buses sold each year in the United States[36]. However, each transit agency typically orders its own line of customized buses. Thus while orders of identical buses may reach 500 vehicles at the high end, sales are typically much lower. Smaller transit agencies sometimes pool their orders to achieve more favorable pricing. Of all bus types[37] in 2011, diesel engine power plants are the most common (63.5%), followed by CNG/LNG/Blends (at 18.6%), and hybrids (electrics or other) (at only 8.8%). Of hybrid electric 40' transit bus power plants, BAE Systems and Alison are the dominant power plant manufacturers. These factors combine to make quite small the expected annual manufacturing output for a particular manufacturer of bus fuel cell power plants. Consequently, 200, 400, 800, and 1,000 buses per year are selected as the annual manufacturing rates to be examined in the cost study. This is considered a representative estimates for near-term fuel cell bus sales, perhaps skewed towards the upper end of production rates to facilitate the general DFMA® cost methodology employed in the analysis. However, these production rates could alternately be viewed as a low annual production estimate if foreign fuel cell bus sales are considered.

In 2016, SA extended the cost analysis to include a life cycle cost (LCC) analysis of the baseline bus system. The LCC analysis was conducted in collaboration with ANL and Aalto University, who provided

[31] "Fuel Cell Transit Buses", R. Ahluwalia, X. Wang, R. Kumar, Argonne National Laboratory, 31 January 2012.
[32] The Ballard bus power systems are typically referred to by their gross power rating (150 kW). They deliver approximately 140 kW net.
[33] "SunLine Unveils Hydrogen-Electric Fuel Cell Bus: Partner in Project with AC Transit", article at American Public Transportation Association website, 12 December 2005, http://www.apta.com/passengertransport/Documents/archive_2251.htm
[34] Such as the Federal Urban Drive Schedule (FUDS), Federal Highway Drive Schedule (FHDS), Combined Urban/Highway Drive Cycle, LA92, or US06.
[35] Personal communication with Leslie Eudy, National Renewable Energy Laboratory, 25 October 2012.
[36] Personal communication with Leslie Eudy, National Renewable Energy Laboratory, 25 October 2012.
[37] 2012 Public Transportation Fact Book, American Public Transportation Association (APTA), 63rd Edition September 2012. Accessed February 2013 at http://www.apta.com/resources/statistics/Documents/FactBook/APTA_2012_Fact%20Book.pdf

bus drive cycle specific fuel consumption based on performance modeling data (in turn based on experimental results). SA then combined the fuel consumption data with other cost and performance parameters (capital cost, maintenance, labor, lifetime, etc.) within a discounted cash flow model to assess effective cost per mile of bus operation. Details of this LCC analysis can be viewed in Section 13.3.

4   System Schematics and Bills of Materials

System schematics are a useful method of identifying the main components within a system and how they interact. System flow schematics for each of the systems in the current report are shown below. Note that for clarity, only the main system components are identified in the flow schematics. As the analysis has evolved throughout the course of the annual updates, there has been a general trend toward system simplification. This reflects improvements in technology to reduce the number of parasitic supporting systems and thereby reduce system cost. The path to system simplification is likely to continue, and, in the authors' opinion, remains necessary to achieve or surpass cost parity with internal combustion engines.

The authors have conducted annually updated DFMA® analysis of automotive fuel cell systems since 2006. Side by side comparison of annually updated system diagrams is a convenient way to assess important changes/advances. However, no configuration changes were made between the 2015 and 2016 auto and bus system diagrams. The 2015/2016 diagrams for the automotive and bus systems are shown below.

4.1   2015/2016 Automotive System Schematic

The system schematic for the 2015/2016 light duty vehicle (auto) fuel cell power system appears in Figure 6.
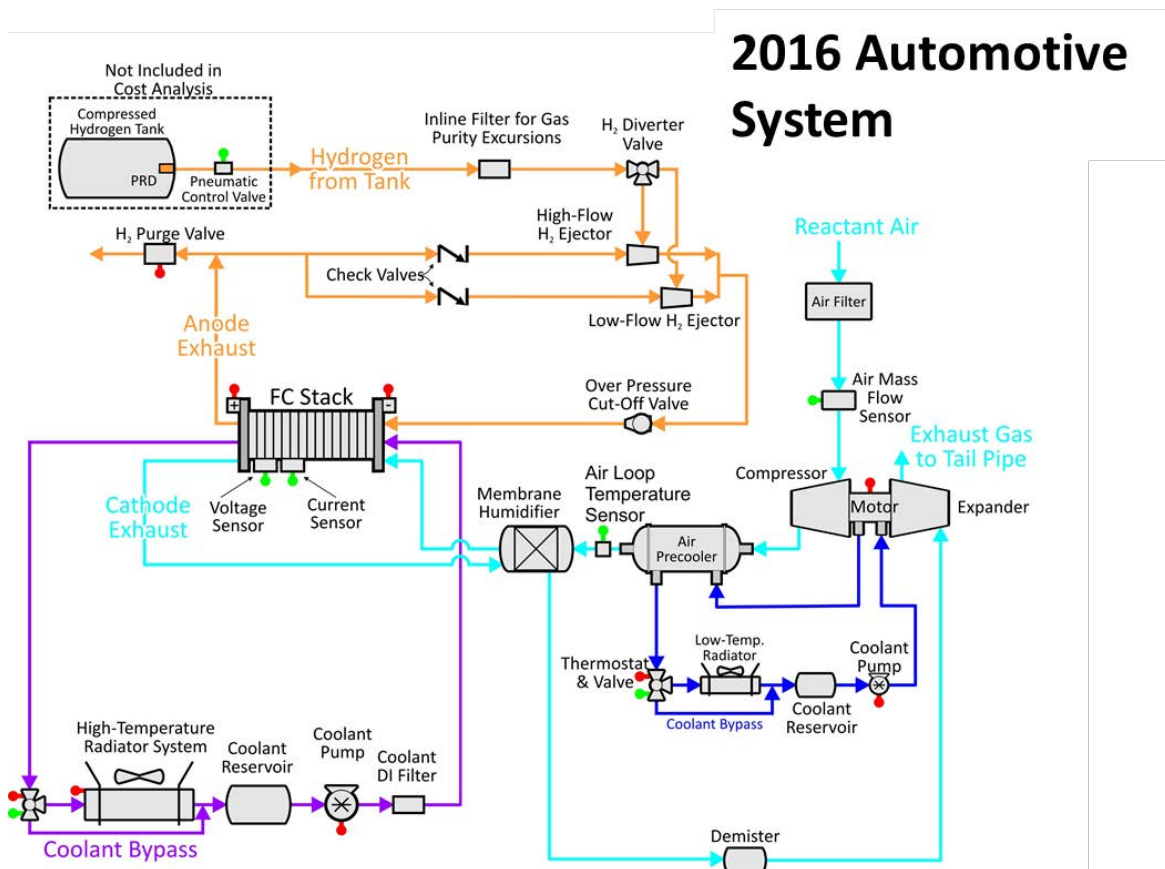
Figure 6. Flow schematic for the 2015/2016 automotive fuel cell system

4.2 2015/2016 Bus System Schematic

The system schematic for the 2015/2016 bus fuel cell power system appears in Figure 7. Power system hardware and layout are directly analogous to the 2015/2016 auto system with the exception of two key differences. 1) The bus system contains two 80 kW stacks whereas the automotive system contains only one 80 kW fuel cell stack, and 2) the automotive system operates at a higher pressure than the bus system, leading to the automotive system's air supply subsystem employing a compressor, motor, and expander (CEM) unit while the bus system uses only a compressor and motor unit.
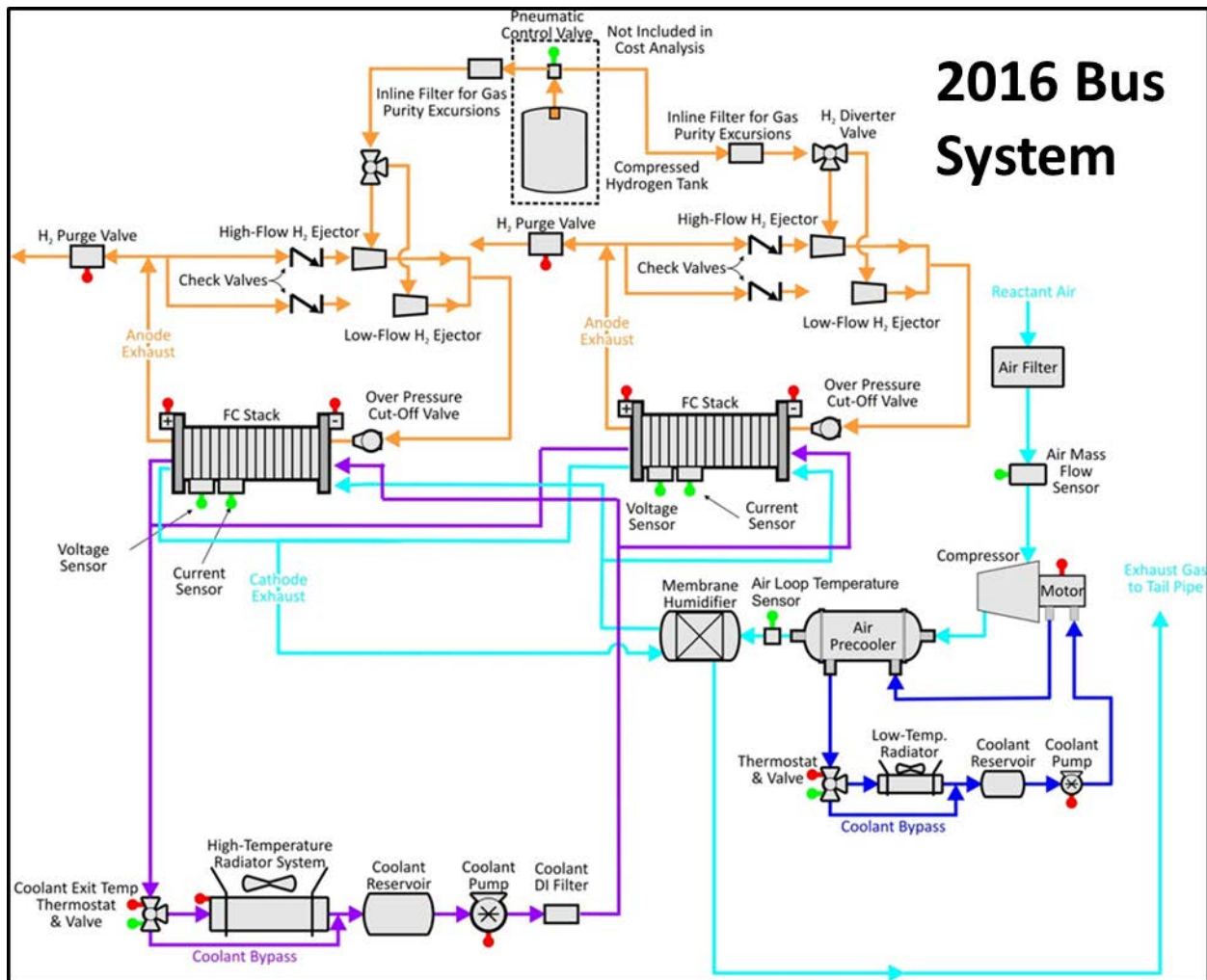
Figure 7. Flow schematic for the 2015/2016 bus fuel cell system

5   System Cost Summaries

Complete fuel cell power systems are configured to allow assembly of comprehensive system Bills of Materials, which in turn allow comprehensive assessments of system cost. Key parameters for the 2015 and 2016 automotive and bus fuel cell power systems are shown in Figure 8 below, with cost result summaries detailed in subsequent report sections.

The bus stack design differs from the automotive stack design in that (1) bus stacks are assumed to operate at a lower pressure and thereby have a lower stack power density; and (2) bus stacks are assumed to operate with a higher Pt catalyst loading so as to meet the greater longevity requirements for buses compared with cars. With a general correlation between Pt loading and stack durability, the bus system, in comparison with the automotive system, has a much higher platinum (Pt) loading due to an assumed longer lifetime. Also, the coolant stack exit temperature is much lower for the bus than for the automotive system primarily due to the typically very low part power operation of the bus stacks. In other words, the bus stacks are typically operating a greater percentage of the time at a lower percentage of their maximum power, compared with passenger cars. As a result, the bus exhaust temperature is lower. A bus is assumed to have a greater surface area available for radiator cooling and therefore is not subject to a Q/ΔT constraint. A more detailed discussion of the key differences between the automotive and bus systems appears in Section 9.1.

5.1   Cost Summary of the 2016 Automotive System

Results of the cost analysis for the 2016 automotive technology system at each of the six annual production rates are shown below. Figure 9 details the cost of the stacks, Figure 10 details the cost of the balance of plant components, and Figure 11 details the cost summation for the system. Figure 12 shows a graph of the stack and total system cost at all manufacturing rates including error bars based on Monte Carlo sensitivity analysis. Assumptions pertaining to the Monte Carlo analysis are detailed in section 14.2.

While the cost results, particularly the $/kW results, are presented to the penny level, this should not be construed to indicate that level of accuracy in all cases. Rather, results are presented to a high level of monetary discretization to allow discernment of the direction and approximate magnitude of cost changes. Those impacts might otherwise be lost to the reader due to rounding and rigid adherence to rules for significant digits, and might be misconstrued as an error or as having no impact.

	2015 Auto Technology System	2016 Auto Technology System	2015 Bus Technology System	2016 Bus Technology System
Power Density (mW/cm^2)	746	749	739	739
Total Pt loading (mgPt/cm^2)	0.142	0.134	0.5	0.5
Pt Group Metal (PGM) Total Content (g/kW$_{gross}$)	0.204	0.191	0.719	0.719
Net Power (kW$_{net}$)	80	80	160	160
Gross Power (kW$_{gross}$)	88.22	87.7	194.7	194.7
Cell Voltage (V)	0.661	0.659	0.659	0.659
Operating Pressure (atm)	2.5	2.5	1.9	1.9
Stack Temp. (Coolant Exit Temp) (°C)	94	94	72	72
Air Stoichiometry	1.5	1.4	1.8	1.8
Q/ΔT (kW$_{th}$/°C)	1.45	1.45	5.4	5.4
Active Cells	378	379	758	758
Membrane Material	Nafion on 25-micron ePTFE	Nafion on 17-micron ePTFE	Nafion on 25-micron ePTFE	Nafion on 20-micron ePTFE
Radiator/ Cooling System	Aluminum Radiator, Water/Glycol Coolant, DI Filter, Air Precooler	No change from 2015	Aluminum Radiator, Water/Glycol Coolant, DI Filter, Air Precooler	No change from 2015
Bipolar Plates	Stamped SS 316L with TreadStone LiteCell™ Coating (Gen1)	Stamped SS 316L with TreadStone LIteCell™ Coating (Gen2)	Stamped SS 316L with TreadStone Litecell™ Coating (Gen1)	Stamped SS 316L with TreadStone Coating (Gen2)
Air Compression	Centrifugal Compressor, Radial-Inflow Expander	No change from 2015	Eaton-Style Multi- Lobe Compressor, Without Expander	No change from 2015
Gas Diffusion Layers	Carbon Paper Macroporous Layer with Microporous Layer (Ballard Cost)	Carbon Paper Macroporous Layer with Microporous Layer (DFMA® cost of Avcarb GDL)	Carbon Paper Macroporous Layer with Microporous Layer (Ballard Cost)	Carbon Paper Macroporous Layer with Microporous Layer (DFMA® cost of Avcarb GDL)
Catalyst & Application	Slot Die Coating of: Cath.: Dispersed 0.092 mgPt/cm^2 d-PtNi$_3$ on C Anode: Dispersed 0.05mgPt/cm^2 Pt on C	Slot Die Coating of: Cath.: Dispersed 0.116 mgPt/cm^2 d-PtNi$_3$ on C Anode: Dispersed 0.018mgPt/cm^2 Pt on C	Slot Die Coating of: Cath.: Dispersed 0.4 mgPt/cm^2 Pt on C Anode: Dispersed 0.1mgPt/cm^2 Pt on C	No change from 2015
CCM Preparation	None	Acid washing	None	None
Air Humidification	Plate Frame Membrane Humidifier	No Change from 2015	Plate Frame Membrane Humidifier	No change from 2015
Hydrogen Humidification	None	None	None	None
Exhaust Water Recovery	None	None	None	None
MEA Containment	Screen Printed Seal on MEA Sub-gaskets, GDL hot pressed to CCM	No Change from 2015	Screen Printed Seal on MEA Sub-gaskets, GDL hot pressed to CCM	No Change from 2015
Coolant & End Gaskets	Laser Welded(Cooling)/ Screen-Printed Adhesive Resin (End)	No Change from 2015	Laser Welded (Cooling), Screen-Printed Adhesive Resin (End)	No Change from 2015
Freeze Protection	Drain Water at Shutdown	No Change from 2015	Drain Water at Shutdown	No Change from 2015
Hydrogen Sensors	2 for FC System[38]	No Change from 2015	3 for FC System[39]	No Change from 2015
End Plates/ Compression System	Composite Molded End Plates with Compression Bands	No Change from 2015	Composite Molded End Plates with Compression Bands	No Change from 2015
Stack Conditioning (hrs)	2	No Change from 2015	2	No Change from 2015

Figure 8. Summary chart of the 2015 and 2016 fuel cell systems

---

[38] There are a total of 4 hydrogen sensors on-board the FC vehicle: 2 under the hood in the power system (within cost estimate), 1 in the passenger cabin (not in cost estimate), and 1 in the fuel system (not in cost estimate).
[39] Additional sensor added to bus system due to the larger fuel cell compartment.

Annual Production Rate	Sys/yr	2016 Automotive System					
		1,000	10,000	30,000	80,000	100,000	500,000
System Net Electric Power (Output)	kWnet	80	80	80	80	80	80
System Gross Electric Power (Output)	kWgross	87.68	87.68	87.68	87.68	87.68	87.68
Bipolar Plates (Stamped)	$/stack	$1,985	$772	$698	$668	$658	$653
MEAs							
Membranes	$/stack	$3,167	$961	$589	$386	$351	$191
d-PtNi Catalyst Ink & Application (Disp	$/stack	$2,307	$1,326	$1,052	$973	$957	$928
CCM Acid Wash	$/stack	$506	$51	$34	$17	$19	$14
GDLs	$/stack	$2,602	$596	$328	$213	$196	$129
M & E Hot Pressing	$/stack	$39	$17	$17	$10	$10	$9
M & E Cutting & Slitting	$/stack	$0	$22	$10	$5	$4	$3
MEA Sub-Gaskets	$/stack	$917	$272	$152	$126	$124	$115
Coolant Gaskets (Laser Welding)	$/stack	$410	$53	$53	$40	$38	$37
End Gaskets (Screen Printing)	$/stack	$1	$1	$1	$1	$1	$0
End Plates	$/stack	$99	$80	$70	$64	$63	$55
Current Collectors	$/stack	$8	$7	$7	$7	$7	$6
Compression Bands	$/stack	$10	$9	$8	$6	$6	$5
Stack Housing	$/stack	$64	$13	$9	$8	$7	$6
Stack Assembly	$/stack	$80	$61	$42	$36	$35	$34
Stack Conditioning	$/stack	$60	$18	$18	$16	$16	$13
Total Stack Cost	$/stack	$12,255	$4,259	$3,087	$2,575	$2,493	$2,199
Total Stacks Cost (Net)	$/kWnet	$153.19	$53.23	$38.58	$32.19	$31.16	$27.49
Total Stacks Cost (Gross)	$/kWgross	$139.77	$48.57	$35.20	$29.37	$28.43	$25.08

Figure 9. Detailed stack cost for the 2016 automotive technology system

Annual Production Rate	Sys/yr	2016 Automotive System					
		1,000	10,000	30,000	80,000	100,000	500,000
System Net Electric Power (Output)	kWnet	80	80	80	80	80	80
System Gross Electric Power (Output)	kWgross	87.68	87.68	87.68	87.68	87.68	87.68
BOP Components							
Air Loop	$/system	$1,813	$1,394	$1,095	$951	$920	$891
Humidifier & Water Recovery Loop	$/system	$1,176	$274	$158	$128	$119	$90
High-Temperature Coolant Loop	$/system	$480	$446	$417	$369	$352	$330
Low-Temperature Coolant Loop	$/system	$71	$68	$65	$61	$59	$56
Fuel Loop	$/system	$346	$306	$291	$261	$251	$238
System Controller	$/system	$172	$152	$138	$103	$97	$83
Sensors	$/system	$512	$290	$226	$184	$176	$131
Miscellaneous	$/system	$263	$165	$136	$123	$119	$115
Total BOP Cost	$/system	$4,833	$3,094	$2,527	$2,181	$2,092	$1,932
Total BOP Cost	$/kW (Net)	$60.41	$38.68	$31.58	$27.27	$26.15	$24.14
Total BOP Cost	$/kW (Gross)	$55.12	$35.29	$28.82	$24.88	$23.86	$22.03

Figure 10. Detailed balance of plant cost for the 2016 automotive technology system

		2016 Automotive System					
Annual Production Rate	**Sys/yr**	**1,000**	**10,000**	**30,000**	**80,000**	**100,000**	**500,000**
System Net Electric Power (Output)	kWnet	80	80	80	80	80	80
System Gross Electric Power (Output)	kWgross	87.68	87.68	87.68	87.68	87.68	87.68
Component Costs/System							
Fuel Cell Stack (High Value)	$/system	$15,093	$5,377	$3,981	$3,398	$3,317	$2,965
Fuel Cell Stack (Nominal Value)	$/system	$12,255	$4,259	$3,087	$2,575	$2,493	$2,199
Fuel Cell Stack (Low Value)	$/system	$10,818	$3,694	$2,575	$2,122	$2,050	$1,755
Balance of Plant (High Value)	$/system	$5,364	$3,558	$2,791	$2,422	$2,324	$2,153
Balance of Plant (Nominal Value)	$/system	$4,833	$3,094	$2,527	$2,181	$2,092	$1,932
Balance of Plant (Low Value)	$/system	$4,542	$2,715	$2,374	$2,051	$1,965	$1,808
System Assembly & Testing	$/system	$148	$103	$101	$101	$101	$101
Cost/System (High Value)	**$/system**	$20,226	$8,702	$6,696	$5,760	$5,585	$5,070
Cost/System (Nominal Value)	**$/system**	$17,236	$7,456	$5,715	$4,858	$4,686	$4,232
Cost/System (Low Value)	**$/system**	$15,858	$6,814	$5,217	$4,422	$4,259	$3,800
Total System Cost	**$/kWnet**	$215.45	$93.20	$71.43	$60.73	$58.57	$52.89
Cost/kWgross	**$/kWgross**	$196.58	$85.04	$65.18	$55.41	$53.44	$48.26

Figure 11. Detailed system cost for the 2016 automotive technology system

Figure 12. Automotive Stack and Total System Cost at all manufacturing rates. Error bars are based on Monte Carlo sensitivity analysis and denote the middle 90% confidence range of results.

5.2 Cost Summary of the 2016 Bus System

Results of the cost analysis of the 2016 bus technology system at 200, 400, 800, and 1,000 systems per year production rates are shown below. Figure 13 details the cost of the stacks, Figure 14 details the cost of the balance of plant components, and Figure 15 details the cost summation for the system. Figure 16 shows a graph of projected stack and total system cost at all manufacturing rates including error bars based on Monte Carlo sensitivity analysis. Assumptions pertaining to the Monte Carlo analysis are detailed in sections 14.2.

		2016 Bus System			
Annual Production Rate	**Sys/yr**	200	400	800	1,000
System Net Electric Power (Output)	kWnet	160	160	160	160
System Gross Electric Power (Output)	kWgross	194.71	194.71	194.71	194.71
Stack Components					
Bipolar Plates (Stamped)	$/stack	$1,873	$1,632	$1,422	$1,876
MEAs					
Membranes	$/stack	$9,563	$6,475	$4,467	$3,980
Catalyst Ink & Application (dispersed l	$/stack	$6,759	$6,167	$5,669	$5,504
GDLs	$/stack	$6,641	$5,340	$3,406	$2,952
M & E Hot Pressing	$/stack	$121	$100	$97	$81
M & E Cutting & Slitting	$/stack	$14	$14	$13	$13
MEA Gaskets (Frame or Sub-Gasket)	$/stack	$621	$503	$481	$432
Coolant Gaskets (Laser Welding)	$/stack	$482	$383	$423	$340
End Gaskets (Screen Printing)	$/stack	$2	$1	$1	$1
End Plates	$/stack	$168	$156	$145	$142
Current Collectors	$/stack	$13	$13	$12	$12
Compression Bands	$/stack	$17	$16	$15	$14
Stack Insulation Housing	$/stack	$275	$146	$83	$70
Stack Assembly	$/stack	$158	$142	$132	$130
Stack Conditioning	$/stack	$290	$151	$146	$120
Total Stack Cost	**$/stack**	**$26,995**	**$21,239**	**$16,516**	**$15,669**
Total Cost for all 2 Stacks	**$/2 stacks**	**$53,989**	**$42,478**	**$33,032**	**$31,338**
Total Stacks Cost (Net)	**$/kWnet**	**$337.43**	**$265.49**	**$206.45**	**$195.86**
Total Stacks Cost (Gross)	**$/kWgross**	**$277.28**	**$218.16**	**$169.65**	**$160.95**

Figure 13. Detailed stack cost for the 2016 bus technology system

		2016 Bus System			
Annual Production Rate	**Sys/yr**	200	400	800	1,000
System Net Electric Power (Output)	kWnet	160	160	160	160
System Gross Electric Power (Output)	kWgross	194.71	194.71	194.71	194.71
BOP Components					
Air Loop	$/system	$8,863	$7,421	$6,445	$6,193
Humidifier & Water Recovery Loop	$/system	$1,278	$1,043	$896	$859
High-Temperature Coolant Loop	$/system	$1,935	$1,873	$1,813	$1,794
Low-Temperature Coolant Loop	$/system	$222	$216	$209	$207
Fuel Loop	$/system	$997	$950	$905	$891
System Controller	$/system	$283	$275	$268	$266
Sensors	$/system	$1,087	$992	$905	$879
Miscellaneous	$/system	$1,118	$909	$792	$766
Total BOP Cost	**$/system**	**$15,784**	**$13,679**	**$12,234**	**$11,856**
Total BOP Cost	**$/kW (Net)**	**$98.65**	**$85.49**	**$76.46**	**$74.10**
Total BOP Cost	**$/kW (Gross)**	**$81.06**	**$70.25**	**$62.83**	**$60.89**

Figure 14. Detailed balance of plant cost for the 2016 bus technology system

			2016 Bus System			
Annual Production Rate	**Sys/yr**	**200**	**400**	**800**	**1,000**
System Net Electric Power (Output)	kWnet	160	160	160	160
System Gross Electric Power (Output)	kWgross	194.71	194.71	194.71	194.71
Component Costs/System					
Fuel Cell Stacks (High Value)	$/system	$69,339	$55,009	$45,471	$42,810
Fuel Cell Stacks (Nominal Value)	$/system	$53,989	$42,478	$33,032	$31,338
Fuel Cell Stacks (Low Value)	$/system	$45,405	$35,209	$27,662	$26,296
Balance of Plant (High Value)	$/system	$17,267	$14,955	$13,374	$12,961
Balance of Plant (Nominal Value)	$/system	$15,784	$13,679	$12,234	$11,856
Balance of Plant (Low Value)	$/system	$14,260	$12,370	$11,083	$10,748
System Assembly & Testing	$/system	$464	$339	$275	$262
Cost/System (High Value)	**$/system**	**$85,688**	**$69,105**	**$58,073**	**$54,982**
Cost/System (Nominal Value)	**$/system**	**$70,237**	**$56,495**	**$45,541**	**$43,456**
Cost/System (Low Value)	**$/system**	**$61,447**	**$49,088**	**$40,029**	**$38,293**
Total System Cost	**$/kWnet**	**$438.98**	**$353.10**	**$284.63**	**$271.60**
Cost/kWgross	**$/kWgross**	**$360.72**	**$290.15**	**$233.89**	**$223.18**

Figure 15. Detailed system cost for the 2016 bus technology system

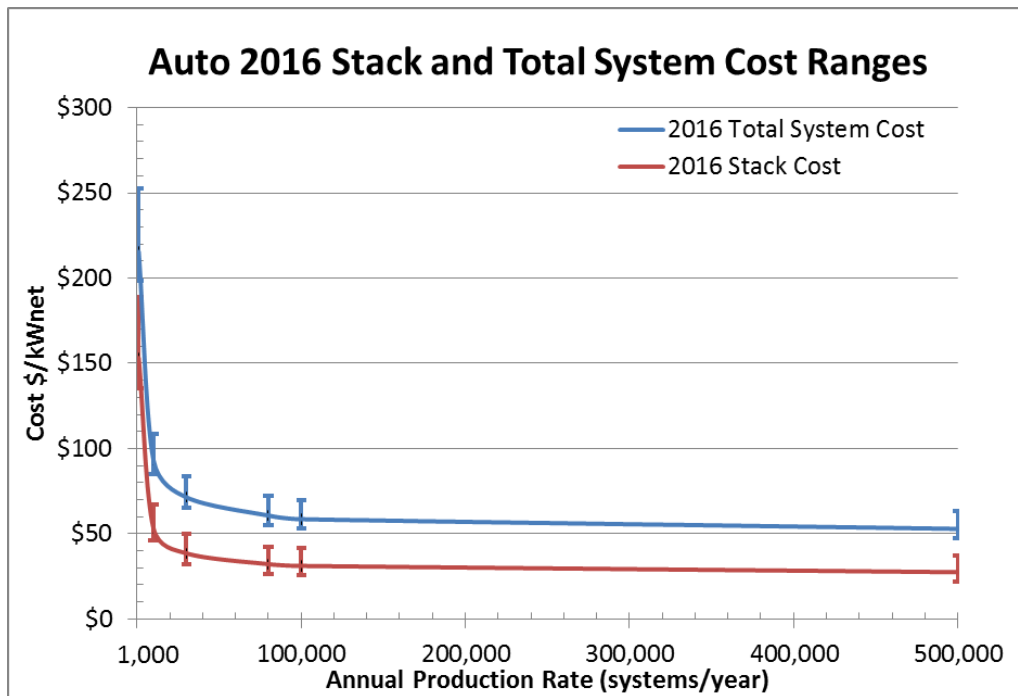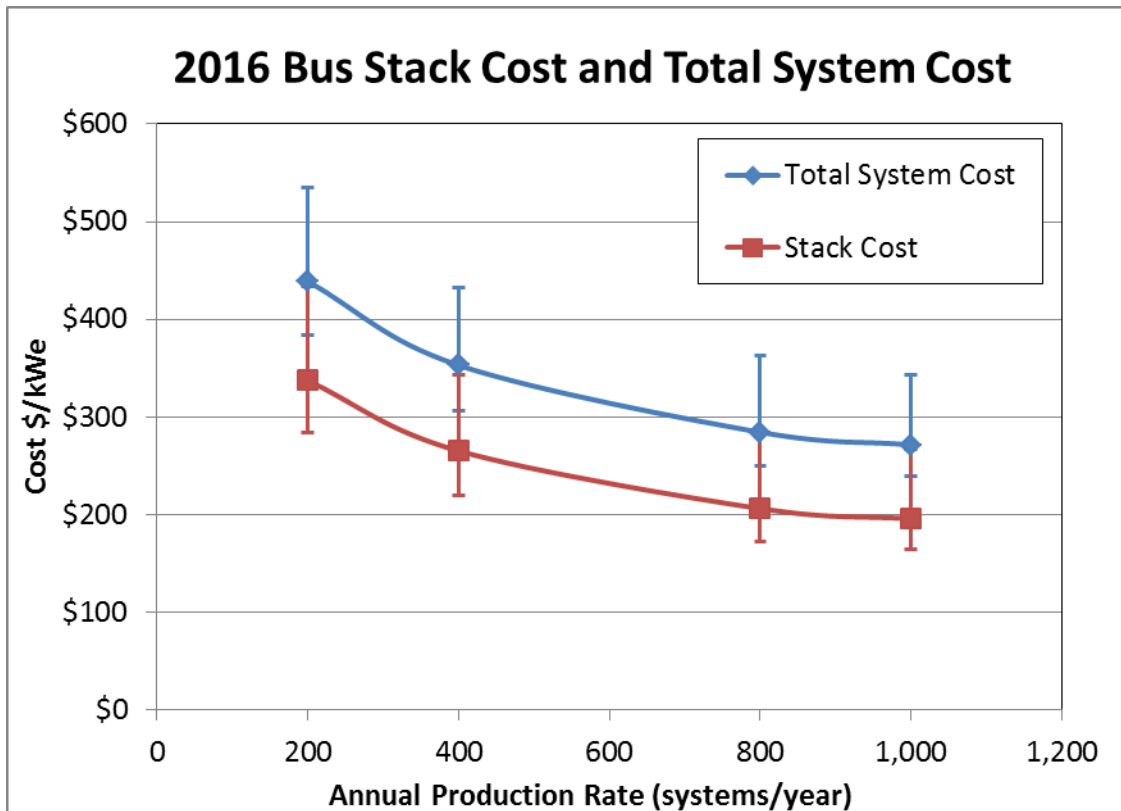**Figure 16. Bus Stack and Total System Cost at all manufacturing rates. Error bars are based on Monte Carlo sensitivity analysis and denote the middle 90% confidence range of results.**

6 Automotive Power System Changes and Analysis since the 2015 Report

This report represents the tenth annual update to the 2006 SA fuel cell cost estimate report[40]. Like the other nine updates before it, this annual report contains updates to the analysis based on advances made over the course of the previous year (i.e. 2016) and reflects new technologies, improvements, and corrections made in the cost analysis. The 2016 analysis closely matches the methodology and results formatting of the 2015 analysis.[41]

The major changes in 2016 result from reduction in total Pt loading (reduced e from 0.05 to 0.0182 mg/cm^2 on the anode and increased from 0.092 to 0.116mg/cm^2 on the cathode with slight variations in operating conditions), re-evaluation of bipolar plate stamping force and related stamping parameter values (i.e. capital cost, stamping speed, etc.), and in switching to TreadStone Generation 2 materials and processing for bipolar plate coating. As in previous updates, SA collaborated with ANL to identify and incorporate a stack operating point optimized for low system cost (i.e. selection of catalyst loading, pressure, humidity, and stoichiometric flow rate for minimum system cost). Additional changes involve updated GDL cost estimates based on DFMA® analysis, updated processing parameter changes to the dispersed catalyst synthesis, and re-evaluation of coolant gasket laser welding process assumptions.

Noteworthy changes since the 2015 update report and their corresponding effects on system cost at 500,000 systems per year are listed in Figure 17 below.

---

[40] "Mass Production Cost Estimation for Direct H_2 PEM Fuel Cell Systems for Automotive Applications", Brian D. James, Jeff Kalinoski, Directed Technologies Inc., October 2007.
[41] "Mass Production Cost Estimation of Direct H_2 PEM Fuel Cell Systems for Transportation Applications: 2015 Update," Brian D. James, Jennie M. Huya-Kouadio & Cassidy Houchins, Strategic Analysis, Inc., December 2015.

Change	Reason	Change from previous value ($/kW)	Cost ($/kW) (@ 500k sys/yr)
2015 Final Cost Estimate		NA	$52.84
Polarization and Catalyst System	Increase of power density from 746 to 749mW/cm^2, reduction of air stoich from 1.5 to 1.4, reduction of catalyst loading from 0.142 to 0.134mg/cm^2, and reduction in membrane humidfier membrane area from 1.2 to 0.7m^2.	($0.93)	$51.91
BPP	Bipolar Plate stamping assumption changes (press force increase from 1,000 to 1,800 tons, capital from $530k to $2M, tooling cost increase from $100k to $600k and increase in tool lifetime of 600k to 10M cycles).	$1.72	$53.63
BPP Coating	Updated Treadstone Coating to Generation 2 materials and process.	($0.81)	$52.82
H$_2$ Sensor	Updated H$_2$ Sensor cost based on FiS model FH2-HY04, used in Toyota Mirai	($1.02)	$51.80
Dispersed Catalyst Synthesis	Numerous updates to dispersed catalyst synthesis based on feedback from catalyst material supplier. (11 changes including limited batch sizes, longer thermal cycle times, increase markups, etc.)	$0.83	$52.63
GDL	Conducted DFMA^{TM} analysis based on Avcarb process and included a 25% markup for profit.	$0.38	$53.01
Coolant Gasket Laser Welding	Added extra laser welding length over the active area of the BPPs, reduced laser welding speed, and increased the number of simultaneous weld heads per station.	$0.12	$53.14
Minor Changes	Re-evaluated air compressor assembly cost to account for automation.	($0.24)	$52.89
2016 Value		$0.05	$52.89

Figure 17. Changes in automotive power system costs at 500,000 systems per year since 2015 update

6.1 De-alloyed Binary Catalyst Selection Process

In 2016, both 3M de-alloyed Pt$_3$Ni$_7$ Nanostructured Thin Film (NSTF) and Johnson Matthey (JM) dispersed de-alloyed platinum/nickel on carbon support (d-PtNi$_3$/C or PtNi$_3$ on C) catalyst systems were examined for use in the baseline system. [42] The JM dispersed d-PtNi$_3$/C was selected for the 2016 baseline as described below. While both cathode and anode catalysts play a vital role, performance and cost are most sensitive to the cathode catalyst. Consequently, catalyst systems are typically categorized by the cathode catalyst specification. Diagrams showing cross-sections and catalyst loadings for the two examined systems are shown here.

---

[42] The subscripts of the catalysts Pt$_3$Ni$_7$ and PtNi$_3$ describe the catalyst material prior to de-alloying the nickel.

1) 3M binary (d-Pt$_3$Ni$_7$) NSTF cathode catalyst with a dispersed interlayer between the GDL and cathode (with PtCoMn NSTF on the anode)
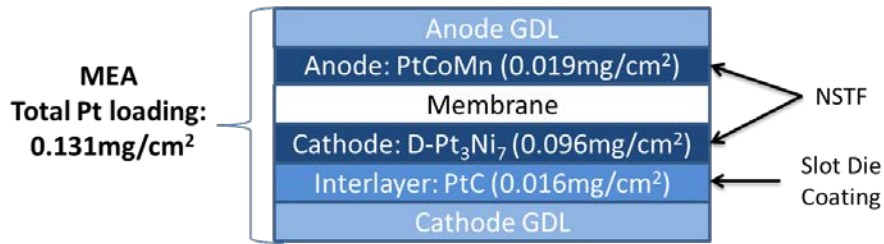
2) JM dispersed d-PtNi$_3$/C (cathode) (with dispersed Pt/C on the anode)
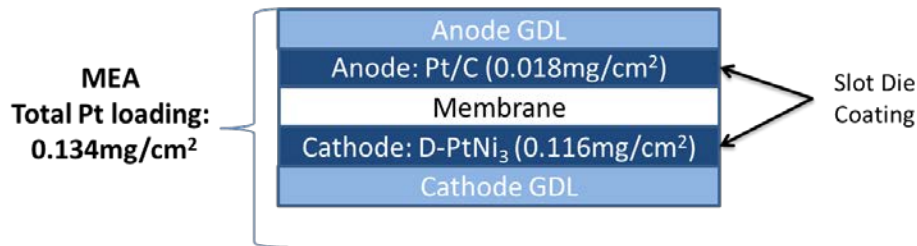
In the past, from 2010 to 2014, NSTF ternary-based catalysts (PtCoMn) were used for both the anode and cathode within the baseline automotive system. Recent progress has led to improved performance of de-alloyed binary catalysts (d-Pt$_3$Ni$_7$ NSTF and dispersed PtNi$_3$/C). Full DFMA® analyses of both dispersed and NSTF de-alloyed binary catalyst synthesis and their applications were completed in 2015 for the automotive system, however, ANL optimized operating conditions were established only for the dispersed d-PtNi$_3$/C and not for the d-Pt$_3$Ni$_7$ NSTF. The 2015 baseline catalyst was switched to the dispersed d-PtNi$_3$/C catalyst per DOE direction and FCTT recommendation.

In 2016, in collaboration with ANL, optimized operating conditions for each catalyst system was paired with SA's DFMA® cost estimates to allow direct comparison between the two catalysts. Optimized operating conditions for the de-alloyed Pt$_3$Ni$_7$ NSTF catalyst system were projected by ANL based on ANL cell and stack models and generally showed high polarization performance (compared to the 2015 projection). The optimized conditions resulted in a system cost reduction of ~$5.40/kW$_{net}$ (and would have resulted in a system cost of ~$47.44/kW$_{net}$) primarily due to increased power density (from 746 mW/cm^2 to 941 mW/cm^2) and reduction in Pt loading (0.142 mg/cm^2 to 0.131 mg/cm^2). However, the FCTT noted that the durability and robustness of the NSTF catalyst had not yet been demonstrated to their satisfaction and did not agree with using NSTF style catalysts for the 2016 baseline analysis. The FCTT instead suggested using only dispersed catalysts for 2016. Based on this advice and in consultation with DOE, SA has selected dispersed de-alloyed PtNi$_3$/C (cathode) and dispersed Pt/C (anode) catalysts for the 2016 baseline analysis. Processing parameter updates made to the 2016 dispersed d-PtNi$_3$/C catalyst DFMA® analysis are described in the next section below. Additional assumptions for the catalyst manufacturing process are detailed in Section 8.1.3. Additional details and full description of de-alloyed Pt$_3$Ni$_7$ NSTF catalyst manufacturing and optimized operating conditions can be viewed in Section 7.5.

6.2 Update of d-PtNi₃/C and d-Pt/C JM-style Catalyst Synthesis Cost

A full DFMA®-style analysis of the de-alloyed $PtNi_3/C$ catalyst system was conducted in 2015 based on open-source, non-proprietary Johnson Matthey literature. Although the analysis was reviewed by Johnson Matthey, the modeled process represents the author's interpretation of the Johnson Matthey processing steps rather than their actual procedures. In 2016, the 2015 results were discussed with additional catalyst suppliers to elicit feedback on the reasonableness of the assumptions and results. The top level processing and material sets were generally validated by the catalyst companies but a more detailed and nuanced description of the processing steps emerged. Consequently, the cost analysis was modified to reflect this additional input and resulted in a substantial percentage increase in catalyst processing costs; however, since processing costs (excluding Pt) had such a low base value from the 2015 analysis, the total dollar impact on system cost was modest.

6.2.1 Changes to Catalyst Processing Steps and Assumptions

Changes to the de-alloyed $PtNi_3/C$ processing steps are detailed below:

- **Pt Handling Charge:** A 2% handling charge was added to the Pt cost to capture broker's fees, physical security, and administrative expenses related to precious metal handling. This percentage markup is considered a reasonable representation of costs regardless of whether the catalyst maker engaged in an internal Pt arbitrage system themselves or bought from a middleman.

- **Pt Precursor Synthesis:** Chloroplatinic acid (CPA) is a common Pt precursor used in catalyst production and in 2015 served as a proxy for the propriety and unspecified Pt salt actually used in the catalyst precipitation reactor. However, all catalyst producers' consults stated that CPA was not the precursor used in their actual d-PtNi₃/C production. Based on industry input, we have modeled the cost of the Pt precursor as the cost of CPA plus an unspecified additional processing step(s) equal in cost. Thus the modeled precursor is effectively 2x the computed CPA cost (excluding Pt).

- **Reactor Size Limitation:** All reactors are limited in size to 1,000 L to reflect industry difficulties in scaling to larger reactor batch sizes.

- **Limited Oven Size:** Drying ovens are limited to 50 kg of catalyst and are modeled as a 0.25 inch powder thickness on stacked horizontal trays with 1 inch tray vertical spacing.

- **Batch Size Tracking:** To facilitate quality control, batch sizes are generally maintained between processing steps.

- **Vacuum Oven Annealing and Drying:** While there is not unanimity in the industry as to whether vacuum ovens are required, the previously modeled atmosphere ovens were converted to vacuum ovens for 2016. Vacuum ovens have much longer cycle times since they rely on radiative rather than convective heat transfer. Consequently, the impact of this change is both in increased oven capital cost and substantially increased cycle time (previously 3.6 hour cycles for atmosphere ovens, now 24+ hours for vacuum ovens).

- **Separate Analysis of Anode and Cathode Catalysts:** In 2015, the anode and cathode catalysts were modeled as the same d-PtNi₃/C catalyst (but with different loadings on each electrode). This was a simplification done solely for analysis convenience. Upon further industry input, the

2016 analysis now analyzes the catalysts separately. Equipment is not shared between the two processing streams.

- o The anode catalyst is modeled as Pt/C without annealing or de-alloying (since there is no Ni to de-alloy).
- o The anode catalyst is modeled using very high surface area carbon (higher than the Vulcan XC-72 carbon assumed in cathode catalyst synthesis). Brand and specifications of the anode carbon are not known but the anode carbon is modeled as 10x the cost of the cathode carbon (10 x ~$9/kg = $90/kg).

- **Pt to Carbon Ratio**: The proportion of Pt to carbon on the anode catalyst is adjusted to 20%wt (previously 30%wt). The cathode remains 30%wt Pt on C.
- **Quality Control:** Quality control testing was not explicitly modeled in 2015. Upon industry input, a per-batch cost of $3,300 is added for a series of powder tests (Pt loading, elemental analysis, water content, BET surface area, particle size, XRD, etc.). Batch sizes range from ~4 to ~36 kg.
- **Process Yield:** A 95% yield is applied to the entire synthesis process (except for Pt metal which is recycled). Thus processing costs and non-Pt material costs are all incurred for a gross amount of catalyst ~5% higher than the net catalyst delivered. Pt recovery of the "extra" catalyst was maintained at the 2015 level of 94%: thus 6% (100%-94%) of the Pt contained in the ~5% extra catalyst (i.e. gross-net catalyst) was lost.
- **Packaging:** A packaging cost was added and is simplistically modeled as bags and boxes for cathode and anode catalyst in sizes of 5 to 100 kg.

6.2.2 Changes to Catalyst Markup Rate

The 2015 catalyst analysis assumed a markup rate of 40% (at 500k systems/year) to 70% (at 1k systems/year). This markup represented the non-production related business expenses incurred by the catalyst company and was denoted as a percentage of the direct catalyst production costs as determined by application of the DFMA® cost methodology (see sections 2.3, 6.2.1, and 8.1.3). The markup was deliberately greater than traditional automotive supplier markup rates to reflect the customized/non-commodity nature of fuel cell catalyst and the resulting higher profit margins and added expenses incurred. However, based on industry input, the markup rates were reconsidered for 2016 and significantly revised.

While material and production costs are estimated based on the DFMA® methodology, catalyst markup rates are based on catalyst supplier pricing data: specifically, markup rates are calculated from the difference between DFMA® materials/processing cost and the catalyst vendor price. This approach yields a representative price (since it is based on vendor input) but also supplies important detail regarding cost drivers (from the DFMA® analysis). Additionally, the derived markup rates were analyzed for reasonableness and greater understanding by re-creating them as the sum of a series of business expenses. The expenses are the authors' estimates based on qualitative vendor input and thus are notional and subject to re-interpretation. However, it is felt that the process of defining cost categories and enumerating expenses can lead to greater understanding and the potential for future cost reduction.

The 2016 markup rates are now set at 0% at 1k systems/year, and 256% to 189% at 10k to 500k systems/year. The rates consist of the following cost elements:

- At 1k systems/year:
  - 0% markup to reflect either of two potential scenarios:
    - business expenses are being borne by the corporate entity so as to grow the market in the early years (a form of "forward-pricing")
    - (because the cost curve is steep at low production volumes) the price of 2 (or more) catalysts produced at low volume is less than half the cost of only 1 produced at that same volume.
- At 10k to 500k systems/year:
  - Base markup of 59-70% (as applied in 2015 for 10k to 500k systems/year) to reflect corporate personnel expenses, profit, warrantee, advertising, etc.
  - Research and Development (R&D) expenses of $1M to $8M per year to reflect the anticipated catalyst research that would be conducted whether or not large scale catalyst sales occur
  - Fire department expenses of $500K to $4M per year to reflect a catalyst company fire department specially trained and equipment to response to catalyst product related emergencies (e.g. powder metal fires, acid accidents, toxic gas releases). (The local municipal fire department may be available to assist but may not possess the specialty knowledge, training, or equipment to respond effectively.)
  - Safety/Environmental department expenses of $70k to $600k per year to reflect staff expenses to monitor and enforce catalyst related safety protocols within the lab and manufacturing facility and the attendant statutory records and filings
  - Physical security department costs of $350k to $3M per year to reflect staff and equipment expenses to provide round the clock security (for the high value Pt stored in the facilities)
  - Waste water department costs of $120k to $600k per year to reflect expenses related to toxic/contaminated waste streams generated from experimentation and catalyst production.

These markup rates are approximations and are expected to vary considerably between companies. Additional vetting of the markup rates is planned for future stages of the project. They are presented here as a representative set of rates, varying with production rate, that lead to a more accurate prediction of catalyst prices charged by the catalyst company. Estimation of the rates is complicated by the expectation that the catalyst company will most likely be a large firm with multiple product lines. Thus expenses for fire, safety, security, wastewater, and administration may be shared among product lines. The extent and circumstances of sharing are expected to vary between companies. The annual costs detailed above thus are the annual expenses apportioned to the fuel cell catalyst: total company expenses for each category would presumably be (much) higher.

Figure 18 plots the expected catalyst annual sales revenue broken down by cost element (production costs, markup expenses, and Pt costs). Production revenues[43] (as assessed by detailed DFMA® analysis) are quite low, only $670k/year at 1k systems/year and even only $11M per year at 500k systems/year. This low base of production costs virtually mandates that markup rates will be a high percentage.

As expected from the magnitude (~200%) of the markup rates, markup rate expenses are much larger than production costs at low system production levels and of more comparable value at high system production levels. However, both expense categories are dwarfed by Pt costs. Thus analysis of a representative catalyst company shows an interesting dichotomy: even at high production levels, the catalyst company has (relatively) modest value-added revenue (~$11M/year) but very high total revenue (~$450M/year), depending on whether the cost of Pt is included. Thus the markup rates are high percentages because they are based on a low level of (non-Pt) production costs, but the rates would be dramatically lower if Pt costs were included in the base.

Finally, it is noted that the catalyst markup rates used in 2016 (~200%) are significantly higher than standard automotive industry markup rates (generally 15%-20%). Since the fuel cell catalyst suppliers are also (generally) auto catalyst (catalytic converter) suppliers and the auto industry is extremely price conscious, it is reasoned that the higher level of markup has been scrutinized by the auto industry and found to reflect legitimate costs (and not unreasonably high profits). However, should the markup rates be lowered in the future, cost of the baseline fuel cell system would presumably be reduced.
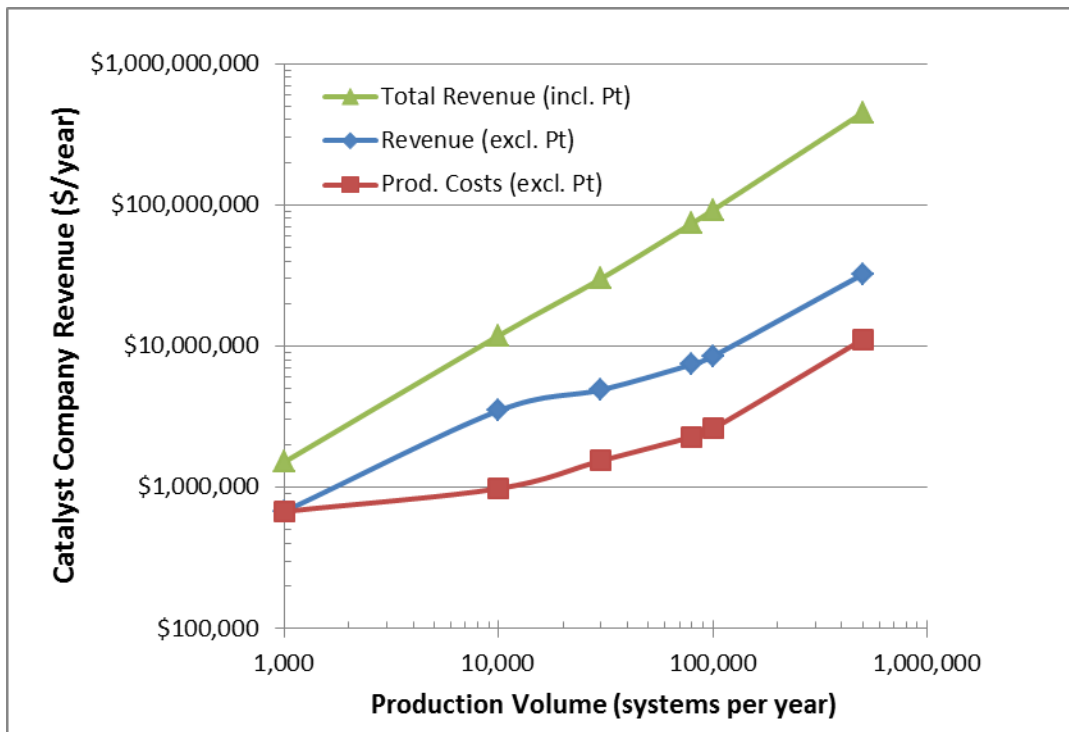
Figure 18. Projected Catalyst Company Revenues from Catalyst Sales

---

[43] As noted in the previous section, a 2% handling charge is applied to the Pt cost. This amounts to ~$8M/year at 500k systems/year and is book-kept under material cost rather than under processing or markup cost.

6.3 2016 Polarization Model

Each analysis year, stack performance is re-examined to incorporate any performance improvements or analysis refinements over the previous year. For 2016, SA collaborated with ANL to define an optimized stack polarization for dispersed de-alloyed PtNi$_3$/C catalyst.

6.3.1 2016 Polarization Model and Resulting Polarization Curves

Historically, ANL supplied SA with a simplified polarization model: a numerical model allowing average stack cell voltage to be projected based on five variables (current density, cathode catalyst loading, air stoichiometry, stack pressure, and coolant temperature at the stack outlet). This simplified model was generated from regression analysis of data generated by ANL's Neural Net first-principals computer model. SA then used Monte Carlo analysis to determine the combination of stack parameters which led to lowest system cost. In 2014, ANL developed an alternative stack polarization model to the Neural Net model used in all previous analysis. This "non-Neural Net" model was specifically developed to better model water balance within the cell and allow optimization of cell inlet humidity levels for optimal performance. In 2015 and 2016, ANL conducted an internal optimization to determine the optimal stack operating conditions using this non-Neural Net model. Unlike previous years, only the optimized stack conditions, rather than a simplified polarization model, were transmitted to SA.

Operating Parameter	2015 Conditions	2016 Optimized Conditions
Cell Voltage	0.661 volts/cell	0.659 volts/cell
Current Density	1,129 mA/cm^2	1,136 mA/cm^2
Power Density	746 mW/cm^2	749 mW/cm^2
Peak Stack Pressure	2.5 atm	2.5 atm
Total Catalyst Loading	0.142 mgPt/cm^2	0.134 mgPt/cm^2
Peak Cell Temperature[44]	100°C	100°C
Air Stoichiometric Ratio	1.5	1.4
Q/ΔT	1.45	1.45

Figure 19. Table of 2016 auto fuel cell system operating conditions compared to 2015 values.

Cell voltage and power density did not change significantly compared to 2015 conditions even though Pt loading and air stoichiometric flow rate went down. The air stoichiometric ratio was reduced from 1.5 to 1.4, leading to a reduction in the stack gross power and compressor/expander/motor cost. Figure 20 graphically compares the 2015 and 2016 polarization curves and design operating points.

---

[44] Peak cell temperature is assumed to be 5 degrees higher than the fuel cell coolant exit temp (same as the single cell testing temperature).
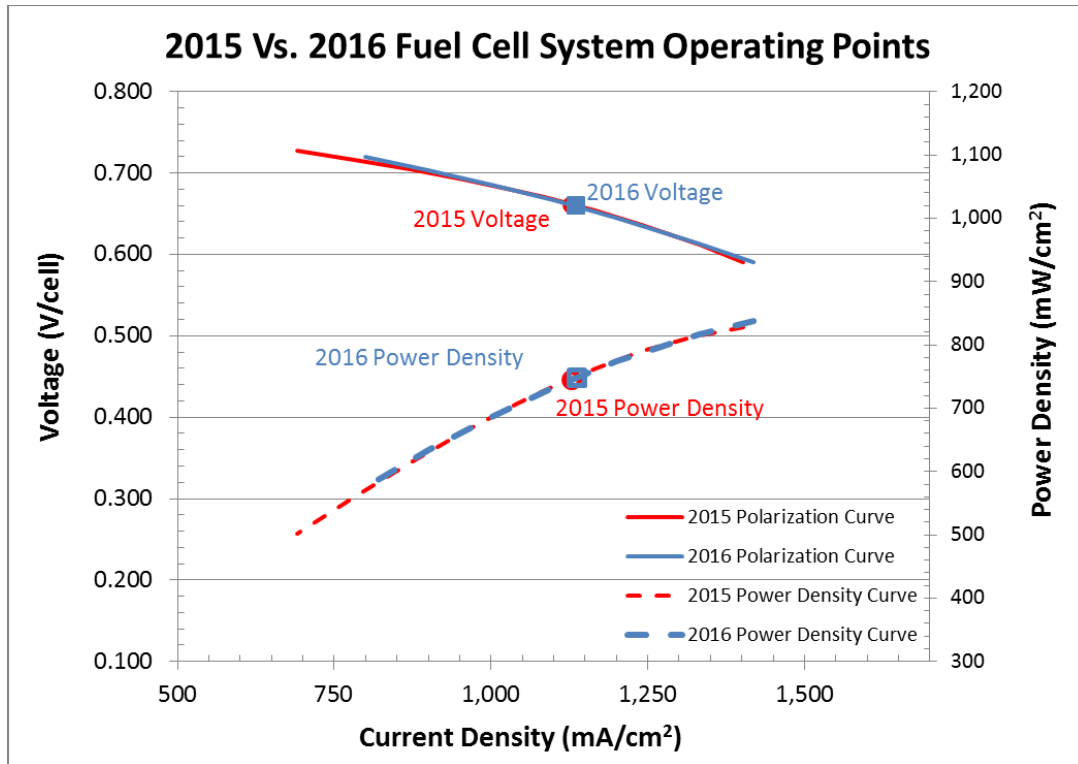
Figure 20. 2016 vs. 2015 polarization modeling results.
(2015 System Operating Point: 0.661 V at 1,129 mA/cm² with 312.8 cm²/cell active area,
2016 System Operating Point: 0.659 V at 1,136 mA/cm² with 308.9 cm²/cell active area)

6.3.2   Q/ΔT Constraint

As directed by DOE and consistent with DOE's 2012 MYRD&D plan, a radiator Q/ΔT constraint was placed on the system beginning in 2013. Q/ΔT is a measure of radiator size, where Q is the fuel cell radiator's heat rejection duty. Q is a function of the temperatures and mass flows of the stack inlet and outlet streams, stack efficiency (i.e. how much heat is generated within the stack), and the extent of liquid product water produced (i.e. how much energy goes into changing the product water from liquid to vapor). ΔT is the difference between the stack coolant exit temperature (typically 80-94 °C) and the worst case ambient air temperature (assumed to be 40 °C). Radiator size scales with Q/ΔT, thus a large Q/ΔT indicates that the stack needs a large radiator to reject waste heat. The DOE 2017 target for Q/ΔT is <1.45 kW$_{th}$/°C and consequently this limit is imposed on the 2013-2016 automotive analyses. All analyses prior to 2013 did not impose a Q/ΔT limit and the 2012 value was ~1.7 kW$_{th}$/°C implying a larger radiator than the automotive community (and DOE) feels is reasonable to incorporate into a light duty automobile.

While the computation of Q/ΔT appears simple (as it is merely the ratio of two easily understood parameters), it is more complex in practice. Q/ΔT is quite sensitive to both Q and ΔT and Q varies considerably depending on the extent of water condensation at the cathode. Water condensation is a function of temperature and gas flows within the cell and is more accurately analyzed by the ANL full polarization model than by the SA cost model. However, the Q/ΔT <=1.45 constraint recommended by the FCTT was based on a simplified, short-hand computation method that assumes all product water

remains in the vapor phase: Q/ΔT = 1.450. Thus for 2015, per DOE directive, the optimization constraint is also assessed by this definition.

$$\frac{Q}{\Delta T} = \frac{P_{gross}\,(1.25 - V_{cell})}{V_{cell}\,(T_{coolant} - T_{ambient})}$$

Where P_{gross} is the gross power of fuel cell stack, V_{cell} is cell voltage at rated power, 1.25 represents the open circuit cell voltage at representative operating conditions, and $T_{coolant}$ and $T_{ambient}$ are the coolant temperature out of the fuel cell stack and ambient temperature (40˚C), respectively.

6.3.3   Parasitic Loads and Gross Power

Changes to the baseline operating conditions directly affect the parasitic load and the mass and volume of the fuel cell system. The changes to parasitic loads and pressure drop within the system since 2015 are summarized in Figure 21.

The pressure at the inlet and outlet of each component must be specified in order to accurately size the compressor and the expander, and to calculate the resulting parasitic power losses for the system. The air compressor outlet pressure is determined by the desired stack inlet pressure (2.5 atm) plus any pressure drop within the BOP components upstream of the stack. The air pressure drops through the pre-cooler and the membrane humidifier were adjusted to ANL model values, ~0.03 atm for each. The same pressure drop was applied to the humidifier after the stack and through the demister, overall reducing the pressure drop after the stack. The pressure into the expander, 2.19 atm, is lower in 2016 than in 2015 (2.23 atm), and the total power out of the expander is lower in 2016 (4.35 kW vs. 4.67 kW) due to the lower air flow rate stoichiometry (1.4 in 2016 vs. 1.5 in 2015).

The high temperature loop coolant pump and radiator fan power were previously constant values for all analyses prior to the 2014 analysis. The coolant pump power was changed to a calculation based on the heat rejection required by the stack and the coolant flow rate. The coolant fan power is now based on a 133 W fan with fan efficiency of 45%, fan motor efficiency of 90%, and DC-DC converter efficiency of 95%.

Air Pressure (atm)	2015 Value	2016 Value
Air Compressor Outlet	2.57	2.57
Air Precooler Outlet	2.54	2.54
Membrane Humidifier Outlet (into stack)	2.50	2.50
Stack Outlet	2.30	2.26
Membrane Humidifier Outlet (into Demister)	2.26	2.23
Air Demister Outlet	2.23	2.19
Parasitic Load (kW)		
Air Compressor Shaft Power	10.42	9.69
Expander Power Out	4.67	4.35
Air Compressor Motor (net of expander)	7.20	6.66
High-Temperature Coolant Loop Pump	0.52	0.51
High-Temperature Coolant Loop Radiator Fan	0.35	0.35
Low-Temperature Coolant Loop Pump	0.06	0.05
Other (Controller, Instruments, etc.)	0.1	0.1
Total Parasitic Loads	**8.22**	**7.68**

Figure 21. Table comparing pressure drop and parasitic loads from 2015 to 2016 values

6.4 Re-evaluation of BPP Stamping

Conversations with multiple bipolar plate vendors suggest SA's overall BPP 2015 costs are below or near the low end of vendor estimates. Figure 22 shows the wide range of BPP cost estimates gathered from vendor discussions: ~$20 to $280/kW$_{net}$ at 1,000 systems per year and $6 to $18/kW$_{net}$ at 500,000 systems per year. Based on this vendor input, the following changes are made to the 2016 analysis.

Stamping Force: Several companies suggested that SA use a higher stamping force (and by association, a higher stamping time, machinery capital cost, and tooling cost). Prior to 2016, progressive stamping forces were calculated from first principles bending force computations based on the plate area, thickness, material, and channel depth[45] with a 5x factor applied to better match vendor input. However, the intricate design of BPPs and the flow field patterns require a much larger force to emboss the material in order to move the material laterally across the face of the plate. The higher press force was suggested by a few companies. The 2016 stamping force is now estimated at 1,800 tons (previously 115 tons) for the five stage progressive die forming a single BPP at each stage (~309 cm^2 active area, ~494 cm^2 total plate area). This stamping force is based on both vendor input and first principles computation for embossing operations and is based on plate area, ultimate tensile strength of the plate material, and an empirical constraint factor.[46] Although not explicitly described, the constraint factor

---

[45] Boothroyd, G., P. Dewhurst, and W. Knight. "Product Design for Manufacture and Assembly, Third Edition," 2011.
[46] Boothroyd, G., P. Dewhurst, and W. Knight. "Product Design for Manufacture and Assembly, Third Edition," 2011.

would account for the thickness and the formation design. As seen in Section 7.2, Hydrogate technology may be a lower cost alternative to progressive stamping.

Stamping Rate: The higher stamping force for 2016 corresponds with a reduction in stamping rate to 24 strokes per minute (previously 60).

Stamping Press Capital Cost: 2016 capital cost is increased to ~$2M from its previous value of $530k.

Stamping Press Power Usage: Larger stamping presses requiring 1,800 tons press force will likely not be of a pneumatic type (max pressure for pneumatic type presses is in the range of 500 tons), but driven by multiple servo torque motors. Power rating is estimated to be 1/3 of the max power (~500 kW x2 = 1 MW for 1,800 ton press), or 330 kW compared to the 23 kW air compressor for the 1,000 ton press.

Die Set Cost: The complete progressive die cost associated with the higher stamping force and intricate flow field patterns is estimated to be ~$660k (previously ~$100k) and is consistent with an estimated 5,000 hours of total machining time.

Die Set Cycle Life: The cycle life for this die set is estimated at 10M cycles compared to 600k cycles used previously.

The combined set of changes results in a BPP cost increase of ~$1.80/kW$_{net}$ compared to the 2015 value (at 500k systems/year). Despite this cost increase, the 2016 BPP cost estimates are still at the low end of the reported vendor values.

The stamped metal plates were selected because of consistent industry feedback suggesting that this material and manufacturing method is the most common approach currently implemented with success.
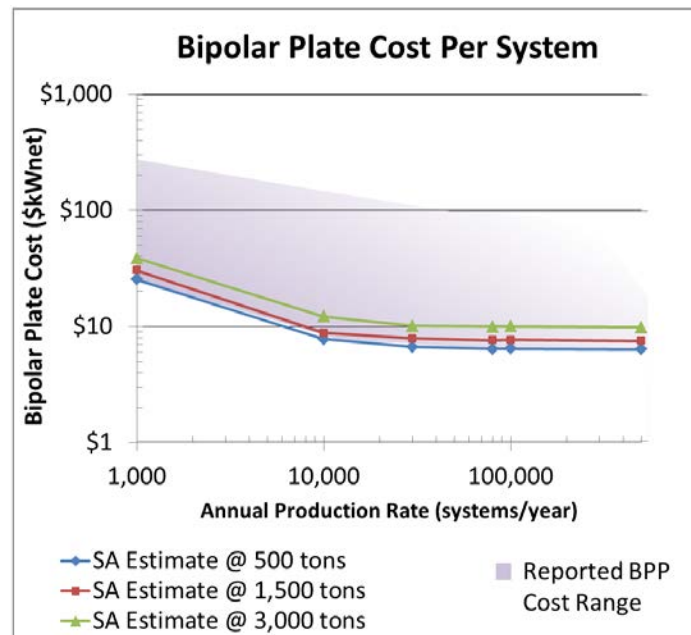
Figure 22. Range in OEM cost and SA's estimate of BPP cost at three stamping forces over all production volumes.

6.5 Re-evaluation of TreadStone Technologies BPP Coating

The TreadStone Technologies Inc. LiteCell™ anti-corrosion coating was first analyzed as part of the 2008 SA baseline system. In 2015, the analysis was re-considered at low production volume to better size the processing equipment for the 1,000 systems/year production rate. In both analyses, the coating was based on TreadStone's Gen 1 "Dot" technology as described in TreadStone's patent US 7,309,540 and conveyed to SA in proprietary discussions with TreadStone. While details are proprietary, the general approach may be described as 1) a continuous coating of an anti-corrosion material applied via physical vapor deposition, 2) application of gold "dots" or "vias" on approximately 1% of the BPP active area to impart high electrical conductivity and low resistance between the BPP and the electrode, and 3) additional proprietary processing steps.

For 2016, the coating was updated to model TreadStone's Gen 2 approach. Gen 2 is also a "Dot" technology but uses a lower cost conductive material in step 2 and eliminates the additional processing step 3. Further details are proprietary to TreadStone and are thus not revealed at this time. Figure 23 illustrates the cost differences between Gen 1 (2015 analysis) and Gen 2 (2016 analysis). Expansion of the analysis to TreadStone's Gen 3 approach is planned for next year.
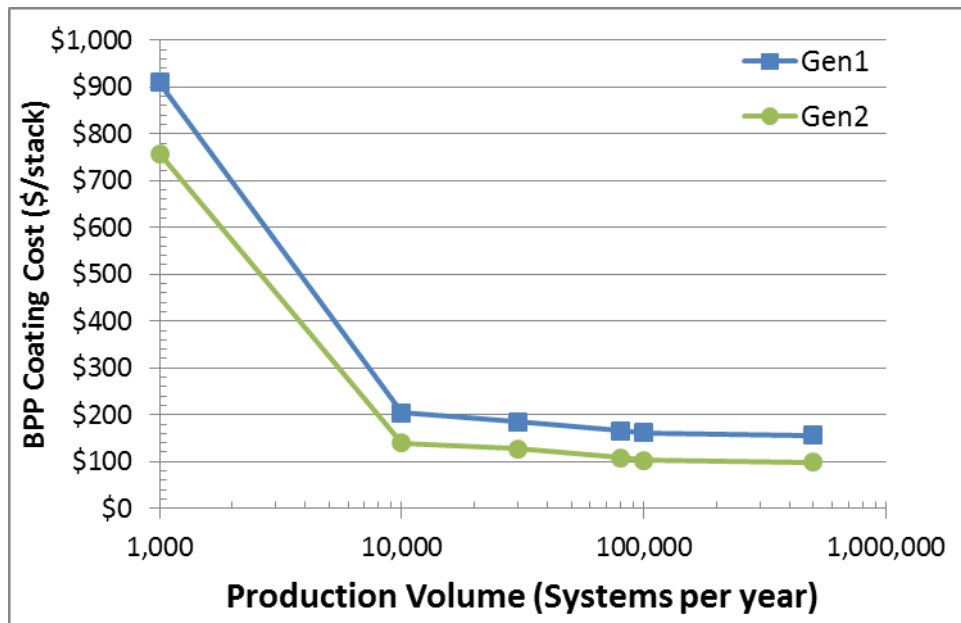
Figure 23. Comparison of TreadStone Gen 1 and Gen 2 BPP coating costs

6.6 Re-evaluation of Laser Welding

Laser welding has been the baseline method of joining bipolar plates since the 2008 SA baseline analysis. For the 2016 analysis, information from additional fuel cell companies and vendors was integrated into the modeled laser welding procedures. Changes to the modeled process are described below.

Extent of weld length: Prior to the 2016 analysis, laser welding was conducted only around the perimeter of the plates and around the manifolds. However, this failed to take into consideration the additional welding required over the active area of the cell to ensure excellent electrical conduction between the plates. Conversations with vendors indicated that this length of welding can vary considerably based on plate design and application: if applied to the entire contact area welding length would dramatically increase. However, based on specific examples from a leading practitioner, welding over the active area is modeled as 2 mm welds every 2 cm with 1 cm lateral spacing. This equates to approximately 5% of the plate-to-plate contact area over the active area and is consistent with feedback from the FCTT. In total (including the perimeter and manifolds), per plate welding length increases from 1.5 m in 2015 to 1.8 m in 2016.

Welding speed: Peak welding speed can be very fast (>1m/s) but the _effective_ speed varies considerably based on the weld path, need to re-position the welding head or the part, and the necessity of avoiding over-heating of the part (if weld paths are tightly spaced). Upon additional input from vendors, the effective laser welding speed is decreased from 0.25 m/s in 2015 to 0.125 m/s in 2016.

Number of welding stations and laser galvanometers: Conversations with Steve Hatkevitch of American Trim elucidated an engineering pathway to reduced laser welding index time. As currently modeled, welding of a 1.8 m length at 0.125 m/s would take 14.4 seconds. This is considerably slower than the expected BPP stamping rate and would lead to a very high number of welding units to achieve high rate system production. Fortunately, welding can be broken into multiple stations much like progressive stamping where only a portion of the work is conducted at each station and the index time between advancements correspondingly reduced. Additionally, multiple laser work heads, or mirror galvanometers[47] (galvos), can be simultaneously supplied from a single laser source and used to increase the effective welding rate at each workstation. Furthermore, welding of more than one plate at each station allows the considerable clamping and index time to be amortized over the multiple plates, rather than adding directly to effective cycle time. The use of multiple stations, each with multiple galvanometers, has several advantages: 1) it allows more versatile clamping of the plates as the clamping system can cover up portions of the plate that will be welded in another station, 2) multiple galvos[48] allow minimization or elimination of x-y movements of the galvos or of the plates thereby increasing effective welding speed and reducing capital cost (i.e. multiple galvos may allow 100% line of sight coverage of the portions to be welded without repositioning), 3) multiple stations allow flexibility in the welding path to avoid localized plate overheating, and 4) multiple stations/galvos allow a dramatic reduction in the effective index time of the parts.

The combined effect of these changes increases the total plate welding time from 6 seconds per weldment (in 2015) to ~14.4 seconds per weldment (in 2016). However, at high production rates, the incorporation of multiple work stations (2), multiple welded assemblies per station (2), and multiple

---

[47] Mirror galvanometers are devices that direct a laser beam by a mirror controlled by a galvanometer sensing unit.
[48] Four galvanometers are selected for full plate coverage without the need for movement of the galvanometers or the plate. For the designed plate geometry this would require an effective field of view (FOV) of up to 130mm. While some laser welding system suppliers say this is feasible, others say the effective FOV is limited to 90mm X 90mm. Should the FOV limit be lower than what is assumed, more galvos and capital cost would be incurred.

galvanometers per assembly (4) allows a significant reduction in effective cycle time. Overall, the time to move the parts from station to station (1 second), clamp the parts (0.75 seconds), weld the parts (1.8 seconds), and unclamp the parts (0.75 seconds) sums to a total 2016 welding index time of 4.3 seconds and an effective per part cycle time of 2.15 seconds (compared to 2 seconds in 2015). Thus the final 2016 effective per part cycle time is nearly identical to the 2015 value but is now based on a more feasible, higher confidence configuration.

Equipment Capital Cost: Based on industry input, the capital cost of the welding process train was updated to reflect multiple stations and multiple galvanometers as described above. Total system capital cost reflects the summation of the following sub-segments (which vary between production rates): laser source ($20k each), galvanometer ($10k each), basic indexed welding station ($100k including clamping system), work piece conveyor system ($50k), Precitec laser welding monitor (for quality control, $45k each), plate handling robots ($87k each), system integration cost ($100k based on 1000 hours at $100/h), and a 20% adder for miscellaneous/non-enumerated costs.

At high production rates, cost of the welding station process line is estimated at $1.03M. A detailed analysis of equipment and process flow is beyond the scope of this report. However, conversations with laser welding specialists revealed a five laser welding systems for a battery application that cost $1-1.5M and a more complex (5 station) fuel cell laser welding system that cost ~$4M. These were one of a kind systems and are expected to have considerable engineering design costs built into their price. In contrast, at moderate fuel cell production rates, multiple welding process lines are required and the design costs would presumably not be incurred on the additional units. Consequently, the 2016 estimate of ~$1M is considered reasonable.

Figure 24 graphically compares 2015 analysis welding cost with the 2016 analysis projections. Overall welding cost is seen to have increased but only by $0.13/kW (at 500k systems/year). A more substantial year-to-year cost increase is observed at low rate. (Cost per welded plate assembly may be converted to $/kW by noting that there are 379 welded assemblies in an 80kW$_{net}$ system.)
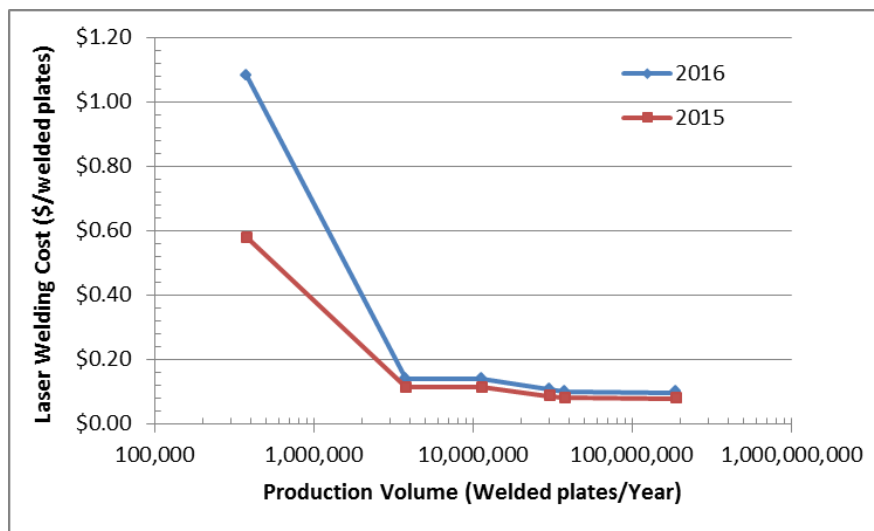
Figure 24. Comparison of 2015 and 2016 BPP welding cost.

Clamping of the BPP to ensure plate contact during welding is identified as a key parameter for welding success. There are many clamping techniques that can be employed and differences between them are not expected to have a large cost impact, although they may lead to substantial performance impacts. Identification and demonstration of BPP clamping and fixturing systems for high rate production is a recommended area of research.

Quality control of laser welds on BPPs is crucial for proper sealing. In addition to the Precitec laser welding monitor, it is postulated that periodic leak checking would be required on the BPP weldments. Vendors suggest that up to a 9 standard deviation (σ) level of reproducibility could be enforced for welded BPPs. Additional quality control cost has not been added in 2016 for this enhanced performance level. Investigation will continue in the next year.

Even with the above changes and a 2.15 sec effective cycle time, 34 parallel lines of welding process trains are needed to achieve a 500k systems/year production rate. Vendors report that such a high level of parallel lines is inconsistent with achievement of high part-to-part plate uniformity: an as-yet-undefined new high rate welding system is needed.

6.7 DFMA® Analysis of GDL Production Process

Discussion with fuel cell companies and vendors about GDL costs and the prices OEMs expect to pay for GDLs resulted in a wide range of values. Figure 25 shows a comparison of the ranges of GDL costs OEMs report against vendor quotes, previous SA analyzed GDL cost, and costs derived from a DOE supported GDL manufacturing project. [49] A 2011 quote from Ballard Material Products (BMP) (purchased by AvCarb in 2013) has been used as the basis for the baseline system GDL cost for the past few years. To provide better insight into cost drivers and to have a more flexible basis for GDL cost, a ground-up DFMA® style model was added to the stack analysis this year.

---

[49] "Reduction in Fabrication Costs of Gas Diffusion Layers," Jason Morgan, Ballard Power Systems, DOE Annual Merit Review, May 2011.
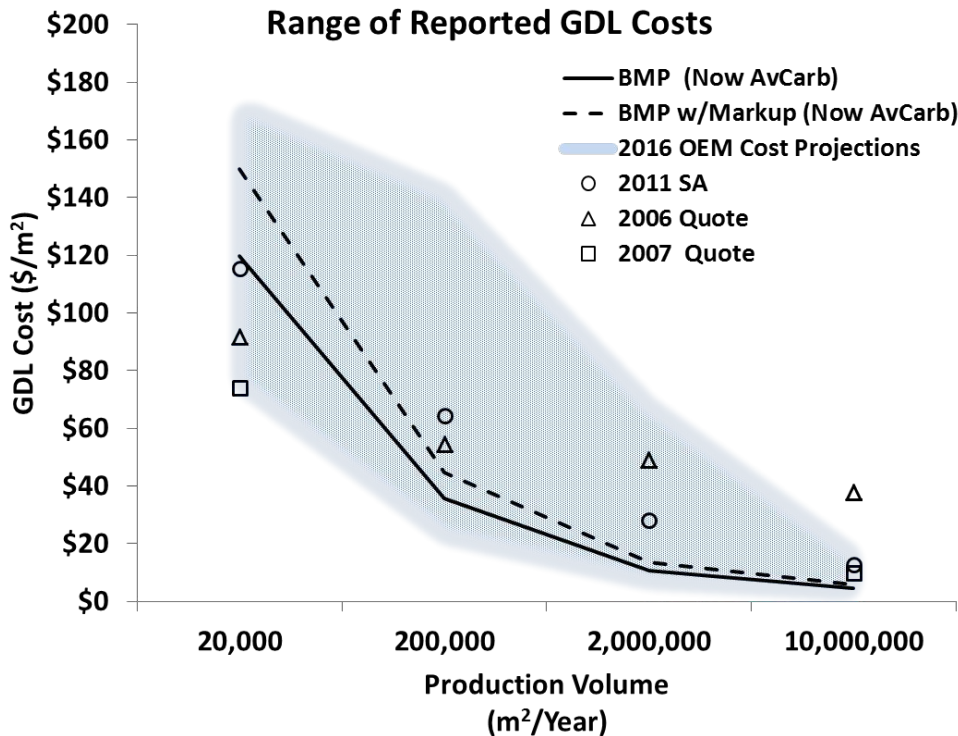
Figure 25. Comparison of GDL costs used in previous SA analysis and as reported by OEMs and GDL suppliers.

The model is based on Ballard Material Products process flow which shares similarities with other GDL manufacturers. Figure 26 graphically illustrates the three main steps of GDL production:

1) Carbon fiber papermaking,

2) Treating the carbon fiber paper for hydrophobicity and pore size, and

3) Application of the microporous layer.

The carbon fiber paper is made using conventional wet-laid papermaking techniques where chopped carbon fiber is dispersed in a solvent (typically water) along with a dispersant such as polyvinyl alcohol, laid onto a web, dried, and re-spooled. Porosity of the carbon fiber paper is adjusted by carbon powder and/or resins, followed by heat treatment in oxidizing conditions, then in graphitizing conditions. Surface properties are adjusted by adding a hydrophobic coating such as fluorinated ethylene propylene (FEP). Finally, a microporous layer (MPL) is applied through an inking step and sintered to compress the MPL to achieve the desired final porosity. A cost breakdown of materials and manufacturing for each of the process steps is presented in Figure 27 (low volume assumptions)[50] and Figure 28 (high volume assumptions), summarizing the results of the cost analysis.

---

[50] Low volume takes into account reduced capital cost of equipment for lower throughput (m^2/hour) compared to high volume machinery. Material cost at all volumes is assumed to remain the same on a $/m^2 basis.
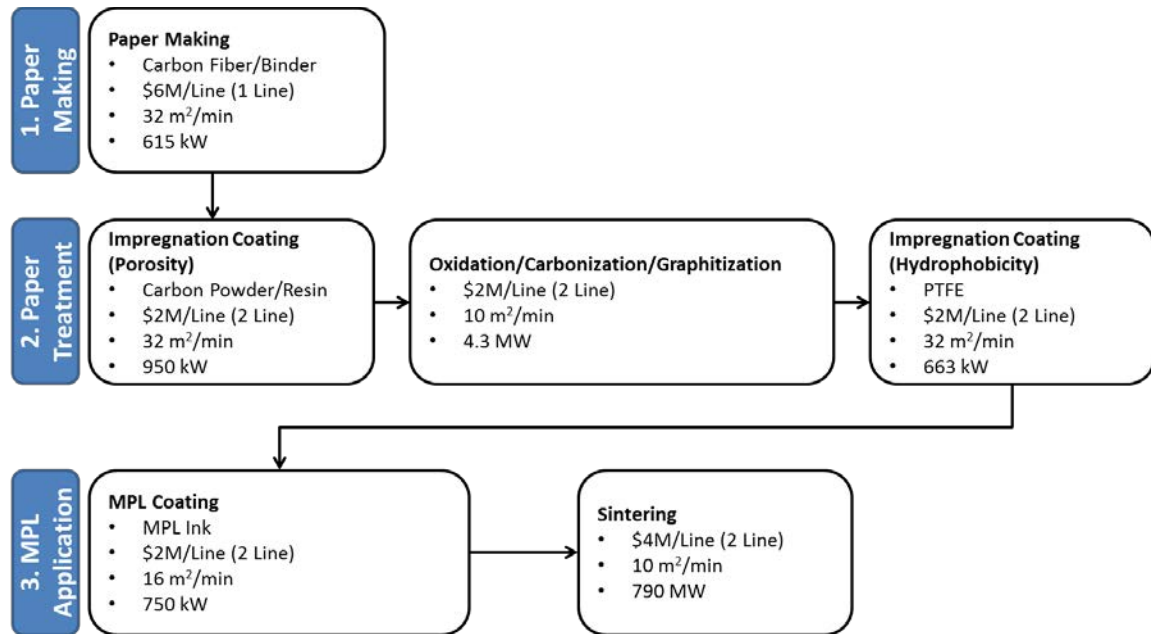
Figure 26. Gas diffusion layer manufacturing process flow diagram for a facility producing GDL to supply 500,000 vehicles per year.

Low Volume Estimates			GDL	
Annual GDL Production	m2/year		200,000	700,000
Paper Making		$/m2	$4.10	$1.70
	Material	$/m2	$0.58	$0.58
	Manufacturing	$/m2	$3.52	$1.12
Impregnation Coating (Porosity)		$/m2	$1.88	$1.06
	Material	$/m2	$0.52	$0.52
	Manufacturing	$/m2	$1.36	$0.54
Oxidation/Carbonization/Graphitization		$/m2	$6.05	$3.91
	Material	$/m2	$0.31	$0.31
	Manufacturing	$/m2	$5.74	$3.60
Impregnation Coating (Hydrophobicity)			$1.61	$0.80
	Material	$/m2	$0.27	$0.27
	Manufacturing	$/m2	$1.35	$0.53
MPL Coating		$/m2	$1.63	$1.25
	Material	$/m2	$0.33	$0.33
	Manufacturing	$/m2	$1.30	$0.92
Sintering		$/m2	$5.45	$1.80
	Material	$/m2	$0.00	$0.00
	Manufacturing	$/m2	$5.45	$1.80
Real Estate		$/m2	$1.66	$0.53
Markup		%	25%	25%
	Material	$/m2	$2.00	$2.00
	Manufacturing	$/m2	$18.72	$8.52
	Facilities	$/m2	$1.66	$0.53
	Total Cost Without Markup	$/m2	$22.39	$11.05
	Total Cost With Markup	$/m2	$27.99	$13.81

Figure 27. Gas diffusion layer cost results for each process for low volume scenario

High Volume Estimates			GDL	
Annual GDL Production	m2/year		2,000,000	10,000,000
Paper Making		$/m2	$1.77	$0.85
	Material	$/m2	$0.58	$0.58
	Manufacturing	$/m2	$1.19	$0.27
Impregnation Coating (Porosity)		$/m2	$0.95	$0.65
	Material	$/m2	$0.52	$0.52
	Manufacturing	$/m2	$0.44	$0.13
Oxidation/Carbonization/Graphitization		$/m2	$1.22	$1.07
	Material	$/m2	$0.31	$0.31
	Manufacturing	$/m2	$0.92	$0.76
Impregnation Coating (Hydrophobicity)			$0.69	$0.39
	Material	$/m2	$0.27	$0.27
	Manufacturing	$/m2	$0.43	$0.12
MPL Coating		$/m2	$0.81	$0.58
	Material	$/m2	$0.33	$0.33
	Manufacturing	$/m2	$0.48	$0.25
Sintering		$/m2	$0.91	$0.61
	Material	$/m2	$0.00	$0.00
	Manufacturing	$/m2	$0.91	$0.61
Real Estate		$/m2	$0.94	$0.29
Markup		%	25%	25%
	Material	$/m2	$2.00	$2.00
	Manufacturing	$/m2	$4.36	$2.15
	Facilities	$/m2	$0.94	$0.29
	Total Cost Without Markup	$/m2	$7.31	$4.45
	Total Cost With Markup	$/m2	$9.13	$5.56

Figure 28. Gas diffusion layer cost results for each process for high volume scenario

At 500,000 systems per year (11.5M m^2/year of GDL), the manufacturing cost is estimated to be $4.40/m^2, very close to Ballard Material Products estimate of $4.45/m^2 used for the baseline system in previous years. The differences between the two estimates are GDL thickness[51], assumptions for labor, electricity, and discount rates. A markup of 25% was estimated[52] to reflect the price the stack integrator would pay, making the total GDL price $5.50/m^2.

The graph in Figure 29 shows the model results over the annual GDL purchase volume for two scenarios: 1) an advanced, roll-to-roll, high volume manufacturing scenario (blue squares) and 2) a conventional, semi-batch, lower volume manufacturing scenario (red squares). For comparison, the Ballard GDL Price (on graph as blue circles) is the cost used in previous year analyses inclusive of a 25% markup for profit. In addition, OEM price projections shown in Figure 25 are included in the graph. A price curve fit was developed with the available data as the basis for GDL price in the 2016 baseline system. At the lowest volume, the OEM price was used as this reflects an average price that accounts for all costs OEMS would pay for GDL including scrap, shipping, etc. At intermediate production rates, SA's modeled conventional GDL price was used in the price curve. Finally, the advanced, high volume manufacturing cost was used

---

[51] Ballard Material Products quotation in 2012 did not specify a GDL thickness. However Jason Morgan's 2011 report on GDL fabrication suggests ~200 microns total, uncompressed. The GDL material modeled in SA's DFMA™ analysis assumes a 150 micron total, uncompressed thickness (105 micron carbon paper thickness and 45micron MPL thickness).

[52] A 25% GDL markup rate is judged to be reasonable based on the approximate company-wide and divisional gross margins shown in SGL's 2015 annual report.

for volumes greater than 2 million m²/year annual GDL production (equivalent to 80,000 to 500,000 systems/year).
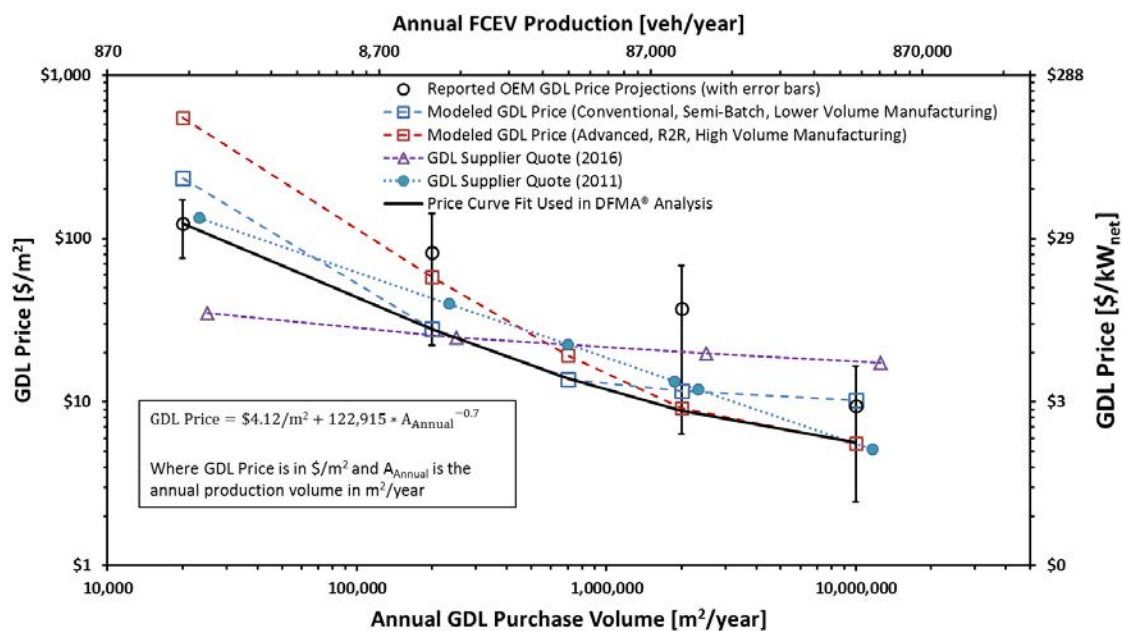
Figure 29. Graph of GDL price over annual GDL purchase volume, showing low and high volume model results and price curve fit used in the baseline.

6.8 Hydrogen Sensor

In 2015, the baseline system used ceramic-based hydrogen sensor with costs based on price quotes from NTM Sensors. While investigating the Toyota Mirai fuel cell vehicle in 2016, SA obtained a projected cost quotation from FiS (A Nissha Company) for hydrogen detectors (model FH2-HY04). In addition to meeting the requirements of a 0-4 vol% detection range in air with less than 2 seconds response time, the FiS detectors do not require calibration and have an estimated lifetime of 10 years. At a quantity of 2,000, these detectors cost around JPY 22,050 per detector ($220 USD/detector). This is very close in cost to the NTM H_2 sensor quotations obtained for the baseline auto and bus systems. However, FiS estimates only JPY2500 ($35 USD) per sensor in 1 million unit orders (with availability at that manufacturing rate in the year 2020). This is approximately half the cost of NTM's projected sensor cost at the same purchase quantity. This cost reduction compared to NTM's projection is not well understood but thought to be related to the size of the company and/or possibly selection of materials. (NTM's sensor is a ceramic sensor that may be made from currently expensive, high purity materials.) Switching to the FiS hydrogen detector reduces the total system cost by $1/kW_{net}$ compared the 2015 analysis.

7 Automotive Power System Side Analyses

This section contains analyses completed during 2016 that either may have helped determine a certain pathway for the baseline system, or may apply to components that will be in a future baseline system when performance has been demonstrated to meet or exceed the performance of current baseline system components.

7.1 Low-Cost Gore MEA Manufacturing and Performance

In 2013, SA evaluated the roll-to-roll Gore MEA manufacturing process as a side study. In that study, SA found that the process was lower cost per area than the baseline process; however, the performance of the Gore MEAs had not yet been characterized. In the past year, the University of Tennessee-Knoxville (UTK) has tested these Gore "direct coated" MEAs at various operating conditions within a 2-cell stack (at 50 cm^2 active area per cell). [53] The operating conditions chosen for these tests were quite different than DOE baseline automotive conditions (1.5 atm and 4 cathode stoichiometry for UTK testing compared to 2.5 atm and 1.5 cathode stoichiometry for baseline system) thereby making a true performance comparison to the baseline MEAs impossible. However, UTK found that the direct coated MEAs had higher performance than commercial MEAs (at the conditions for which they tested). Consequently, it is inferred that the Gore direct coated MEAs would also have higher polarization performance than the SA analysis baseline MEAs at baseline operating conditions, but a quantitative assessment is not possible. If and when additional testing results can be shared, a more quantitative comparison with the baseline MEA fabrication process can be made.

7.2 Evaluation of Borit Hydrogate BPP Forming Process

The baseline system assumes use of progressive stamping to form the stainless steel bipolar plates. However, sequential stamping and hydroforming are also viable alternatives to form very thin metal plates and were examined, particularly in low volume applications, as part of SA's 2015 cost analysis. For 2016, hydroforming was revisited to examine the Hydrogate process, a specific version of continuous hydroforming offered by Borit NV of Belgium.

The Hydrogate process of continuous hydroforming combines continuous metal coil feed with a hydrostatic press to form low residual stress flat plates. Compared to traditional stamping presses, the Hydrogate process offers:

- Reduced press capital cost (due to a compact press system and single station operation)
- Reduced tooling costs since only one forming step (rather than a sequence) and one forming is required (rather than both a top and bottom die).
- Potentially increased die life due to reduction of metal-on-metal impacts.
- Low cycle times (specifically when accounting for forming of multiple parts in one press cycle).
- Greater feasibility of forming multiple parts in a single operation (i.e. more formed parts per cycle).

---

[53] Based on pre-publication extract of a W.L. Gore, Inc. Preliminary Report on University of Tennessee Cell Testing, 2016.

- Forming of BPP with a reduced number of stations. (The BPP flow field may be formed in a single operation, but the manifold piercings and part cut must be done in a separate operation (mechanical stamping, laser cutting, etc.).)
- Ability to form detailed features that may not be dimensionally possible with conventional stamping.

Because the Hydrogate process uses high pressure fluid to deform the sheet metal parts, it is ill-suited for piercing operations (however, at very high volumes the integration of cutting steps in the forming step may be feasible). Consequently, cutting of the BPP manifold holes and part cut-out must be done by some other operation. Borit currently uses high precision laser cutting for smaller to medium volumes and already uses mechanical cutting for higher volumes. (Coiling of the formed BPPs is considered infeasible as it would deform the flow fields: consequently any stamping operation must be done in-line with the Hydrogate process.) Press tonnage to cut the manifolds and trim the part is low compared to the tonnage required for the flow fields. Consequently, the stamping press is expected to be quite small and (relatively) inexpensive. All stamped features are anticipated to be captured in a single die-set.

Figure 30 and Figure 31 contrast a conventional 5-stage inline progressive die stamping process train (as used in the baseline design) with the Hydrogate process (followed by a conventional stamping operation for manifold forming and part cut-off). As shown, the Hydrogate process has considerable advantages in capital cost for the press and die costs. The cost impact of Hydrogate's lower forming speed is off-set by the greater number of parts formed per stroke. Overall, the Hydrogate process is projected to yield lower part cost at all production rates. At 500k systems/year, Hydrogate offers a potential cost reduction of $2.35/kW ($4.59/kW vs. $6.93/kW) compared to baseline stamping. After further analysis, the Hydrogate forming process will be considered for inclusion in the 2017 baseline system.

	SA Baseline (5-stage Progressive Die Stamping)	Borit Hydrogate (with manifold/separation cutting)
Plate Active Area	312 cm^2	312 cm^2
Plate Total Area	500 cm^2	500 cm^2
Plates per stamp	1	4
BPP Stamping/Hydrogate Force	16,000 kN or 1,600 tons	41,200 kN or 4,200 tons (2,000 bar over active area)
Plate Material	316 SS, 3 mils	316 SS, 3 mils
Forming Machine Capital Cost	$1.8M (Prog. Stamp) $2.1M total system	$1M (Hydrogate) $89k (Cutting Press) $1.2M total system
Forming Rate	2.47sec per plate	7.5 sec per 4 plates
Labor	0.25 workers per press (min)	0.25 workers per press (min) (oversees Hydrogate & stamping)
Stamping Die Set Lifetime	10M cycles	10M cycles (Cutting die)
Stamping Die Set Cost	$662k	$100k (Cutting die)
Hydrogate Die Set Lifetime	Not applicable	10M cycles
Hydrogate Die Cost	Not applicable	$60k

Figure 30. Parameter comparison of progressive die stamping with the Hydrogate hydroforming process.
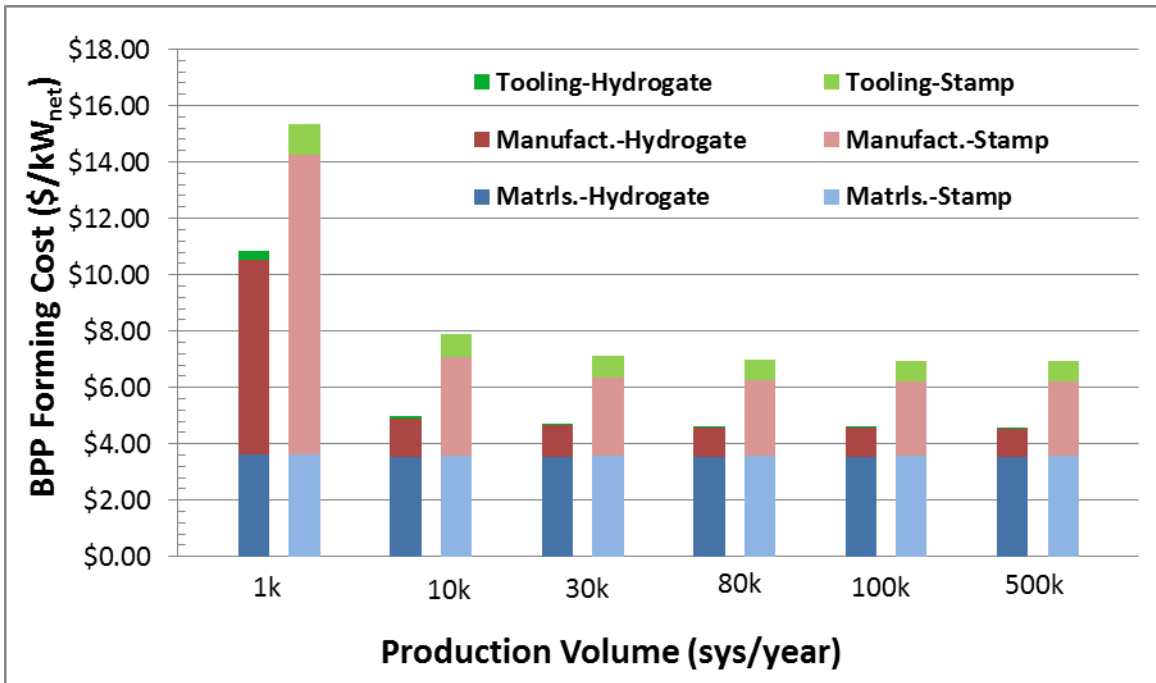
Figure 31. Cost comparison of progressive die stamping with the Hydrogate hydroforming process.

Of note is the high number of forming process trains required for 500k systems/year: ~111 for progressive die stamping and ~72 for Hydrogate (based on 2 shifts/day, 240 days/year).[54] As previously discussed, these are extremely high numbers of parallel process trains and are not deemed a feasible arrangement (while still maintaining plate tolerances).

Both processes currently assume a 15 minute coil change out time. This temporary line shut-down adds approximately $0.2/kW to BPP cost. Systems which employ coil changes with continuous operation would presumably result in cost savings.

7.3 DFMA® Analysis of Toyota Mirai Fuel Cell System

The unveiling of the Toyota Mirai fuel cell vehicle provides a unique opportunity for SA to compare the baseline automotive system to a mass produced FCS. While Toyota has not released details of the power system operating conditions, much top level component information is publicly available. SA is able to make educated guesses for many aspects of the Mirai system based on Toyota news releases and publications[55], discussions with OEMs and the DOE Fuel Cell Tech Team, and the patent literature.[56, 57] Given reported stack sizing and operating techniques such as power output, number of cells, and

---

[54] The number of required process trains would be proportionally lower of 24/7 operation were implemented.

[55] Konno, Norishige, Seiji Mizuno, Hiroya Nakaji, and Yuji Ishikawa. "Development of Compact and High-Performance Fuel Cell Stack." SAE International Journal of Alternative Powertrains 4, no. 2015-01–1175 (2015): 123–129.

[56] Tabata, Toshiharu, Tomoaki Terada, Takahiro Nagata, Susumu Enomoto, Yosuke Horiuchi, Hiroaki Takahashi, Tetsuo Kawamura, and Hideyasu Kawai. Conductive Carbon Carrier for Fuel Cell, Electrode Catalyst for Fuel Cell and Solid Polymer Fuel Cell Comprising Same. US8372562 (B2), issued February 12, 2013.

[57] Fujii, Toshiro, and Yoshiyuki Nakane. Electric pump. US7980830 (B2), issued July 19, 2011.

60

internal cell humidification, SA was able to make educated guesses for a complete set of operating conditions that is deemed reasonable by the DOE Fuel Cell Tech Team.

Stack humidification (external vs. internal) is one of the key differences between SA's baseline system and the Toyota Mirai system. In the Mirai stack, a thinner than typical PEM membrane facilitates product water transport across the membrane and into the H_2 flow. An H_2 recirculation blower is then used to circulate humidified H_2 from the anode exhaust back to the anode inlet, where it can humidify the membrane at the stack inlet, a region where there is otherwise limited product water.

There are three aspects of this benchmarking analysis: 1) Detailed definition of the Mirai system and stack design, 2) DFMA® analysis and cost sensitivities of unknown aspects of the system, and 3) side-by-side comparison and evaluation of the component and cost differences between SA's baseline automotive system and the Toyota Mirai system.

The baseline automotive DFMA® model is used as the analysis framework of the Mirai system, as they have much in common. Many of the lower cost components for which there is little or no detail provided by Toyota, are adopted without change from the baseline system. Additionally, many design assumptions are held constant between systems when there were no documented changes reported for the Mirai. Larger impact values are incorporated into a sensitivity study to estimate the ranges of the potential Mirai cost impact. For example, the bipolar plate thickness is unknown so a range in thicknesses (affecting titanium cost) is postulated to estimate the spread of potential bipolar plate costs. Figure 32 details specific modeled differences between the Toyota Mirai fuel cell system and the baseline automotive fuel cell system.

Component	2016 Baseline System	Change made to model Toyota Mirai System
BPP	Stamped stainless steel	Exchanged stainless steel for titanium
BPP Coating	TreadStone Coating	Exchanged for amorphous carbon coating
Coolant Gaskets	Laser Welding of BPPs	Exchanged with injection molded EPDM BPP gasket
MEA Sealing	2-part Subgasket	Exchanged with injection molded EPDM frame gasket
Compression	Compression bands	Removed compression bands (uses constant dimension compression)
Housing	Vacuum thermoformed polypropylene	Exchanged for aluminum casting
End Plates	Compression molding of LYTEX® composite	Exchanged with sand cast aluminum
Gas Distribution Manifold	Not Included	Added component for gas distribution connection to stack (external to housing). Sand cast aluminum plate with insertion molded resin.
Humidifier	External plate frame membrane humidifier	Removed humidifier (uses internal humidification via a thin membrane, BPP flow channels, and H_2 recirculation pump)
Air compressor	Honeywell centrifugal compressor/expander	Exchanged with Roots-type compressor (modeled as two-shaft Eaton-style system without expander)
H_2 Recirculation Pump	Not Included (2 passive ejectors are used for recirculation)	Added electrically driven gear-type compressor based on Toyota Industries Corporation patent

Figure 32. List of changes made to the baseline DFMA® model to represent a Toyota Mirai system

The estimated cost for the Toyota Mirai FCS is $233/kW$_{net}$ at 1,000 systems per year production and is approximately 18% higher than the $197/kW$_{net}$ projected cost of SA's baseline automotive system (scaled to 91 kW$_{net}$ at 1,000 systems per year). This section of the report will describe the design and cost differences between the Mirai FCS and the baseline system; however, there are two main fundamental concepts that must be acknowledged while comparing systems:

1) The baseline auto DFMA® model is modified each year to optimize the cost of the system. While performance parameters are considered, durability for state-of-the-art technology may not yet be proven in a complete integrated system.
2) The design of the baseline auto system is primarily designed (on paper) with high production in mind and the design kept constant for all lower manufacturing volumes. In contrast, the Mirai is presumably primarily designed (in hardware) with low production in mind. Consequently, the design of the Mirai is more likely to change with increased production volumes as the limitations of early production/development are alleviated.

7.3.1 Mirai Operating Conditions

The power density estimate (1.3 W/cm^2) is derived from the estimated total active area (9 m^2/stack) and Toyota reported gross power (114 kW).[58] The calculation for the active area is based on Toyota's documented stack sizing (37 L, at 1.34 mm thickness per cell) and number of cells (370 cells/stack) [58], SA's estimate for ratio of active cell height to active cell width (0.5:1), SA's estimate for the housing thickness (1 cm), and SA's estimate of the cell active to total area ratio (0.4:1). The net power of the stack is not specified by Toyota; however, with air compressor sizing and other ancillary loads from the system, net power is estimated to be 91 kW. Ancillary loads include 21 kW for the air compressor, 1 kW for the H$_2$ recirculation blower, and 1 kW for the coolant loop pumps and fans. Estimated Mirai operating conditions are listed in Figure 33.

Note that power density is normally a key parameter for determination of the size and cost of the stack, and that the Mirai power density in this study is derived rather than stated by Toyota. While this would suggest enhanced uncertainty in cost projection, for this particular analysis the power density (and also voltage operating point) are of lesser importance because the physical dimensions for the stack are defined and thus the total plate area of the BPPs is fairly well established. Note, however, that deviations from the estimated power density would impact membrane total area required and catalyst cost (as Pt usage is determined by active area and assumed catalyst loading).

---

[58] Konno, Norishige, Seiji Mizuno, Hiroya Nakaji, and Yuji Ishikawa. "Development of Compact and High-Performance Fuel Cell Stack." SAE International Journal of Alternative Powertrains 4, no. 2015-01–1175 (2015): 123–129.

Estimated Mirai Operating Condition	
Stack Power Net/Gross	91 kW/114 kW
Cell Voltage	0.67 V, 370 cells/stack
Current Density	1.9 A/cm^2
Power Density	1,295 mW/cm^2
Stack Pressure	est. <=2.5 atm
Total Pt loading	0.3 mg/cm^2
Peak Cell Temp	est. <86 °C
Total Active Area per system	8.78 m^2
Active to Total Area ratio	0.4
Active/Total plate area	237 cm^2/593 cm^2
Q/ΔT	2.5 kW/°C

Figure 33. Table of estimated Toyota Mirai operating conditions for SA side study

7.3.2   Mirai Stack Components

There are multiple stack components provided to Toyota by lower tier vendors such as bipolar plate material, rubber gaskets, GDLs, catalyst, and membrane material. The table below in Figure 34 describes many of these stack components and their publically identified Mirai supplier. Information on the material and technique used to manufacture the catalyst and the rubber gaskets is used in the Mirai DFMA® cost analysis. Cost quotes for GORE-SELECT® membranes were not obtained for this study; rather cost was based on use of the baseline membrane process. When including components provided by external vendors, a markup is applied to the manufacturing cost to estimate a price to Toyota Motor Company (TMC).

Component Description	Vendor	Reference
PtCoCe/C catalyst includes increased durability with graphitized carbon black and free radical quenchers (cerium oxide)	Cataler	Cataler Website: http://www.cataler.co.jp/en/innovation/index.php Patent: US 8,372,562 B2 (2013) Patent: US 8,338,051 B2 (2012)
GORE-SELECT® membrane	W.L. Gore	http://www.gore.com/en_xx/products/electronic/fuelcells/fuelcells_series57_available.html
GDL carbon paper	Toray	http://www.toray.com/news/carbon/detail.html?key=D144E85F1C996C5149257D950007222B
Flat rolled specialty titanium bipolar plate material	Kobelco	http://www.kobelco.co.jp/english/releases/2015/1190697_14516.html
Rubber gaskets for coolant gasket and MEA gasket	Sumitomo Riko	https://www.sumitomoriko.co.jp/english/companynews/pdf/2014/n51910191.pdf Patent Application: US 2015/0380694 A1 (2015)
H$_2$ Detector: FH2-HY04	FiS (a Nissha Company)	http://www.nissha.com/english/news/2014/12/12th_1.html

Figure 34. Second tier vendor list for Mirai components with references

7.3.2.1   *Mirai Catalyst Fabrication*

A DFMA® analysis was conducted for the Mirai catalyst system (assumed to be PtCoCe on graphite for both anode and cathode). Two patents from Cataler were used to define the synthesis steps, as seen in Figure 35. The processing steps are quite similar to dispersed de-alloyed PtNi$_3$/C synthesis, although an

additional processing step for graphitizing the carbon powder is assumed for increased durability. The addition of cerium oxide to the catalyst is also reported to improve durability through free radical quenching. The Pt loading is assumed to be 0.3 mgPt/cm^2 based on some references[59], thus implying ~30 grams Pt per stack; however, this value was subjected to sensitivity analysis because there is no reference directly from Toyota that verifies this catalyst loading.
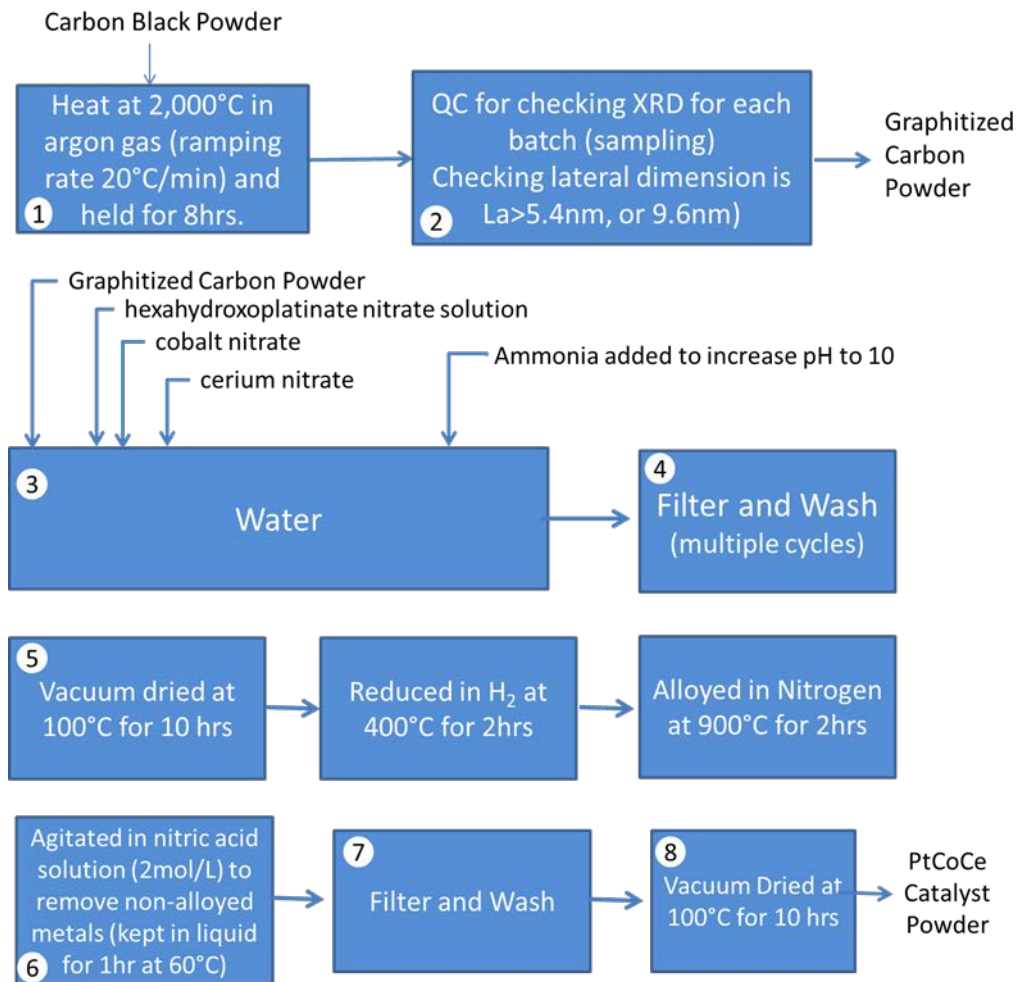
Figure 35. Process flow diagram for Mirai catalyst PtCoCe on graphite synthesis

In the process to make PtCoCe, the cost of platinum donor material (hexahydroxoplatinate) is assumed to be twice the cost of the platinum donor material (chloroplatinic acid). The breakdown in materials, manufacturing, and markup for the catalyst synthesis is shown in Figure 36. At 1,000 systems per year, the markup associated with materials (excluding Pt) and processing for the catalyst synthesis and

---

[59] http://energyfuse.org/three-challenges-confronting-the-toyota-mirai-fuel-cell-vehicle/
https://newenergytreasure.com/2014/07/08/100-kw-hydrogen-fuel-cell/

application is 25% at 1,000 systems per year. The catalyst is applied via sequential slot die coating at a cost of roughly $800 per system.

Component Costs per 80kWnet Fuel Cell System		All at 1k systems per year			
		Materials	Manuf.	Markup	Total
Platinum Cost		$1,418	$0	$0	$1,418
Step 1: Catalyst PtCoCe Precursor	$/system	$171	$56	$57	$284
Step 2: Precursor Filtration	$/system	$0	$18	$4	$22
Step 3: Precusor Wash	$/system	$0	$7	$2	$9
Step 4: Precursor Drying	$/system	$0	$47	$12	$59
Step 5: Precursor Crushing	$/system	$0	$25	$6	$31
Step 6: Precursor Annealing	$/system	$0	$88	$22	$111
Step 7: Catalyst Dealloying	$/system	$1	$54	$14	$68
Step 8: Catalyst Filtration	$/system	$0	$13	$3	$16
Step 9: Catalyst Wash	$/system	$0	$7	$2	$9
Step 10: Catalyst Dry	$/system	$0	$26	$7	$33
Step 11: Catalyst Crushing	$/system	$0	$25	$6	$31
Total Cost		$1,589	$366	$134	$2,089

Figure 36 Table of PtCoCe catalyst synthesis costs at 1,000 systems per year production.

7.3.2.2 *Amorphous Carbon Bipolar Plate Coating*

The Mirai bipolar plates (BPPs) are modeled as stamped titanium plates with an amorphous carbon anti-corrosion coating based on reports from Toyota.[60] The amorphous carbon application process is modeled assuming plasma enhanced chemical vapor deposition (PECVD) of a pyridine precursor in a nitrogen carrier gas with an argon plasma cleaning step to prepare the titanium plate surface. The cost model is based on Toyota's patents which identify example precursor gas formulations to form amorphous carbon as well as film thicknesses.[61, 62] In the DFMA® analysis, plates are manually loaded into the PECVD vacuum chamber (96cm diameter x 1.2m tall chamber) which can hold ~ 196 parts per batch. After evacuating the chamber, an argon plasma is used to clean the surface for 5 minutes. A 2 μm amorphous carbon film is deposited from pyridine precursor (100 mTorr) in a nitrogen carrier gas. The plasma is formed by field ionization and confined using a fixed magnetic field. The targets (BPPs) are biased to facilitate ion bombardment of the surface of the BPP. After a 40 minute deposition time (20 min/μm), the plates are manually unloaded. Figure 37 is a flow diagram showing these steps and processing times.

---

[60] Konno, Norishige, Seiji Mizuno, Hiroya Nakaji, and Yuji Ishikawa. "Development of Compact and High-Performance Fuel Cell Stack." SAE International Journal of Alternative Powertrains 4, no. 2015-01–1175 (2015): 123–129.

[61] Patent: US 8,119,242 B2 (2012)

[62] Patent Application: US 2012/0183887 A1
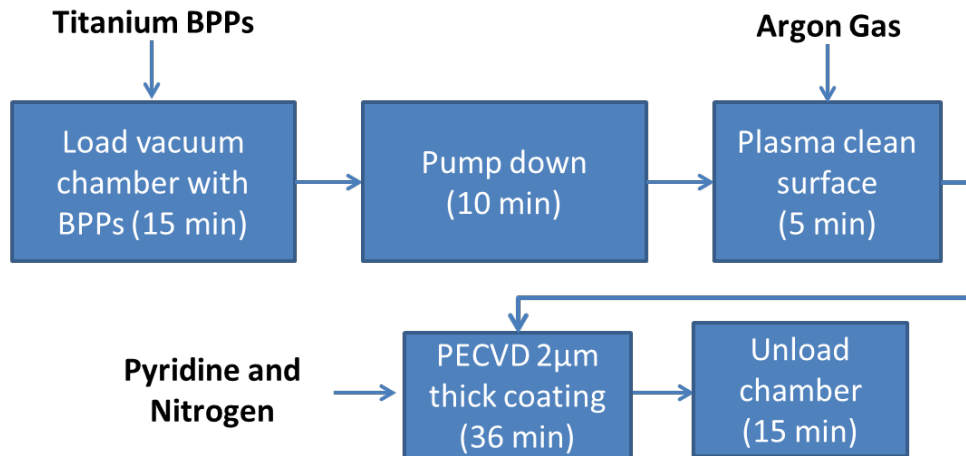
Figure 37. Process flow diagram of amorphous carbon coating onto BPPs

7.3.2.3 Mirai Gasket Sealing

The gasket sealing design of the Mirai stack includes an injection molded frame gasket around the MEA and injection molded bipolar plate (BPP) gasket (as an alternative to the laser welding in the baseline system). The design of the two gaskets is described in a Sumitomo Riko patent application[63] and is illustrated in Figure 38 (which shows a cross-sectional view of the cell from the patent application).
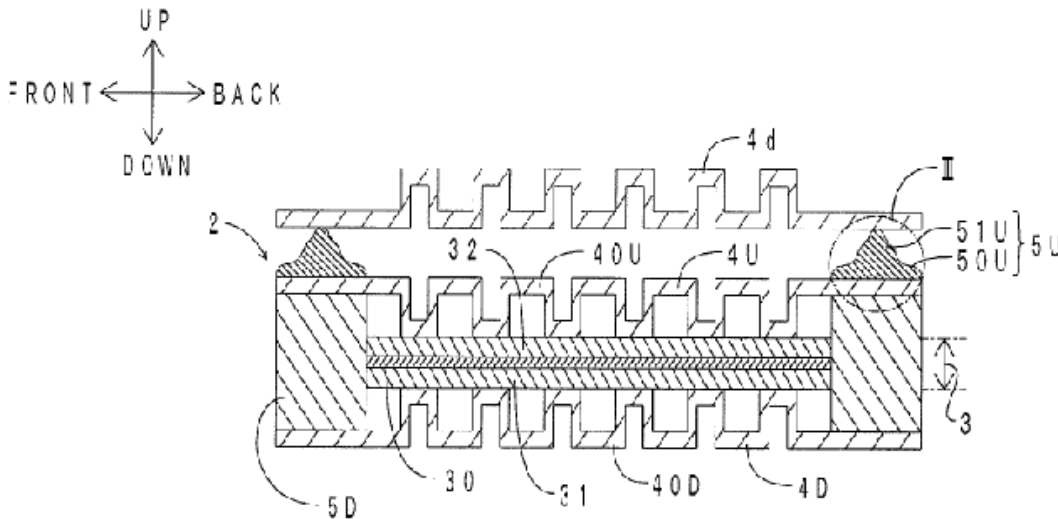
Figure 38. Cross-sectional view of cell showing the anode bipolar plate (4D), BPP gasket (5U), cathode bipolar plate (4U) and MEA frame gasket (5D). Figure 3 of US Patent Application 2015/0380694 A1 (2015).

Within the patent application, an example is given using EPDM as the rubber gasket material and using the following process (as further shown in Figure 39).

---

[63] Patent Application: US 2015/0380694 A1 (2015)

A) **Injection Molding:** Injection mold unlinked EPDM into two pre-form shapes
   a. a free-standing BPP gasket (step 1 of Figure 39) and
   b. a free-standing Frame gasket (step 2 of Figure 39).

B) **Application of gaskets to BPPs:** temporary attachment (via clamping) of the free-standing gaskets to form 2 sub-assemblies (as a precursor to creation of the full BPP assembly)
   a. Sub-assembly #1: Room temperature clamping of the cathode BPP and the free-standing BPP gasket. (Primer is first applied to the BPP surface facing the gasket to improve gasket adhesion.)
   b. Sub-assembly #2: Room temperature clamping of the anode BPP, the frame gasket, and the MEA. (Primer is first applied to the BPP surface facing the frame gasket to improve gasket adhesion.)

C) **Cell Assembly:** Place sub-assembly #1 and sub-assembly #2 into a single mold and apply primer to the cathode bipolar plate, then clamp and heat for 10 minutes at 150 °C to cross-link EPDM. Final result is a gasketed and assembled cell.

Cost estimates show the cell assembly (C) is more than 60% of the total gasket process cost (A+B+C=$939/stack) due to the long processing time and limited number of parts simultaneously heated in the same mold. The application to the BPP (B) is only 10% of the total cost and injection molding (A) is about 30%. A 30% markup is applied to only the injection molded gaskets based on the assumption that Sumitomo Riko would be the vendor supplying the injection molded gaskets to Toyota. Toyota would then assemble the individual cells in a fuel cell stack.
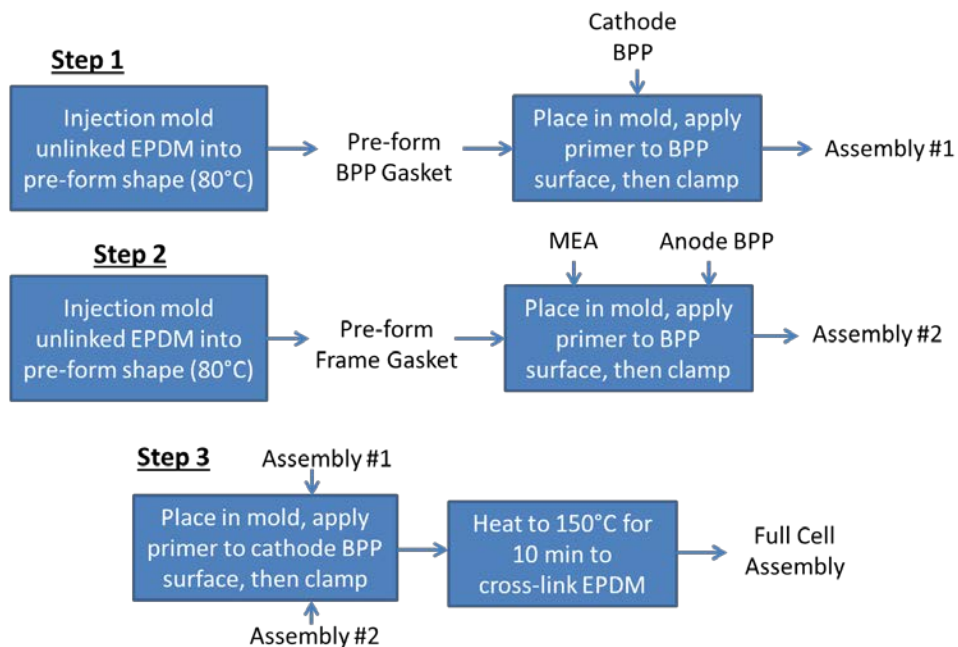
Figure 39. Process flow diagram for Sumitomo Riko MEA and coolant gaskets

7.3.2.4 Mirai Gas Distribution Manifold

Unlike the SA baseline system, the Toyota Mirai stack includes a gas distribution manifold made of aluminum and Kuraray *GENESTAR* resin.[64,65] The manifold plate replaces one of the stack end plates, piping fittings at stack inlet/outlet, and insulator between current collector and end plate. The resin is a proprietary polyamide material that electrically insulates the aluminum plate from the rest of the stack. Additionally, the resin contains additives for decreased electric conductivity and is designed for lower water absorption (high water absorption at higher temperatures can reduce electrical insulation within the resin material). The manifold is modeled as a sand casted aluminum plate with insertion molding of the resin around the part. The insertion molding process contributes to 80% of the total manifold cost (~$1,600/manifold).

7.3.3 Mirai Stack Cost Results

This section covers the results of a side-by-side comparison of the Toyota Mirai stack and SA's baseline DFMA® stack model scaled to 91 kW_{net} at a production rate of 1,000 systems per year. The stack cost for the Mirai is about $15,400/stack compared to $12,800/stack for the 91 kW_{net} baseline system. Figure 40 enumerates the cost elements within the Mirai stack and Figure 41 is a bar chart comparing the component costs for the two systems. A majority of the cost difference is explained by a few key features:

- The Mirai's titanium BPPs have higher material cost than the stainless steel used in the baseline),
- The Mirai's higher (estimated) Pt loading (0.3 mg/cm^2 compared to 0.134 $mgPt/cm^2$ for the baseline) is likely driven by the desire to ensure durability, and
- The Mirai's balance of stack cost is much higher than the SA baseline balance of stack due to extra components in the Mirai stack (including a manifold for gas feed connections).
- All other Mirai stack components that use the same process and methods as the baseline system are slightly lower cost due to the lower total active area required per stack (8.8m^2 for the Mirai compared to 13.3m^2 for the baseline system at 91 kWnet).

---

[64] Nobuhiko Nakagaki, 'The Newly Developed Components for the Fuel Cell Vehicle, Mirai', *SAE International Journal of Alternative Powertrains*, 2015 <http://dx.doi.org/10.4271/2015-01-1174>.
[65] http://www.kuraray.com/release/2015/150825.html

Annual Production Rate	Sys/yr	1,000
System Net Electric Power (Output)	**kWnet**	91
System Gross Electric Power (Output)	**kWgross**	114
Stack Components		
Bipolar Plates (Stamped)	$/stack	$4,660
MEAs		
Membranes	$/stack	$2,800
PtCoCe Catalyst Ink & Application	$/stack	$2,896
GDLs	$/stack	$2,177
M & E Hot Pressing	$/stack	$36
Bipolar Plate and MEA Gaskets	$/stack	$939
End Gaskets (Screen Printing)	$/stack	$1
End Plates	$/stack	$77
Manifold	$/stack	$1,605
Current Collectors	$/stack	$7
Stack Housing	$/stack	$57
Stack Assembly	$/stack	$78
Stack Conditioning	$/stack	$61
Total Stack Cost	**$/stack**	**$15,393**
Total Stacks Cost (Net)	**$/kWnet**	**$169.16**
Total Stacks Cost (Gross)	**$/kWgross**	**$135.41**

Figure 40. Breakdown in Mirai stack cost
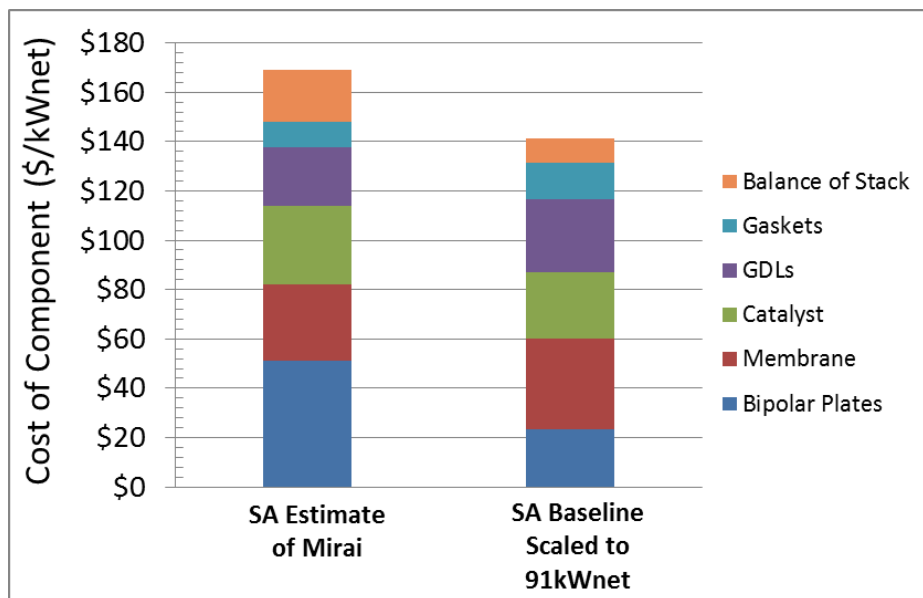
Figure 41. Comparison of SA's estimate of Mirai stack cost with SA baseline auto system scaled to 91 kW$_{net}$

7.3.4   Mirai BOP Components

Figure 42 is a diagram of the Toyota Mirai fuel cell system as used for cost modeling purposes. The Mirai system contains no expander in the air loop and no external humidifier or low temperature coolant loop for the air compressor (after air compression the air is cooled by the intercooler using the same water coolant loop as the stack). The air compressor is based on a Roots-type blower with cost based on

DFMA® analysis previously conducted for the bus fuel cell system (Roots blower, electric motor, and motor controller, with scaling to the appropriate power level required for the Mirai).

As consistent with past SA cost analysis, the hydrogen regulator is considered part of the hydrogen storage system and is not included as part of the Mirai's BOP cost analyzed here. The injector component for flow control, upstream of the hydrogen recirculation loop, is some type of integrated unit functioning as three solenoid valves: its cost is simplistically modeled as three times the cost of a single hydrogen ejector cost used in the baseline system.[66] The cost of these components could reasonably be tabulated with the hydrogen storage system but are included in the fuel cell subsystem for completeness. Whereas the baseline system uses two hydrogen ejectors to recirculate hydrogen, the Mirai uses an electrically driven hydrogen recirculation pump to facilitate hydrogen and water recycle within the stack. A DFMA® analysis was completed for the Mirai hydrogen recirculation pump as described below.
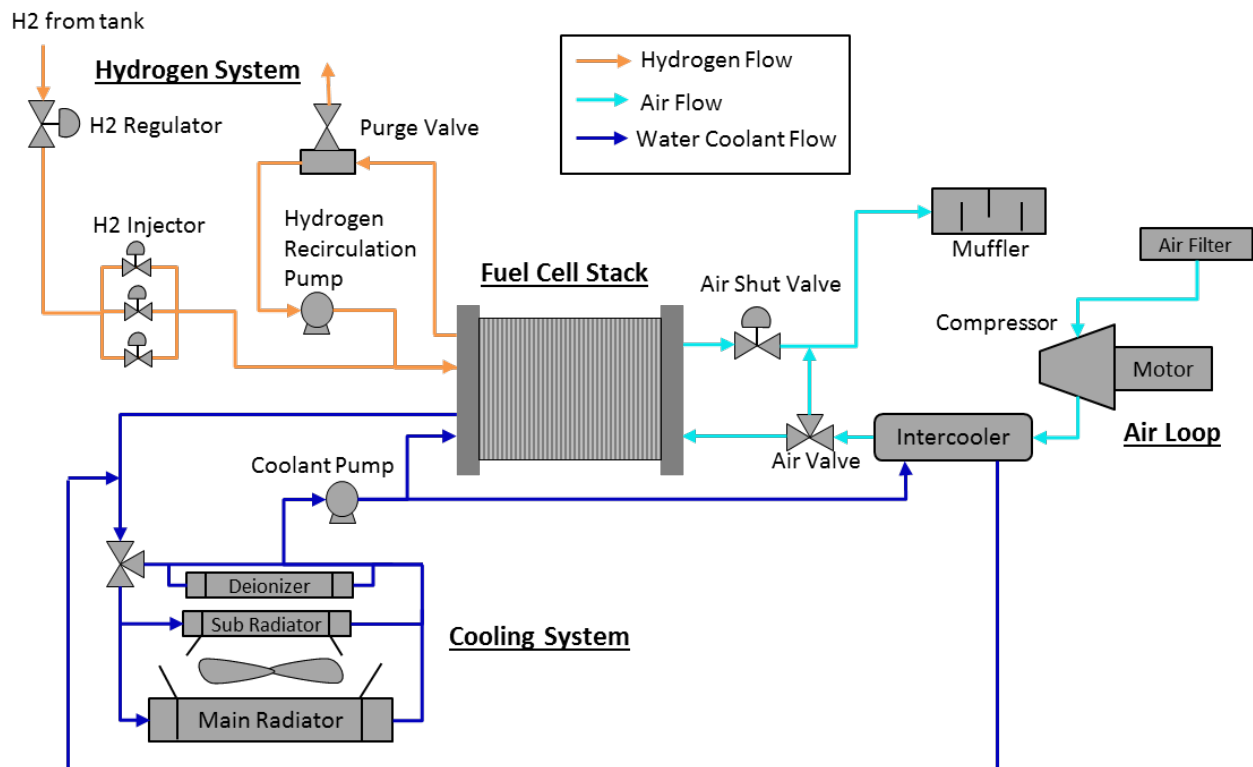
Figure 42. Toyota Mirai system diagram derived from EVS28 KINTEX, Korea, May 3-6, 2015 Toyota Fuel Cell System (TFCS)[67]

---

[66] The H$_2$ injector used in the Mirai system is made by Aisan (http://www.aisan-ind.co.jp/en/products/greenvehicle.html). The cost is estimated at ~$130 but this is a preliminary value and will likely change with further investigation.

[67] http://www.a3ps.at/site/sites/default/files/downloads/evs28/papers/A8-04.pdf

7.3.4.1 Mirai H₂ Recirculation Pump

Based on the Toyota Industries Corporation (TIC) patent[68] for an electrical pump, the pump is specially designed to have the ability to break-up ice if needed upon startup. One of the pumps main purposes is to recycle water from the anode exhaust to the anode inlet. Consequently, liquid water may accumulate in the pump. If left in freezing temperatures, the hydrogen pump motor can rotate the drive shaft in both directions, breaking up any ice that may accumulate within the pump. The patent contains a detailed description of all the components including a diagram of the cross-section of the pump, as seen in Figure 43. The list of pump components analyzed and their respective costs are shown in Figure 44.

Figure 43. Cross-section of hydrogen recirculation pump from Toyota Industries Corporation patent[69]

[68] US Patent 7,980,830 B2, "Electrical Pump", 2011.
[69] US Patent 7,980,830 B2, "Electrical Pump", 2011.

Pump Cost per System			
Component Costs per System			
Pump Rotor	$/sys	Laser Cut SS316 2-Lobe Straight Roots Type Rotors	$8.39
Pump Housing	$/sys	SS316 Investment Casting	$65.10
Pump End Plate	$/sys	SS316 Machined Plate	$11.02
Gear Housing	$/sys	Aluminum Investment Casting	$33.24
Gears	$/sys	Laser Cut SS316 Gears	$18.30
Gear Plate	$/sys	SS316 Machined Plate	$8.11
Driven Shaft	$/sys	High Carbon Steel Machined Rod	$16.57
Large Bearings	$/sys	Steel Ball Bearings	$8.60
Screws	$/sys	1/4-20 socket head	$5.35
O-Ring Seals	$/sys	1x motor housing, 2x gear housing, and 1 x pump housing	$16.00
Motor Housing	$/sys	Aluminum Investment Casting	$61.60
Small Bearings	$/sys	Steel Ball Bearings	$6.45
Motor Drive Shaft	$/sys	High Carbon Steel Machined Rod	$19.37
Stator Lamination Stamping	$/sys	Electrical Steel (high silicon content) Stamped	$12.18
Stator Lamination Stacking and Laser Weld	$/sys		$1.97
Stator Coil Winding	$/sys	Copper coil	$4.38
Motor Dip Coating	$/sys	Epoxy Polyester Resin Dip Coating	$18.49
Motor Heat Treat	$/sys	Heat for 3hrs at 350F	$29.59
Rotor Core	$/sys	Electrical Steel (high silicon content) Stamped	$9.40
Rotor	$/sys	Copper Die Casting	$29.75
Brass Weight	$/sys	Machined Brass Plate	$3.15
Hammer	$/sys	Machined SS316 Plate	$5.94
Collision Member	$/sys	Machined SS316 Plate	$2.91
Motor and Pump Assembly	$/sys	~7min Assembly	$14.01
Motor Testing	$/sys	~30 min Testing	$40.10
Motor Controller Cover	$/sys	Aluminum Plate	$5.00
Motor Controller	$/sys	Previous DFMA model for motor controller adjusted for rpm and power	$202.61
Contingency (5% of total)	$/sys		$32.88
Total Pump Manufacturing and Material Cost	**$/sys**		$690.46
Markup on Compressor and Motor (23%)	**$/sys**		$114.43
Total Pump Unit Cost	**$/sys**		$804.89
Total Pump Cost (Net)	**$/kWnet**		$8.84
Total Pump Cost (Gross)	**$/kWgross**		$7.08

Figure 44. Bill of Materials for Hydrogen Recirculation Pump.

7.3.4.2   *Hydrogen Detectors*

The Mirai is modeled as requiring two hydrogen sensors, the same number as the baseline automotive system. Quotations were requested from FiS (A Nissha Company) for hydrogen detectors (model FH2-HY04). Compared to NTM sensors used in the 2015 baseline system, the FH2-HY04 detectors are able to detect 0 to 4 vol% hydrogen in air with less than 2 seconds response time (compared to 5 seconds for NTM sensors), and the FiS detectors do not require calibration over their estimated 10 year lifetime (compared to a 5 year lifetime for NTM sensors). At a quantity of 2,000, these detectors cost around JPY 22,050 per detector ($220 USD/detector). FiS estimates JPY2500 ($35 USD) per sensor in 1 million unit orders (with availability at that manufacturing rate in the year 2020).

7.3.5   **Mirai BOP Cost Results**

The Mirai's BOP cost breakdown is listed in Figure 45 and shows the air loop and fuel loop as primary contributors to cost. Figure 46 shows a side-by-side BOP cost comparison between the Mirai and SA baseline (scaled to 91 kW$_{net}$ at 1,000 systems per year). The BOP cost for the Mirai is about $5,700/BOP compared to $5,000/BOP for the 91 kW$_{net}$ baseline system.

As described previously, the baseline system uses a combination of low and high flow ejectors for H_2 recirculation while the Mirai system incorporates a hydrogen recirculation pump. Due to internal humidification, the Mirai does not require an external humidifier like the one used within the baseline system. This trade-off in BOP components makes the systems surprisingly close in BOP cost, making it quite clear that variation in the stack components is the primary source of the power system cost variance.

Annual Production Rate	Sys/yr	1,000
System Net Electric Power (Output)	kWnet	91
System Gross Electric Power (Output)	kWgross	114
BOP Components		
Air Loop	$/system	$2,733
Humidifier & Water Recovery Loop	$/system	$167
High-Temperature Coolant Loop	$/system	$606
Low-Temperature Coolant Loop	$/system	$99
Fuel Loop	$/system	$1,160
System Controller	$/system	$152
Sensors	$/system	$512
Miscellaneous	$/system	$256
Total BOP Cost	$/system	$5,685
Total BOP Cost	$/kW (Net)	$62.47
Total BOP Cost	$/kW (Gross)	$50.00

Figure 45. Breakdown in Mirai BOP sub-systems
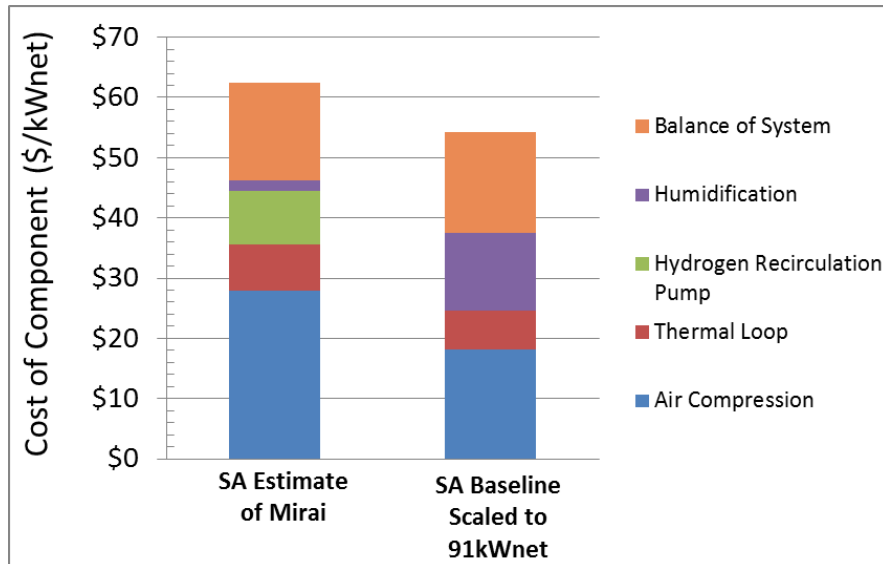
Figure 46. Comparison of Mirai BOP cost with SA baseline model scaled to 91 kW$_{net}$.

7.3.6 Total System Cost Comparison

The total Mirai FCS cost is estimated to be ~$233/kW$_{net}$ with about 73% of the cost from the stack cost (at 1,000 systems per year production). Figure 47 show the Mirai system next to the baseline auto system scaled to 91 kW$_{net}$.
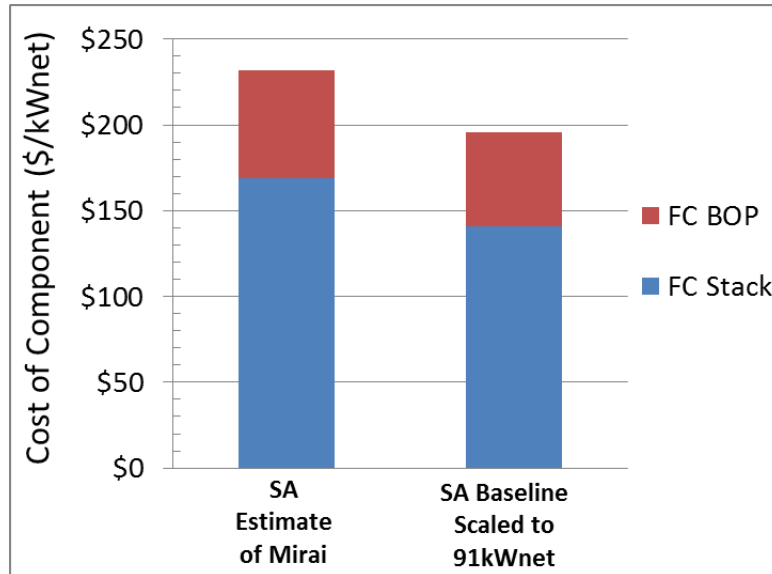
Figure 47. Comparison of Mirai total system cost with SA baseline model scaled to 91 kW$_{net}$

7.3.7 Variation in Mirai Fuel Cell System Cost Estimates

A Tornado chart showing the cost sensitivity of multiple components within the Mirai system (with range and rationale of parameters in Figure 48) is shown in Figure 49. Bipolar plate thickness is observed to be an especially sensitive cost parameter. The Mirai's BPP thickness is modeled at 3.5mils (0.09 mm) but the actual thickness is not known. The Tornado chart cost spread for thickness only reflects the change in mass of material required for the stack. It does not reflect the sheet-metal mill cost changes due to thickness variation (thicker sheet metal is often lower cost per mass due to less processing to thin the sheet metal) nor the BPP stamping press changes due to thickness variation. Consequently, the cost spread due to BPP thickness changes is most likely wider than displayed in the Tornado chart. The bounds for the power density are not selected via the same methodology as in the baseline system Tornado analysis: whereas the baseline system range is based on polarization performance, the Mirai power density range is constrained by the known power (114kW$_{gross}$), cell pitch, known number of cells (370/stack), known stack volume, and (mostly known) active to total area ratio. The total active area in the Mirai stack is not provided in the open literature, therefore an estimate is made for the range in end plate thicknesses (estimated to be between 2 and 4 cm thick whereas real values are unknown). When combined with the other parameters, the possible range of power density is back calculated.

Toyota Mirai Sensitivity Ranges (1,000 sys/year)					
Parameter	Units	Min Param. Value	Base Value	Max Param. Value	Rationale
GDL Cost	$/m2	$75	$124	$170	Approx. upper and lower bounds of OEM reported values
Amorphous Carbon Cost	$/kW	$7	$13	$20	Low end: 5deg half angle of rotation in chamber and 50nm thickness.
BPP Thickness	microns	76	89	102	Between 3 and 4 mils
Power Density (active area)	mW/cm^2	1,244	1,295	1,350	Based on estimate range of end plate thicknesses (4cm at high end and 8cm at low end) to match up the volume and total active area.
H2 Recirculation Pump Cost	$/system	$604	$805	$1,006	+/-25% of system cost
Catalyst Cost	$/system	$1,921	$2,089	$2,257	+/- 25% of catalyst cost (exluding Pt)
Pt Loading	mgPt/cm^2	-	0.3	0.350	+ 0.05mg Pt/cm2 based on "30g of Pt in stack"
2016 Mirai System Cost ($/kWnet)			$233.29		

Figure 48. Parameter sensitivity range and rationale for Toyota Mirai Tornado Chart
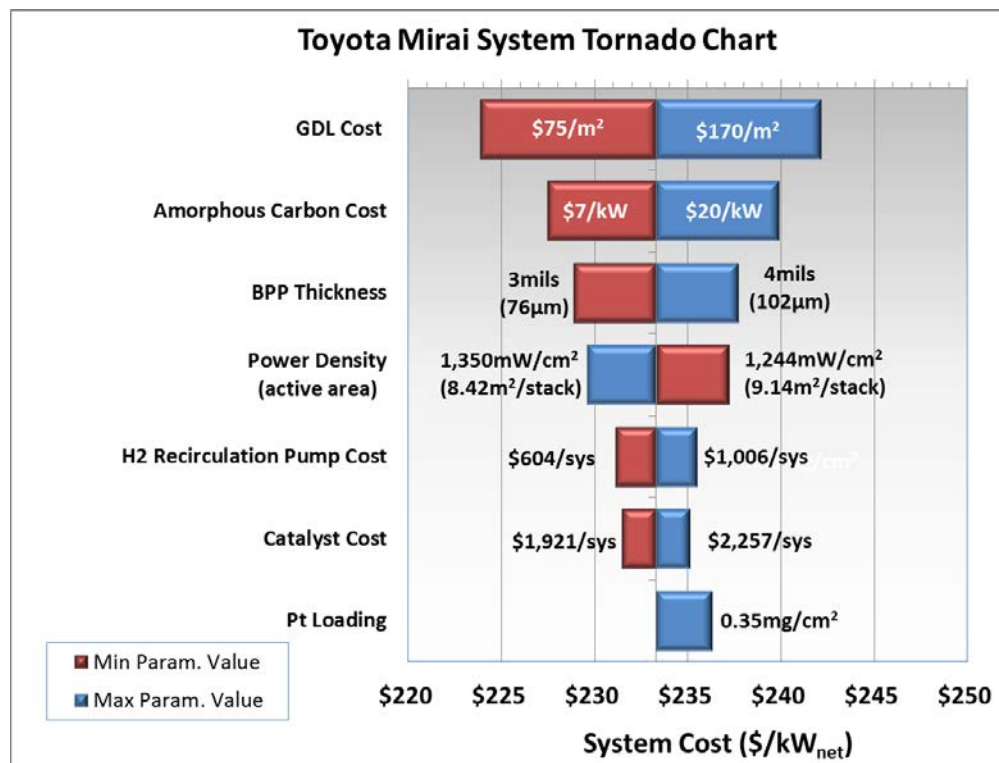
Figure 49. Single variable sensitivity Tornado chart for the Toyota Mirai fuel cell system.

7.4 Alternative Bipolar Plate Coating Research

Numerous BPP coating materials and methods on metal plates are currently in use:

- TreadStone Technologies Inc. LiteCell[TM] (Gen 1 and Gen2) (Gen 2 used in 2016 baseline system and is described in Section 6.5 and Section 8.1.1.2)
- Amorphous carbon (described in Toyota Mirai Section 7.3.2.2)
- Dana Reinz – polymer matrix (described below)
- Impact Coatings Ceramic MaxPhase™ (to be examined in the future)
- Metal nitride coatings (i.e. titanium nitride, chromium nitride) (to be examined in the future)

For a better understanding of the various technology advancements in this area, SA began investigating two new types of coatings. In Section 7.3.2.2, amorphous carbon coating for the Toyota Mirai bipolar plates was analyzed for direct coating onto titanium. Future analysis is planned to explore the cost impact of similar amorphous carbon coatings onto SS316 plates. Additionally, SA began gathering information on Dana Reinz BPP coating method.

Dana Reinz Coating Technology for Bipolar Plates:

Patents to Reinz [70, 71, 72] describe an alternative bipolar plate coating consisting of an electrically conductive coating with an organic binder to reduce corrosion. Notably, the coating is applied in a non-vacuum process (screen printing or roller printing) to only the top surface of the bipolar plates (not to the sides/bottom of the flow channels). The coating is composed of conductive fillers and metal powders dispersed in a polymer matrix:

- Conductive filler: such as graphite
- Metal Powders: such as niobium, rare earth metals, precious metals such as gold, platinum, silver, palladium and/or rhodium, metal boride, metal nitride and/or metal carbide such as titanium boride, titanium nitride, titanium carbide and/or chromium nitride, silicon carbide
- Polymer: thermoplastic or thermoset such as polyurethane, polyacrylic, polyester, or phenol resins.

Coatings are typically between 0.05 – 0.5 mm in thickness, with a loading between 0.32 g/m^2 and 80 g/m^2. Continued work and possibly a DFMA$^®$ analysis of this process may be investigated in the future.

7.5 DFMA® of Binary De-alloyed Pt$_3$Ni$_7$ Catalyst Application using 3M NSTF

As described in Section 6.1, attention has shifted toward binary de-alloyed PtNi catalysts. To compare dispersed d-PtNi$_3$ and NSTF de-alloyed Pt$_3$Ni$_7$ catalyst, a side study was conducted in 2015/2016 for the NSTF de-alloyed Pt$_3$Ni$_7$ catalyst system.

---

[70] US Patent 8,053,141 B2 (2011)
[71] DE Patent Application 10235598 A1 (2002)
[72] DE Patent Grant 10235598 B4 (2005)

In 2016, 3M provided single cell polarization data (at specified operating conditions) to ANL for d-Pt_3Ni_7 NSTF catalyst MEAs (inclusive of a catalyst interlayer coated on the cathode GDL). ANL incorporated this data into their non-neural net performance model and used SA's 2015 simplified system cost model (based on 3M NSTF stack cost) to establish optimized operating conditions for lowest system cost. Figure 50 lists the optimized operating conditions for the 3M d-Pt_3Ni_7 NSTF catalyst system and the resulting stack and system cost.

Cathode Catalyst		d-Pt_3Ni_7 NSTF (3M)
Anode Catalyst		PtCoMn NSTF
Cathode Interlayer		Dispersed Pt/C
Pressure	atm	2.5
O_2 Stoich	--	1.5
Stack Coolant Exit Temperature	°C	95
Total PGM	mg_{PGM}/cm^2	0.131
Voltage	mV	664
Power Density	mW/cm^2	941
Stack Cost	$/kW_{net}$	$22
System Cost	$/kW_{net}$	$47

Figure 50. List of 3M d-Pt_3Ni_7 NSTF optimized operating conditions and resulting stack and system cost

A cross-section of the MEA (not to scale) is shown in Figure 51. The single cell test data is for an MEA with a de-alloyed Pt_3Ni_7 NSTF cathode with a Pt/C interlayer on the GDL and a ternary PtCoMn NSTF anode. The NSTF application cost model is the same for both the PtCoMn and the d-Pt_3Ni_7 with the exception of an additional de-alloying step for d-Pt_3Ni_7. The block diagram for the NSTF catalyst application process is shown in Figure 52 (top) with the de-alloying step highlighted in blue. In the de-alloying step, the web is submerged in a ferric acid bath for 2.5 minutes (0.8 m/min web speed), rinsed, dried, and re-wound onto a roll. Calendaring of the NSTF electrodes onto the membrane is not shown in the diagram, but is assumed to follow the same methods used for ternary PtCoMn NSTF catalyst application (described in SA's 2014 Update report).[73] The process used to apply an interlayer of catalyst onto the GDL of the cathode using slot die coating is shown at the bottom of Figure 52.

---

[73] "Mass Production Cost Estimation of Direct H_2 PEM Fuel Cell Systems for Transportation Applications: 2014 Update" Brian D. James, Jennie M. Moton & Whitney G. Colella, Strategic Analysis, Inc., January 2015.
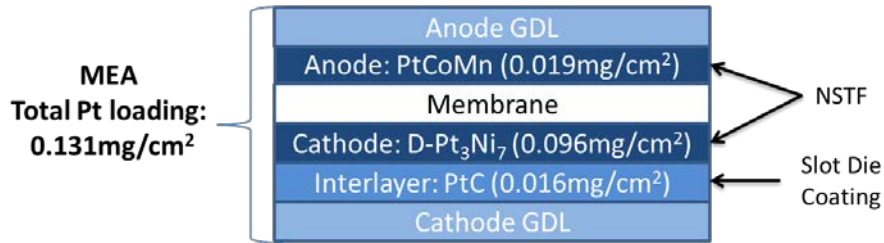
Figure 51. Pt Loading for each layer of the 3M test cell

Figure 52. Process diagram for de-alloyed Pt_3Ni_7 catalyst processing using NSTF (top) and process for interlayer coating (bottom)

Cost results are shown in Figure 53 for d-Pt_3Ni_7 NSTF catalyst synthesis and application. The results illustrate that the processing costs dominate at low volume and material costs dominate at high volume. The two material costs appear to remain constant over all production volumes due to the constant cost of platinum ($1,500/tr.oz.) making up the majority of the material cost. The cost results are expressed in $/kWnet based on ANL's optimized operating conditions. At 1,000 systems per year, the processing cost dominates because of the extra de-alloying and interlayer of the d-Pt_3Ni_7 catalyst. However, at higher

volumes, the processing cost becomes insignificant compared to the cost of platinum. The total system cost of d-Pt$_3$Ni$_7$ NSTF is lower than JM dispersed d-PtNi$_3$/C at all volumes as seen in Figure 54 due to the lower Pt loading and higher power density. This comparison uses ANL's optimized conditions for each catalyst system and also assumes that all other components of the system remain constant. The development of higher performing catalysts with reduced platinum content (from either the unique and complex application techniques or creative catalyst structures) outweighs the impact of any sort of custom application process when it comes to lowering the cost of catalyst systems.
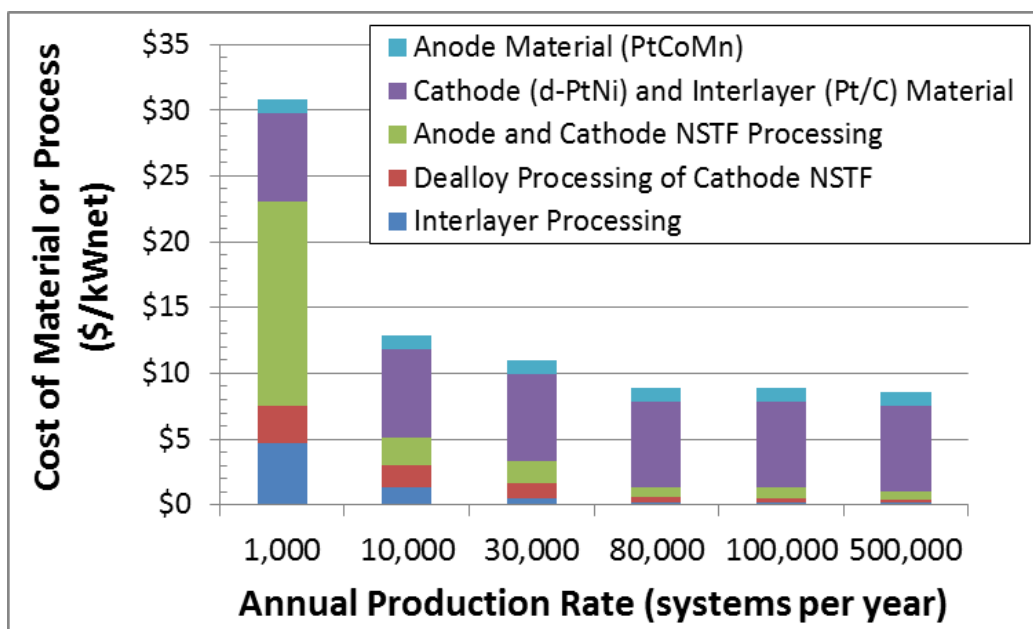
Figure 53. Breakdown in binary d-Pt$_3$Ni$_7$ NSTF catalyst and application at all production rates

	D-PtNi NSTF	Dispersed D-PtNi
Power Density (mW/cm^2)	941	749
Cell Voltage (V)	0.664	0.659
Coolant Exit Temp (°C)	95	94
Stack Pressure (atm)	2.5	2.5
Air Stoich	1.5	1.4
Total Pt Loading (mg/cm^2)	0.131	0.134
Membrane Thickness (μm)	14	17
Active Area per stack (m^2)	9.37	11.71
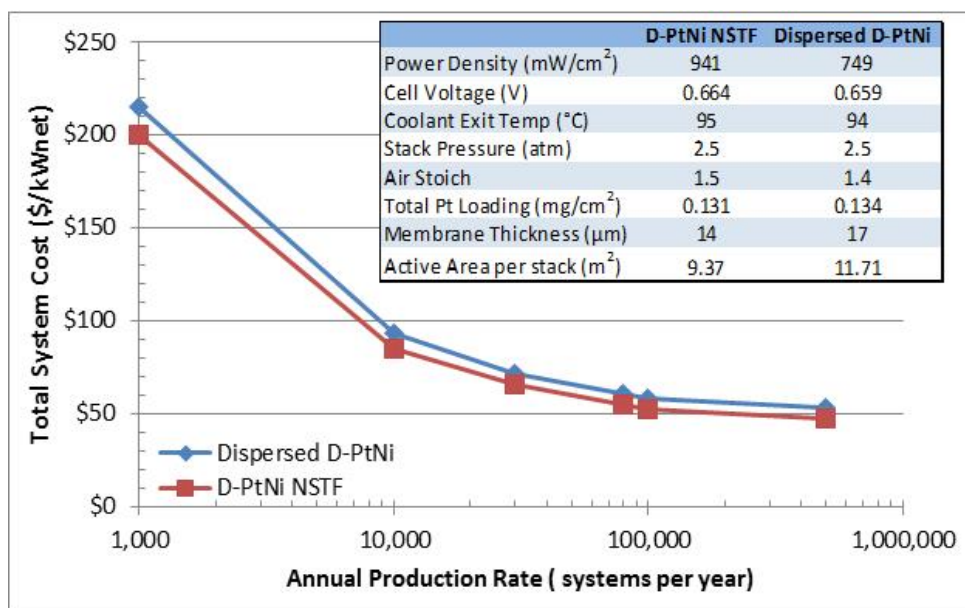
Figure 54. Comparison of system cost for 3M d-Pt$_3$Ni$_7$ NSTF and JM dispersed d-PtNi$_3$/C catalysts (assuming all other system components remain constant).

8 Description of 2016 Automotive Fuel Cell System Manufacturing Assumptions and Cost Results

8.1 Fuel Cell Stack Materials, Manufacturing, and Assembly

8.1.1 Bipolar Plates

Each stack in the system consists of hundreds of active cells, each of which contains two bipolar plates. A one-to-one (1:1) ratio of active cells to cooling cells is assumed, to facilitate better temperature uniformity throughout the stack. Consequently, one side of the bipolar plate is a cooling cell flow field and the other side is an active cell flow field. Specially-designed end gaskets are used to block off the flow into the gas channel side of the cooling plates.

In previous estimates, the cathode and anode flow field sides of the bipolar plates were envisioned as having identical flow patterns and being symmetrical. Consequently, only one bipolar plate design was needed and the cells could be flipped 180 degrees to alternate between cathode flow fields and anode flow fields. However, based on feedback from Ballard Power Systems Inc. given in previous years, different designs are assumed for the anode plates compared with the cathode plates.

Because each system contains hundreds of bipolar plates, hundreds of thousands of plates are needed even at the lowest production rate. This high level of production of a repeating component even at low system production levels means that bipolar plate mass-manufacturing techniques are applicable across a wide range of system production rates.

The stamped metal plates were selected because of consistent industry feedback suggesting that this material and manufacturing method is the most common approach currently implemented with success. Other options for bipolar plate forming include hydroforming (Grabener, Borit Hydrogate™), adiabatic forming (Cell Impact), embossing, coining, etching, machining, and molding (injection, compression).

8.1.1.1 Progressive Die Stamping of the Bipolar Plates

Sheet metal stamping is selected for production of the bipolar plates and is inferred to be employed by GM, Dana Reinz, and Mercedes Benz.[74] Since ~738 plates are needed per system and multiple features are required on each plate (flow fields, manifolds, etc.), progressive die stamping is a logical choice for manufacturing method. In progressive die stamping, coils of sheet metal are fed into stamping presses having a series of die stations, each one sequentially imparting one or more features into the part as the coil advances. The parts move through the stationary die stations by indexing and a fully formed part emerges from the last station. As shown in Figure 55, the four main sequential die stations envisioned are (1) shearing of the intake manifolds, (2) shearing of the exhaust manifolds, (3) embossing of the flow field paths, and (4) shearing off of the part.

---

[74] The composition and manufacturing method for production of GM bipolar plates is a trade secret and is not known to the authors. However, a review of GM issued patents reveals that they are actively engaged in metallic plate research.
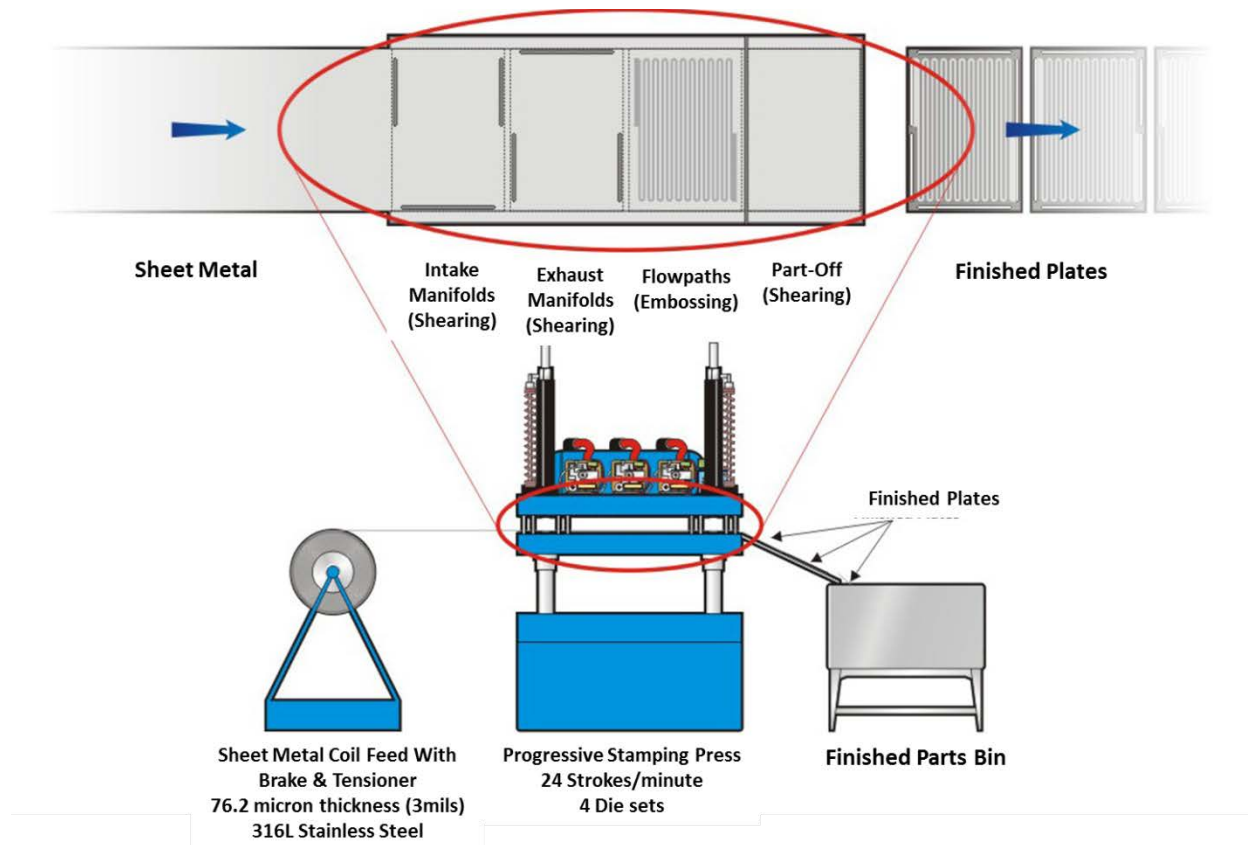
Figure 55. Bipolar plate stamping process diagram

Costs for bipolar plate progressive die stamping were obtained following the standard SA methodology described above. In summary, capital costs, maintenance costs, and electric power requirements were derived from manufacturer price and performance quotes and also survey data supplied within Boothroyd Dewhurst Inc. (BDI) proprietary software. These data were then used to estimate true annual operating costs when the manufacturing line is operated at less than full capacity and 100% utilization. The cost estimation process and assumptions are described more fully below.

Capital Cost and Press Tonnage: Press clamping force is the primary factor influencing both the size and cost of a metal forming press. Prior to 2016, price quotes and performance data for AIRAM Press Co. Ltd pneumatic presses ranging from 50 tons to 210 tons of clamping force were analyzed to develop a function describing the approximate purchase cost as a function of clamping force. As mentioned in Section 6.4, the press force for the stamping machine increased to 1,800 tons (16,000kN) due to more complicated flow paths and embossing, rather than shallow bending, of the flow field. Based on industry feedback, the base capital cost of the press was roughly estimated as $1,000/ton of press force. The cost of supporting equipment required for press operation was then added to the base press cost. Some of the supporting equipment has a fixed cost regardless of press size, while other supporting equipment costs scale with press size. A sheet metal coil feeder was judged necessary and its cost was found to be largely independent of press size. To ensure part accuracy, a sheet metal straightener was added, although it may prove to be ultimately unnecessary due to the thin material used (76.2 microns, or 3 mils).

Press force needed in the progressive die is a function of the material thickness, the material tensile strength, the perimeter of cutting, and the perimeter and depth of bending or other forming. In early modeling efforts, the press force was computed based on the assumption that the channels in the plate active area were merely formed by bending. Thus, in the 2006 report[75], it was estimated that a 65-ton press was necessary to produce the bipolar plates. However, as noted above, embossing rather than bending is required for the flow field channels. Embossing (similar to coining or swaging[76]) moves the material laterally, requiring more force, and is calculated based on the ultimate tensile strength, the area formed, and a constraint factor. The constraint factor can vary by plate design, but for this analysis it is carried as 1.

Press Speed: The speed of the press (in strokes per minute) varies with press size (kilo-Newtons (kN)): a small press is capable of higher sustained operating speeds than a large press. Press speed is a function of press size, and this relationship is shown in Figure 56. At 16,000 kN (used as baseline press force for BPPs), the press speed is about 24 strokes/min.
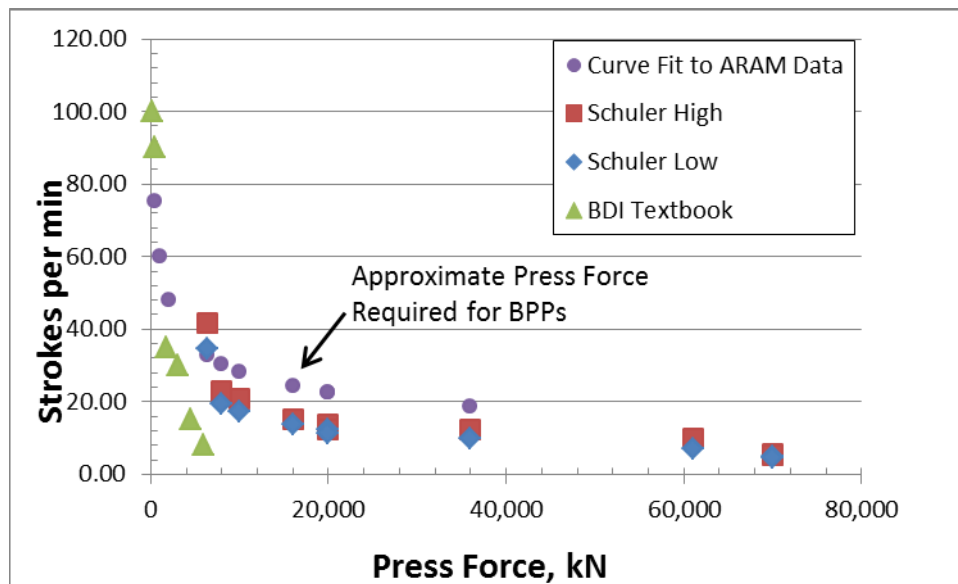
Figure 56. Press speed vs. press force

Quality Control System: A non-contact laser triangulation probe developed by NIST provides detailed information concerning flow field depth, plate size, thickness and defects for the stamped bipolar plate. As shown in Figure 57, the sensor must be able to scan three plates at a time in order to match the speed of the stamping press, which is producing nearly three plates every two seconds. The measurement area for each sensor is 600 mm by 300 mm, significantly larger than the size of a single plate. The line speed has been proven at roughly 300 mm/second but further R&D could increase the effective speed to an estimated maximum of 2 m/sec. Since the probes are inexpensive, they add little

---

[75] "Mass Production Cost Estimation for Direct H_2 PEM Fuel Cell Systems for Automotive Applications," Brian D. James & Jeff Kalinoski, Directed Technologies, Inc., October 2007.
[76] Use of the word "swaging" is meant to denote a more substantial lateral movement of metal during the process than is typically observed within bending or stamping operations.

additional capital cost; consequently, three sensors are envisioned for the system to ensure adequate measurement overlap for each plate and to match the stamping speed.

At 1,000 systems per year, the bipolar plates are stacked manually (extra FTE added for this process). Therefore the optical system is removed from the QC at 1,000 systems per year as the worker is manually stacking plates and can observe any placement anomalies. This reduced the QC system to only the laser triangulation probe capital cost ($70k). The optical system was estimated at $30k and kept only for the high production volumes.

**Part Collection Robot
(3 plates simultaneously)**

**NIST Non-Contact Laser Triangulation Probe
Optical Detection System**
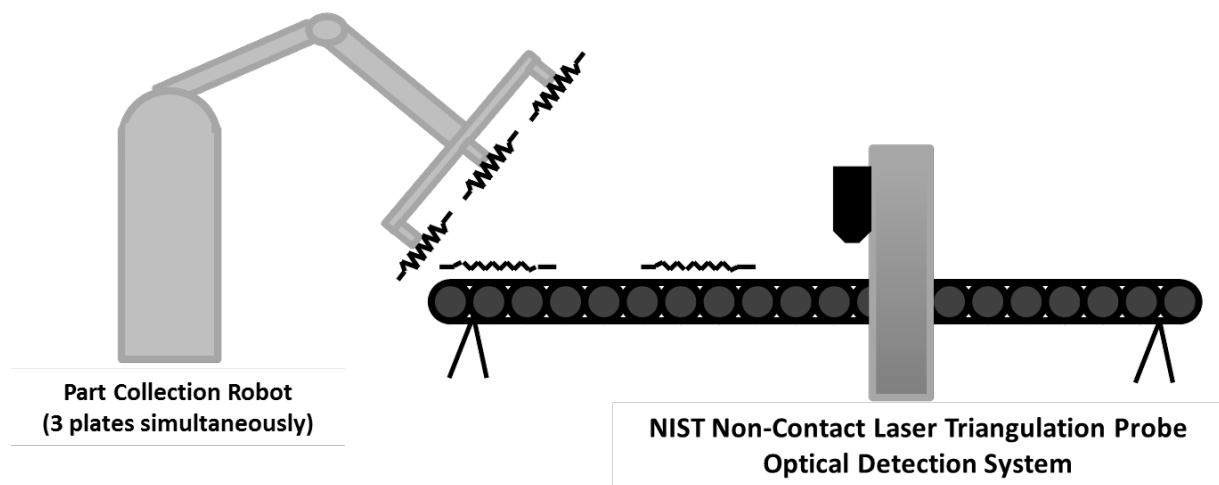
Figure 57. Bipolar plate part collection and quality control: NIST Non-Contact Laser Triangulation Probe, Optical Detection System

Maintenance: The same press operated at higher speeds tends to require maintenance more frequently. Based on discussion with industry vendors, the minimum life of a set of these stamping machine wear parts was estimated to be 10 million cycles, with a total replacement cost estimated to be 20 to 25% of complete press initial capital cost depending on machine size. Since the above cycle life is the minimum number of cycles, but could be substantially more, an approximation is applied to this latest modelling iteration such that the maintenance cost of the press is estimated to be 15% of initial press capital cost every 10 million cycles. This approach deviates from SA's historically-implemented methodology, which estimates maintenance costs as a percentage of initial capital costs per year rather than per cycle. Applying a similar cycle-based lifetime criterion, feeder equipment maintenance is estimated to be 5% of initial feeder capital cost every 10 million cycles.

Utilities: Prior to 2016, the principal sources of demand for electricity in the progressive die process train were the air compressor for the pneumatic press and the electric motor for turning the coil feeder. After updating the stamping force in 2016, a larger stamping press using two torque motors is used (opposed to the pneumatic type stamping press used previously). The max capacity power requirement

for a 16,000 kN machine is roughly 1 MW.[77] It is postulated that the stamping press would on average use 33% of the max capacity (~335 kW). Further data will need to be obtained in order to define a mathematical relationship to describe electric power consumption as a function of press size.

Machine Rate: Using the above information for total line capital, maintenance, and utility costs, mathematical expressions can be generated that relate machine rates with various size presses at varying utilization. Basic input parameters are summarized in Figure 59 and Figure 60.

Die Cost: Die costing is estimated according to the equations outlined in the Boothroyd and Dewhurst section on sheet metal stamping. As expected, complex stamping operations require more intricate, and therefore more expensive, dies. The first two, and final, press steps are simple punching and shearing operations and therefore do not require expensive dies. The flowpath-forming step involves forming a complex, possibly serpentine, shape, which requires a highly complex die that is significantly more expensive (requiring approximately 500 hours of machining time) than the dies for other steps in the process (requiring a combined 160 hours of machining time). This step also requires the majority of press force. The die cost figures are listed below in Figure 58 (under "Tooling"). Note that "secondary operations" refers to the coating process that will be further discussed in Section 8.1.1.2.

Annual Production Rate	1,000	10,000	30,000	80,000	100,000	500,000
Materials ($/stack)	$291	$286	$284	$284	$284	$284
Manufacturing ($/stack)	$848	$279	$223	$216	$212	$212
Tooling ($/stack)	$88	$66	$62	$60	$58	$58
Secondary Operations: Coating ($/stack)	$757	$140	$128	$108	$103	$99
Total Cost ($/stack)	$1,985	$772	$698	$668	$658	$653
Total Cost ($/kWnet)	$24.81	$9.65	$8.72	$8.35	$8.22	$8.17

Figure 58. Cost breakdown for stamped bipolar plates

Die Lifetime: Over time, the repetitive use of the dies to form the metallic bipolar plates will cause these tools to wear and lose form. Consequently, the dies require periodic refurbishing or replacement depending on the severity of the wear. Based on communication with American Trim, titanium nitride dies for progressive bipolar plate stampings are estimated to last in the tens of millions of cycles. Thus, a die (tooling) lifetime of 10 million cycles is specified, with a die cost of $660,000.

Annual Production Rate	1,000	10,000	30,000	80,000	100,000	500,000
Equipment Lifetime (years)	15	15	15	15	15	15
Interest Rate	10%	10%	10%	10%	10%	10%
Corporate Income Tax Rate	40%	40%	40%	40%	40%	40%
Capital Recovery Factor	0.175	0.175	0.175	0.175	0.175	0.175
Equipment Installation Factor	1.4	1.4	1.4	1.4	1.4	1.4
Maintenance/Spare Parts (% of CC)	13%	13%	13%	13%	13%	13%
Miscellanous Expenses (% of CC)	2%	2%	2%	2%	2%	2%
Power Consumption (kW)	335	342	342	342	342	342

Figure 59. Machine rate parameters for bipolar plate stamping process

---

[77] Based on 16,000 kN Schuler progressive stamping machines that utilizes two torque motors, each with 500kW power: https://www.schulergroup.com/technologien/produkte/pressen_twin_servo/index.html

Annual Production Rate	1,000	10,000	30,000	80,000	100,000	500,000
Capital Cost ($/line)	$1,992,576	$2,119,298	$2,119,298	$2,119,298	$2,119,298	$2,119,298
Costs per Tooling Set ($)	$661,557	$661,557	$661,557	$661,557	$661,557	$661,557
Tooling Lifetime (cycles)	10,000,000	10,000,000	10,000,000	10,000,000	10,000,000	10,000,000
Simultaneous Lines	1	3	7	18	22	110
Laborers per Line	1.25	0.25	0.25	0.25	0.25	0.25
Line Utilization	22.0%	73.4%	94.3%	97.8%	100.0%	100.0%
Cycle Time (s)	2.47	2.47	2.47	2.47	2.47	2.47
Effective Total Machine Rate ($/hr)	$1,145.69	$377.36	$302.13	$292.80	$287.17	$287.21
Stainless Steel Cost ($/kg)	$11.37	$11.17	$11.10	$11.10	$11.10	$11.10

Figure 60. Bipolar plate stamping process parameters

8.1.1.2 *Alloy Selection and Corrosion Concerns*

One of the challenges presented by using metallic plates is that they are more susceptible to corrosion than carbon-based plates. For this reason, alloy selection is very important. There is much uncertainty in the fuel cell community as to which alloy and surface treatments are needed to provide adequate corrosion resistance. Although some believe that suitable stainless steel alloys exist that adequately address this problem, others insist that protective coatings are necessary. If the right coating method were selected, it may be possible to use a cheaper and/or lighter (but less corrosion-resistant) material for the plates, which could help offset the cost of coating. In determining the coating method and/or plate material, consideration must be given to the different corrosion environments each plate will encounter: hydrogen and coolant for the anode plates, and oxygen and coolant for the cathode plates.

Literature and patent reviews and conversations with researchers indicate that coatings/surface treatments may not be needed and that 316L stainless steel (or another commercial alloy of similar cost) is appropriate. However, further input from the FCTT suggested that coatings *are* necessary. At the direction of the Fuel Cell Tech Team, coatings were included in the system cost and are based on a 76.2-micron (3-mil) stainless steel 316L alloy metallic bipolar plates coated using a proprietary process from TreadStone Technologies, Inc.

An anti-corrosion coating is applied to both sides of the bipolar plates based on TreadStone's proprietary LiteCell™ process. A DFMA® analysis was conducted based on information from TreadStone's patent US 7,309,540, as well as information transferred under a non-disclosure agreement, with close collaboration with C.H. Wang and Gerry DeCuollo of TreadStone Technologies, Inc.

According to the patent, the coating consists of "one or more resistant layers, comprising conductive vias through the resistant layer(s)" (see Figure 61). The resistant layer provides excellent corrosion protection, while the vias provide sufficient electrical conduction to improve overall conductivity through the plate.
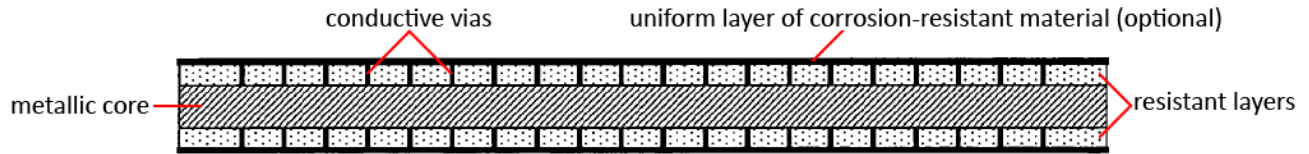
Figure 61. Conductive vias shown in US patent 7,309,540 for TreadStone Technologies, Inc. anti-corrosion coating

The resistant layer is applied via a physical vapor deposition (PVD) process. Details of the manufacturing process are considered proprietary, so only limited explanation is provided here.

In 2016, the coating process was updated to reflect TreadStone Gen 2 "dot" anti-corrosion coating technology. The postulated coating application follows a two-step process: 1) PVD application of a continuous proprietary anti-corrosion layer, and 2) low cost proprietary deposition of a non-continuous layer of proprietary conductive material (~5-10% surface coverage). Both layers are applied after bipolar plate stamping. The conductive layer is only applied to one side of the plates because only one side requires low contact resistance.

At 1,000 systems per year, a smaller system is envisioned for the PVD process to improve utilization of the coating equipment. Quotations were obtained from Vergason Technologies for a smaller deposition area machine requiring a manual load system. Extra labor was added in addition to a slower processing time. However, at a lower capital cost and higher utilization (>30%), the cost for the TreadStone coating decreased.

The cost breakdown for the TreadStone process is shown in Figure 62. The coating cost is observed to be primarily a function of annual production rate, with cost spiking at low quantities of only 1,000 systems per year. This is a reflection of low utilization of the coating system, and the application cost could perhaps be reduced with an alternate application technique.

Annual Production Rate	1,000	10,000	30,000	80,000	100,000	500,000
Materials ($/stack)	$20	$20	$20	$20	$20	$20
Manufacturing ($/stack)	$737	$120	$108	$88	$83	$78
Total Cost ($/stack)	$757	$140	$128	$108	$103	$99
Total Cost ($/kWnet)	$9.47	$1.75	$1.60	$1.35	$1.29	$1.23

Figure 62. Cost breakdown for TreadStone LiteCell™ bipolar plate coating process

8.1.2 Membrane

The total cost of the fuel cell membrane (uncatalyzed) is estimated as the summation of three components:

1. ionomer (input material cost)
2. ePTFE substrate (input material cost)
3. manufacturing cost of casting into membrane form

Each component is described in detail below.

8.1.2.1 Ionomer Cost

Ionomer cost is based upon a 2010 Dow Chemical reference report[78] on high-volume manufacture of Nafion-like long side chain perfluorosulfonic acid proton exchange membranes from hexafluoropropylene oxide (HFPO) raw material. In this report, ionomer material and manufacturing costs are analyzed at extremely high volumes: as high as 6,000 MT/year (although only ~400 MT/year of material is suitable for 500k vehicles/year). The combination of extremely high production volume and simpler manufacturing process—the industry report models membrane casting rather than application to an ePTFE substrate—results in a reported finished membrane cost much lower than calculated by the SA model. Rather than using the direct results of the Dow cost report, the 2012 FCTT recommended that the membrane continue to be modeled as an ePTFE-supported membrane and that we adapt the Dow ionomer price to plant sizes more in line with expected annual demand. Consequently, for the 2012-2015 analyses, a production-volume-dependent scaling relationship was derived from the Dow report data and used to estimate ionomer price at various fuel cell system annual production rates. This ionomer price curve is shown in Figure 63. Data points on the graph correspond to the six annual system manufacturing rates analyzed in the study.
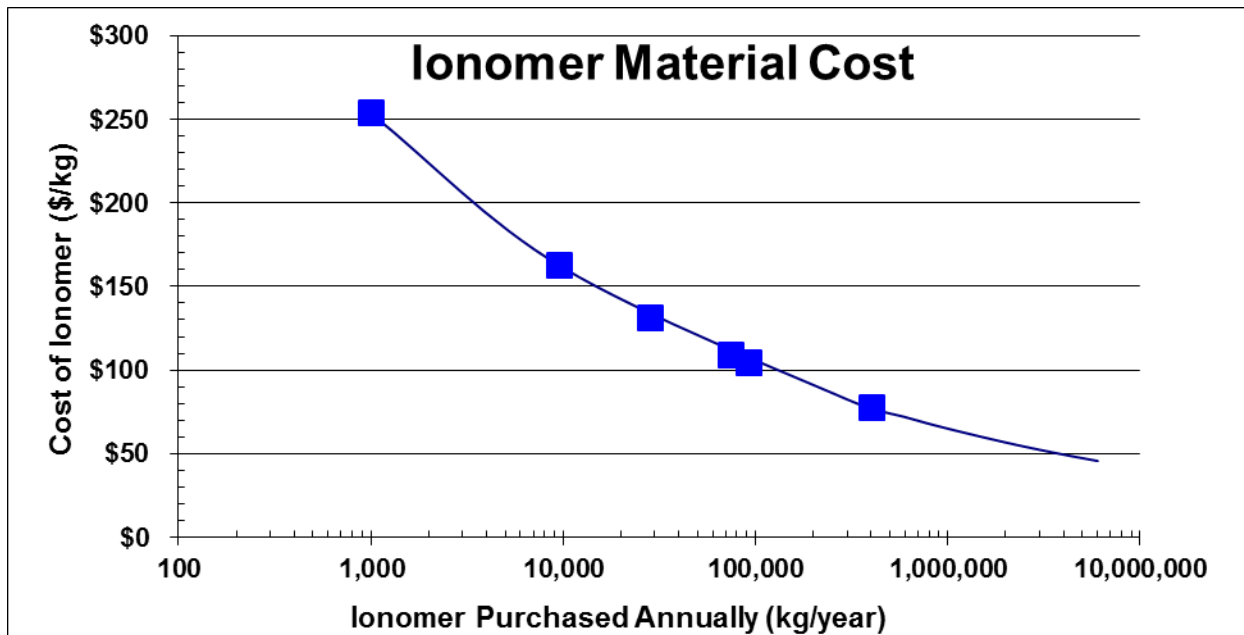
Figure 63. Ionomer material cost curve

8.1.2.2 ePTFE Cost

An expanded polytetrafluoroethylene (ePTFE) porous layer is modeled as a mechanical substrate for the ionomer membrane. Use of an ePTFE supported fuel cell membrane is well documented in the literature and is a continuation of past SA cost analysis practice. A ground-up DFMA® cost analysis of ePTFE was initiated but it soon became evident that such an analysis was impractical as the specific (and crucial)

---

[78] "High Volume Cost Analysis of Perfluorinated Sulfonic Acid Proton Exchange Membranes," Tao Xie, Mark F. Mathias, and Susan L. Bell, GM, Inc., May 2010.

processing steps[79] were closely guarded industry secrets unavailable as inputs into the cost analysis. While ePTFE is manufactured in high production volume for the textiles industry (e.g. Gore-Tex), there are different qualities available and also potentially different processing steps for fuel cell applications. For this reason, a quote based cost estimate is used within the 2016 report.

Quotes from multiple ePTFE manufacturers were obtained, all on the basis of confidentially. These cost quotes (without attribution to their source) are shown in Figure 64. W.L. Gore & Associates, Inc., the predominant supplier of ePTFE to the fuel cell industry, did not provide a cost quotation, although they did review this cost analysis.

A wide range of prices is observed in Figure 64 due to both differences between manufacturers and uncertainty in projection to high manufacturing volumes. ePTFE prices are affected by the quality and cost of the starting PTFE material and one manufacturer suggested that only the better quality "fuel cell grade" of PTFE was suitable for fuel cell applications. The lower red curve in Figure 64 represents an ePTFE price quote from a Chinese supplier of textile grade ePTFE which probably isn't well suited to fuel cell applications but is included in the graph to illustrate the ePTFE price floor. The other price quotations are from U.S. suppliers. Price quotes were obtained for both 10 micron and 25 micron ePTFE thickness but prices did not vary appreciably, indicating that the majority of cost was in the processing steps. A mid-range price of ePTFE is used in the cost analysis, with the upper and lower bound price quotes used as limits in the sensitivity analysis.
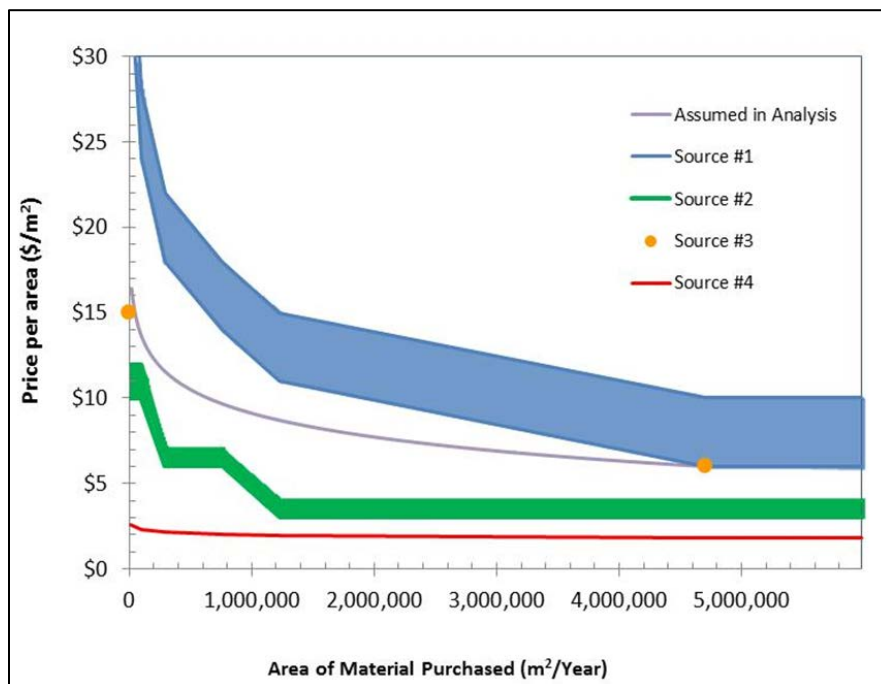
Figure 64. ePTFE price quotations and data selected for use in SA DFMA® models

---

[79] ePTFE uses a particular grade of non-expanded PTFE as a precursor material and then applies a multi-stage, presumably bi-axially, mechanical stretching regiment to attain an optimized node and fibril end structure of the 95+% porous ePTFE. Exact parameters of those stretching steps, along with proprietary heat treatments or other non-disclosed steps, are highly confidential to W.L. Gore and other fuel cell ePTFE manufacturers.

8.1.2.3 Membrane Manufacturing Cost

The membrane manufacturing method for 2016 is modeled as factory-based roll-to-roll processing, unchanged from previous SA analyses. The analysis is not based on a detailed enumeration of capital costs but rather uses industry supplied approximate plant cost estimates combined with estimated yield rates, labor requirements, line speeds, and markup rates to derive a simplified cost curve representing manufacturing cost as a function of membrane annual production rate.

As schematically detailed in Figure 65, the membrane fabrication process consists of eight main steps:

Unwinding: An unwind stand with tensioners is used to feed the previously procured ePTFE substrate into the process line. A web width of ~ 1 m is deemed feasible for both the membrane fabrication line and the subsequent catalyzation.

First Ionomer Bath: The ePTFE substrate is dipped into an ionomer/solvent bath to partially occlude the pores.

First Infrared Oven Drying: The web dries via infrared ovens. A drying time of 30 seconds is postulated. Since the web is traveling quickly, considerable run length is required. The ovens may be linear or contain multiple back-and-forth passes to achieve the total required dwell time.

Second Ionomer Bath: The ionomer bath dipping process is repeated to achieve full occlusion of the ePTFE pores and an even thickness, pinhole-free membrane.

Second Infrared Oven Drying: The web is dried with a second bank of infra-red ovens after the second ionomer bath.

Boiling Water Hydration: The web is held in boiling water for 5 minutes to fully hydrate the ionomer. Optimal selection of the ionomer may reduce or eliminate this boiling step.

Air Dryer: High velocity air is used to dry the web after the hydration step.

Rewind: The finished membrane is wound onto a spool for transport to the catalyzation process line.
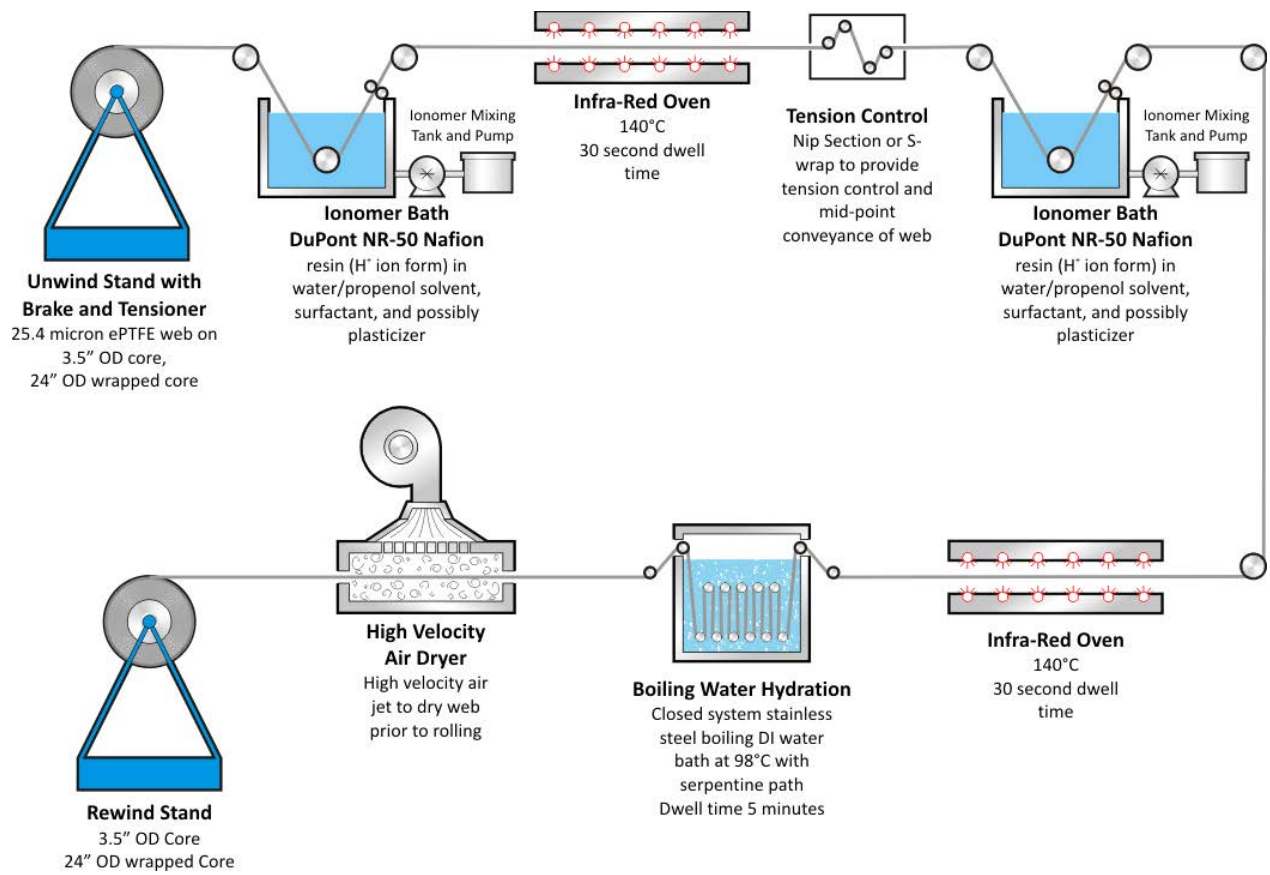
Figure 65. Membrane fabrication process diagram

Details of the simplified membrane fabrication cost analysis are shown in Figure 66. Two roll-to-roll plants are postulated: a "low-speed plant" (5 m/min) and a "high-speed" plant (35 m/min). Run at partial load, they cover the full span of membrane production requirements (1,000 to 500,000 vehicles/year).

Key assumptions are noted below.

Capital Cost: Capital costs are coarsely estimated based on industry input and are significantly greater than previous element-by-element summations based on component price quotes.

Web speed: Even the "high-speed" web (35 m/min) is very slow by converting machinery standards where speeds of 100 m/min are often achieved. This is a nod toward cost conservativeness and a reflection that the upper bound of membrane web speed is not known at this time.

Discount Rate: The discount rate is increased to 20% to reflect the increased business risk of a membrane production line.[80]

---

[80] While all fuel cell system manufactured components share similar market risk in that the demand for fuel cell vehicles is uncertain, some components (e.g. the membrane manufacturing line) utilize specialized equipment that

Production for Simultaneous Product Lines: In virtually all other components of the automotive fuel cell stack, it is assumed that there is vertical integration and dedicated component production for a single vehicle product. For the membrane, however, it is likely that a separate company would fabricate the membrane for multiple car companies or, at least, that the membrane plant would produce membrane for more than one line of vehicles. Consequently, a multiplier on the yearly membrane demand is included to reflect supply to multiple vehicle product lines. This multiplier is not constant as production rate increases since the plant is at some point limited by capacity. The non-constant nature of the multiplier leads to unevenness in the resulting $/m² cost projections.

Peak Equipment Utilization: Input from a membrane supplier raised the point that average plant utilization would be significantly affected under scenarios of rapid demand growth. Consequently, utilization (at most manufacturing rates) is limited to 67% to reflect the five-year average utilization assuming 25% per year demand growth. For the 500,000 vehicles per year case, plant utilization is allowed to increase to 80% to reflect a more stable production scenario.

Production/Cutting Yield: There are appreciable cutting losses associated with the roll-to-roll manufacturing process, which directly affect the membrane material costs. ePTFE yield was assessed at 77% to 98%. It is assumed that a portion of ionomer in the scrap membrane is able to be recycled. Consequently, it is assumed for costing purposes that the ionomer material wastage rate is half that of the overall membrane areal scrap rate (making the ionomer yield 89% to 99%). Manufacturing yield is assessed at the same yield as ePTFE.

Workdays and Hours: The maximum plant operating hours are assumed to be 20 hours per day, 240 days per year. Actual hours vary based on actual plant utilization.

Cost Markup: The standard methodology throughout the analysis has been not to apply manufacturer markups, in keeping with the vertically integrated manufacturing assumption, and the directives of the DOE on this costing project. However, since it is likely that the membrane producer will not be vertically integrated, a markup is included in our membrane cost estimate. Furthermore, because the membrane is a critical component of the stack, significantly higher margins are allocated than are typical to the automotive industry where there is a large supplier base with virtually interchangeable products competing solely on price. Markup on the manufacturing process varies from 40% to 70%. A constant 25% markup rate is applied to the materials (ePTFE and ionomer) in keeping with auto industry practice of the auto company supplying high cost materials to the vendor rather than paying a full markup for the vendor to procure the materials.

Revenue: Annual membrane fabricator revenue is not an input in the analysis. Rather it is an output. However, it is worth noting that even at high membrane production rates, company revenues are still only about $35M per year. This is a modest company size and supports the notion of allowing higher-than-average markups as a means to entice people into the business.

---

can't be resold or repurposed for other markets. Furthermore, the membrane manufacturing line is one of the largest capital investments thereby amplifying the consequences of missing production projections.

Simplified Computation of Membrane Manufacturing Cost							
Annual Veh Prod. (1 product line)	vehicle/year	1,000	10,000	30,000	80,000	130,000	500,000
Capital Amortization							
Capital Cost (Membrane Fabrication)	$	$15,000,000	$15,000,000	$15,000,000	$35,000,000	$35,000,000	$35,000,000
Machine Lifetime	years	10	10	10	10	10	10
Discount Rate	%	20%	20%	20%	20%	20%	20%
Corporate Income Tax Rate	%	40%	40%	40%	40%	40%	40%
Capital Recovery Factor (CRF)		0.331	0.331	0.331	0.331	0.331	0.331
Labor Costs							
Min. Mfg. Labor Staff (Simul. on 1 Shift)	FTE	5	25	25	50	50	50
Labor Rate	$/min	1	1	1	1	1	1
Machine Costs							
Maintenance/Spare Parts (% of installed C.C./year)	%	5%	5%	5%	5%	5%	5%
Miscellaneous Expenses	%	5%	5%	5%	5%	5%	5%
Total Power Consumption	kW	200	200	250	350	350	350
Electrical Utility Cost	$/kWh	0.07	0.07	0.07	0.07	0.07	0.07
Membrane Production Parameters							
Simul. Product Lines to Which Memb. is Supplied		5	3.25	2.2	2	1.75	1.5
Vehicle Annual Production	veh/year	5,000	32,500	66,000	160,000	227,500	750,000
m^2 per Vehicle	m^2/vehicle	13.00	13.00	13.00	13.00	13.00	13.00
Peak Equipment Utilization Due to Growth	%	67%	67%	67%	67%	67%	100%
Production/Cutting Yield	%	77%	84%	88%	91%	93%	97.956%
Gross Production @ 100% Utilization (plant)	m^2/year	1,440,000	1,440,000	1,440,000	10,080,000	10,080,000	10,080,000
Gross Production (plant)	m^2/year	83,927	500,053	974,185	2,275,706	3,176,927	9,953,438
Net Production (plant)	m^2/year	65,000	422,500	858,000	2,080,000	2,957,500	9,750,000
Net Production of 1 Line	m^2/year	13,000	130,000	390,000	1,040,000	1,690,000	6,500,000
Design Web Speed	m/min	5	5	5	35	35	35
Web Width	m	1	1	1	1	1	1
Work Days per Year	days/year	240	240	240	240	240	240
Plant Utilization	% of 20hr days	5.8%	34.7%	67.7%	22.6%	31.5%	98.7%
Hours per Year of Production	hrs/year	280	1,667	3,247	1,084	1,513	4,740
Hours per Day of Production	hrs/day	1.17	6.95	13.53	4.52	6.30	19.75
Annual Cost Summation							
Capital Recovery Cost	$/year	$4,963,069	$4,963,069	$4,963,069	$11,580,494	$11,580,494	$11,580,494
Labor Cost	$/year	$576,000	$2,880,000	$4,870,927	$5,760,000	$5,760,000	$14,219,197
Maintenance/Spares Cost	$/year	$750,000	$750,000	$750,000	$1,750,000	$1,750,000	$1,750,000
Miscellaneous Expenses	$/year	$750,000	$750,000	$750,000	$1,750,000	$1,750,000	$1,750,000
Utility Cost	$/year	$3,917	$23,336	$56,827	$26,550	$37,064	$116,123
Effective Machine Rate	$/min	$420	$94	$58	$321	$230	$103
Total Manufacturing Cost ($/net m2, pre-markup)							
From computations	$/m²	$108.35	$22.17	$13.28	$10.03	$7.06	$3.02
From simplified curve fit	$/m²	$ 93.83	$ 25.84	$ 13.97	$ 8.06	$ 6.15	$ 2.89
Manufacturing Cost Markup %	%	70%	59%	54%	49%	47%	40%
Gross Margin	%	41%	37%	35%	33%	32%	29%
Annual Revenue (on manufacturing only)	$/year	$10,368,358	$17,348,407	$18,407,310	$24,970,418	$26,626,707	$39,451,822
Total Manufacturing Cost ($/net m2, post-markup)							
From computations	$/m²	$184.21	$35.22	$20.39	$14.93	$10.34	$4.22
From simplified curve fit	$/m²	$ 159.51	$ 41.06	$ 21.45	$ 12.01	$ 9.00	$ 4.05

Figure 66. Simplified membrane manufacturing cost analysis assumptions

Membrane manufacturing cost is plotted against membrane annual volume in Figure 67 below. Note that membrane material costs (ionomer and ePTFE) are not included. Membrane manufacturing costs are computed using the multiple production line assumption. To aid in numerical calculation, a power curve was curve-fit to the cost computations.
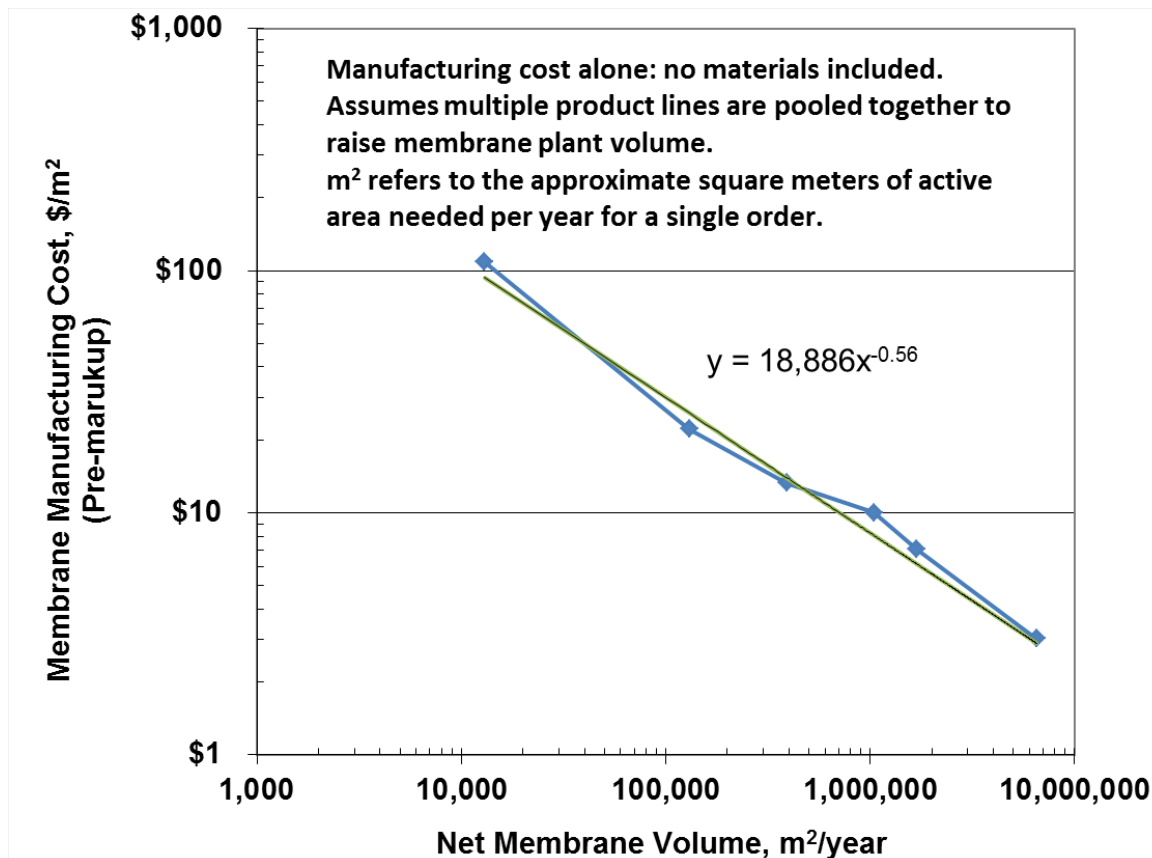
Figure 67. Membrane manufacturing cost vs. annual membrane manufacturing volume

Quality Control: An Optical Detection System (ODS) is used for detecting membrane defects on the order of 20μm such as pinholes, folds, bends, scratches, and thickness non-uniformity in the ionomer. The entire membrane fabrication process is assumed to be completed at 1 m web width and requires 13 cameras to cover the entire web width at the targeted detection resolution. A high web processing speed is accommodated by a camera with a high refresh rate (125 kHz).

8.1.2.4 Total Membrane Cost

Figure 68 summarized cost results for the un-catalyzed ePTFE supported membrane.

Annual Production Rate	1,000	10,000	30,000	80,000	100,000	500,000
Materials ($/m²)	$44	$28	$23	$18	$16	$11
Manufacturing ($/m²)	$208	$48	$24	$13	$11	$4
Total Cost ($/m2 (total) total)	$252	$76	$47	$31	$28	$15
Total Cost ($/stack)	$3,167	$961	$589	$386	$351	$191
Total Cost ($/kWnet)	$39.58	$12.02	$7.37	$4.83	$4.39	$2.39

Figure 68. Cost breakdown for the membrane (un-catalyzed)

8.1.3 Fuel Cell Catalyst

Numerous catalysts have been proposed for PEM fuel cells, including:

- PtCo/C (Brookhaven National Lab/ChemCat, Toyota/Tanaka)

- PtNi (3M, Johnson Matthey/General Motors)
- PtMnCo (3M-NSTF)
- Pt/C (typically an anode catalyst)
- PANI (Los Alamos National Lab)

As described previously in Section 6.1, a dispersed binary d-PtNi$_3$/C cathode catalyst is used for the 2016 baseline catalyst system and is applied in catalyst ink form via a slot die coating deposition method. The synthesis of the dry powder d-PtNi$_3$/C catalyst (before being made into a catalyst ink) is described within this section and may be summarized as a wet chemistry based mixture of platinum and nickel with carbon. The cost of platinum, one of the greatest influencers on stack cost, is assumed to be $1,500/troy ounce for the baseline system.

8.1.3.1 Platinum Cost

The raw material cost of platinum is the major cost element of the catalyst ink. At the direction of the DOE, a platinum cost of $1,500 per troy ounce is selected (and represents a price increase from the $1,100/troy ounce used in 2013 and prior SA analyses). As shown in Figure 69, the $1,500/troy ounce Pt price reflects the average and likeliest value of Pt within the last eight year span. Interestingly, as shown in Figure 70, Pt is currently at a multi-year price low ($855/tr.oz. in December 2015).
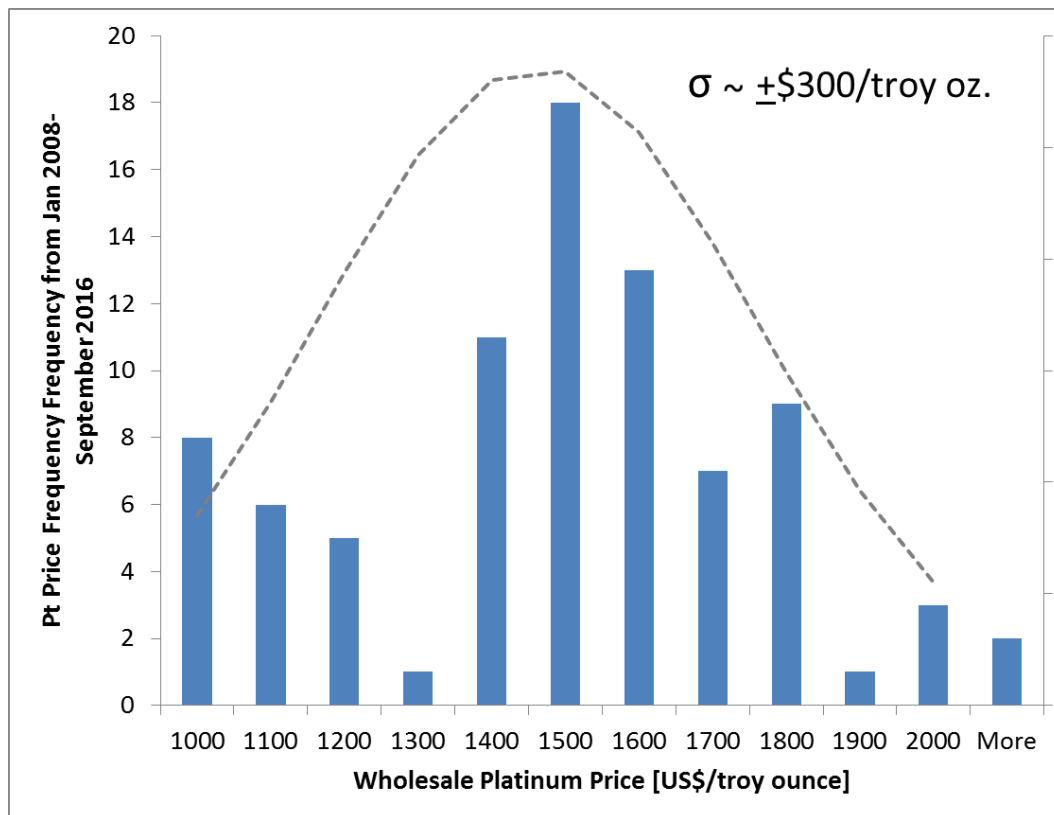
Figure 69. Pt price distribution over eight years (2008-2016)
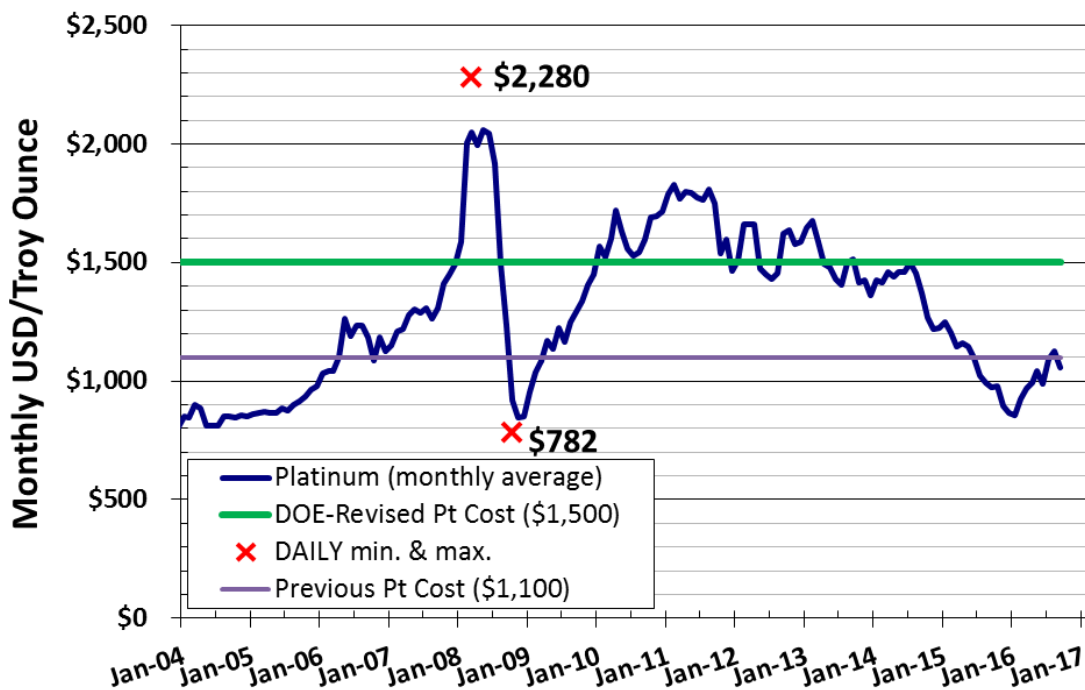
Figure 70. Twelve-year graph of monthly Pt prices

8.1.3.2 Catalyst Powder Synthesis

The de-alloyed PtNi$_3$/C analysis draws from open literature sources and vendor discussions for definition of representative processing steps. While inspired by the de-alloyed binary catalysts of Johnson Matthey (JM), the analysis does not purport to model the JM catalyst synthesis exactly and may differ from JM catalysts in important and unknown ways. The de-alloyed PtNi$_3$/C catalyst analysis results are incorporated into the 2016 baseline system.

The binary catalyst powder synthesis processing steps are outlined in Figure 71. A variety of Pt donor compounds are available as inputs to catalyst synthesis. Chloroplatinic acid (CPA) is selected as a representative starting reactant as its production method is described in the literature and it is a common Pt catalyst precursor. However, the Pt compound preferred by JM is not discernable from the patent literature and many other reactants may viably be used. Discussions with catalyst manufacturers suggest that CPA is a reasonable precursor to the desired Pt donor reactant and thus it is reasonable to model the unknown compound at a cost equal to CPA plus some additional processing. Based on industry feedback and in the absence of detailed knowledge regarding this unknown processing step, the modeled cost is assessed at 2x the computed CPA cost (excluding Pt).

Preparing the CPA involves dissolving platinum sponge into a 4:1 mix of hydrochloric and nitric acids, called "aqua regia," via the reaction:

$$\text{Pt} + 4\ \text{HNO}_3 + 6\ \text{HCl} \rightarrow \text{H}_2\text{PtCl}_6 + 4\ \text{NO}_2 + 4\ \text{H}_2\text{O}$$

The CPA (H_2PtCl_6) is brownish-red in color, and is isolated by evaporating the solution to a thick syrup, which becomes solid at room temperature. Cost of the CPA was obtained by combining Pt material cost with CPA preparation cost, derived from a DFMA® analysis. The CPA is used to create the Pt donor reactant in an additional process before the PtNiC precursor. As mentioned previously, this processing step is considered to be the same processing cost as the CPA fabrication process (without Pt material cost). Further costs associated with precipitating the Pt donor reactant onto the carbon were obtained using DFMA®.

The Pt donor reactant is next reacted with nickel chloride and Ketjen carbon within a precipitation reactor to form the PtNiC precursor. The precipitate precursor slurry (solid precursor in excess acid liquids) is run through a press filter and washed with water, then dried and crushed, resulting in a precursor powder. Based on literature[81] parameters, the precursor powder is annealed at 1,000˚C to improve the activity and stability of the catalyst powder. The de-alloying step uses nitric acid to etch away nickel over 24 hours. Filter, wash, dry, and catalyst crush steps are needed to form the final catalyst d-PtNi$_3$ on C powder used in the catalyst electrode inks.
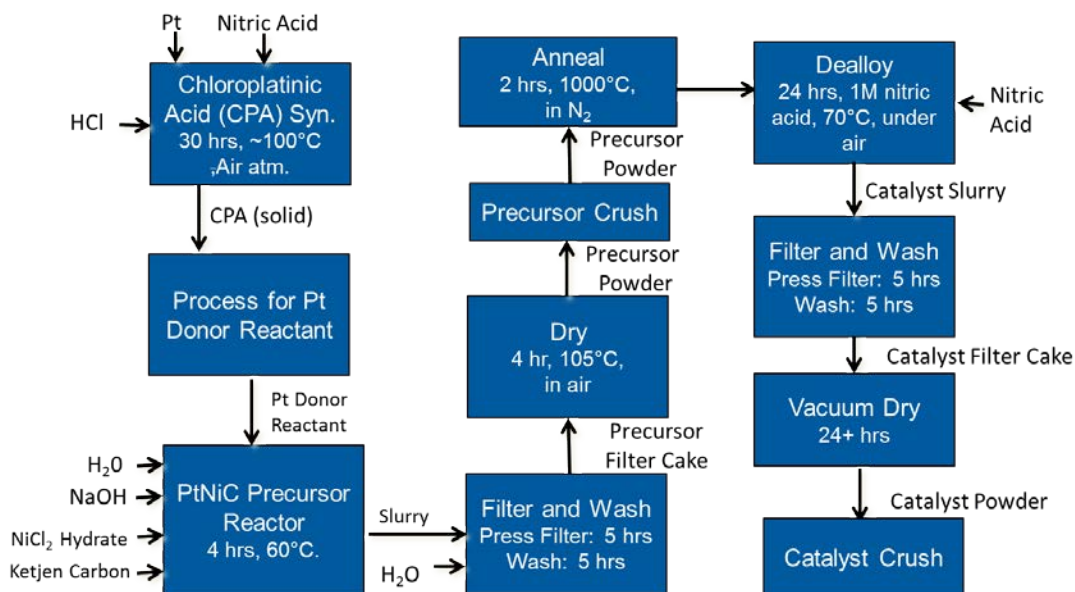
Figure 71. Processing steps for de-alloyed binary d-PtNi$_3$/C cathode catalyst powder synthesis

Final cost results of the cathode de-alloyed catalyst powder synthesis and anode catalyst powder synthesis process are shown in Figure 72 and Figure 75, respectively, where the tables show the cost of each processing step at all manufacturing rates. Figure 73 shows a further breakdown of cathode materials, manufacturing, markup, and total cost for each processing step at both 1,000 and 500,000

---

[81] Wang, C., et al., "Design and synthesis of bimetallic electrocatalyst with multilayered Pt-skin surfaces", Journal of the American Chemical Society, 2011. 133(36): p. 14396-14403.

systems per year manufacturing rates. Highlighted in Figure 73 are the dominant cost of Pt (circled in red), other material costs (circled in blue), and the most expensive processing step (circled in green).

PtNi/C Cathode Catalyst Powder Synthesis		Annual System Prodution Rate					
Component Costs per 80kWnet Fuel Cell System		1,000	10,000	30,000	80,000	100,000	500,000
Step 1: Catalyst PtNiC Precursor	$/system	$849.92	$801.02	$758.70	$747.04	$744.58	$739.26
Step 2: Precursor Filtration	$/system	$14.64	$6.16	$2.12	$0.98	$0.82	$0.33
Step 3: Precusor Wash	$/system	$7.37	$3.22	$1.20	$0.56	$0.51	$0.33
Step 4: Precursor Drying	$/system	$47.74	$17.84	$5.66	$2.32	$1.95	$0.64
Step 5: Precursor Crushing	$/system	$25.01	$9.15	$3.21	$1.29	$1.06	$0.29
Step 6: Precursor Annealing	$/system	$134.57	$52.50	$30.69	$12.57	$10.62	$9.30
Step 7: Catalyst Dealloying	$/system	$42.92	$23.94	$10.39	$6.18	$5.69	$4.57
Step 8: Catalyst Filtration	$/system	$14.58	$6.10	$2.10	$0.97	$0.81	$0.33
Step 9: Catalyst Wash	$/system	$7.37	$3.22	$1.20	$0.56	$0.51	$0.33
Step 10: Catalyst Dry	$/system	$50.76	$21.81	$8.02	$5.40	$4.78	$3.63
Step 11: Catalyst Crushing	$/system	$26.69	$11.56	$4.74	$1.70	$1.48	$0.29
Step 12: Catalyst Quality Control Testing	$/system	$33.33	$43.88	$26.13	$15.46	$15.43	$13.69
Step 13: Cathode Catalyst Packaging	$/system	$11.07	$4.18	$1.72	$0.80	$0.70	$0.33
Total Catalyst Synthesis Cost	$/system	$1,265.98	$1,004.58	$855.87	$795.83	$788.93	$773.34

Figure 72. Cost of each processing step for the cathode de-alloyed catalyst at production rates between 1,000 and 500,000 systems/year.

		All at 100k systems per year				All at 500k systems per year			
Component Costs per 80kWnet Fuel Cell System		Materials	Manuf.	Markup	Total	Materials	Manuf.	Markup	Total
Platinum Cost		$720.04	$0.00	$0.00	$720.04	$720.04	$0.00	$0.00	$720.04
Step 1: Catalyst PtNiC Precursor	$/system	$4.53	$3.00	$17.01	$24.54	$4.23	$2.41	$12.58	$19.22
Step 2: Precursor Filtration	$/system	$0.00	$0.25	$0.57	$0.82	$0.00	$0.12	$0.22	$0.33
Step 3: Precusor Wash	$/system	$0.00	$0.16	$0.35	$0.51	$0.00	$0.11	$0.22	$0.33
Step 4: Precursor Drying	$/system	$0.00	$0.60	$1.35	$1.95	$0.00	$0.22	$0.42	$0.64
Step 5: Precursor Crushing	$/system	$0.00	$0.32	$0.73	$1.06	$0.00	$0.10	$0.19	$0.29
Step 6: Precursor Vacuum Annealing	$/system	$0.00	$3.26	$7.36	$10.62	$0.00	$3.22	$6.08	$9.30
Step 7: Catalyst Dealloying	$/system	$0.60	$1.15	$3.95	$5.69	$0.60	$0.98	$2.99	$4.57
Step 8: Catalyst Filtration	$/system	$0.00	$0.25	$0.56	$0.81	$0.00	$0.11	$0.22	$0.33
Step 9: Catalyst Wash	$/system	$0.00	$0.16	$0.35	$0.51	$0.00	$0.11	$0.22	$0.33
Step 10: Catalyst Vacuum Dry	$/system	$0.00	$1.47	$3.31	$4.78	$0.00	$1.26	$2.38	$3.63
Step 11: Catalyst Crushing		$0.00	$0.45	$1.02	$1.48	$0.00	$0.10	$0.19	$0.29
Step 12: Quality Control	$/system	$0.00	$4.73	$10.69	$15.43	$0.00	$4.73	$8.95	$13.69
Step 13: Cathode Catalyst Packaging	$/system	$0.08	$0.14	$0.49	$0.70	$0.08	$0.04	$0.22	$0.33
Total Cost		$725.25	$15.93	$47.75	$788.93	$724.95	$13.52	$34.87	$773.34

Figure 73. Detailed cost breakdown for each cathode de-alloyed catalyst processing step at 1,000 and 500,000 systems per year.

The anode catalyst is composed of platinum on carbon with a much more simplified process (shown in Figure 74) than the cathode de-alloyed catalyst. Final cost results of anode catalyst powder synthesis process are shown in Figure 75, showing the cost of each processing step at all manufacturing rates.

Pt/C Anode Catalyst Processing Steps
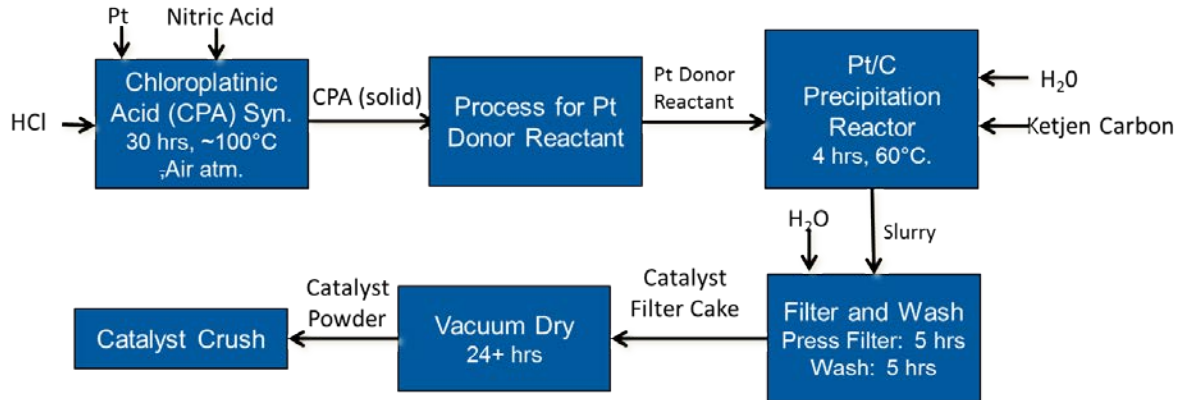
Figure 74. Processing steps for Pt/C anode catalyst powder synthesis

Anode Pt/C Catalyst Powder Synthesis		Annual System Prodution Rate					
Component Costs per 80kWnet Fuel Cell System		1,000	10,000	30,000	80,000	100,000	500,000
Step 1: Catalyst PtC Synthesis	$/system	$138.08	$131.41	$123.04	$121.04	$120.53	$119.16
Step 2: Anode Catalyst Filtration	$/system	$11.30	$4.31	$1.37	$0.58	$0.47	$0.12
Step 3: Anode Catalyst Wash	$/system	$2.77	$1.14	$0.40	$0.18	$0.16	$0.08
Step 4: Anode Catalyst Vacuum Drying	$/system	$48.03	$18.06	$5.75	$2.37	$2.02	$0.94
Step 5: Anode Catalyst Crushing	$/system	$25.26	$9.51	$3.44	$1.43	$1.20	$0.30
Step 6: Anode Catalyst QC Testing	$/system	$10.00	$11.86	$6.71	$3.93	$4.02	$3.51
Step 7: Anode Catalyst Packaging	$/system	$6.91	$2.65	$1.40	$0.57	$0.47	$0.13
Total Catalyst Synthesis Cost	$/system	$242.35	$178.94	$142.11	$130.10	$128.88	$124.23

Figure 75. Cost of each processing step for the anode catalyst at production rates between 1,000 and 500,000 systems/year.

8.1.3.3 Total Catalyst Synthesis and Material Cost

Figure 76 and Figure 77 summarize cost results for the catalyst synthesis process and materials on cathode and anode.

Annual Production Rate	1,000	10,000	30,000	80,000	100,000	500,000
Material ($/stack)	$803	$736	$730	$726	$725	$725
Manufacturing ($/stack)	$463	$65	$34	$18	$16	$14
Markup ($/stack)	$0	$204	$92	$53	$48	$35
Total Cost ($/stack)	$1,266	$1,005	$856	$796	$789	$773
Total Cost ($/kWnet)	$15.82	$12.56	$10.70	$9.95	$9.86	$9.67

Figure 76. Cost summary for de-alloyed cathode catalyst synthesis and materials

Annual Production Rate	1,000	10,000	30,000	80,000	100,000	500,000
Material ($/stack)	$127	$116	$115	$115	$115	$115
Manufacturing ($/stack)	$115	$15	$7	$4	$3	$2
Markup ($/stack)	$0	$47	$20	$12	$11	$7
Total Cost ($/stack)	$242	$179	$142	$130	$129	$124
Total Cost ($/kWnet)	$3.03	$2.24	$1.78	$1.63	$1.61	$1.55

Figure 77. Cost summary for Pt/C anode catalyst synthesis and materials

8.1.4 Dispersed Catalyst Ink and Application to Membrane

There are numerous methods to apply the catalyst ink into the membrane electrode assembly. Some systems apply the catalyst ink (either directly or via decal transfer) onto the membrane to form a catalyst coated membrane (CCM). Others apply the catalyst ink directly onto the gas diffusion layer (GDL) to form a gas diffusion electrode (GDE).

SA analysis from 2006 to 2010 was based on the CCM-based inking application (specifically slot die coating of the catalyst ink directly onto a moving membrane web via a Coatema VertiCoater system). Such an approach had the advantage of being one of the least costly application techniques judged adequate for high production rates and reasonably high MEA performance. In 2011, SA switched to a new method of catalyst deposition that had shown significant improvements in power density and reported durability at low Pt loadings. Developed at 3M, the Nanostructured Thin Film Catalyst (NSTF) deposition process begins with vapor sublimation of a layer of crystalline finger-like projections, or "whiskers", to create a high surface area substrate on which the active catalysts may be deposited. Vapor deposition methods are utilized to deposit a very thin layer of platinum and other metals (cobalt and manganese) onto the whiskers in a very precise and uniform manner. The resulting catalyst coated whiskers can then be pressed into the fuel cell membrane to form a porous mat electrode intimately bonded to the membrane. This NSTF catalyst application method was used in SA analyses from 2011 to 2014. In 2015, the baseline reverted back to a slot die coating method for applying the de-alloyed binary catalyst to the membrane and is continued to be used in the 2016 baseline.

In 2014/2015, SA examined two types of slot die coating methods: 1) dual-sided simultaneous slot die coating of anode and cathode onto the membrane, and 2) single-sided sequential (anode then cathode) slot die coating. Feedback from industry indicated differing opinions as to the best method of applying the catalyst ink. The simultaneous coating process would seem to be the obviously lower cost pathway given its 2x processing time advantage. However, at low production rates, the higher capital cost of the simultaneous coating system more than offsets its speed advantage and makes it more expensive than sequential coating. It is estimated that the two application methods would yield similar performance and are compared to each other in that respect. Both methods were examined for each volume of the baseline system and results show that sequential single-sided coating is lower cost only at 1,000 systems per year.

Multiple slot die coating companies provided information on dual-sided simultaneous and single-sided sequential coating techniques and input parameters. The results of the analysis reflect a combination of different machines with respective capital costs and operating conditions. Due to the proprietary nature of the detailed cost breakdown, SA is unable to provide this information. However, top-level operating parameters are shown in Figure 78 and specify coating web width and web speeds of both dual-sided and single-sided coating machines. In all cases, the process starts with ultrasonic mixing of the dry catalyst powder (15 wt% $PtNi_3$/C) with methanol (37.5 wt%), water (37.5 wt%), and ionomer (10 wt% Nafion) to form catalyst ink slurry.[82]

---

[82] Assuming ionomer to carbon ratio of 1.

In some dual-sided coating cases the membrane is carried vertically through a set of rollers after coating so as to avoid web sag and eliminate/minimize roller contact with the wet slurry. Other machines execute dual sided horizontal coating (within one meter distance between anode and cathode coatings). In both cases, the catalyst coated membrane is dried under multiple sets of heaters before being rewound onto a take-up spool. The membrane that is coated vertically allows the CCM a long unsupported span during which the coating can dry before touching a roller. The horizontal coating includes flotation drying, eliminating any smearing or damage to the CCM before it is dried. The vertical and horizontal dual-sided simultaneous slot die coating methods are described in Figure 79 and Figure 80, respectively. The capital cost of equipment for all methods includes an ultrasonic mixer, web handling equipment (unwind, tension control, and rewind), coating machine (frame, backing roll, slot die, and fluid delivery), and drying system (supply and exhaust fans).

Parameter	Sequential Slot Die Coating Machine	Dual-Sided Vertical Coating Machine	Dual-Sided Horizontal Coating Machine
Power Consumption	80kW	60kW	500kW[83]
Line Speed	12m/min	13m/min	25m/min
Web Roll Length	1,500m	1,500m	1,500m
Web Width	30cm	50cm	90cm
Number of Laborers	1	1	3

Figure 78. Table of Slot Die Coating parameters comparing three different machines
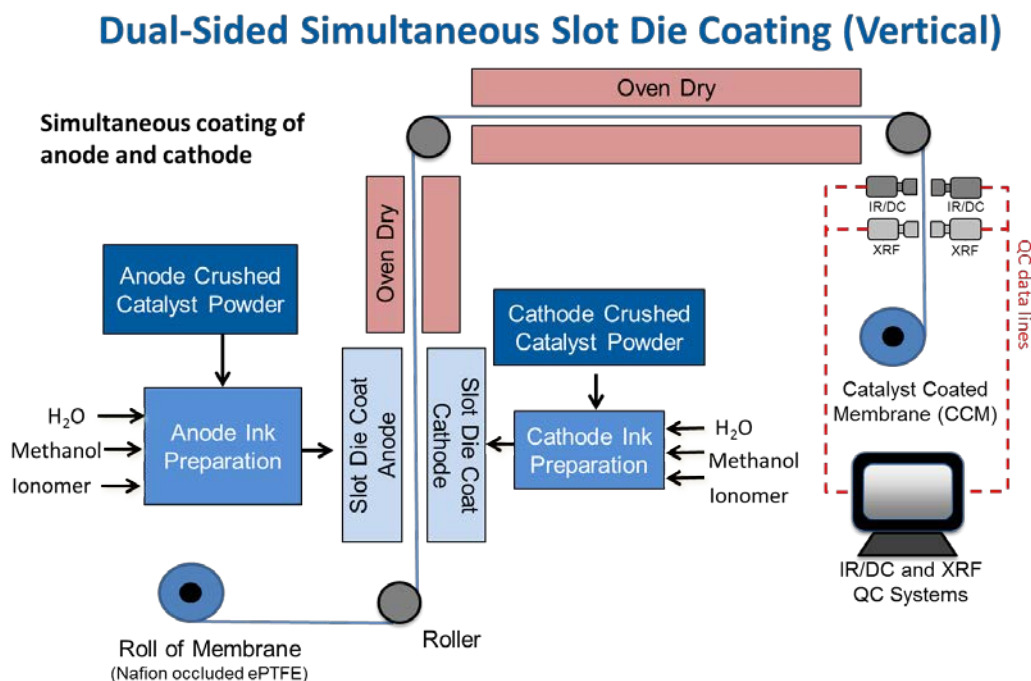
Figure 79. Vertical dual-sided simultaneous slot die coating of de-alloyed PtNi$_3$/C catalyst process flow diagram

---

[83] Electrical power used for heating the air for drying is 455kW or 91% of the total 500kW. All other components in process require the remaining 45kW or 9% of the total 500kW.
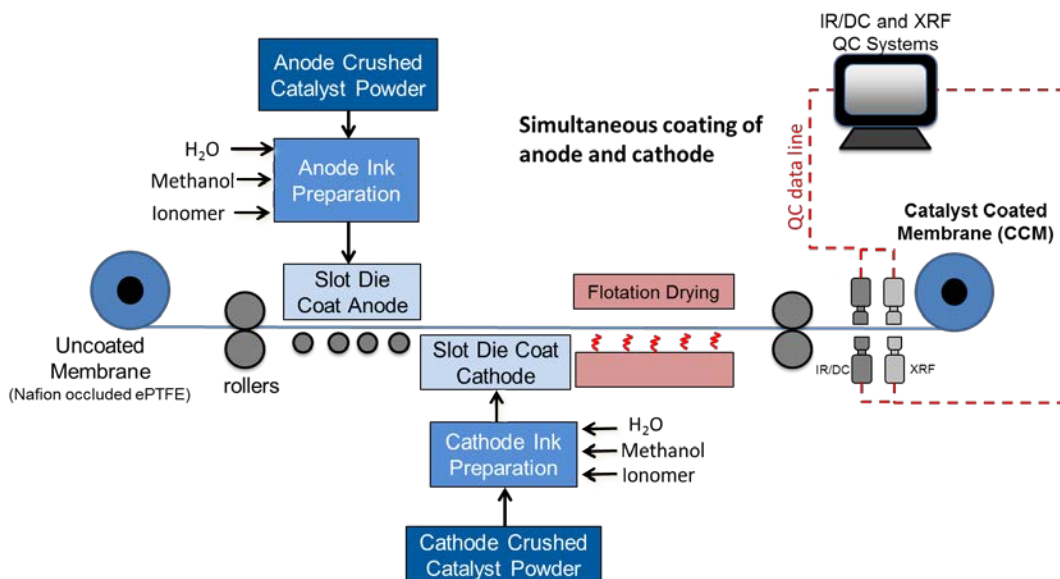
Figure 80. Horizontal dual-sided simultaneous slot die coating of de-alloyed PtNi$_3$/C catalyst process flow diagram

The second slot die coating method (sequential or single-sided coating) is illustrated in Figure 81. In the first step, the anode ink is prepared within an ultrasonic mixer by mixing dry anode catalyst powder with water, methanol, and ionomer. In the second step, the membrane is unrolled while the anode ink is slot die coated onto the continuously moving membrane. This single layer is dried under heaters and rolled onto a take-up spool. The coating operation is then repeated in a second slot die coater to apply the cathode ink to the opposite face of the membrane. It is possible to use one coating line to alternately apply anode and cathode layers. Therefore, the cost analysis is based on use of one coater for both lines (anode and cathode). For the sequential process, extra time is required to coat two sides (compared to simultaneous coating), and longer roll change-out times are needed (due to sequential operation). Additionally, there may be difficulties with registering the web, particularly after it goes through the drying oven a single time.

Sequential Slot Die Coating Catalyst
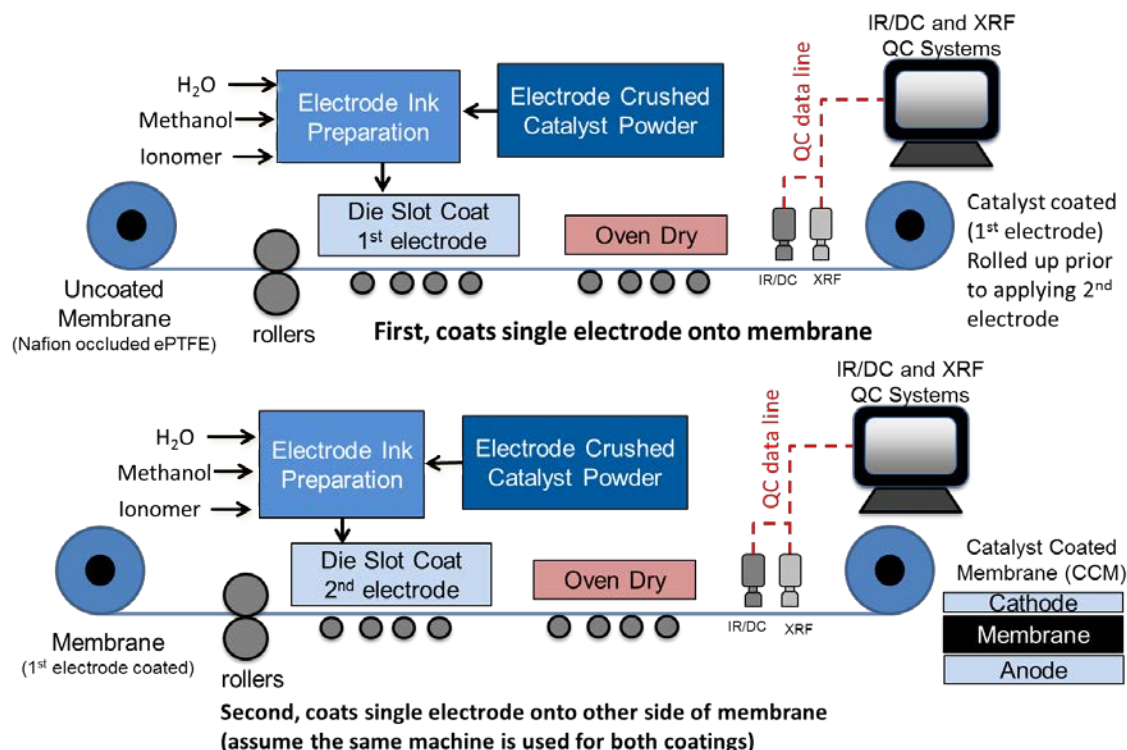
Figure 81. Flow Diagram of Sequential Slot Die Coating of Electrodes

Patch, island coating, window coating, "window frame", or interrupted coating all describe coating techniques to pattern the ink onto the web rather than provide a 100% fully coated coverage. Such non 100% coverage coating is not assumed in this analysis. Patch coating is generally desirable in that it reduces catalyst coating on areas of the membrane that will not be active within the fuel cell, thereby reducing catalyst cost. Within the DFMA® model, SA does not include this capability for two reasons 1) the sub-gasket process assumes a continuous coating of the membrane that is cut into separate parts and realigned with appropriate spacing between active areas, 2) when presented to the Fuel Cell Technical Team, it is assumed to be a future capability of slot die coating that has not been demonstrated successfully at high volumes while maintaining polarization performance.

The quality control equipment associated with the slot die coating process includes IR/DC and XRF. An IR/DC system is used to assess the uniformity of the electrode layers at a single location within the slot die coating production sequence. The IR/DC system[84] operates by placing two conductive rollers across the width of the web a short distance from one another. An electric current is fed to one of the rollers, and then down the length of the electrode layer (anode and cathode) to be collected by the other roller.

---

[84] Niccolo V. Aieta, Prodip K. Das, Andrew Perdue, Guido Bender, Andrew M. Herring, Adam Z. Weber, Michael J. Ulsh, "Applying infrared thermography as a quality-control tool for the rapid detection of polymer-electrolyte-membrane-fuel-cell catalyst-layer-thickness variations", Journal of Power Sources, Volume 211, 1 August 2012, Pages 4-11.

An IR camera mounted above the electrode and peering down onto the moving web is used to visually assess the temperature signature of the electrode and detect anomalies that would be indicative of electrode thickness variation, improper catalyst loading, improper particle size, non-uniform platinum distribution, or other general defects.[85] Due to the simplicity of the signal processing required, IR camera systems can easily match the line speed of the catalyst deposition (25 m/min). To achieve appropriate resolution (at 500k systems/year), six IR cameras are needed at each analysis site to achieve a 1m total field of view (the web width) at a 25 m/min web speed. Two systems are needed per line for all production volumes using dual-sided coating method corresponding to viewing of 1) the anode after drying, and 2) the cathode after drying. This equates to a total of 12 IR cameras for a dual-sided coating line. Only one system is needed for sequential single-sided coating at 1k systems per year as it is assumed that the IR/DC equipment is viewing one catalyst layer at a time after coating. X-Ray Fluorescence (XRF) is included as an additional QC feature for the catalyst coating processing that was not originally included in the 2014 NSTF catalyst application. It was recommended by NREL to be included for the baseline as it is currently used in addition to IR/DC QC by many CCM suppliers. XRF is appropriate for the determination of material composition (i.e. Pt loading and content of material) and electrode thickness that can directly affect performance.

8.1.4.1   Total Catalyst Ink and Application Cost

Machine rate and process parameters are shown in Figure 82 and Figure 83 . The overall cost breakdown at various production rates is summarized in Figure 84.

Annual Production Rate	1,000	10,000	30,000	80,000	100,000	500,000
Equipment Lifetime (years)	14	13	13	13	13	13
Interest Rate	10%	10%	10%	10%	10%	10%
Corporate Income Tax Rate	40%	40%	40%	40%	40%	40%
Capital Recovery Factor	0.177	0.181	0.181	0.186	0.186	0.186
Equipment Installation Factor	1.40	1.40	1.40	1.40	1.40	1.40
Maintenance/Spare Parts (% of CC)	5%	5%	5%	5%	5%	5%
Miscellanous Expenses (% of CC)	1%	1%	1%	1%	1%	1%
Power Consumption (kW)	83	58	58	503	503	503

Figure 82. Slot die coating application process parameters

Annual Production Rate	1,000	10,000	30,000	80,000	100,000	500,000
Capital Cost ($/Line)	Proprietary					
Coating Web Width (cm)	30	50	50	91	91	91
Simultaneous Lines	1	1	1	1	1	4
Laborers per Line	1.00	1.00	1.00	3.00	3.00	3.00
Line Utilization	9.6%	16.1%	48.4%	54.4%	68.0%	85.0%
Effective Total Machine Rate ($/hr)	$1,410.49	$1,526.97	$543.33	$1,149.95	$955.24	$799.47
Line Speed (m/s)	0.1	0.2	0.2	0.4	0.4	0.4

Figure 83. Machine rate parameters for slot die coating process

---

[85] Private conversation with Michael Ulsh, NREL.

Annual Production Rate	1,000	10,000	30,000	80,000	100,000	500,000
Material ($/stack)	$16	$10	$9	$7	$7	$5
Manufacturing ($/stack)	$463	$84	$30	$27	$23	$18
Total Cost ($/stack)	$799	$143	$54	$47	$40	$30
Total Cost ($/kWnet)	$9.98	$1.78	$0.67	$0.59	$0.49	$0.38

Figure 84. Cost summary for slot die coating process

8.1.5 Catalyst Coated Membrane Acid Washing

Since 2013, ANL has been working toward optimization of cathode electrode catalyst materials in order to meet DOE targets for Pt loading (<0.125 mg/cm^2) and performance (>1,000 mW/cm^2 @ 675 mV).[86] De-alloyed PtNi$_3$/C catalysts tend to have reduced performance (i.e., low mass activity and/or limited exposure of O$_2$ or protons to three phase boundaries at the cathode) at low relative humidity conditions. One way of mitigating this reduction in performance is by acid washing the CCM. PtNi$_3$ alloy is susceptible to oxidation during FC operation and will create Ni(2+) ions on the surface, creating mass transport resistance at low relative humidity conditions. Acid washing removes these Ni(2+) ions, allowing operation at low humidity without these mass transport losses.

In 2016, acid washing of the CCM was included in the DFMA$^®$ cost analysis by adapting a lab process provided by Zhiwei Yang at United Technologies Research Center (UTRC). The current lab process involves the soaking of individual CCM pieces in a heated acid bath of 0.5 M sulfuric acid for ~3 hours, then washing in DI water several times (3 x 1 hour cycles) before drying. In a high rate manufacturing scenario, the process would likely be optimized for a roll-to-roll process, where washing times and possibly number of water wash steps could be reduced. However, this type of roll-to-roll process has not yet been demonstrated for slower processing times. Therefore, to maintain the same processing times as has been demonstrated in the lab, a batch process is postulated where a 1,500 m roll of CCM material is loosely wound with a porous spacer material and submerged in a bath. Figure 85 shows the postulated high volume acid washing process. The acid is pumped into the bath, heated to 60 °C (~30 min), and held at that temperature for 2.5 hours. The acid is then drained and fresh DI water is pumped into the same chamber and heated to 60 °C and held four about 1 hour. The water washing step is then repeated twice before the washed CCM is removed from the chamber. This equates to about 6 hours of processing. While one roll goes through this process, the previous roll is unwound and dried under heaters and then re-wound for the sub-gasket process. The effective areal acid washing rate is about 4m^2/min at the highest volume. The preliminary analysis of this concept assumes acid disposal costs equal to 50% of the acid purchase price and 3-4 re-use cycles of the acid (before flowing fresh acid).

There are numerous opportunities for process optimization and cost reduction. Acid and water can be pumped through the wound coil described above to enhance effectiveness. Acid/water washing times can be decreased through process optimization. Roll-to-roll processing (instead of batch processing) can be implemented. Acid usage amount can be reduced. Acid disposal costs can be significant and the

---

[86] Myers, D., Kariuki, N., Ahluwalia, R., Wang, X., and Peng, K., "Rationally Designed Catalyst Layers for PEMFC Performance Optimization", Argonne National Lab Annual Progress Report for the U.S. Department of Energy, 2015.

extent of acid reuse (before it becomes unacceptably saturated with contaminants) is not clear. Consequently, maximizing acid reuse is a cost reduction strategy. In another scenario envisioned, the CCM could be initially washed with recycled acid (perhaps for 2 hours) and then washed with fresh acid at the end (perhaps for the last half hour).
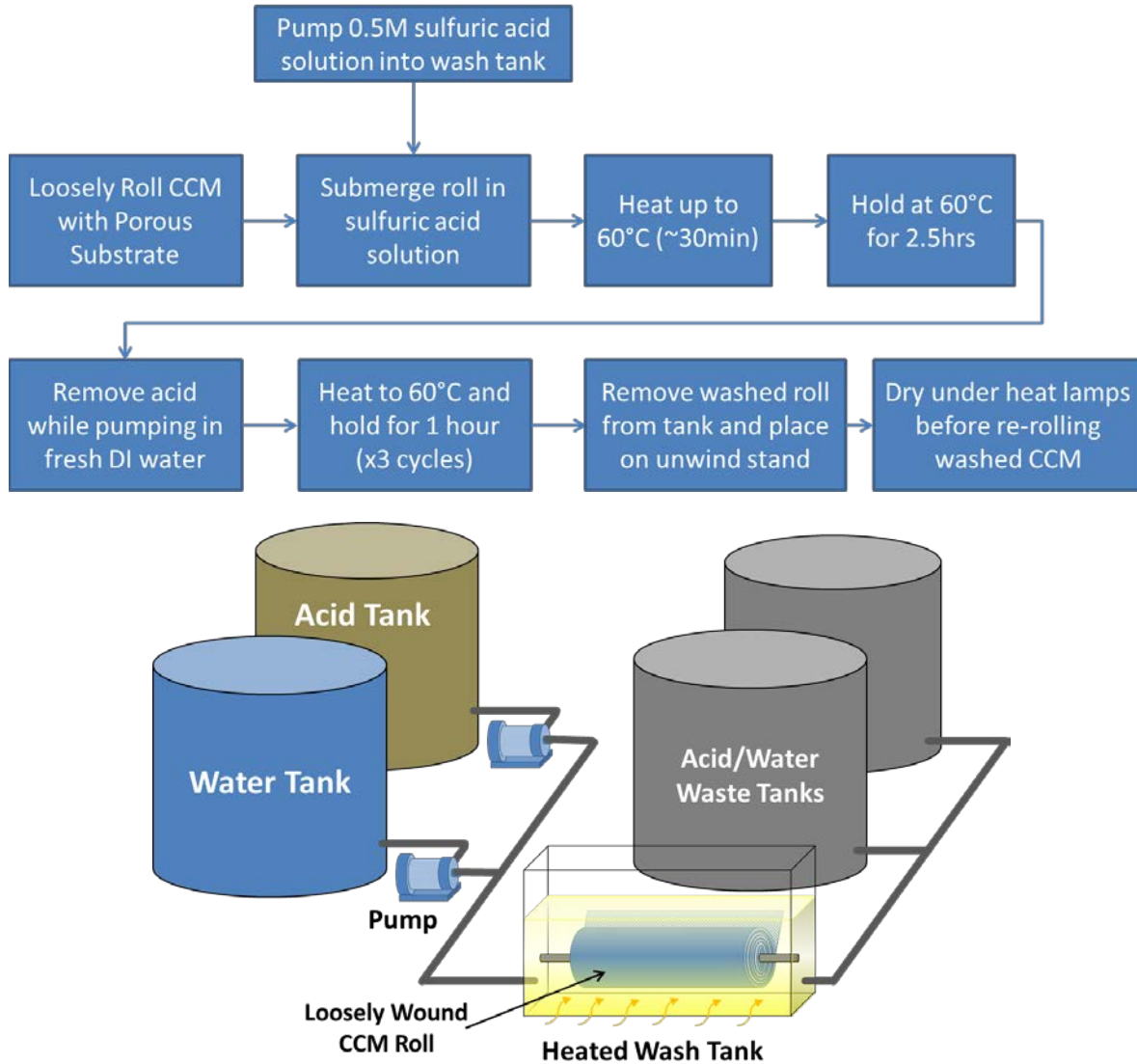
Figure 85. Diagram of CCM Acid Wash Process

Machine rate and process parameters for acid washing are shown in Figure 86 and Figure 87. The overall cost breakdown at various production rates is summarized in Figure 88.

Annual Production Rate	1,000	10,000	30,000	80,000	100,000	500,000
Equipment Lifetime (years)	15	15	15	15	15	15
Interest Rate	10%	10%	10%	10%	10%	10%
Corporate Income Tax Rate	40%	40%	40%	40%	40%	40%
Capital Recovery Factor	0.175	0.175	0.175	0.175	0.175	0.175
Equipment Installation Factor	1.40	1.40	1.40	1.40	1.40	1.40
Maintenance/Spare Parts (% of CC)	10%	10%	10%	10%	10%	10%
Miscellanous Expenses (% of CC)	7%	7%	7%	7%	7%	7%
Power Consumption (kW)	20	20	20	30	30	30

Figure 86. Acid Wash Process Parameters

Annual Production Rate	1,000	10,000	30,000	80,000	100,000	500,000
Capital Cost ($/Line)	$692,000	$692,000	$692,000	$907,000	$907,000	$907,000
Simultaneous Lines	1	1	2	2	3	11
Laborers per Line	0.33	0.33	0.33	0.33	0.33	0.33
Line Utilization	13%	41%	59%	91%	75%	97%
Effective Total Machine Rate ($/hr)	$651.67	$224.56	$161.18	$140.33	$166.12	$133.34
Batch Cycle Time (hrs)	6.0	6.0	6.0	6.0	6.0	6.0
Roll Length (m)	1,500.0	1,500.0	1,500.0	1,500.0	1,500.0	1,500.0
Roll Width (m)	0.3	0.5	0.5	0.9	0.9	0.9
Effective Acid Wash Rate (m2/min)	1.3	2.1	2.1	3.8	3.8	3.8

Figure 87. Machine Rate Parameters for CCM Acid Wash

Annual Production Rate	1,000	10,000	30,000	80,000	100,000	500,000
Material ($/stack)	$4	$1	$1	$1	$1	$1
Manufacturing ($/stack)	$294	$31	$21	$11	$13	$10
Total Cost ($/stack)	$506	$51	$34	$17	$19	$14
Total Cost ($/kWnet)	$6.32	$0.63	$0.43	$0.21	$0.24	$0.18

Figure 88. Cost Summary for CCM Acid Wash

8.1.6 Gas Diffusion Layer

The gas diffusion layer (GDL) costs for 2011 and previous analyses were based on a price quote for a vendor macroporous layer combined with a DFMA® analysis of a microporous layer addition. This resulted in a GDL cost of ~$11/m^2 at 500k systems/year (~$2.54/kWnet).

Between 2012 and 2015, the GDL cost estimates were based on DOE-funded research by Ballard Power Systems for cost reduction of a teflonated ready-to-assemble GDL consisting of a non-woven carbon base layer with two microporous layers.[87] The Ballard analysis[88] estimated a cost of ~$4.45/m^2 at 10M m^2/year (approximately equivalent to 500k systems/year) and a cost of $56/m^2 at less than 100k m^2/year (approximately equivalent to 5k systems/year). Based upon these data points, a learning curve exponent of 0.6952 was derived and used to estimate the GDL cost at intermediate production rates.

In 2016, feedback from industry indicated a wide range in current low volume and projected high volume GDL cost. In an effort to understand this disparity in cost, SA performed a DFMA® analysis of the GDL material. Section 6.7 provides a detailed description of this analysis, breaking down each processing step. The results of the model indicate only a modest cost difference between 2015 and 2016 but a

---

[87] "Reduction in Fabrication Costs of Gas Diffusion Layers," Jason Morgan, Ballard Power Systems, DOE Annual Merit Review, May 2011.
[88] Personal communication with Jason Morgan of Ballard Power Systems, 24 July 2012.

larger difference to cost vs. price assumptions: the 2015 analysis used GDL manufacturing *cost* whereas the 2016 analysis more correctly uses GDL *price* reflecting our understanding the GDL would not be vertically integrated. For 2016, it is assumed that the GDL is supplied to the OEM by a vendor and therefore includes a 25% markup to the manufacturing cost to depict price to the OEM. Thus the appropriate year to year GDL comparison is between $4.45/m^2 *cost* in 2015 and $5.50/m^2 *price* in 2016. Figure 89 graphically portrays the GDL price used in the analysis as a function of annual GDL production.

Materials and manufacturing breakdown for each of the GDL fabrication steps are shown in Figure 90. GDL production rates were modeled from a GDL manufacturer's perspective and based on process equipment for a facility sized to produce 10,000,000 m^2 of GDL per year. This leads to the GDL production and vehicle production rates not lining up exactly. Since the total amount of GDL used changes with stack power density, and because the GDL manufacturing rate doesn't scale exactly with stack production rates, a curve fit for GDL price is used in the DFMA® stack cost model. The overall cost from this curve fit at each vehicle production volume is shown in Figure 91.
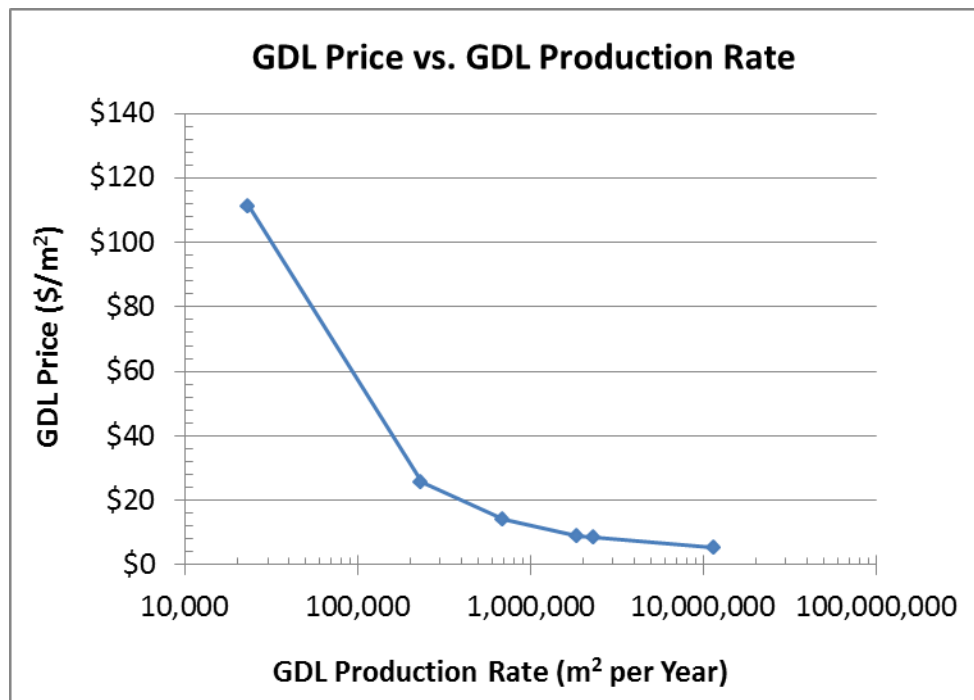
Figure 89. Price OEMs pay for GDL as a function of production rate

		m2/year	GDL 200,000	700,000	GDL 2,000,000	10,000,000
Annual GDL Production		m2/year	**200,000**	**700,000**	**2,000,000**	**10,000,000**
Paper Making		$/m2	**$4.10**	**$1.70**	**$1.77**	**$0.85**
	Material	$/m2	$0.58	$0.58	$0.58	$0.58
	Manufacturing	$/m2	$3.52	$1.12	$1.19	$0.27
Paper Impregnation Coating		$/m2	**$1.88**	**$1.06**	**$0.95**	**$0.65**
	Material	$/m2	$0.52	$0.52	$0.52	$0.52
	Manufacturing	$/m2	$1.36	$0.54	$0.44	$0.13
Saturation Coating Oxidation		$/m2	**$6.05**	**$3.91**	**$1.22**	**$1.07**
	Material	$/m2	$0.31	$0.31	$0.31	$0.31
	Manufacturing	$/m2	$5.74	$3.60	$0.92	$0.76
Hydrophobic Paper Coating			**$1.61**	**$0.80**	**$0.69**	**$0.39**
	Material	$/m2	$0.27	$0.27	$0.27	$0.27
	Manufacturing	$/m2	$1.35	$0.53	$0.43	$0.12
MPL Coating		$/m2	**$1.63**	**$1.25**	**$0.81**	**$0.58**
	Material	$/m2	$0.33	$0.33	$0.33	$0.33
	Manufacturing	$/m2	$1.30	$0.92	$0.48	$0.25
MPL Sintering		$/m2	**$5.45**	**$1.80**	**$0.91**	**$0.61**
	Material	$/m2	$0.00	$0.00	$0.00	$0.00
	Manufacturing	$/m2	$5.45	$1.80	$0.91	$0.61
Real Estate		$/m2	**$1.66**	**$0.53**	**$0.94**	**$0.29**
Markup		%	**25%**	**25%**	**25%**	**25%**
	Material	$/m2	**$2.00**	**$2.00**	**$2.00**	**$2.00**
	Manufacturing	$/m2	**$18.72**	**$8.52**	**$4.36**	**$2.15**
	Facilities	$/m2	**$1.66**	**$0.53**	**$0.94**	**$0.29**
	Total Cost Without Markup	$/m2	**$22.39**	**$11.05**	**$7.31**	**$4.45**
	Total Cost With Markup	$/m2	**$27.99**	**$13.81**	**$9.13**	**$5.56**

Figure 90. Materials and manufacturing cost for GDL fabrication processes for two low volume (left) and two high volume (right) production levels

Annual Production Rate	1,000	10,000	30,000	80,000	100,000	500,000
GDL Cost ($/stack)	$2,602	$596	$328	$213	$196	$129
Total Cost ($/stack)	$2,602	$596	$328	$213	$196	$129
Total Cost ($/kWnet)	$32.53	$7.45	$4.10	$2.66	$2.45	$1.61

Figure 91. Cost breakdown for GDL

8.1.7   MEA Sub-Gaskets

Prior to 2012, the fuel cell systems analyzed by SA were assumed to use MEA frame gaskets for gas and liquid sealing between the membrane and the bipolar plate.[89] The frame gaskets were insertion-molded around the periphery of the MEA and added substantial cost due to high cycle time and the relatively high cost of custom injection-moldable sealant. Consequently, during the 2012 analysis, an examination was conducted of fuel cell manufacturer processes and patents to identify an alternative lower cost sealing approach. The use of sub-gaskets was identified as a promising alternative and was selected for the 2012 to 2016 fuel cell systems.

The sub-gasket sealing approach consists of thin layers of PET gasketing material, judiciously cut into window-frame shapes and laminated to themselves and the periphery of the MEA to form a contiguous

---

[89] "Mass Production Cost Estimation for Direct H2 PEM Fuel Cell Systems for Automotive Applications: 2010 Update," Brian D. James, Jeffrey A. Kalinoski & Kevin N. Baum, Directed Technologies, Inc., 30 September 2010.

and flat sealing surface against the bipolar plate. A thin bead of adhesive sealing material is screen-printed onto the bipolar plates to form a gas- and liquid-tight seal between the bipolar plate and the sub-gasket material. The bipolar plate design has been changed to incorporate a raised surface at the gasket bead location to minimize the use of the gasket material. Screen printing of the gasket bead onto the bipolar plates is a well-understood and demonstrated process. The sub-gasket layers are bonded to the MEA in a roll-to-roll process, shown in Figure 92, based upon a 3M patent application.[90] While the construction is relatively simple in concept, fairly complex machinery is required to handle and attain proper placement and alignment of the thin sub-gasket and MEA layers. This sub-gasket process has four main steps:

1. Formation of a catalyst coated membrane (CCM) web
2. Attachment of CCMs to the first half of the sub-gasket ladder web
3. Attachment of the second half of the sub-gasket ladder web to the half sub-gasketed CCM
4. Attach GDLs to sub-gasketed membrane to form five-layer MEAs (in roll form)

---

[90] "Fuel Cell Subassemblies Incorporating Sub-gasketed Thrifted Membranes," US2011/0151350A1
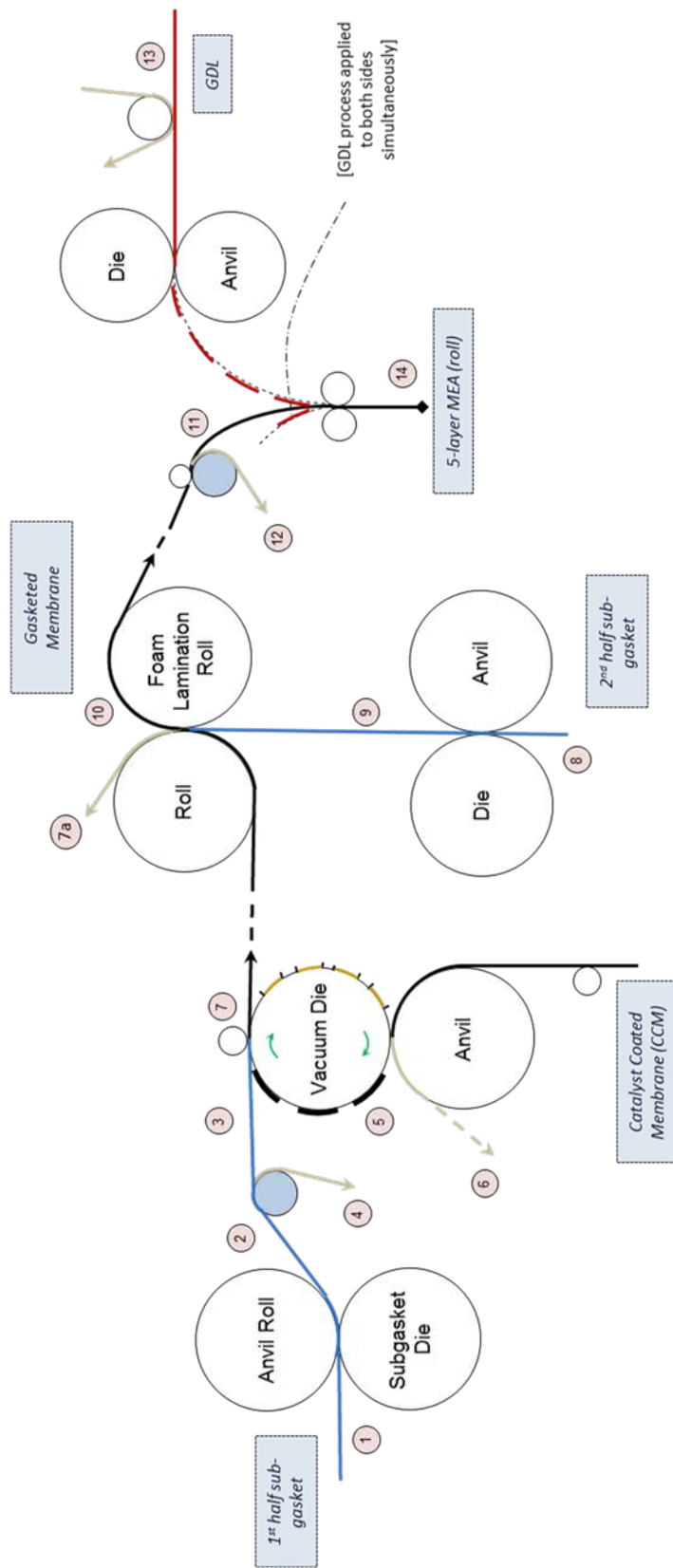
Figure 92. Roll-to-roll sub-gasket application process

1st half sub-gasket

Anvil Roll

Subgasket Die

Catalyst Coated Membrane (CCM)

Vacuum Die

Anvil

Die

2nd half sub-gasket

Roll

Foam Lamination Roll

Gasketed Membrane

Die

Anvil

GDL

[GDL process applied to both sides simultaneously]

5-layer MEA (roll)

110

First half Sub-gasket

Carrier Web
Adhesive
Aperture "slug"

Gasket layer
Release Liner

① ② ③

Release Liner "Ladder"
④

CCM

Vacuum Die

CCM

⑤

⑥

⑦

(Scrap)

7a

2nd half Sub-gasket

No Adhesive
Carrier Web
2nd aperture slug

Gasket

⑧ ⑨

⑩

Adheres & seals 1
& 2 sub-gaskets

⑪

(Scrap)
⑫

⑪

~1/8 in. overlap of sub-gasket over
membrane on each side

GDL
GDL Adhesive

⑭

5-layer MEA

Figure 92. (continued)

111

The process uses a proprietary 3M "pressure sensitive adhesive," which is modeled at a notional $20/kg based on high-end generic adhesive surrogates. The sub-gasket layer consists of two layers of 0.1mm PET film at $1.67/m^2 based on a high-volume internet price quote. These materials experience significant waste using this process, as the center section of both the sub-gasket layers (corresponding to the fuel cell active area) and the adhesive liner is scrapped. The process capital equipment is based on component analogy to membrane web processing units and is assumed to operate at a line speed of 30m/min with five line workers.

While the process train illustrated in Figure 92 is based on a 3M patent, the implementation of it for cost modeling purposes differs in two important respects. First, the process shows a "ladder" of scrap CCM being left over (component 6) after the vacuum die cutter separates the CCM active area (component 5) from the CCM roll. This amount of CCM wastage would normally be approximately equal to the difference between the bipolar plate total area and the membrane active area: a substantial scrap fraction.[91] Consequently, to minimize this CCM wastage, additional machinery is postulated for cost modeling purposes to allow the active area CCM pieces to be cut from the CCM roll contiguously (i.e. with no scrap between pieces) and then placed appropriately to fit into the picture portion of the picture-frame sub-gaskets. This may be accomplished by rotary, indexed, or robotic pick-and-place machinery. While this approach adds mechanical complexity and capital cost, it avoids the high CCM scrap rates that otherwise would occur. Second, the 3M patent is silent on the issue of how many cells are processed simultaneously in the web width direction. While 1 cell wide is inferred, use of multiple cells across the width is a reasonable engineering extrapolation. Cost computations are based on a nominal 1 meter web width that can process 5 cells simultaneously. This adds mechanical complexity and capital cost but overall leads to reduced part cost due to an increased processing rate.

A thin bead of sealing material is screen printed onto the bipolar plates to form a gas and liquid tight seal between the bipolar plate and the sub-gasket material. This process is directly analogous to the screen-printed coolant gaskets analyzed in past cost analyses.[92] The cost of this screen printing step is combined with that of the sub-gasket procedure described above, and presented as a single cost result in Figure 9.

In 2015, an alternative processing method was implemented for the sub-gasket at 1,000 systems per year production. The sub-gasket process assumed for high volume has quite high capital cost with very high throughput resulting in very low utilization at low volumes. For low volume, an alternative robotic stacking approach was used where the material for each of the sub-gasket components is cut to the cell size and stacked with a robot. This change in process affects the processing methods of the hot pressing and cutting and slitting. More on these changes are described in their respective sections. Figure 93 shows the step-by-step process (view of through-cell cross-sections) for the low volume sub-gasket technique.

---

[91] For an active to total area ratio of 0.625, scrap as a percentage of active area would be 0.375/0.625 = 60%.
[92] The reader is directed to section 4.4.9.3 of the 2010 update of the auto fuel cell cost analysis for a more detailed discussion. "Mass Production Cost Estimation for Direct H$_2$ PEM Fuel Cell Systems for Automotive Applications: *2010 Update*," Brian D. James, Jeffrey A. Kalinoski & Kevin N. Baum, Directed Technologies, Inc., 30 September 2010.

In switching to a discretized operation of robotic stacking, the capital cost reduces to $800k with an 88.5% utilization of equipment at 1,000 systems per year. This change affects the cutting/slitting cost at (low volume) which is unnecessary since the MEAs are already in discrete cells. The manufacturing cross-over point for this process (the point at which the high throughput roll-to-roll process becomes less expensive than robotic stacking) is approximately 2,000 systems per year (25k m^2 MEA area per year), as shown in Figure 94. At such a low cross-over point, a vehicle OEM may be willing to accept the sub-optimal high cost roll-to-roll process at 1,000 systems per year, confident that cost savings are in the near future.
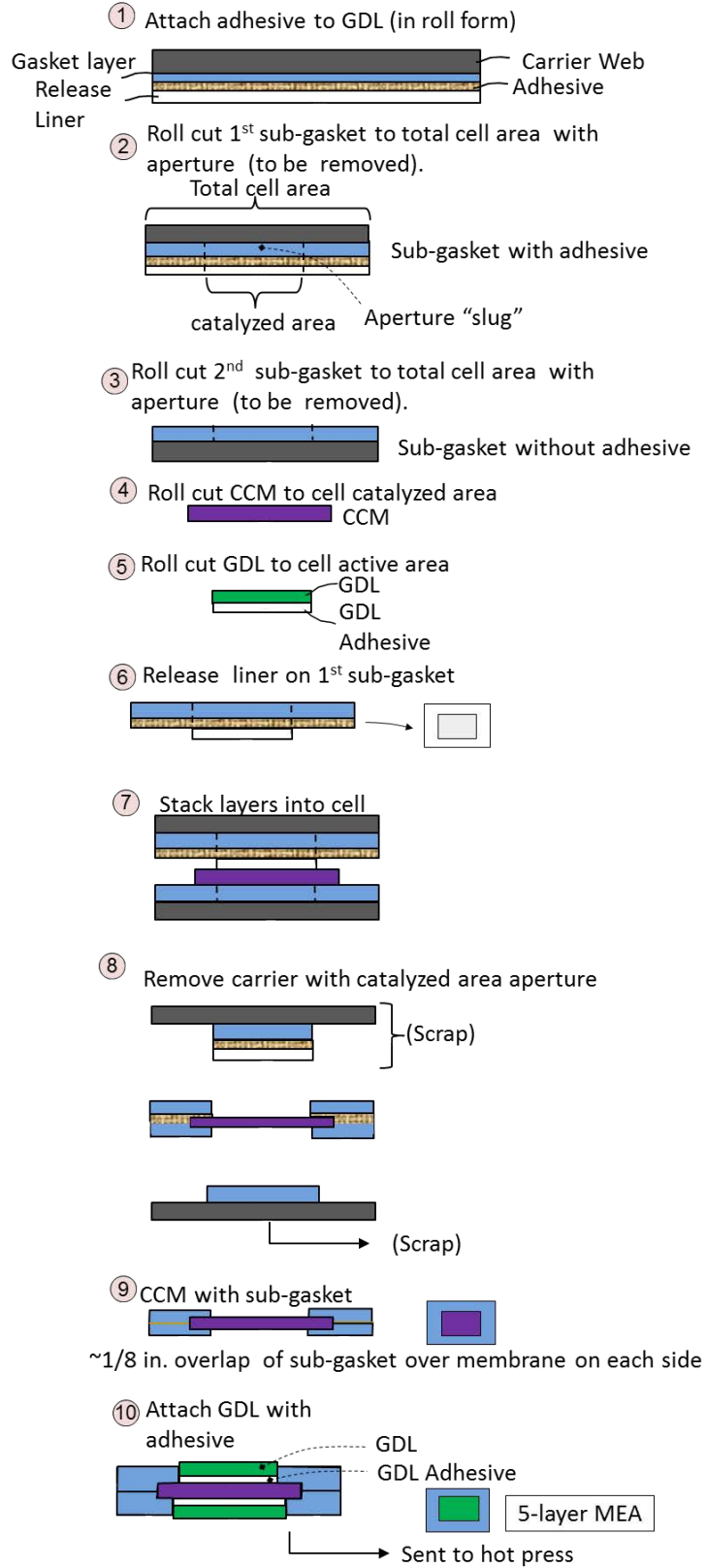
Figure 93. Labeled processing steps for sub-gasket manufacturing at low volumes
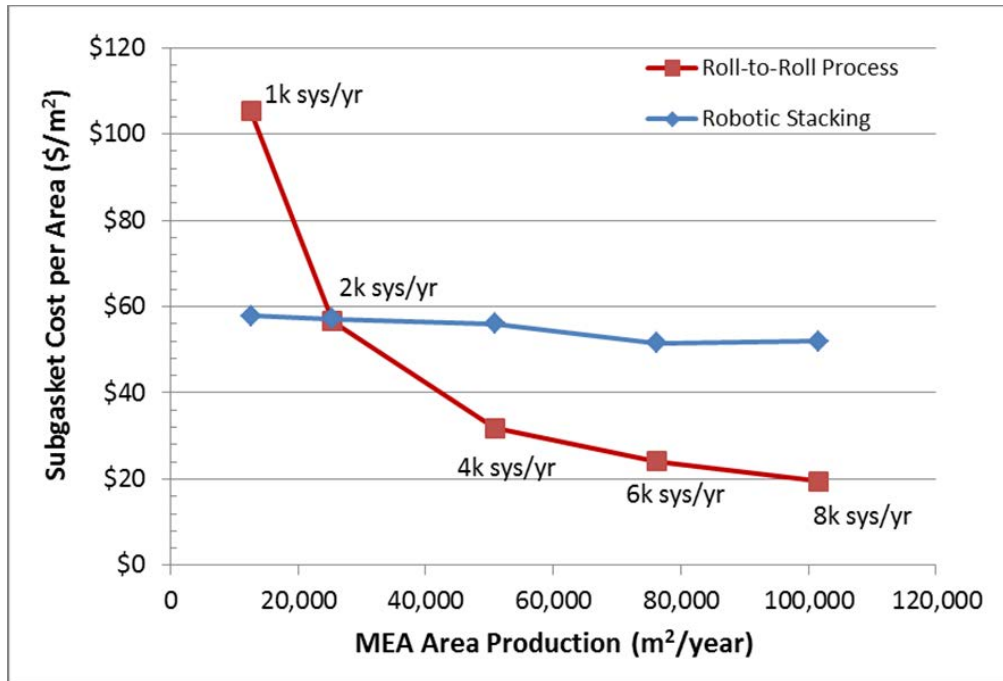
Figure 94. Graph showing cost cross-over for low volume to high volume sub-gasket process

Quality Control: An optical detection system (ODS) QC system is used on the sub-gasket process to detect misalignment of sub-gasket and membrane, folds, bends, tears, or scratches in the membrane or sub-gasket material. The sub-gasketed MEA is laid on a conveyor belt during inspection and passed beneath a camera. The capital cost of the QC system is adjusted at each manufacturing rate to account for changes in web width (cell material across width), and whether a conveyor system is required. At low volume (only 1,000 systems per year) the ODS system is assumed to be vertically mounted above the MEA with sub-gasket while being stacked due to the assembly process being discrete, not continuous. Therefore, the conveyor system for the QC of sub-gaskets was removed when there was no need for a continuous process at low volume.

8.1.8 Sub-gasket Formation

Details of the MEA sub-gasket formation process appear in Figure 95 and Figure 96 with cost results shown in Figure 97.

Annual Production Rate	1,000	10,000	30,000	80,000	100,000	500,000
Equipment Lifetime (years)	15	13	13	13	13	13
Interest Rate	10%	10%	10%	10%	10%	10%
Corporate Income Tax Rate	40%	40%	40%	40%	40%	40%
Capital Recovery Factor	0.175	0.186	0.186	0.186	0.186	0.186
Equipment Installation Factor	1.4	1.4	1.4	1.4	1.4	1.4
Maintenance/Spare Parts (% of CC)	10%	10%	10%	10%	10%	10%
Miscellanous Expenses (% of CC)	7%	7%	7%	7%	7%	7%
Power Consumption (kW)	101	101	101	101	101	101

Figure 95. MEA Sub-gasket process parameters

115

Annual Production Rate	1,000	10,000	30,000	80,000	100,000	500,000
Capital Cost ($/Line)	$864,129	$2,908,600	$2,908,600	$2,958,600	$2,958,600	$2,958,600
Simultaneous Lines	1	1	1	1	1	3
Laborers per Line	2	5	5	5	5	5
Line Utilization	89.0%	8.4%	24.2%	37.2%	46.2%	72.4%
Effective Total Machine Rate ($/hr)	$219.00	$4,676.52	$1,779.03	$1,254.07	$1,057.38	$759.83
Line Speed (m/s)	0.3	0.5	0.5	0.5	0.5	0.5
Kapton Tooling Cost ($/m2)	$6.47	$3.56	$3.34	$3.28	$3.27	$3.24
Subgasket Material Cost ($/m2)	$1.67	$1.67	$1.67	$1.67	$1.67	$1.67

Figure 96. MEA Sub-gasket machine parameters

Annual Production Rate	1,000	10,000	30,000	80,000	100,000	500,000
Material ($/stack)	$63	$63	$63	$63	$63	$63
Manufacturing ($/stack)	$655	$132	$48	$20	$16	$11
Tooling (Kapton Web) ($/stack)	$18	$9	$9	$8	$8	$8
Total Cost ($/stack)	$735	$204	$119	$91	$87	$82
Total Cost ($/kWnet)	$9.19	$2.55	$1.49	$1.13	$1.09	$1.03

Figure 97. Cost breakdown for MEA Sub-gasket

8.1.8.1   Screenprinted Sub-gasket Seal

Details of the screenprinted sub-gasket seal application step appear in Figure 98 and Figure 99 with cost results shown in Figure 100.

Annual Production Rate	1,000	10,000	30,000	80,000	100,000	500,000
Screen Printing Machine Type	DEK Horizon	DEK PV 1200	DEK PV 1200	DEK PV 1200	DEK PV 1200	DEK PV 1200
Equipment Lifetime (years)	15	15	15	15	15	15
Interest Rate	10%	10%	10%	10%	10%	10%
Corporate Income Tax Rate	40%	40%	40%	40%	40%	40%
Capital Recovery Factor	0.175	0.175	0.175	0.175	0.175	0.175
Equipment Installation Factor	1.4	1.4	1.4	1.4	1.4	1.4
Maintenance/Spare Parts (% of CC)	3%	1%	1%	1%	1%	1%
Miscellanous Expenses (% of CC)	12%	12%	12%	12%	12%	12%
Power Consumption (kW)	61	166	166	166	166	166

Figure 98. Screenprinted Sub-gasket process parameters

Annual Production Rate	1,000	10,000	30,000	80,000	100,000	500,000
Screen Printing Machine Type	DEK Horizon	DEK PV 1200	DEK PV 1200	DEK PV 1200	DEK PV 1200	DEK PV 1200
Capital Cost ($/Line)	$392,735	$1,458,755	$1,458,755	$1,458,755	$1,458,755	$1,458,755
Simultaneous Lines	1	1	1	3	4	17
Laborers per Line	0.25	0.25	0.25	0.25	0.25	0.25
Line Utilization	30.7%	32.5%	97.6%	86.8%	81.4%	95.7%
Effective Total Machine Rate ($/hr)	$164.79	$519.91	$189.58	$210.23	$222.61	$192.88
Line Speed (m/s)	1.00	1.00	1.00	1.00	1.00	1.00
Index Time (s)	$9.62	$4.00	$4.00	$4.00	$4.00	$4.00
Resin Cost ($/kg)	$15.19	$15.19	$15.19	$15.19	$15.19	$15.19

Figure 99. Screenprinted sub-gasket machine parameters

Annual Production Rate	1,000	10,000	30,000	80,000	100,000	500,000
Material ($/stack)	$12	$12	$12	$12	$12	$12
Manufacturing ($/stack)	$170	$57	$21	$23	$24	$21
Total Cost ($/stack)	$182	$69	$33	$35	$36	$33
Total Cost ($/kWnet)	$2.27	$0.86	$0.41	$0.44	$0.45	$0.41

Figure 100. Cost breakdown for screenprinted sub-gasket

8.1.8.2 *Total MEA Sub-gasket & Seal Cost*

The total cost of the sub-gasket (sub-gasket formation plus screenprinted seal) appears in Figure 101.

Annual Production Rate	1,000	10,000	30,000	80,000	100,000	500,000
Material ($/stack)	$74	$74	$74	$74	$74	$74
Manufacturing ($/stack)	$825	$189	$69	$43	$41	$32
Tooling (Kapton Web) ($/stack)	$18	$9	$9	$8	$8	$8
Total Cost ($/stack)	$917	$272	$152	$126	$124	$115
Total Cost ($/kWnet)	$11.46	$3.40	$1.90	$1.57	$1.54	$1.44

Figure 101. Cost breakdown for total MEA sub-gasket

8.1.9 Hot Pressing CCM and GDLs

Bonding of the three layers of the MEA (the catalyst-coated membrane plus GDL on either side) is desirable for intimate electronic/ionic contact, proper alignment of the parts, and ease of subsequent MEA handling. In switching from a NSTF-based catalyst coating process to a slot die coating process, an alternative method was needed to bond the GDLs to the CCM. Industry feedback[93] confirmed that the procedure of hot pressing the CCM and GDL to bond the parts was incompatible with the NSTF catalyst layer.[94] Consequently, for the 2014 cost analysis (NSTF-based), the layers of the MEA were crimped together periodically along the edges (between the MEA gasketing process and the cutting and slitting process) to sufficiently hold the assembly together. For NSTF, hot pressing is incompatible because there is no ionomer material in the catalyst to melt to the GDL. However, for the 2015 and 2016 baseline systems (catalyst ink based, not NSTF), hot pressing to bond the ionomer in the catalyst ink to the GDL layers was added back into the analysis.

As described in Figure 102, the hot-pressing process starts with the roll that comes off the sub-gasket line; the gasketed catalyzed membrane sandwiched between two GDLs. Each of the two wind stands (wind and unwind) is equipped with a brake and a tensioner. The sandwiched MEA travels through the hot press and then is rewound back into a roll. The press is heated to 160°C, and is indexed with a press time of 90 seconds. It takes 3 seconds to open the press, advance the roll to the next section, and re-close the press, making the cycle time 93 seconds. The section advance time could be quicker, but because of the limited tensile strength of the materials, 3 seconds is appropriate. Furthermore, 3

---

[93] Personal communication with Mark Debe of 3M, November 2011.
[94] Previous cost analysis postulated bonding of the GDL and catalyst coated membrane through a hot pressing procedure since the ionomer within the catalyst ink composition could serve as a bonding agent for the GDL. However, there is no ionomer in the NSTF catalyst layer and thus hot pressing would not be effective for NSTF MEA's.

seconds is only 1/30th of the press time, and for an already-inexpensive process, the savings in speeding up the section advance would be minimal. The press is 100 cm wide by 150 cm in length, so approximately 18 to 22 cells get hot-pressed at a time, depending on the cell geometry. The idea of hot pressing the MEA with the sub-gasket is a potential problem. This assumption was not based on what is currently done in practice and has not been demonstrated in industry. However, the PET film melting point is 250˚C while the hot pressing is only at 160˚C and the press die is portioned to only press the GDL and not the gaskets.

At 1,000 systems per year, the cells are prematurely cut into single cell units, requiring an alternative delivery method to the hot pressing machine. Normally an automated process would only require a worker ¼ of their time, but for the 1,000 system per year production rate, SA assumed a full-time worker that manually inserts the MEA into the press and then visually inspects them afterward for holes, delamination, etc. As is described in the cutting and slitting section, no additional cutting or slitting is required for the MEA at 1k systems per year because the cells are already in final form. The visual inspection of the cell by the worker after the hot pressing is important because it takes the place of the Optical Detection System (ODS) QC inspection after the cutting and slitting process.

| CCM with GDL | Hot-Pressing Station | Hot-Pressed M&E |
| Unwind Stand with Brake & Tensioner 0.6m ID spool, 1 m width | Large, flat surface, 1m wide, 1.5m length, 160˚C, 90 second clamp time. | Rewind Stand with Tensioner 0.6m ID spool, 1m width |
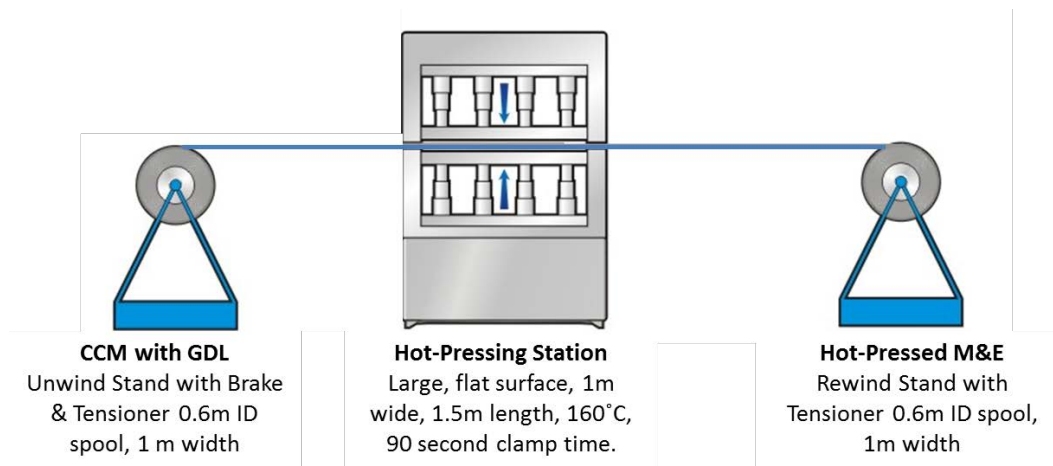
Figure 102. Hot-pressing process diagram for pressing two GDL layers and the CCM.

8.1.9.1 *Hot Pressing CCM and GDLs Cost Breakdown*

Machine rate and process parameters are shown in Figure 103 and Figure 104. The overall cost breakdown at various production rates is summarized in Figure 105.

Annual Production Rate	1,000	10,000	30,000	80,000	100,000	500,000
Equipment Lifetime (years)	15	15	15	15	15	15
Interest Rate	10%	10%	10%	10%	10%	10%
Corporate Income Tax Rate	40%	40%	40%	40%	40%	40%
Capital Recovery Factor	0.175	0.175	0.175	0.175	0.175	0.175
Equipment Installation Factor	1	1	1	1	1	1
Maintenance/Spare Parts (% of CC)	5%	5%	5%	5%	5%	5%
Miscellanous Expenses (% of CC)	7%	7%	7%	7%	7%	7%
Power Consumption (kW)	15	16	16	16	16	16

Figure 103. Hot-pressing process parameters

Annual Production Rate	1,000	10,000	30,000	80,000	100,000	500,000
Capital Cost ($/Line)	$56,062	$126,795	$126,795	$126,795	$126,795	$126,795
Simultaneous Lines	$1	$2	$6	$9	$11	$51
Laborers per Line	1	0	0	0	0	0
Line Utilization	11%	84%	84%	90%	92%	99%
Effective Total Machine Rate ($/hr)	$101.41	$29.00	$29.00	$27.98	$27.64	$26.55
Total Cycle Time (seconds)	105	95	95	95	95	95

Figure 104. Machine rate parameters for hot-pressing process

Annual Production Rate	1,000	10,000	30,000	80,000	100,000	500,000
Manufacturing ($/stack)	$38	$16	$16	$9	$9	$9
Tooling ($/stack)	$1	$0	$0	$0	$0	$0
Total Cost ($/stack)	$39	$17	$17	$10	$10	$9
Total Cost ($/kWnet)	$0.48	$0.21	$0.21	$0.12	$0.12	$0.11

Figure 105. Cost summary for hot-pressing process

8.1.10 MEA Cutting, and Slitting

As shown in Figure 106, the rolls of hot-pressed MEA are fed through cutters and slitters to trim to the desired dimensions for insertion into the stack. The 100-cm-wide input roll (width at 500k systems per year) is slit into ribbon streams of the appropriate width (again, depending on cell geometry). The streams continue through to the cutters, which turn the continuous material into individual rectangles. These rectangles are then sorted into magazine racks.
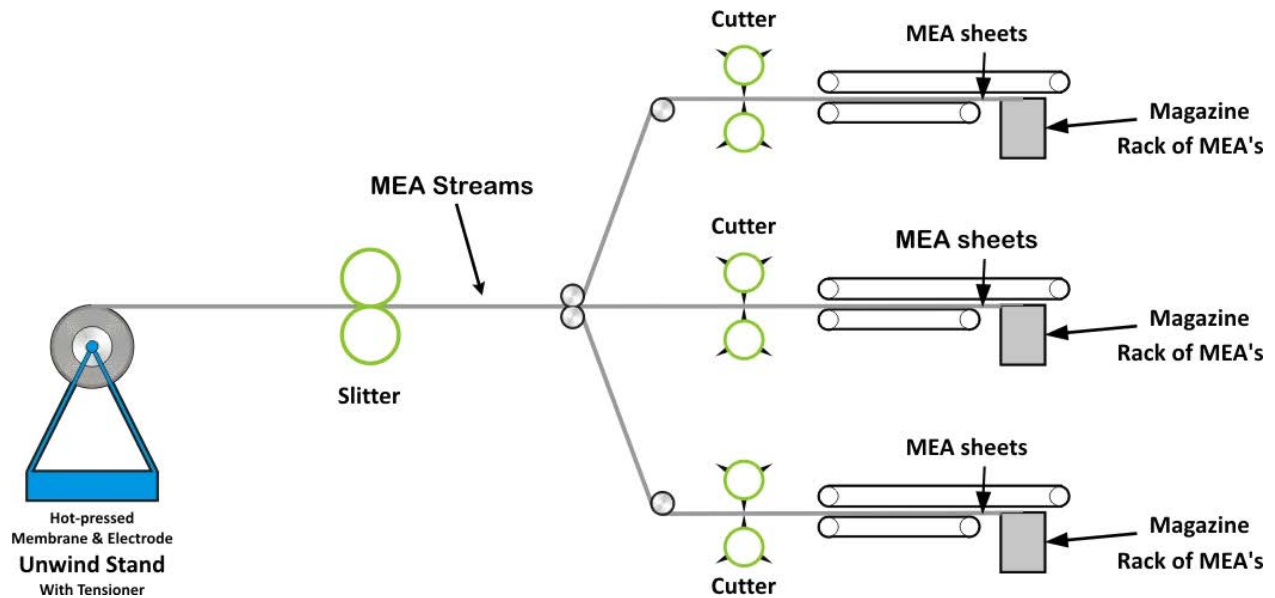
Figure 106. Cutting & slitting process diagram

Figure 107 and Figure 108 further detail the process parameters. This process is not used at all production rates. At 1,000 systems per year, there is no cutting and slitting due to the fact that the cells are already discretized for the sub-gasket process. Figure 109 summarizes the overall cost of the cutting and slitting operation.

Annual Production Rate	1,000	10,000	30,000	80,000	100,000	500,000
Equipment Lifetime (years)	0	14	14	14	14	14
Interest Rate	0%	10%	10%	10%	10%	10%
Corporate Income Tax Rate	0%	40%	40%	40%	40%	40%
Capital Recovery Factor	0.000	0.180	0.180	0.180	0.180	0.180
Equipment Installation Factor	0	1.4	1.4	1.4	1.4	1.4
Maintenance/Spare Parts (% of CC)	0%	10%	10%	10%	10%	10%
Miscellanous Expenses (% of CC)	0%	7%	7%	7%	7%	7%
Power Consumption (kW)	0	18	18	18	18	18

Figure 107. Cutting & Slitting process parameters

Annual Production Rate	1,000	10,000	30,000	80,000	100,000	500,000
Capital Cost ($/line)	$0	$419,136	$419,136	$469,136	$469,136	$469,136
Costs per Tooling Set ($)	$0	$5,606	$5,606	$5,606	$5,606	$5,606
Tooling Lifetime (cycles)	0	200,000	200,000	200,000	200,000	200,000
Simultaneous Lines	0	1	1	1	1	2
Laborers per Line	0	0.25	0.25	0.25	0.25	0.25
Line Utilization	0.0%	4.7%	13.7%	21.7%	27.1%	67.8%
Effective Total Machine Rate ($/hr)	$0.00	$1,135.02	$396.36	$284.19	$229.95	$99.67
Line Speed (m/s)	0.0	1.2	1.3	1.3	1.3	1.3

Figure 108. Machine rate parameters for Cutting & Slitting process

Annual Production Rate	1,000	10,000	30,000	80,000	100,000	500,000
Manufacturing ($/stack)	$0	$18	$6	$3	$2	$1
Tooling ($/stack)	$0	$4	$4	$2	$2	$2
Total Cost ($/stack)	$0	$22	$10	$5	$4	$3
Total Cost ($/kWnet)	$0.00	$0.27	$0.12	$0.06	$0.06	$0.04

Figure 109. Cost breakdown for Cutting & Slitting process

8.1.11 End Plates

In a typical PEM fuel cell stack, the purposes of an end plate are threefold:

- Evenly distribute compressive loads across the stack

- Cap off and protect the stack

- Interface with the current collector

Typically there is also a separate insulator plate at each end to electrically insulate the stack from the rest of the vehicle. However the SA end plate design, based on a UTC patent (see Figure 110), eliminates the need for separate insulators. Thus, the SA modeled end plates also serve a fourth function: electrical insulation of the ends of the stack.

The end plate is made from a compression-molded composite (LYTEX 9063), is mechanically strong (455 MPa) to withstand the compressive loading, and is sufficiently electrically non-conductive (3×10^{14} ohm-cm volume resistivity). Use of this material allows for an end plate with lower cost and lower thermal capacity than the typical metal end plates, with the additional benefit of having very low corrosion susceptibility. The benefits of lower cost and corrosion resistance are obvious, and the low thermal capacity limits the thermal energy absorbed during a cold start, effectively accelerating the startup period.
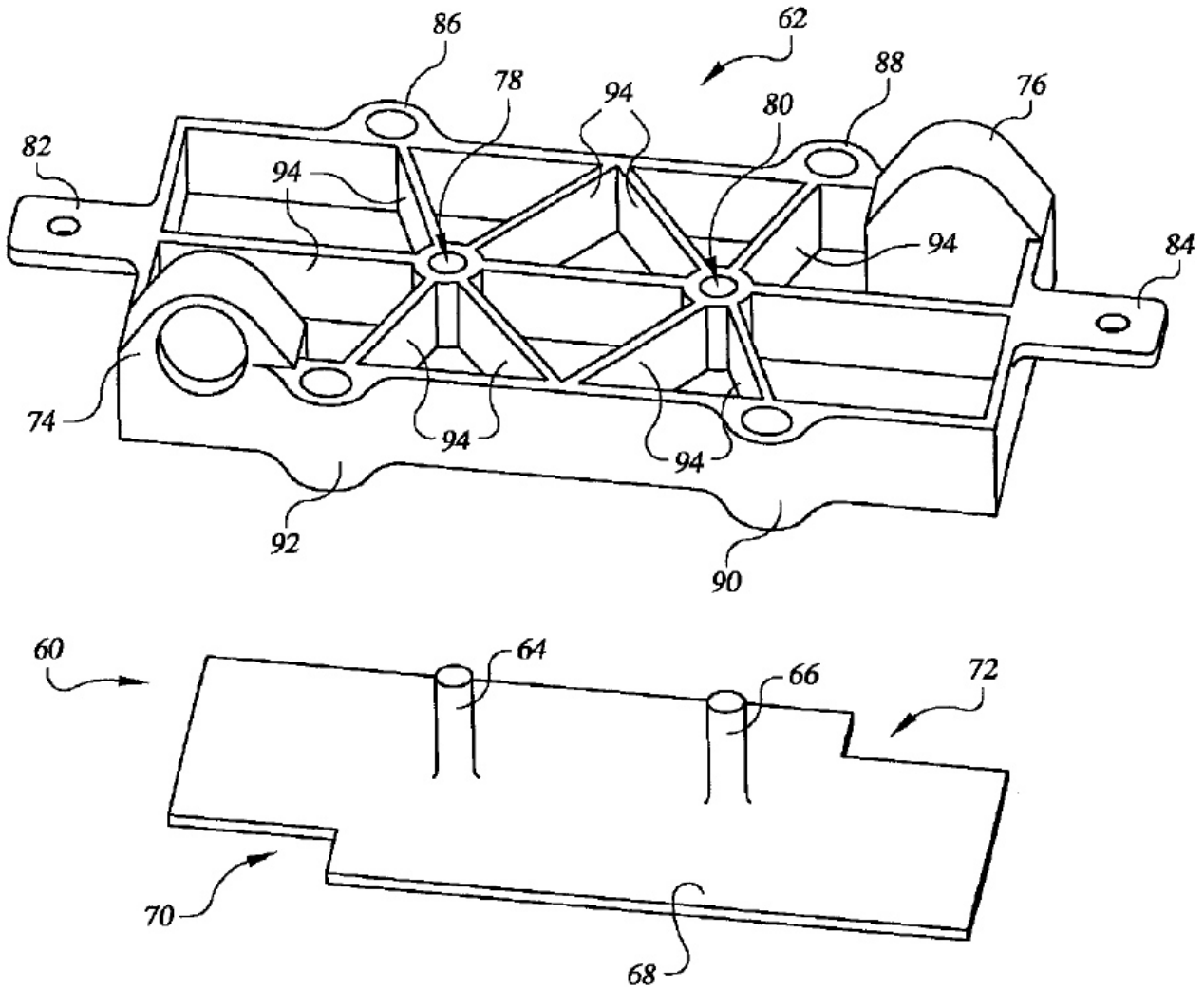
Figure 110. End plate concept (Figure courtesy of US patent 6,764,786)

LYTEX 9063 is a high performance engineered structural composite (ESC) molding compound consisting of epoxy and glass fiber reinforcement. It is designed for military and aerospace structural applications requiring excellent mechanical properties, retention of properties at elevated temperatures, good chemical resistance and excellent electrical properties. For all of these reasons, it is ideally suited for this application.

The end plates are manufactured via compression molding. A summary of the procedure is as follows:[95]

- Remove enough LYTEX from cold storage for one day's usage. Allow it to warm to room temperature.

- Clean mold thoroughly. Apply a uniform thin coating of a mold release. (Note: Once the mold is conditioned for LYTEX, only periodic reapplications are required.)

---

[95] Based on Quantum Composites recommended procedures for LYTEX molding.

- Adjust mold temperature to 300°F (148°C).

- Adjust molding pressure on the material to 1,500 psi (105 kg/cm).

- Remove protective film completely from both sides of the LYTEX.

- Cut mold charge so the LYTEX covers approximately 80% of the mold area and is about 105% of the calculated part weight.

- Dielectrically preheat the LYTEX quickly to 175°F (80°C).

- Load material into mold and close the mold.

- Cure for 3 minutes

- Remove part from mold. Because of low shrinkage and high strength, the part may fit snugly in the mold.

- Clean up mold and begin again.

- Re-wrap unused LYTEX and return to cold storage.

In 2015, alternative low production volume techniques were investigated including job shop of non-repeat stack components. End plates were found to be an excellent candidate for job shop due to the low volume of parts and status as a low proprietary level component. Details of the end plate processing parameters are shown in Figure 111 and Figure 112.

Annual Production Rate	1,000	10,000	30,000	80,000	100,000	500,000
Equipment Lifetime (years)	15	15	15	15	15	15
Interest Rate	10%	10%	10%	10%	10%	10%
Corporate Income Tax Rate	40%	40%	40%	40%	40%	40%
Capital Recovery Factor	0.175	0.175	0.175	0.175	0.175	0.175
Equipment Installation Factor	1.4	1.4	1.4	1.4	1.4	1.4
Maintenance/Spare Parts (% of CC)	10%	10%	10%	10%	10%	10%
Miscellanous Expenses (% of CC)	12%	12%	12%	12%	12%	12%
Power Consumption (kW)	29	29	60	63	63	68

Figure 111. End plate compression molding process parameters

As seen in Figure 113, the material represents the majority of the end plate costs, ranging from 86% to 96%, depending on the production rate.

Annual Production Rate	1,000	10,000	30,000	80,000	100,000	500,000
Capital Cost ($/line)	$229,297	$229,297	$444,462	$475,200	$475,200	$536,676
Costs per Tooling Set ($)	$25,802	$25,802	$73,942	$79,602	$79,602	$90,438
Tooling Lifetime (cycles)	300,000	300,000	300,000	300,000	300,000	300,000
Simultaneous Lines	1	1	1	1	1	3
Laborers per Line	0.5	0.5	0.5	0.5	0.5	0.5
Cycle Time (s)	310.16	310.16	345.72	350.80	350.80	360.96
Cavities/Platen	2	2	9	10	10	12
Effective Total Machine Rate ($/hr)	$1,249.13	$148.64	$349.98	$169.32	$141.00	$117.64
LYTEX Cost ($/kg)	$30.92	$25.90	$23.80	$22.07	$21.69	$19.16
Job Shop or Manufactured	Job Shop	Job Shop	Job Shop	Manufactured	Manufactured	Manufactured
Job Shop Line Utilization (%)	39.6%	62.7%	56.1%	46.4%	58.0%	82.9%
Job Shop Machine Rate ($/min)	$2.28	$1.64	$2.97	$3.67	$3.06	$2.55
Manufactured Line Utilization (%)	2.6%	25.7%	19.1%	46.4%	58.0%	82.9%
Manufactured Machine Rate ($/min)	$20.82	$2.48	$5.83	$2.82	$2.35	$1.96
Line Utilization Used (%)	39.6%	62.7%	56.1%	46.4%	58.0%	82.9%
Manufacturing Rate Used ($/min)	$2.28	$1.64	$2.97	$2.82	$2.35	$1.96

Figure 112. Machine rate parameters for compression molding process

Annual Production Rate	1,000	10,000	30,000	80,000	100,000	500,000
Material ($/stack)	$86	$72	$66	$61	$60	$53
Manufacturing ($/stack)	$12	$8	$4	$3	$3	$2
Tooling ($/stack)	$2	$0	$0	$0	$0	$0
Total Cost ($/stack)	$99.22	$80.35	$69.85	$64.45	$62.85	$55.08

Figure 113. Cost breakdown for end plates

8.1.12 Current Collectors

The function of the current collectors is to channel the electrical current that is distributed across the active area of the stack down to the positive and negative terminals. In the SA modeled design, based on the UTC patent (Figure 110) and shown in Figure 114 , two copper current studs protrude through the end plates to connect to a copper sheet in contact with the last bipolar plate.
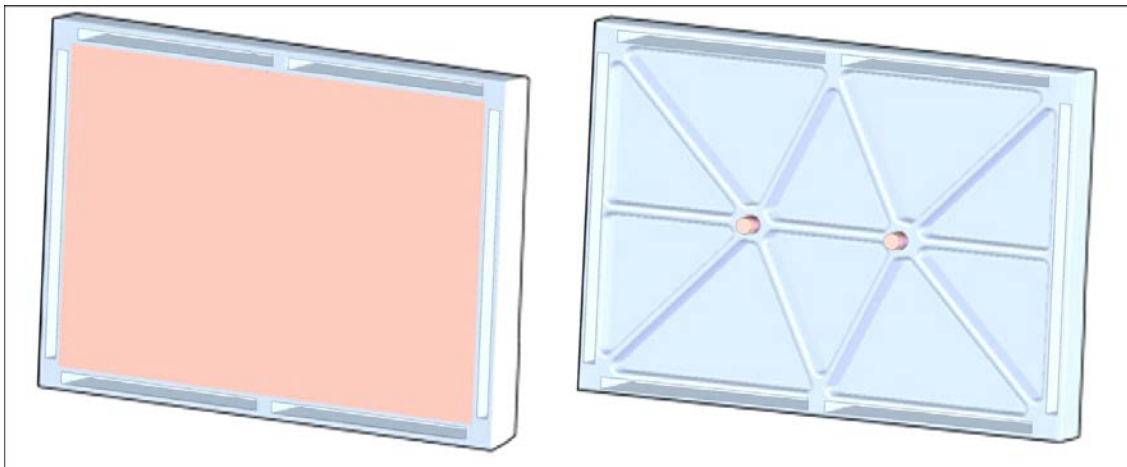
Figure 114. End plate and current collector[96]

---

[96] Some details of the port connections are not shown in the illustration.

The current collectors were designed to fit snugly within the end plate. A shallow (0.3 mm) cavity in the end plate provides room for the 1 mm thick copper sheet, sized to the active area of the cells. The remaining 0.7 mm of the sheet thickness protrudes from the end plate, and the end plate gasket seals around the edges.

The face of the current collector is pressed against the coolant side of the last bipolar plate in the stack. With the compression of the stack, it makes solid electrical contact with the bipolar plate, and thus can collect the current generated by the stack.

The other side of the current collector is flush against the inner face of the end plate. Two copper studs protrude through their corresponding holes in the end plate, where they are brazed to the current collector sheet. On the outside of the end plate, these studs serve as electrical terminals to which power cables may be attached.

Manufacturing the current collectors is a fairly simple process. A roll of 1 mm thick copper sheeting is stamped to size, and 8 mm diameter copper rod is cut to 2.43 cm lengths. The ends of the rods are then brazed to one face of the sheet. At low production (1,000 systems per year), a manual cutting process is used. All other manufacturing rates use an automated process that cuts parts from a roll of copper sheet stock.

Similar to the end plates, current collector cost estimates are based on job shopping to attain a lower cost. Details of current collector processing parameters are shown in Figure 115 and Figure 116. Cost results are shown in Figure 117.

Annual Production Rate	1,000	10,000	30,000	80,000	100,000	500,000
Equipment Lifetime (years)	10	10	15	15	15	15
Interest Rate	10%	10%	10%	10%	10%	10%
Corporate Income Tax Rate	40%	40%	40%	40%	40%	40%
Capital Recovery Factor	0.205	0.205	0.175	0.175	0.175	0.175
Equipment Installation Factor	1.4	1.4	1.4	1.4	1.4	1.4
Maintenance/Spare Parts (% of CC)	13%	13%	13%	13%	13%	13%
Miscellanous Expenses (% of CC)	2%	2%	2%	2%	2%	2%
Power Consumption (kW)	17	17	23	23	23	23

Figure 115. Current collector manufacturing process parameters

Annual Production Rate	1,000	10,000	30,000	80,000	100,000	500,000
Costs per Tooling Set ($)	$1,882	$1,882	$1,882	$1,882	$1,882	$1,882
Tooling Lifetime (cycles)	400,000	400,000	400,000	400,000	400,000	400,000
Capital Cost ($/line)	$35,483	$70,029	$166,443	$166,443	$166,443	$166,443
Simultaneous Lines	1	1	1	1	1	1
Laborers per Line	1.00	1.00	0.25	0.25	0.25	0.25
Line Utilization	0.1%	0.6%	0.4%	1.1%	1.4%	7.1%
Effective Total Machine Rate ($/hr)	$8,085.63	$1,682.51	$4,569.84	$1,729.54	$1,389.87	$288.83
Index Time (s)	3.00	3.00	0.53	0.53	0.53	0.53
Copper Cost ($/kg)	$15.78	$12.92	$11.50	$10.23	$9.94	$7.86
Job Shop or Manufactured	Job Shop	Job Shop	Job Shop	Job Shop	Job Shop	Job Shop
Job Shop Line Utilization (%)	37.1%	37.6%	37.4%	38.1%	38.4%	44.1%
Job Shop Machine Rate ($/min)	$1.29	$1.54	$1.42	$1.40	$1.39	$1.25
Manufactured Line Utilization (%)	0.1%	0.6%	0.4%	1.1%	1.4%	7.1%
Manufactured Machine Rate ($/min)	$134.76	$28.04	$76.16	$28.83	$23.16	$4.81
Line Utilization Used (%)	37.1%	37.6%	37.4%	38.1%	38.4%	44.1%
Manufacturing Rate Used ($/min)	$1.29	$1.54	$1.42	$1.40	$1.39	$1.25

Figure 116. Machine rate parameters for current collector manufacturing process

Annual Production Rate	1,000	10,000	30,000	80,000	100,000	500,000
Material ($/stack)	$7.28	$6.51	$6.44	$6.38	$6.37	$5.76
Manufacturing ($/stack)	$0.15	$0.17	$0.04	$0.04	$0.04	$0.04
Tooling ($/stack)	$0.13	$0.01	$0.01	$0.01	$0.01	$0.01
Secondary Operations ($/stack)	$0.53	$0.53	$0.53	$0.53	$0.53	$0.53
Total Cost ($/stack)	$8	$7	$7	$7	$7	$6
Total Cost ($/kWnet)	$0.10	$0.09	$0.09	$0.09	$0.09	$0.08

Figure 117. Cost breakdown for current collector manufacturing process

8.1.13 Coolant Gaskets/Laser-welding

Coolant gaskets seal between the facing coolant-flow sides of the bipolar plates, around the perimeter of the flow fields, and thus prevent coolant from leaking into the air or hydrogen manifolds. There is a coolant gasket in every repeat unit, plus an extra at the end of the stack. Thus each stack has hundreds of coolant gaskets.

Three methods coolant gaskets methods have been previously analyzed:

- insertion molding to apply the coolant gasket

- screen printing of the coolant gasket

- laser welding

Laser welding of the bipolar plate edges (to eliminate the need of a separate coolant) has been selected for every system analyzed since 2008 and is also selected for the 2016 design.

Laser welding is an option that only applies to use with metallic bipolar plates. The idea of welding two plates together to form a seal is a popular approach in the fuel cell industry and is an alternative to

gasketed or adhesive bonding approaches. Conversations with Richard Trillwood of Electron Beam Engineering of Anaheim, California indicate that grade 316L stainless steel is exceptionally well-suited to laser welding. Additionally, the thinness of the plates allows welding from the plate face, which is significantly quicker and thus less expensive than edge welding around the perimeter. As described in Section 6.6, the laser welding process for the coolant gasket was updated in 2016 to reflect current practices by BPP vendors. The most impactful changes include extension of laser welding length (added 1.5 m length over active area to ensure excellent electrical contact between plates), laser welding speed (decreased from 0.25 m/s in 2015 to 0.125 m/s in 2016), restructuring of the welding equipment (defining the number of laser work heads per station and number of stations per line), and capital cost. Figure 118 details key process parameters.

Annual Production Rate	1,000	10,000	30,000	80,000	100,000	500,000
Equipment Lifetime (years)	12	12	12	12	12	12
Interest Rate	10%	10%	10%	10%	10%	10%
Corporate Income Tax Rate	40%	40%	40%	40%	40%	40%
Capital Recovery Factor	0.191	0.191	0.191	0.191	0.191	0.191
Equipment Installation Factor	1.4	1.4	1.4	1.4	1.4	1.4
Maintenance/Spare Parts (% of CC)	10%	10%	10%	10%	10%	10%
Miscellanous Expenses (% of CC)	12%	12%	12%	12%	12%	12%
Power Consumption (kW)	7	7	7	7	7	7

Figure 118. Coolant gasket laser welding process parameters

Laser welding provides a number of distinct advantages compared to traditional gasketing methods. The welds are extremely consistent and repeatable, and do not degrade over time as some gaskets do. It also has extremely low power requirements, and very low maintenance and material costs. Consumables include argon gas, compressed air, and a cold water supply. Maintenance involves lamp replacement every three months, lens cleaning, and general machine repair. Trillwood suggests that the welding speed is limited to a range of 60 to 100 inches per minute, with a maximum of three parts being welded simultaneously. However, according to *Manufacturing Engineering & Technology*,[97] laser welding speeds range from 2.5m/min to as high as 80 m/min. An average welding speed of 7 m/min (0.125m/s) is selected as a conservative middle value and was also recommended by a BPP vendor in 2016.

Figure 119 shows the machine rate parameters, and Figure 120 shows the cost breakdown.

---

[97] *Manufacturing Engineering & Technology*, by Kalpakjian & Schmid (5th edition), p. 957.

Annual Production Rate	1,000	10,000	30,000	80,000	100,000	500,000
Capital Cost ($/line)	$815,444	$1,031,444	$1,031,444	$1,031,444	$1,031,444	$1,031,444
Parts per station	1	2	2	2	2	2
Effective Cycletime per Welded assembly	9.8	2.2	2.2	2.2	2.2	2.2
Simultaneous Lines	1	1	3	6	7	34
Laborers per Line	0.25	0.25	0.25	0.25	0.25	0.25
Line Utilization	31%	68%	68%	90%	97%	100%
Effective Total Machine Rate ($/hr)	$398.34	$232.94	$232.94	$177.68	$166.63	$162.21
Material Cost ($/kg)	$0.00	$0.00	$0.00	$0.00	$0.00	$0.00

Figure 119. Machine rate parameters for gasket laser-welding process

Annual Production Rate	1,000	10,000	30,000	80,000	100,000	500,000
Material ($/stack)	$0	$0	$0	$0	$0	$0
Manufacturing ($/stack)	$410	$53	$53	$40	$38	$37
Tooling ($/stack)	$0	$0	$0	$0	$0	$0
Total Cost ($/stack)	$410	$53	$53	$40	$38	$37
Total Cost ($/kWnet)	$5.12	$0.66	$0.66	$0.51	$0.47	$0.46

Figure 120. Cost breakdown for coolant gasket laser welding

8.1.14 End Gaskets

The end gaskets are very similar to the coolant gaskets but are sandwiched between the last bipolar plate and the end plate, rather than between two bipolar plates. This means that welding is not an option, as the end plates are non-metallic. They also have a slightly different geometry than the coolant gaskets, due to their function as a seal against reactant gasses rather than the coolant. Like the coolant gaskets, they were initially modeled using insertion molding, but were switched to a screen printing approach beginning in 2008. The largest difference between coolant gaskets and end gaskets is simply the quantity needed; with only two end gaskets per stack, there are far fewer end gaskets than coolant gaskets. Screen printing of the end gaskets is selected for the 2014 design.

Conversations with DEK International confirmed initial SA assumptions and various screen printers were examined for their efficacy at five production levels. To screen print a seal onto a bipolar plate, a single plate, or a pallet holding several plates, is first fed into the machine by conveyor. Once in the screen printer, it is locked into place and cameras utilize fiducial markers on either the plate itself or the pallet for appropriate alignment. A precision emulsion screen is placed over the plates, allowing a wiper to apply the sealing resin. After application, the resin must be UV cured to ensure adequate sealing.

Two different scenarios were examined in the screen printing process. In the first, one plate would be printed at a time, reducing costs by halving the need for handling robots to align plates. It would also avoid the necessity of a pallet to align multiple plates in the screen printer. The second scenario requires two handling robots to place four plates onto prefabricated self-aligning grooves in a pallet, ensuring proper alignment in the screen printer. The advantage of this technique is reduced cycle time per plate. However, it would result in increased capital costs due to more expensive screen printers, increased necessity for handling robots and precise mass-manufacture of pallets. Small variations in the grooves of pallets would lead to failure of the screen printer to align properly or apply the resin appropriately.

Printers: Three different screen printer models were examined as recommended by representatives from the DEK Corporation. The Horizon 01i machine was suggested for one-plate printing. The Europa VI and the PV-1200 were both evaluated for four plate printing. Comparison of the screen printers can be seen in Figure 121. After cost-analysis, it was determined that, despite the reduced cycle time (12.26 second to 4 seconds), the PV-1200 and Europa VI machines were more expensive, even at higher volumes. The Horizon was cheapest at all production levels.

		Screen Printers (DEK)		
Machine		Horizon	Europa VI	PV-1200
Cycle Time	s	9.63	12.26	4
Cost	$	$150,000	$200,000	$1,000,000
Power Consumption	kW	3.5	3.5	0.7
Print Area	in^2	400	841	841

Figure 121. Screen printer comparison

Resin: The selected resin formula is based on information gleaned from the Dana Corporation US patent 6,824,874. The patent outlines several resins that would be suitable to provide an effective seal between bipolar plates and resin "A" was selected for its formulaic simplicity. However, any of the other recommended resins could be substituted with negligible changes in cost and performances.

UV Curing: Following printing, a short conveyor is needed to transfer the printed plate to a UV curing system. Consultation with representatives from UV Fusion Systems Inc. of Gaithersburg, Maryland, along with information from the Dana Corporation resin patent indicated that the VPS 1250 lamp carrying 350 Watt type D and type H+ bulbs[98] would be adequate to cure the resin. If it is only necessary to cure a single plate, then one seven inch type D, and one seven inch type H+ bulb should be used. In order to ensure full UV coverage, for a 24 inch pallet holding four plates, three side-by-side ten inch bulbs of both types would be employed.

Patent research indicates that roughly two seconds of exposure for each type of lamp is sufficient for curing. When using the PV-1200 screen printer the curing time for both lamps matches the cycle time for the screen printer. If using the Horizon printer, the cure time is less than half the cycle time for the printer, yet in both situations the plates could be indexed to match the screen printer cycle time. A shutter would be built into the lamp to block each bulb for half of the time the plate is within the system to ensure adequate exposure of both light types. Rapidly turning the bulbs on and off is more destructive to the bulb life than continuous operation, making a shutter the preferred method of alternating light sources.

Cost estimation for UV curing system includes the cost of lamps, bulbs, power supply rack, light shield to protect operators, and blowers for both lamp operation and heat reduction.

---

[98] Type D and Type H+ bulbs refer to the specific light wavelength emitted. Both wavelengths are needed for curing.

Maintenance: Communication with DEK has indicated that, if properly cared for, the screen printers have a lifetime of twenty years, but on average are replaced after only eight years due to poor maintenance practices. The modeled lifetime is specified as ten years. Regular maintenance, including machine repair, cleaning, and replacement of screens every 10,000 cycles costs an estimated $10,000 per year.

Utilities: Relatively little power is used by the printers. A belt-drive system that collects and releases parts is the primary power consumer of the screen printers. Additional consumption comes from the alignment system, the wiper blade and the screen controls. Depending on the specifications of the individual printer, power consumption varies from 0.7 to 3.5 kW. On the other hand, the UV curing system has higher power demand. The total power usage, ranging from 61 to 166 kW, is primarily consumed by the lamps, but also by the exhaust blowers and the modular blowers for the lamps.

Low Volume Job Shop: Due to the small number of end gaskets required in a stack (2), the machine utilization can be quite low at 1,000 systems per year. Even when a smaller screen printing unit is used, the cost does not go below $52/part at 1,000 systems per year (2,000 parts per year). The table in Figure 122 shows how the cost could be significantly reduced if the part was outsourced to a third party vendor or "Job-Shop". Note that although both the in-house and job-shop costs are labeled as "costs", the job-shop "cost" contains job-shop markup and thus represents their selling price. Job shopping the end gasket component provides the OEM a cost benefit due to the higher utilization of equipment.

Machine	"Small" Machine (Keywell KY-912GL)	"Production" Machine (DEK Horizon)
Projected In-House (1k sys/yr) Cost, $/part	$52.23/part (0.05% util.)	$76.63 (0.16% util.)
Projected Job-Shop (1k sys/yr) Cost, $/part	$0.11/part (37% util.)	$0.50/part (37% util.)

Figure 122. Table showing two types of screen printing machines for "In-House" and "Job-Shop" and the associated cost per part of the end gasket with corresponding machine utilization.

Figure 123 shows the key process parameters, as selected for the end-gasket model. The capital cost includes the cost of the screen printer, plus a UV curing system, plate handling robots, and a conveyor belt. Figure 124 shows the assumed machine rate parameters and Figure 125 the cost breakdown. Being a non-repeat component, the end gasket benefits from lower cost when job shopped, like the end plate and current collector. The machine rate table compares the effective machine rates for in-house manufacture versus job shopping and shows the job shop option to always be less expensive except at 500,000 systems/year.

Annual Production Rate	1,000	10,000	30,000	80,000	100,000	500,000
Equipment Lifetime (years)	15	15	15	15	15	15
Interest Rate	10%	10%	10%	10%	10%	10%
Corporate Income Tax Rate	40%	40%	40%	40%	40%	40%
Capital Recovery Factor	0.175	0.175	0.175	0.175	0.175	0.175
Equipment Installation Factor	1.4	1.4	1.4	1.4	1.4	1.4
Maintenance/Spare Parts (% of CC)	3%	3%	3%	3%	3%	3%
Miscellanous Expenses (% of CC)	12%	12%	12%	12%	12%	12%
Power Consumption (kW)	61	61	61	61	61	61

Figure 123. End gasket screen printing process parameters

Annual Production Rate	1,000	10,000	30,000	80,000	100,000	500,000
Screen Printing Machine Type	DEK Horizon	DEK Horizon	DEK Horizon	DEK Horizon	DEK Horizon	DEK Horizon
Capital Cost ($/line)	$392,735	$392,735	$392,735	$392,735	$392,735	$392,735
Gaskets Printed Simultaneously	1	1	1	1	1	1
Runtime per Gasket (s)	9.62	9.62	9.62	9.62	9.62	9.62
Simultaneous Lines	1	1	1	1	1	1
Laborers per Line	0.25	0.25	0.25	0.25	0.25	0.25
Line Utilization	0.2%	1.6%	4.8%	12.9%	16.2%	80.8%
Effective Total Machine Rate ($/hr)	$28,100	$2,836	$957	$369	$298	$73
Material Cost ($/kg)	$15.19	$15.19	$15.19	$15.19	$15.19	$15.19
Job Shop or Manufactured	Job Shop	Job Shop	Job Shop	Job Shop	Job Shop	Manufactured
Job Shop Line Utilization (%)	37.2%	38.6%	41.8%	49.9%	53.2%	80.8%
Job Shop Machine Rate ($/min)	$3.01	$2.91	$2.71	$2.33	$2.21	$1.57
Manufactured Line Utilization (%)	0.2%	1.6%	4.8%	12.9%	16.2%	80.8%
Manufactured Machine Rate ($/min)	$468.34	$47.27	$15.95	$6.15	$4.97	$1.21
Line Utilization Used (%)	37.2%	38.6%	41.8%	49.9%	53.2%	80.8%
Manufacturing Rate Used ($/min)	$3.01	$2.91	$2.71	$2.33	$2.21	$1.21

Figure 124. Machine rate parameters for end gasket screen printing process

Annual Production Rate	1,000	10,000	30,000	80,000	100,000	500,000
Material ($/stack)	$0.07	$0.07	$0.07	$0.07	$0.07	$0.07
Manufacturing ($/stack)	$0.98	$0.95	$0.88	$0.76	$0.72	$0.39
Tooling ($/stack)	$0.00	$0.00	$0.00	$0.00	$0.00	$0.00
Total Cost ($/stack)	$1.06	$1.02	$0.96	$0.83	$0.79	$0.47
Total Cost ($/kWnet)	$0.01	$0.01	$0.01	$0.01	$0.01	$0.01

Figure 125. Cost breakdown for end gasket screen printing

8.1.15 Stack Compression

Traditional PEM fuel cells use tie-rods, nuts, and Belleville washers to supply axial compressive force to ensure fluid sealing and adequate electrical connectivity. However, the use of metallic compression bands is assumed, as used by Ballard Power Systems and described in US Patent 5,993,987 (Figure 126). Two stainless steel bands of 2 cm width are wrapped axially around the stack and tightened to a pre-determined stack compressive loading, and then the ends of the bands are tack welded to each other. The end plates' low conductivity allows them to act as insulators, to prevent shorting of the stack. Custom recesses in the end plates are used to provide a convenient access to the lower surface of the bands to enable welding. The edges of the bipolar plates do not contact the compressive bands as this would electrically short the stack. The costs are reported as part of the stack assembly section, as shown in Figure 130.
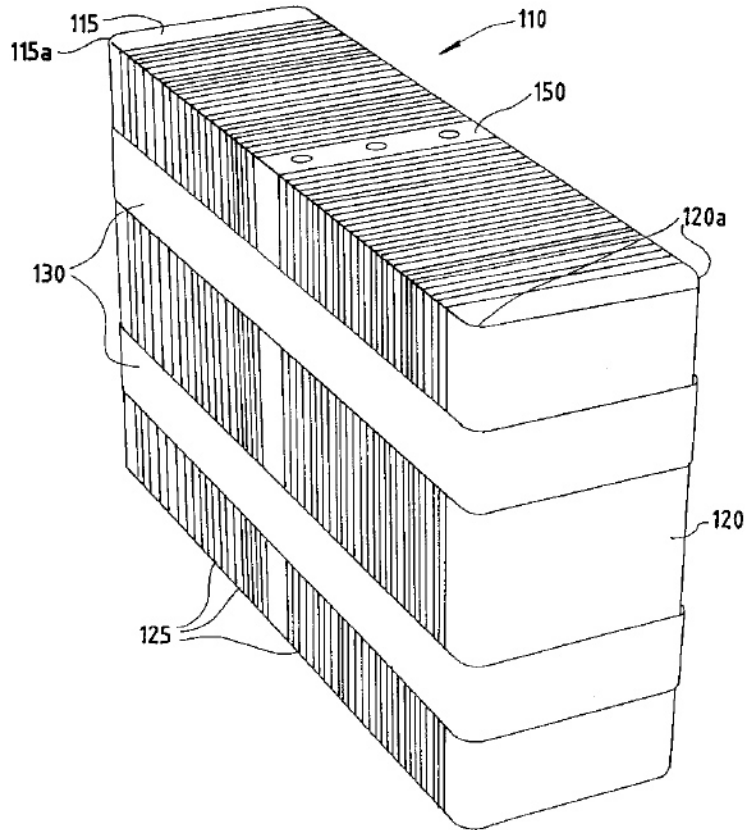
Figure 126. Stack compression bands concept (Figure courtesy of US patent 5,993,987)

8.1.16 Stack Assembly

Stack assembly costs were based on the amortized workstation costs and the estimated times to perform the required actions. Two methods of stack assembly were analyzed: manual and semi-automated.

At the lowest production rate of 1,000 systems per year, manual assembly was selected. Manual assembly consists of workers using their hands to individually acquire and place each element of the stack: end plate, insulator, current collector, bipolar plate, gasketed MEA, bipolar plate, and so on. An entire stack is assembled at a single workstation. The worker sequentially builds the stack (vertically) and then binds the cells with metallic compression bands. The finished stacks are removed from the workstation by conveyor belt.

At higher production levels, stack assembly is semi-automatic, requiring less time and labor and ensuring superior quality control. This is termed "semi-automatic" because the end components (end plates, current conductors, and initial cells) are assembled manually but the ~378 active cell repeat units are assembled via automated fixture. Figure 127 details the layout of the assembly workstations and Figure 128 and Figure 129 list additional processing parameters.
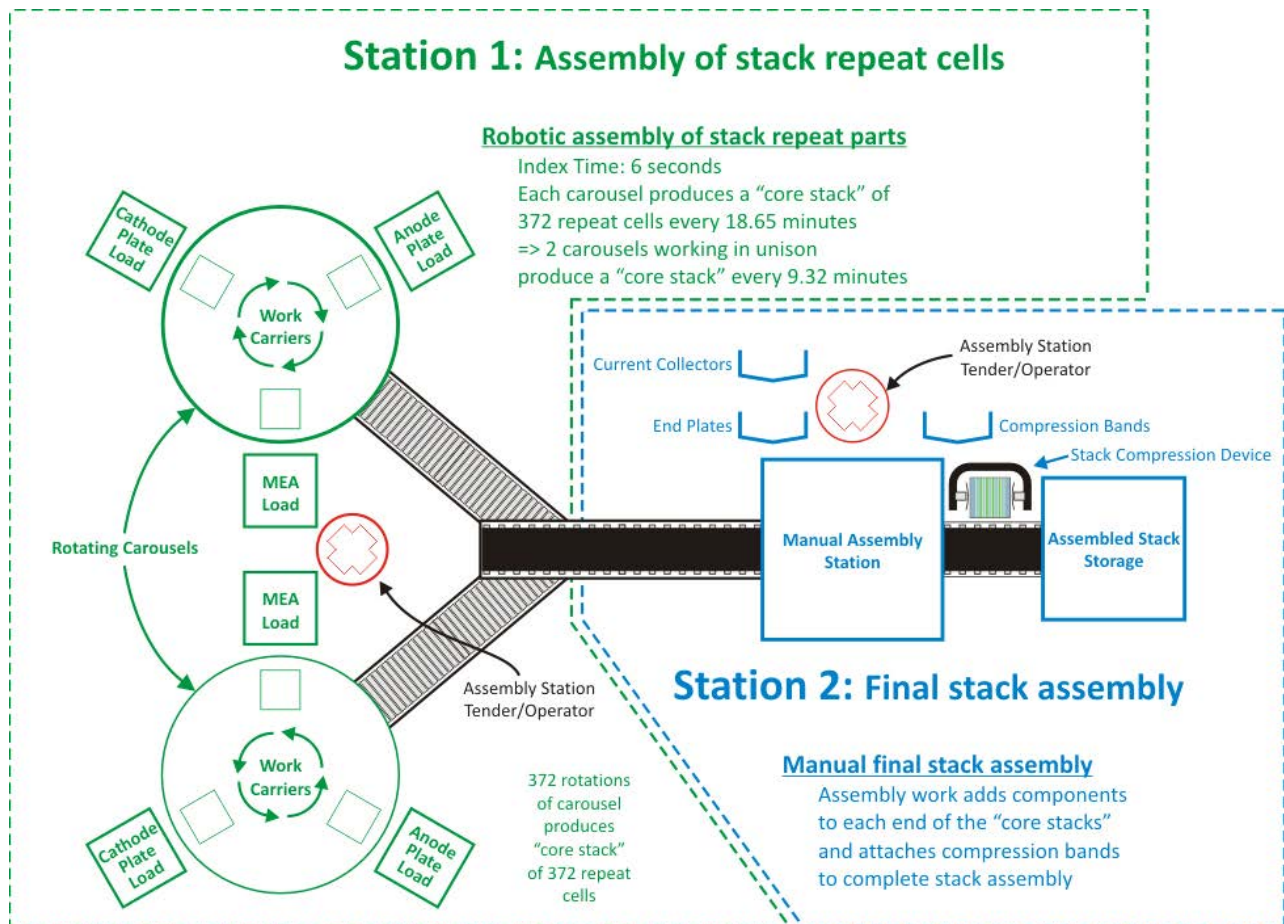
Figure 127. Semi-automated stack assembly work flow diagram

Following assembly, each stack is transported to a leak-check station where the three sets of fluid channels (hydrogen, air, and coolant) are individually pressurized with gas and monitored for leaks. This test is very brief and meant only to verify gas and liquid sealing. Full performance testing of the stack will occur during stack conditioning.

As shown in Figure 130, stack assembly is quite inexpensive, ranging from $1.00/kW$_{net}$ at the most to only $0.42/kW$_{net}$. The only material costs are those of the compressive metal bands.

Annual Production Rate	1,000	10,000	30,000	80,000	100,000	500,000
Equipment Lifetime (years)	5	15	15	15	15	15
Interest Rate	10%	10%	10%	10%	10%	10%
Corporate Income Tax Rate	40%	40%	40%	40%	40%	40%
Capital Recovery Factor	0.306	0.175	0.175	0.175	0.175	0.175
Equipment Installation Factor	1.4	1.4	1.4	1.4	1.4	1.4
Maintenance/Spare Parts (% of CC)	10%	10%	10%	10%	10%	10%
Miscellanous Expenses (% of CC)	7%	7%	7%	7%	7%	7%
Power Consumption (kW)	1	7	7	7	7	7

Figure 128. Stack assembly process parameters

Annual Production Rate	1,000	10,000	30,000	80,000	100,000	500,000
Assembly Method	Manual	Semi-Auto	Semi-Auto	Semi-Auto	Semi-Auto	Semi-Auto
Capital Cost ($/line)	$11,212	$821,339	$821,339	$821,339	$821,339	$821,339
Simultaneous Lines	1	2	4	9	11	52
Laborers per Line	1.00	0.25	0.25	0.25	0.25	0.25
Line Utilization	48.9%	51.8%	77.6%	92.0%	94.1%	99.5%
Effective Total Machine Rate ($/hr)	$48.97	$174.65	$120.53	$103.56	$101.53	$96.64
Index Time (min)	98	21	21	21	21	21

Figure 129. Machine rate parameters for stack assembly process

Annual Production Rate	1,000	10,000	30,000	80,000	100,000	500,000
Compression Bands ($/stack)	$0	$0	$0	$0	$0	$0
Assembly ($/stack)	$80	$61	$42	$36	$35	$34
Total Cost ($/stack)	$80	$61	$42	$36	$35	$34
Total Cost ($/kWnet)	$1.00	$0.76	$0.52	$0.45	$0.44	$0.42

Figure 130. Cost breakdown for stack assembly

8.1.17 Stack Housing

The stack insulation housing is a plastic housing that encases the stack. It is meant primarily for protection from physical damage caused by road debris and liquids, as well as for protection from electrical shorting contacts and a small amount of thermal insulation. It is modeled as vacuum-thermoformed polypropylene. It is 0.5 cm thick, and is separated from the stack by a 1 cm gap. At high production rate, the cycle time is seven seconds: three for insertion, and four for the vacuum thermoforming. Processing parameters are shown in Figure 131 and Figure 132. A cost breakdown of the stack housing production is shown below in Figure 133.

Annual Production Rate	1,000	10,000	30,000	80,000	100,000	500,000
Equipment Lifetime (years)	8	8	8	15	15	15
Interest Rate	10%	10%	10%	10%	10%	10%
Corporate Income Tax Rate	40%	40%	40%	40%	40%	40%
Capital Recovery Factor	0.229	0.229	0.229	0.175	0.175	0.175
Equipment Installation Factor	1.4	1.4	1.4	1.4	1.4	1.4
Maintenance/Spare Parts (% of CC)	5%	5%	5%	5%	5%	5%
Miscellanous Expenses (% of CC)	6%	6%	6%	6%	6%	6%
Power Consumption (kW)	30	30	30	35	35	40

Figure 131. Stack housing vacuum thermoforming process parameters

Annual Production Rate	1,000	10,000	30,000	80,000	100,000	500,000
Capital Cost ($/line)	$50,000	$50,000	$50,000	$250,000	$250,000	$655,717
Costs per Tooling Set ($)	$96,352	$96,352	$96,352	$96,352	$96,352	$96,352
Tooling Lifetime (years)	3	3	3	3	3	3
Cavities per platen	1	1	1	1	1	1
Total Cycle Times (s)	71	71	71	15	15	7
Simultaneous Lines	1	1	1	1	1	1
Laborers per Line	1.00	1.00	1.00	1.00	1.00	0.25
Line Utilization	0.6%	5.9%	17.7%	10.1%	12.6%	28.9%
Effective Total Machine Rate ($/hr)	$1,136.85	$156.88	$84.29	$310.80	$258.32	$253.68
Material Cost ($/kg)	$1.48	$1.48	$1.48	$1.48	$1.48	$1.48

Figure 132. Machine rate parameters for stack housing vacuum thermoforming process

Annual Production Rate	1,000	10,000	30,000	80,000	100,000	500,000
Material ($/stack)	$6	$6	$6	$6	$6	$6
Manufacturing ($/stack)	$22	$3	$2	$1	$1	$0
Tooling ($/stack)	$36	$4	$1	$0	$0	$0
Total Cost ($/stack)	$64	$13	$9	$8	$7	$6
Total Cost ($/kWnet)	$0.81	$0.16	$0.11	$0.09	$0.09	$0.08

Figure 133. Cost breakdown for stack housing

8.1.18 Stack Conditioning and Testing

PEM fuel cell stacks have been observed to perform better in polarization tests if they first undergo "stack conditioning." Consequently, a series of conditioning steps are modeled based on a regulation scheme discussed in GM Global Technology Operations LLC's (subsidiary of General Motors (GM)) US patent 9,099,703 B2.[99] The GM patent describes voltage variation (current cycling), a fuel/oxidant stoichiometry, and temperature for conditioning. The conditioning would occur immediately after stack assembly at the factory. Because the conditioning process finishes with a final performance verification, the conditioning process also serves a stack quality control purpose and no further system checkout is required.

Figure 134 details the stack conditioning steps. The GM patent states that while prior-art conditioning times were 1-15 hours, the GM accelerated break-in methodology is able to achieve 70% of the performance benefit in 1.5 hours (with expectation of achieving 100% performance after additional hours). Two hours of conditioning time is selected for cost modeling.

---

[99] US Patent 9,099,703 B2, Rapaport et. al., "Fast MEA Break-In and Voltage Recovery", August 4, 2015.

Step	Description	H$_2$ Stoic.	Air Stoic.	Temp(°C)	Voltage (V)	Current Density (A/cm^2)
1	Shorting check (prior to voltage cycling)					
2	Room temp voltage cycling: Once voltage stops increasing, move to step 3, otherwise repeat step 2.	1.5	1.1	22	0.1-0.4	0.1-0.2
3	35°C voltage cycling: Once voltage stops increasing, move to step 4, otherwise repeat step 3.	1.5	1.1	35	0.1-0.4	0.2-0.3
4	50°C voltage cycling: Once voltage stops increasing, move to step 5, otherwise repeat step 4.	1.5	1.1	50	0.1-0.4	0.3-0.4
5	65°C voltage cycling: Once voltage stops increasing, move to step 6, otherwise repeat step 5.	1.5	1.1	65	0.1-0.4	0.4-0.5
6	80°C voltage cycling: Once voltage stops increasing, move to step 7, otherwise repeat step 6.	1.5	1.1	80	0.1-0.4	0.5-0.7
7	95°C voltage cycling: Once voltage stops increasing, move to step 8, otherwise repeat step 7.	1.5	1.1	95	0.1-0.4	0.7-0.85
8	Performance verification: If performance level adequate, move to step 9, otherwise, repeat step 7 and 8.					
9	H$_2$ Take-over test: confirm absence of cross-over leaks after voltage cycling					

Figure 134. Stack conditioning process based on US patent 9,099,703 B2 ("Fast MEA Break-In and Voltage Recovery")

Conditioning cost is based on proprietary capital cost quotation of a programmable load bank to run the stacks up and down the polarization curve according to the power-conditioning regimen. The fuel cells load banks are assumed to condition two stacks simultaneously (between 30k and 100k systems per year production) and eight stacks simultaneously at 500k systems per year. Since the stacks can be staggered in starting time, peak power can be considerably less than 2 or 8 times the individual stack rated power of ~88.2 kW$_{gross}$. It is estimated that simultaneous peak power would be approximately 270 kW at 500,000 fuel cell systems per year. Hydrogen usage is estimated based on 50% fuel cell efficiency and $3/kg hydrogen. SA's standard machine rate methodology yields machine rates as low as $0.28/min for each load bank. Process parameters are shown in Figure 135 and Figure 136. Total costs for stack conditioning are shown in Figure 137. Note that considerable power is generated, and rather than dumping the load to a resistor bank, it may be advantageous to sell the electricity back to the grid. This would require considerable electrical infrastructure and is expected to provide only a relatively small benefit; sale of electricity to the grid is not included in our cost estimates.

Annual Production Rate	1,000	10,000	30,000	80,000	100,000	500,000
Equipment Lifetime (years)	19	19	19	19	19	19
Interest Rate	10%	10%	10%	10%	10%	10%
Corporate Income Tax Rate	40%	40%	40%	40%	40%	40%
Capital Recovery Factor	0.159	0.159	0.159	0.159	0.159	0.159
Equipment Installation Factor	1.4	1.4	1.4	1.4	1.4	1.4
Maintenance/Spare Parts (% of CC)	10%	10%	10%	10%	10%	10%
Miscellanous Expenses (% of CC)	7%	7%	7%	7%	7%	7%
Power Consumption (kW)	2	2	2	2	2	9

Figure 135. Stack conditioning process parameters

Annual Production Rate	1,000	10,000	30,000	80,000	100,000	500,000
Capital Cost ($/line)			Proprietary			
Simultaneous Lines	1	2	6	14	18	22
Laborers per Line	0.1	0.1	0.1	0.1	0.1	0.1
Line Utilization	99.2%	86.8%	86.8%	99.2%	96.5%	98.6%
Effective Total Machine Rate ($/hr)	$30.19	$17.86	$17.72	$16.24	$16.50	$51.35
Test Duration (hrs)	2	2	2	2	2	2

Figure 136. Machine rate parameters for stack conditioning process

Annual Production Rate	1,000	10,000	30,000	80,000	100,000	500,000
Conditioning/Testing ($/stack)	$60	$18	$18	$16	$16	$13
Total Cost ($/stack)	$60	$18	$18	$16	$16	$13
Total Cost ($/kWnet)	$0.75	$0.22	$0.22	$0.20	$0.21	$0.16

Figure 137. Cost breakdown for stack conditioning

8.2 Balance of Plant (BOP)

While the stack is the heart of the fuel cell system, many other components are necessary to create a functioning system. In general, our cost analysis utilizes a DFMA®-style analysis methodology for the stack but a less detailed methodology for the balance of plant (BOP) components. Each of the BOP components is discussed below along with its corresponding cost basis.

8.2.1 Air Loop

The air loop of the fuel cell power system consists of five elements:

- Air Compressor, Expander and Motor (CEM) Unit
- Air Mass Flow Sensor
- Air Filter and Housing
- Air Ducting

These components are described in the subsections below. The cost breakdown is shown below in Figure 138.

Annual Production Rate	1,000	10,000	30,000	80,000	100,000	500,000
Filter and Housing ($/system)	$56	$56	$56	$56	$56	$56
Compressor, Expander & Motor ($/system)	$1,591	$1,178	$884	$752	$729	$708
Mass Flow Sensor ($/system)	$21	$19	$17	$13	$12	$10
Air Ducting ($/system)	$136	$132	$130	$124	$118	$112
Air Temperature Sensor ($/system)	$10	$9	$8	$6	$6	$5
Total Cost ($/system)	$1,813	$1,394	$1,095	$951	$920	$891
Total Cost ($/kW$_{net}$)	$22.67	$17.42	$13.69	$11.89	$11.50	$11.13

Figure 138. Cost breakdown for air loop

8.2.1.1 *Compressor-Expander-Motor Unit & Motor Controller*

The air compression system is envisioned as an integrated air compressor, exhaust gas expander, and permanent magnet motor. An electronic CEM controller is also included in the system. For the 2015 system analysis, the CEM is based on a Honeywell design for a high rpm, centrifugal compressor, radial inflow expander integrated unit.

In the 2008 and prior year system cost analyses, the fuel cell CEM unit was based on a multi-lobe compressor and expander from Opcon Autorotor of Sweden with cost based on a simplified DFMA® analysis in which the system was broken into seven cost elements: wheels/lobes, motor, controller, case, bearings, variable geometry, and assembly/test.

For the 2009 analysis, an all-new, extremely detailed CEM cost estimate was conducted in collaboration with Honeywell. It is a bottom-up cost analysis based directly on the blueprints from an existing Honeywell design, which pairs a centrifugal compressor and a radial-inflow expander, with a permanent-magnet motor running on air bearings at 100,000 rpm. After analyzing the base design, engineers from both SA and Honeywell simplified and improved the design to increase its performance and lower cost, to better reflect a mass-production design. Ultimately, six different configurations were examined; three main configurations, plus a version of each without an expander.

The six different configurations examined are listed in Figure 139. "Design #1" is based on an existing Honeywell design, which runs at 100,000 rpm. Design #2 is an optimized version of Design #1 running at 165,000 rpm, in order to reduce its size. Design #3 is a further-optimized future system, based on Design #2 but with slightly more aggressive design assumptions. Designs #4, 5, and 6 are identical to Designs #1, 2, and 3 respectively, but with the expander removed.

	Baseline: 100k rpm	Current: 165k rpm	Future: 165k rpm
With Expander	Design 1	Design 2 (2015 cost estimate)	Design 3
Without Expander	Design 4	Design 5	Design 6

Figure 139. Matrix of CEM design configurations

The cost estimate utilizes a combination of DFMA® methodology and price quotes from established Honeywell vendors. Excluding repeat parts, the existing Honeywell turbocompressor design (Design #1) has 104 different components and assemblies. Each of these components is categorized into one of three different tiers. "Tier 1" consists of the 26 largest/most-significant components in need of the most careful cost analysis. "Tier 2" corresponds to the 42 mid-level components for which a vendor quote is sufficient. The "Tier 3" components are the minor components such as screws and adhesives that are insignificant enough that educated guesses are sufficient in lieu of vendor quotes. Honeywell engineers solicited price quotes from their existing supplier base for components in the top two tiers, as well as for some of the components in Tier 3, and supplied these values to SA for review and analysis.

In some cases, the high-volume quotes were judged to be inappropriate, as they were merely based on repeated use of low-production-rate manufacturing methods rather than low-cost, high-manufacturing-rate production and assembly methods. Consequently, these quotes were replaced with cost estimates based on a mix of DFMA® techniques and our best judgment.

After having completed the initial cost summation for Design #1, the unit costs seemed prohibitively high. Consequently, Honeywell engineers reviewed their design and created a list of potential improvements. SA augmented the list with some ®-based suggestions, the list was vetted by both parties, and the design changes incorporated into the cost model. Changes deemed reasonable to describe as "current technology" were applied to Design #2, and the more aggressive improvements were used to define Design #3. The most important of these improvements is the switch from 100,000 to 165,000 rpm, which facilitates a reduction in the size of the CEM by roughly 35%, thereby saving greatly on material (and to a lesser extent, manufacturing) costs, while also providing the intrinsic benefits of reduced size. These improvements are listed in Figure 140, showing that Design #2 is used for the 2015 cost estimate.

Each of the six CEM designs was analyzed across the range of five production rates (1,000 to 500,000 systems per year): this yields 30 different cost estimates for each of the 100+ components. Summed together, they provide 30 different estimates for the CEM cost. The five Design #2 estimates provide the compressor costs across the range of production rates.

For the 2010 update, the CEM cost model was fully integrated into the fuel cell system cost model, and adjusted to scale dynamically based on the pressure and power requirements of the system. This was achieved via a complex system of multipliers that are applied differently for almost every different component since there are a wide variety of combinations and permutations for costing methods across the range of components, and not everything scales at the same rate. For example, as the pressure ratio increases and the CEM increases in size, the diameter of the turbine wheel increases, and its volume increases at a rate proportional to the square of its diameter. The diameter of the compressor wheel scales at a different rate than that of the turbine (expander) wheel, and the shaft length and motor mass each scale at yet another rate. The geometric scaling factors were derived from data that Honeywell provided showing dimensions of key components across a range of performance parameters such as pressure ratio, mass flow rate, and shaft power.

		2015 Cost Estimate				
Design #	1	2	3	4	5	6
	With Expander			Without Expander		
	Baseline (100k rpm)	Current (165k rpm)	Future (165k rpm)	Baseline (100k rpm)	Current (165k rpm)	Future (165k rpm)
Removed Turbine (Expander)	[Baseline System Design]			x	x	x
Increased speed from 100,000 to 165,000 rpm		x	x		x	x
Improved turbine wheel design		x	x		x	x
Improved variable nozzle technology		x	x		x	x
Lower cost electrical connectors		x	x		x	x
Design change to integrate housing into single casting			x			x
Integrate/eliminate mounting bosses on main housing			x			x
compressor housing design change to re-route cooling air over motor			x			x
Improved foil bearing design			x			x
Back-to-back compressor wheel			x			x
Removed washers/face bolts			x			x
Improved bearing installation/design			x			x
Impreoved labryinth seal			x			x
Changed fasterns to more common, inexpensive design			x			x
Changed threaded inserts to more common, inexpensive design			x			x
Reduced testing of machine/cast parts			x			x
Aluminum turbine wheel			x			x

Figure 140. List of Improvements for the 6 compressor configurations

The materials cost of each component increases proportionately with the volume of material needed, and the manufacturing costs scale separately, at rates dependent on the manufacturing processes involved and the specifics of each process.

For components whose cost estimates are derived partially or completely from price quotes rather than full DFMA® analysis (such as those in Tier 2 and Tier 3), assumptions were made about the fractional split between the component's material and manufacturing costs, so that each fraction can be scaled independently.

With this new scaling and integration into the main fuel cell system cost model, the size and cost of the CEM now scale dynamically based on the performance requirements of the system. So if a new electrical component is added to the BOP that increases the parasitic load (and thus increases the gross power required), the CEM will automatically scale to accommodate.

The SA/Honeywell CEM analysis also examined the motor controller, for which the same design was deemed applicable to control all six compressor designs. Unlike with the custom parts involved in the

compressor, the motor controller uses almost exclusively off-the-shelf parts that are already manufactured at high volume. As such, there is limited value in conducting a detailed DFMA® analysis, so the cost analysis is primarily based on vendor quotation. The original Honeywell controller design was a standalone unit with its own air or water cooling. However, in order to cut costs, it is now assumed that the CEM controller is integrated into the water-cooled electronics housing for the overall fuel cell system controller. Thirty percent of the controller base cost is assumed to correspond to logic functions, with the remaining 70% corresponding to power management. Accordingly, to scale the controller cost for different input powers (as is necessary when varying stack operating parameters to determine the lowest possible system cost), the 30% of the baseline controller cost (i.e. the portion for logic circuitry) is held at a constant cost, the remaining 70% of baseline cost (i.e. the portion for power management) is assumed to scale linearly with input power.

The CEM and motor controller costs for the various configurations are shown below in Figure 141 for the various 2016 system CEM options. Design 2 is selected for the 2016 cost analysis. Note that the costs at 10k and 30k systems per year are reported as identical values. This is a slight inaccuracy based on not scaling the 10k/year cost estimates.

8.2.1.2   Air Mass Flow Sensor
A high-performance (~2% signal error) automotive hot-wire mass flow sensor is used for measuring the air flow rate into the fuel cell system. Since these devices are already produced in very high quantities, little change in cost is expected between high and low production rates.

8.2.1.3   Air Ducting
The air ducting is modeled as conformal polymer tubes to guide the cathode air in and out of the stack.

8.2.1.4   Air Filter and Housing
Some fuel cell manufacturers filter inlet air both for particles and for volatile organic compounds. However, while particle filters are needed, it is not clear that VOC filters are necessary. Consequently, a standard automotive air particle filter and polymer filter housing are assumed.

| Design | Sys/yr | 2016 CEM | | | 2016 Motor Controller | | | 2016 Total |
		Cost	Assy	Markup	Cost	Assy	Markup	Cost
Design #1 Baseline Tech. 100,000 RPM	1,000	$1,297.35	$23.00	15%	$458.02	$7.67	10%	$2,030.66
	10,000	$571.20	$11.50		$380.94	$3.83		$1,093.36
	30,000	$571.20	$11.50		$380.94	$3.83		$1,093.36
	80,000	$444.60	$11.50		$368.43	$3.83		$934.00
	100,000	$437.26	$11.50		$351.96	$3.83		$907.45
	500,000	$426.02	$11.50		$339.82	$3.83		$881.17
Design #2 Current Tech. 165,000 RPM	1,000	$914.73	$23.00	15%	$458.02	$7.67	10%	$1,590.64
	10,000	$389.41	$11.50		$380.94	$3.83		$884.30
	30,000	$389.41	$11.50		$380.94	$3.83		$884.30
	80,000	$286.72	$11.50		$368.43	$3.83		$752.45
	100,000	$281.97	$11.50		$351.96	$3.83		$728.86
	500,000	$275.03	$11.50		$339.82	$3.83		$707.53
Design #3 Future Tech. 100,000 RPM	1,000	$776.29	$23.00	15%	$458.02	$7.67	10%	$1,431.43
	10,000	$339.95	$11.50		$380.94	$3.83		$827.42
	30,000	$339.95	$11.50		$380.94	$3.83		$827.42
	80,000	$245.14	$11.50		$368.43	$3.83		$704.63
	100,000	$241.01	$11.50		$351.96	$3.83		$681.76
	500,000	$234.96	$11.50		$339.82	$3.83		$661.45
Design #4 Baseline Tech. 100,000 RPM No Expander	1,000	$941.36	$23.00	15%	$458.02	$7.67	10%	$1,621.27
	10,000	$377.70	$11.50		$380.94	$3.83		$870.83
	30,000	$377.70	$11.50		$380.94	$3.83		$870.83
	80,000	$262.37	$11.50		$368.43	$3.83		$724.44
	100,000	$258.58	$11.50		$351.96	$3.83		$701.96
	500,000	$253.32	$11.50		$339.82	$3.83		$682.57
Design #5 Current Tech. 165,000 RPM No Expander	1,000	$753.04	$23.00	15%	$458.02	$7.67	10%	$1,404.70
	10,000	$282.10	$11.50		$380.94	$3.83		$760.90
	30,000	$282.10	$11.50		$380.94	$3.83		$760.90
	80,000	$185.59	$11.50		$368.43	$3.83		$636.14
	100,000	$182.87	$11.50		$351.96	$3.83		$614.90
	500,000	$178.81	$11.50		$339.82	$3.83		$596.87
Design #6 Future Tech. 100,000 RPM No Expander	1,000	$628.25	$23.00	15%	$458.02	$7.67	10%	$1,261.19
	10,000	$244.86	$11.50		$380.94	$3.83		$718.06
	30,000	$244.86	$11.50		$380.94	$3.83		$718.06
	80,000	$155.88	$11.50		$368.43	$3.83		$601.98
	100,000	$153.71	$11.50		$351.96	$3.83		$581.37
	500,000	$150.42	$11.50		$339.82	$3.83		$564.23

Figure 141. CEM cost results

8.2.2 Humidifier & Water Recovery Loop

The humidifier and water recovery loop consists of three components:

- Air precooler
- Demister
- Humidifier

Total subsystem cost is shown in Figure 142. Further details of each subsystem component appear below.

Annual Production Rate	1,000	10,000	30,000	80,000	100,000	500,000
Air Precooler ($/system)	$32	$32	$32	$32	$32	$32
Demister ($/system)	$119	$22	$13	$9	$8	$6
Membrane Air Humidifier ($/system)	$1,025	$221	$113	$87	$78	$52
Total Cost ($/system)	$1,176	$274	$158	$128	$119	$90
Total Cost ($/kW$_{net}$)	$14.70	$3.43	$1.98	$1.60	$1.48	$1.13

Figure 142. Cost breakdown for humidifier & water recovery loop

8.2.2.1 Air Precooler

The air precooler sits between the air compressor and the membrane humidifier, where it cools the hot compressed air to the humidifier's optimal inlet temperature. The design is based on the ANL-supplied key parameters for a compact liquid/air cross-flow intercooler, and the dimensions are scaled based on the specific heat transfer requirements. The unit is 100% aluminum and uses an array of 0.4-mm-thick tubes with 0.08-mm-thick fins spaced at 24 fins per inch, which cool the air with a very minimal pressure drop (0.1 psi). Because the cost impact of the precooler is small, a full DFMA® analysis was not conducted. Instead, the mass and volume of the radiator core were determined by heat transfer calculations conducted at ANL, and the materials cost of the unit was estimated based on detailed geometry assumptions and the cost of aluminum ($6.82/kg). The materials cost was then simply doubled to account for the cost of manufacturing. As a result of this simplified costing methodology, air precooler cost does not vary with annual production rate. Air precooler cost is detailed in Figure 143.

Annual Production Rate	1,000	10,000	30,000	80,000	100,000	500,000
Material ($/system)	$16	$16	$16	$16	$16	$16
Manufacturing ($/system)	$16	$16	$16	$16	$16	$16
Total Cost ($/system)	$32	$32	$32	$32	$32	$32
Total Cost ($/kWnet)	$0.40	$0.40	$0.40	$0.40	$0.40	$0.40

Figure 143. Cost breakdown for air precooler

8.2.2.2 Demister

The demister removes liquid water droplets from the cathode exhaust stream and thereby prevents erosion of the turbine blades. Designed by SA, the demister's housing consists of two threaded, hollow 2-mm-thick polypropylene frustums that unscrew from one another to allow access to the filter inside. The filter is a nylon mesh Millipore product designed for water removal and cost $5.84 each at high volume (assuming 81 cm^2 per demister). The polypropylene adds only ~10 cents of material cost per part, and at high volume, the injection molding process is only 15 cents per part. Because the housing is so inexpensive, the filter dominates the total demister cost ($6.30/demister, or $0.08/kW$_{net}$ at 500,000 systems per year).

Figure 144 and Figure 145 show demister processing parameters. Figure 146 details demister cost results.

Annual Production Rate	1,000	10,000	30,000	80,000	100,000	500,000
Equipment Lifetime (years)	15	15	15	15	15	15
Interest Rate	10%	10%	10%	10%	10%	10%
Corporate Income Tax Rate	40%	40%	40%	40%	40%	40%
Capital Recovery Factor	0.175	0.175	0.175	0.175	0.175	0.175
Equipment Installation Factor	1.4	1.4	1.4	1.4	1.4	1.4
Maintenance/Spare Parts (% of CC)	5%	5%	5%	5%	5%	5%
Miscellanous Expenses (% of CC)	6%	6%	6%	6%	6%	6%
Power Consumption (kW)	21	21	21	21	21	21

Figure 144. Demister injection molding process parameters

Annual Production Rate	1,000	10,000	30,000	80,000	100,000	500,000
Capital Cost ($/line)	$288,522	$288,522	$288,522	$288,522	$288,522	$288,522
Costs per Tooling Set ($)	$16,193	$16,193	$16,193	$16,193	$16,193	$16,193
Tooling Lifetime (cycles)	1,000,000	1,000,000	1,000,000	1,000,000	1,000,000	1,000,000
Cavities per platen	1	1	1	1	1	1
Total Cycle Time (s)	6	6	6	6	6	6
Simultaneous Lines	1	1	1	1	1	1
Laborers per Line	0.50	0.50	0.50	0.50	0.50	0.50
Line Utilization	0.1%	0.6%	1.6%	4.3%	5.4%	26.5%
Effective Total Machine Rate ($/hr)	$27,124.97	$5,219.18	$1,895.87	$756.53	$616.26	$162.10
Material Cost ($/kg)	$1.33	$1.33	$1.33	$1.33	$1.33	$1.33

Figure 145. Machine rate parameters for demister injection molding process

Annual Production Rate	1,000	10,000	30,000	80,000	100,000	500,000
Material ($/system)	$12	$11	$10	$7	$7	$6
Manufacturing ($/system)	$102	$10	$3	$1	$1	$0
Tooling ($/system)	$4	$0	$0	$0	$0	$0
Total Cost ($/system)	$119	$22	$13	$9	$8	$6
Total Cost ($/kWnet)	$1.49	$0.27	$0.17	$0.11	$0.10	$0.08

Figure 146. Cost breakdown for demister

8.2.2.3 *Membrane Humidifier*

The 2012 and prior year cost analyses were based on a tubular membrane design from Perma Pure LLC (model FC200-780-7PP) as shown in Figure 147.
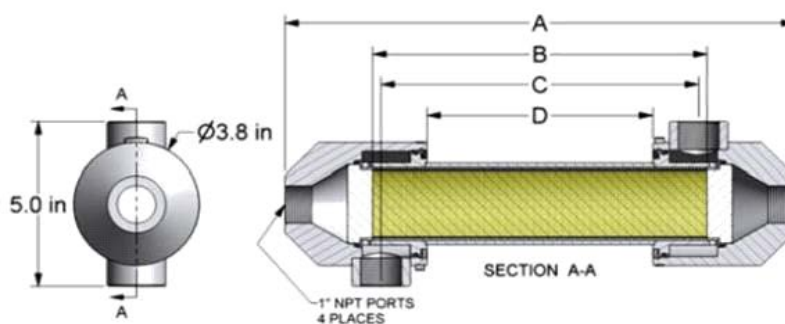
Figure 147. Perma Pure FC200-780-7PP humidifier

In 2013, the plate frame air humidifier was examined as a potentially lower cost and smaller volume alternative to the previously modeled tubular membrane humidifier. Compared to tubular membrane designs, the plate frame membrane humidifiers allow a thinner membrane (5 microns) to be used. Since membrane thickness correlates with required membrane area for a given amount of water transport, plate frame humidifiers are expected to be more compact and lower cost than tubular humidifiers.

The design and projected manufacturing methods for the 2013-2016 plate frame humidifier are based on publicly available information from W.L Gore & Associates, Inc. and dPoint Technologies Inc.[100] Both companies were consulted and provided input during the cost analysis process but information transfer was entirely public domain and non-proprietary. The resulting design is thus a Strategic Analysis Inc. interpretation of the Gore/dPoint Technologies unit and may differ in design and manufacturing process from the actual unit. However, it is expected that the key cost influencing aspects have been adequately captured in the cost analysis.

The modeled Gore plate frame humidifier design is composed of multiple stacked cell pouches made of a 4-layer composite membrane with stainless steel flow fields inside the pouch and stainless steel rib spacers between each pouch in the stack. The total process consists of eight steps:

1. Fabrication of Composite Membranes
2. Fabrication of Stainless Steel Flow Fields and Separators
3. Pouch Formation
4. Stainless Steel Rib Formation
5. Stack Formation
6. Formation of the Housing
7. Assembly of the Composite Membrane and Flow Fields into the Housing
8. System Testing

---

[100] Johnson, William B. "Materials and Modules for Low-Cost, High Performance Fuel Cell Humidifiers," W.L. Gore & Associates, Inc., presentation at the 2012 DOE Hydrogen and Fuel Cell Program Annual Merit Review, Washington, DC, 17 May 2012.

The cost for the membrane humidifier is estimated to be about $52 for a 36-cell pouch stack (sized for an 80-kWe automotive fuel cell system operating at 1.4 air stoichiometry) including housing, assembly, and testing at 500,000 systems per year. Over 50% of the total cost is attributed to materials, primarily the composite membrane.

2016 cost results are based on a humidifier containing 0.7 m^2 of membrane area (0.57m^2 x 1.25 oversizing for degradation) based on ANL modeling analysis for membrane water transport at the 2016 fuel cell operating conditions. Much discussion surrounded selection of this membrane area.

Past analysis has sought to reconcile various estimates of required humidifier membrane area. Separately funded experimental testing was conducted at Ford on the Gore/dPoint humidifier and showed very good correlation with ANL modeling predictions.[101] Both experimental and modeling results showed that ~2m^2 of humidifier membrane area was required for an 80kWe fuel cell system at the 2013 DOE specified operating conditions. However, when ANL applied their performance model at the 2013 SA/ANL specified system operating conditions, the required membrane area dropped to 0.5m^2. This significant membrane area reduction was due primary to higher pressure, lower air flow, and higher temperature conditions included in the model. Additionally, Gore raised a concern that membrane performance degradation was not factored into any of the modeled estimates. Consequently, in 2013 a value of 1.6m^2 humidifier membrane area was selected for SA cost modeling to reflect both a deliberate humidifier oversizing (to offset the expected but quantitatively unknown rate of degradation) and a conservative estimate. dPoint was consulted on this area selection and expressed acceptance. Gore continues to prefer the use of 2 m^2 membrane area (or even greater). In 2014, the automotive fuel cell air stoichiometric ratio increased from 1.5 to 2, therefore the amount of membrane area was linearly scaled from 1.6m^2 at air stoic of 1.5 to 2.13m^2 at air stoic 2. In 2015, the air stoic went back down to 1.5, although SA did not scale with stoic but rather used a calculated membrane area provided by ANL (0.92m^2). SA added a 1.25 oversizing factor to account for degradation over the life of the humidifier, yielding 1.15m^2 for the 2015 baseline total humidifier area. In 2016, ANL's optimized operating conditions resulted in a 1.4 air stoich with decreased humidity at the cathode inlet (from 82% RH in 2015 down to 68% RH in 2016). The dispersed d-PtNi$_3$/C dispersed catalyst experimental testing results have shown improved performance at low RH and due to acid washing of CCM (see Section 0). The addition of 1.25 oversizing factor is still included for the 2016 baseline (0.57 m^2 x 1.25 = 0.7 m^2).

For the automotive application, the modeled design is composed of 36 "cell pouches" where each cell pouch is a loop of membrane with a metal spacer within the loop. The dimension of each cell pouch is 10cm by 10cm, summing to a total humidifier membrane area of 0.7 m^2. The cell pouches allow dry primary inlet air to flow through the inside of the pouch and humid secondary outlet oxygen-depleted air from the cathode to flow cross-wise over the outside of the pouch (as seen in Figure 148). Stamped metal "ribs" are used to separate the pouches and thus enable gas flow between the pouches. The cell pouches are arranged in a simple aluminum cast-metal housing to direct the gas flows.

---

[101] Ahluwalia, R., K., Wang, X. , *Fuel Cells Systems Analysis*, Presentation to the Fuel Cell Tech Team, Southfield, MI, 14 August, 2013.
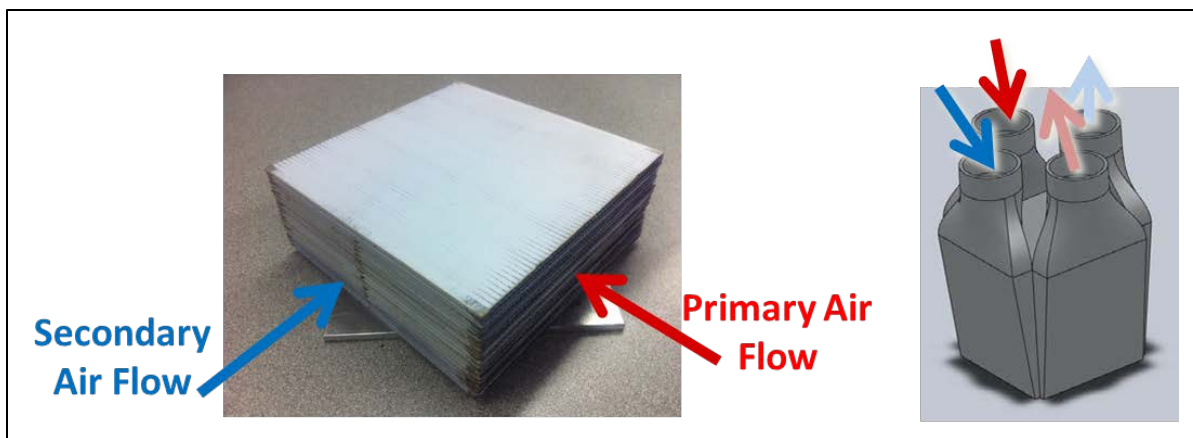
Figure 148. Images from W.L. Gore & Associates presentation[102] showing (Left) stack of cell pouches with primary flow (dry air) flowing through the cell pouches and secondary flow (wet air) flowing over/under and between pouches and (Right) humidifier housing with four ports: primary and secondary flow inlet and outlet ports.

8.2.2.3.1   Membrane Humidifier Manufacturing Process

The manufacturing process for the plate frame membrane humidifier is modeled as eight steps:

1. Fabrication of Composite Membranes
2. Fabrication of Etched Stainless Steel Flow Fields
3. Pouch Formation
4. Stainless Steel Rib Formation
5. Stack Formation
6. Formation of the Housing
7. Assembly of the Composite Membrane and Flow Fields into the Housing
8. Humidifier System Testing

Manufacturing details and cost components for each process are described in the following sections.

Fabrication of Composite Humidifier Membranes

The postulated process for the manufacture of the composite humidifier membrane is based on a slot die coating roll-to-roll system.

a. A 10µm thick ePTFE layer is unrolled onto a Mylar backer.
b. A 5µm thick slot die coated layer of Nafion® ionomer is laid on top of the ePTFE.
c. A second layer of 10µm thick ePTFE is unrolled onto the ionomer layer.
d. The stacked layers are passed through a continuous curing oven.
e. In the final step, all three layers are hot laminated to a 180µm polyethylene terephthalate (PET) non-woven porous layer, also known as a gas diffusion layer (GDL).

---

[102] Johnson, William B. "Materials and Modules for Low-Cost, High Performance Fuel Cell Humidifiers," W.L. Gore & Associates, Inc., presentation at the 2012 DOE Hydrogen and Fuel Cell Program Annual Merit Review, Washington, DC, 17 May 2012.

The ePTFE layers bracket and mechanically support the very thin, and thus high water flux, ionomer layer and are arranged in a symmetrical orientation to minimize stresses during thermal cycling and thereby enhance lifetime. The much thicker PET layer provides additional mechanical support and abrasion resistance. Figure 149 shows a schematic of the postulated fabrication process inspired by a Ballard patent for composite membrane manufacturing[103] and a Gore patent for integral composite membranes.[104]
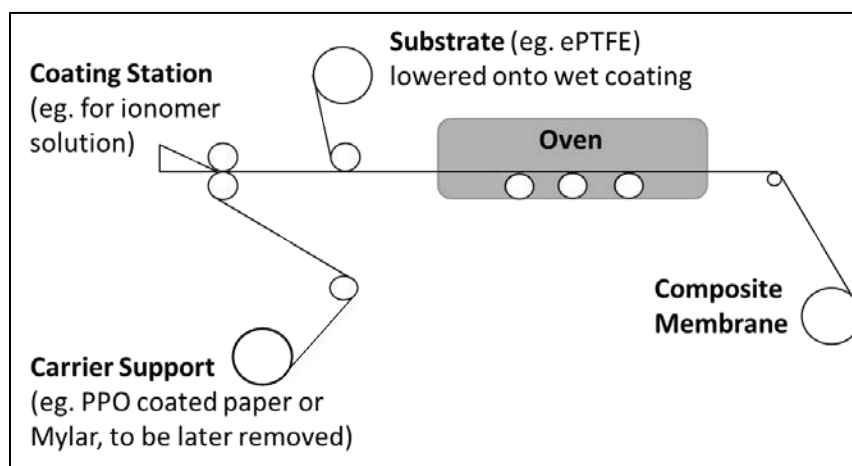
Figure 149. Design for ionomer addition to ePTFE, followed by oven drying to form a composite membrane from combination of Ballard Patent (U.S. Patent 6,689,501 B2) and Gore patent (U.S. Patent 5,599,614).

Key elements of composite membrane fabrication process include:
- Adding a porous substrate (eg. ePTFE) onto a wet impregnate solution (eg. ionomer) (shown in Figure 149).
- Coating ionomer directly onto a porous substrate (eg. Slot die coating onto the top of the ePTFE) (not shown in Figure 149).
- Adding a second porous substrate (eg. ePTFE) onto the top of a wet solution layer (eg. ionomer) (not shown in Figure 149).

The process is modeled using a 1m web width at a baseline speed of 10m/min (based on DuPont patent).[105] Curing oven residence time is a total of 9 minutes (3 minutes at 40°C, 3 minutes at 60°C and 3 minutes at 90°C), also based on the DuPont patent. The total capital cost of manufacturing equipment for the composite membrane is approximately $3M with the cost breakdown and cost basis listed in Figure 150.

The membrane production for 1,000 air humidifiers is roughly 700 m^2. At such a low volume of membrane production, the slot die coating process is heavily underutilized. However, SA postulates that the humidifier manufacturer would most likely have multiple products and customers with similar

---

[103] Ballard Patent: U.S. Patent 6,689,501 B2

[104] Gore Patent: "Integral composite Membrane" U.S. Patent 5,599,614.

[105] DuPont Patent US 7,648,660 B2

membrane requirements. Therefore, the cost of membrane per m^2 is based on aggregate process line production rather than on the production of only one product. To model this aggregate production, a 5x multiplier is placed on the membrane fabrication at the 1,000 systems/year level for purposes of computing membrane cost per square meter. This reduces the cost of membrane for the humidifier by approximately $8/kW$_{net}$.

Figure 151 and Figure 152 show membrane processing parameters. Cost results are shown Figure 153 and reveal that (at 500,000 systems per year) material cost is the largest cost contributor, with ePTFE cost being the dominating cost element. Consequently, ePTFE cost was carefully assessed and found to vary substantially vendor to vendor, partly due to variations in ePTFE precursor materials and processing steps (together referred to as ePTFE "quality"). A discussion of the range of ePTFE costs used within the cost analysis appears in Section 8.1.2.2.

Component	Capital Cost	Basis
Web Casting Operation		
Base slot die coating system	**$800k**	**Frontier Industrial Technology Inc. quote**
Additional Pump Cart	**$25k**	**Frontier Industrial Technology Inc. quote**
ePTFE Unwind stands	**2 x $60k**	**Machine Works Inc. quote**
Customization Adder	**2x**	**Conservatism for custom machinery**
Total Web Casting Capital Cost	**$1.9M**	
Additional heating zones	**$37k**	**Modified Wisconsin Ovens quote**
Tensioner for laminator	**$60k**	**Estimated based on similar machinery**
Laminator	**$864k**	**Modified Andritz Kuster quote**
Clean Room	**$166k**	**Industrial ROM estimate**
Quality Control Equipment	**$165k**	**Line Cameras to provide 100micron anomaly resolution after ionomer addition and 350 micron resolution of each ePTFE layer.**
Total Capital (uninstalled)	**$3M**	

Figure 150. Capital cost of manufacturing equipment required for the composite membrane fabrication process at 500k sys/yr.

Annual Production Rate	1,000	10,000	30,000	80,000	100,000	500,000
Equipment Lifetime (years)	16	15	15	15	15	15
Interest Rate	10%	10%	10%	10%	10%	10%
Corporate Income Tax Rate	40%	40%	40%	40%	40%	40%
Capital Recovery Factor	0.175	0.175	0.175	0.175	0.175	0.175
Equipment Installation Factor	1.4	1.4	1.4	1.4	1.4	1.4
Maintenance/Spare Parts (% of CC)	10%	10%	10%	10%	10%	10%
Miscellanous Expenses (% of CC)	7%	7%	7%	7%	7%	7%
Power Consumption (kW)	278	278	278	294	294	294

Figure 151. Fabrication of composite membranes process parameters

Annual Production Rate	1,000	10,000	30,000	80,000	100,000	500,000
Capital Cost ($/line)	$1,275,047	$1,247,716	$1,247,716	$2,836,683	$2,836,683	$3,019,397
Simultaneous Lines	1	1	1	1	1	1
Laborers per Line	0.67	0.67	0.67	0.67	0.67	0.67
Line Utilization	0.2%	2.2%	6.4%	5.7%	7.1%	23.4%
Casting Line Rate (m/s)	0.24	0.13	0.13	0.17	0.17	0.17
Effective Total Machine Rate ($/hr)	$98,942	$6,939	$2,450	$6,161	$4,983	$1,648
Backer Cost ($/m^2)	$0.96	$0.96	$0.96	$0.96	$0.96	$0.96

Figure 152. Machine rate parameters for fabrication of composite membranes

Annual Production Rate	1,000	10,000	30,000	80,000	100,000	500,000
Materials ($/stack)	$44	$32	$27	$24	$23	$15
Manufacturings ($/stack)	$111	$54	$18	$15	$12	$3
Toolings ($/stack)	$0	$0	$0	$0	$0	$0
Markups ($/stack)	$62	$30	$16	$12	$10	$5
Total Costs ($/stack)	$217	$117	$61	$51	$45	$23
Total Costs ($/kWnet)	$2.71	$1.46	$0.77	$0.64	$0.56	$0.28

Figure 153. Cost breakdown for fabrication of composite membranes

Fabrication of Etched Stainless Steel Flow Fields

The humidifier flow field plates serve to separate the sides of the cell pouch and open a channel through which the air may pass. The plates are fabricated by electrochemical etching of 0.6mm stainless steel 316L sheet. Etching is selected as it grants the design flexibility and dimensional tolerance critical to achieving low pressure drop and high membrane water transport performance. To reduce the cost of the etching process, multiple flow fields are etched from a single large panel of SS. The process includes the following stages:

- **Stage 1 (Add Photoresist)**: Photoresist is first laminated to both sides of a 0.6mm (24mils) SS316 metal coil and cut to 1m by 2m panel size (holding 180 parts).
- **Stage 2 (Illuminate with light):** Two SS/photoresist panels are manually loaded into a light chamber, covered with stencils (one stencil on each side of each panel), exposed to light simultaneously on each side of panel for 7.5 minutes to activate the photoresist not covered by the stencil, and then the panels are removed from the light chamber. The photoresist has now been selectively removed from the panel in the exact pattern desired for etching.
- **Stage 3 (Stripping):** Ten panels are loaded into a vertical fixture, simultaneously lowered into a stripping tank of alkaline solution (sodium carbonate), the exposed portions of photoresist are stripped/dissolved by the alkaline solution over a 5 minutes submersion, the panel are then lifted from the tank.
- **Stage 4 (Etching):** The ten panels fixture is moved to an electrochemically etching bath, electrodes are connected to each panel, the panels are simultaneously lowered into the etching tank, an electric current is applied to electrochemically etch the exposed SS surface. The electrochemical etching rate is estimated at 6.7 µm per minute, taking a total of 45 minutes to etch 600 microns (300 microns from each side simultaneously). Perforations are also etched into the material to allow for easy flow field separation using a low force stamping machine. The average power consumption estimated is approximately 1.2kW per 100cm^2 part (2.16MW for 10 panels).

- **Stage 5 (Cleaning):** After the etching is complete, the panels are lowered into a wash tank of alkaline solution (sodium hydroxide) for 4 minutes to remove the remaining photoresist.

Additionally, the etched plates are anodized for corrosion resistance, separated by stamping into 10cm by 10cm pouch cell sizes, and packaged into magazines for robotic assembly. Anodizing cost is estimated at 1.6 cents per 50cm^2 of anodizing surface ($3 for a 100 cell stack) with the parts being anodized while in panel form before separated. Figure 154 and Figure 155 show flow field processing parameters. Cost results for the etching process are shown in Figure 156.

Annual Production Rate	1,000	10,000	30,000	80,000	100,000	500,000
Equipment Lifetime (years)	15	15	15	15	15	15
Interest Rate	10%	10%	10%	10%	10%	10%
Corporate Income Tax Rate	40%	40%	40%	40%	40%	40%
Capital Recovery Factor	0.175	0.175	0.175	0.175	0.175	0.175
Equipment Installation Factor	1.4	1.4	1.4	1.4	1.4	1.4
Maintenance/Spare Parts (% of CC)	13%	13%	13%	13%	13%	13%
Miscellanous Expenses (% of CC)	2%	2%	2%	2%	2%	2%
Power Consumption (kW)	2,226	2,226	2,226	2,226	2,226	2,226

Figure 154. Fabrication of etched stainless steel flow fields process parameters

Annual Production Rate	1,000	10,000	30,000	80,000	100,000	500,000
Capital Cost ($/line)	$1,018,602	$1,018,602	$1,018,602	$1,018,602	$1,018,602	$1,693,602
Stage 1 Simultaneous Lines	1	1	1	1	1	1
Stage 2 Simultaneous Lines	1	1	1	1	1	2
Stage 3 Simultaneous Lines	1	1	1	1	1	1
Stage 4 Simultaneous Lines	1	1	1	1	1	3
Stage 5 Simultaneous Lines	1	1	1	1	1	1
Stage 1 Line Utilization	0.0%	0.1%	0.3%	0.8%	1.0%	5.0%
Stage 2 Line Utilization	0.4%	4.0%	11.9%	31.7%	39.7%	99.2%
Stage 3 Line Utilization	0.1%	0.5%	1.6%	4.4%	5.5%	27.3%
Stage 4 Line Utilization	0.5%	4.6%	13.7%	36.5%	45.6%	76.1%
Stage 5 Line Utilization	0.0%	0.5%	1.5%	4.0%	5.0%	24.8%
Stage 1 Laborers per Line	1	1	1	1	1	1
Stage 2 Laborers per Line	2	2	2	2	2	2
Stage 3 Laborers per Line	1	1	1	1	1	1
Stage 4 Laborers per Line	0	0	0	0	0	0
Stage 5 Laborers per Line	1	1	1	1	1	1
Stage 1 Cycle Time (s)	6	6	6	6	6	6
Stage 2 Cycle Time (s)	480	480	480	480	480	480
Stage 3 Cycle Time (s)	330	330	330	330	330	330
Stage 4 Cycle Time (s)	2,761	2,761	2,761	2,761	2,761	2,761
Stage 5 Cycle Time (s)	300	300	300	300	300	300
Effective Total Machine Rate ($/hr)	$24,698.50	$2,683.68	$1,052.96	$543.35	$482.20	$318.93
Stainless Steel Cost ($/kg)	$3.93	$3.93	$3.93	$3.93	$3.93	$3.93

Figure 155. Machine rate parameters for fabrication of etched stainless steel flow fields

Annual Production Rate	1,000	10,000	30,000	80,000	100,000	500,000
Materials ($/stack)	$7	$7	$7	$7	$7	$7
Manufacturings ($/stack)	$406	$44	$17	$9	$8	$5
Total Costs ($/stack)	$413	$51	$24	$16	$15	$12
Total Costs ($/kWnet)	$5.16	$0.64	$0.30	$0.20	$0.18	$0.15

Figure 156. Cost breakdown for fabrication of etched stainless steel flow fields

Pouch Formation

The cell pouches are formed using custom machinery to wrap a flow field with composite membrane and apply adhesive to seal the ends of the membrane and form a membrane loop. An image of a complete single cell pouch is shown in Figure 157. The process order used to fabricate these cell pouches is as follows:

a. Composite humidifier membrane material is unrolled onto a cutting deck.
b. The custom machine cuts the composite membrane to a 20 cm length.
c. A flow field is placed in the center of the membrane.
d. One end of the membrane is wrapped around the flow field.
e. A bead of silicone adhesive is applied to the membrane end wrapped around the flow field.
f. The other end of the membrane is wrapped around the flow field and onto the adhesive bead. The ends are held in place until bonded.
g. A vision quality control system is used to verify alignment of the cell pouch.
h. The cell pouch is removed and stacked in a magazine to be used in the next stack assembly process.

A schematic of the process steps is shown in Figure 158. (The schematic does not show the quality control system.) The complete system is estimated at $413,000 and able to simultaneously prepare 10 pouches with a 9 second cycle time (i.e. 9 seconds per 10 pouches).

Figure 157. Plate Frame Membrane Humidifier single cell pouch (Source: Johnson, William B. "Materials and Modules for Low-Cost, High Performance Fuel Cell Humidifiers," W.L. Gore & Associates, Inc., presentation at the 2012 DOE Hydrogen and Fuel Cell Program Annual Merit Review, Washington, DC, 17 May 2012.)
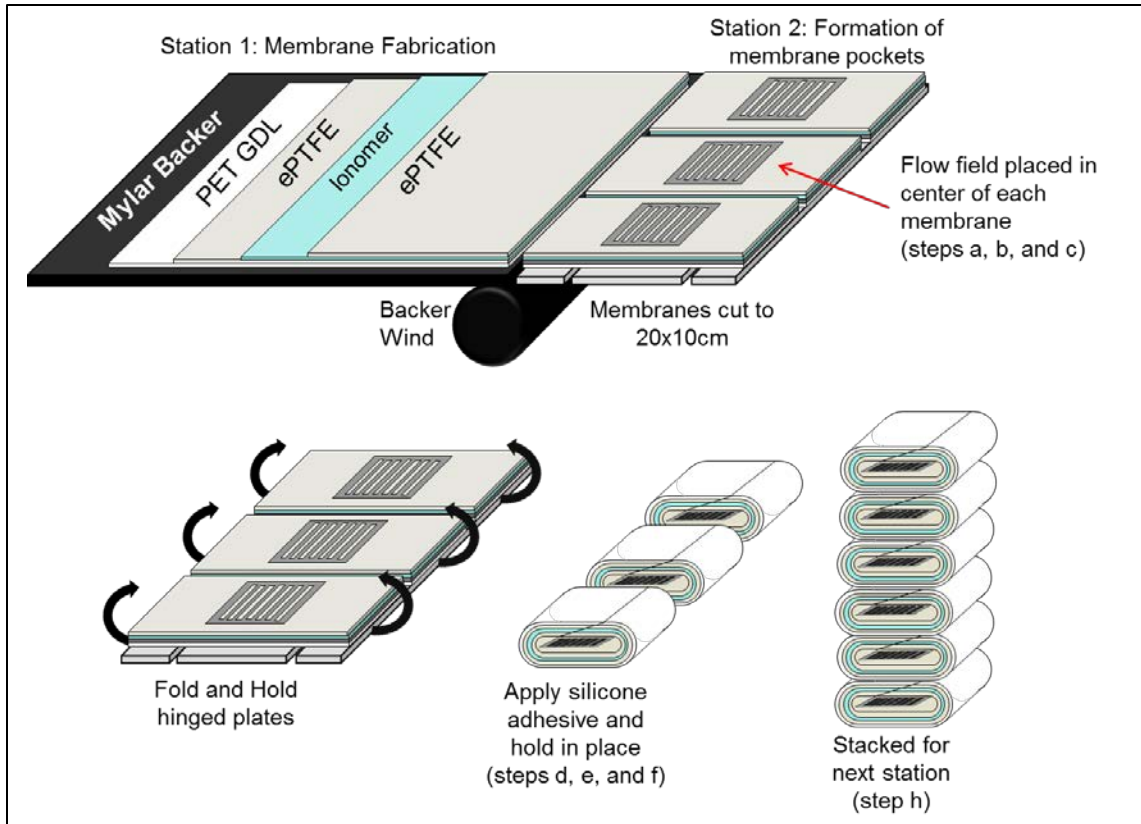
Figure 158. Process steps used in DFMA® analysis for humidifier cell pouch formation.

Figure 159 and Figure 160 show cell pouch formation processing parameters. Cost results for the cell pouch formation process are in Figure 161.

Annual Production Rate	1,000	10,000	30,000	80,000	100,000	500,000
Equipment Lifetime (years)	15	15	15	15	15	15
Interest Rate	10%	10%	10%	10%	10%	10%
Corporate Income Tax Rate	40%	40%	40%	40%	40%	40%
Capital Recovery Factor	0.175	0.175	0.175	0.175	0.175	0.175
Equipment Installation Factor	1.4	1.4	1.4	1.4	1.4	1.4
Maintenance/Spare Parts (% of CC)	10%	10%	10%	10%	10%	10%
Miscellanous Expenses (% of CC)	7%	7%	7%	7%	7%	7%
Power Consumption (kW)	27	27	27	27	27	27

Figure 159. Pouch formation process parameters

Annual Production Rate	1,000	10,000	30,000	80,000	100,000	500,000
Capital Cost ($/line)	$413,179	$413,179	$413,179	$413,179	$413,179	$413,179
Costs per Tooling Set ($)	$1,259	$1,259	$1,259	$1,023	$900	$359
Costs per Tooling Set 2 ($)	1,400	1,400	1,400	1,400	1,400	1,400
Tooling Lifetime (cycles)	2,000,000	2,000,000	2,000,000	2,000,000	2,000,000	2,000,000
Simultaneous Lines	1	1	1	1	1	2
Laborers per Line	0.25	0.25	0.25	0.25	0.25	0.25
Line Utilization	0.3%	2.9%	8.6%	21.7%	27.1%	66.9%
Cycle Time (s)	0.875	0.875	0.875	0.875	0.875	0.875
Effective Total Machine Rate ($/hr)	$17,677.77	$1,798.58	$609.39	$248.63	$201.65	$89.65
Silicon Adhesive Cost ($/kg)	$12.05	$12.05	$12.05	$12.05	$12.05	$12.05

Figure 160. Machine rate parameters for pouch formation

Annual Production Rate	1,000	10,000	30,000	80,000	100,000	500,000
Materials ($/stack)	$0	$0	$0	$0	$0	$0
Manufacturings ($/stack)	$171	$17	$6	$2	$2	$1
Toolings ($/stack)	$0	$0	$0	$0	$0	$0
Total Costs ($/stack)	$172	$18	$6	$3	$2	$1
Total Costs ($/kWnet)	$2.15	$0.22	$0.08	$0.03	$0.03	$0.01

Figure 161. Cost breakdown for pouch formation

Stainless Steel Rib Formation

Metal ribs are used to create air passageways between the cell pouches of the plate frame humidifier. The ribs are stamped from 0.6mm thick stainless steel 316L sheeting and formed into 10cm by 0.25cm by 0.6mm ribs. Plate handling robots are used to collect and stack the ribs into magazines to be used during stack assembly. The capital cost of the stamping press is $160,000 and the cycle time is approximately 0.67 seconds per rib (90 stamps per minute).

Figure 162 and Figure 163 show rib formation processing parameters. Cost results for rib formation are shown in Figure 164.

Annual Production Rate	1,000	10,000	30,000	80,000	100,000	500,000
Equipment Lifetime (years)	15	15	15	15	15	15
Interest Rate	10%	10%	10%	10%	10%	10%
Corporate Income Tax Rate	40%	40%	40%	40%	40%	40%
Capital Recovery Factor	0.175	0.175	0.175	0.175	0.175	0.175
Equipment Installation Factor	1.4	1.4	1.4	1.4	1.4	1.4
Maintenance/Spare Parts (% of CC)	13%	13%	13%	13%	13%	13%
Miscellanous Expenses (% of CC)	2%	2%	2%	2%	2%	2%
Power Consumption (kW)	18	18	18	18	18	18

Figure 162. Stainless steel rib formation process parameters

Annual Production Rate	1,000	10,000	30,000	80,000	100,000	500,000
Capital Cost ($/line)	$158,587	$158,460	$158,460	$158,460	$158,460	$158,460
Costs per Tooling Set ($)	$6,000	$6,000	$6,000	$6,000	$6,000	$6,000
Tooling Lifetime (cycles)	400,000	400,000	400,000	400,000	400,000	400,000
Simultaneous Lines	1	1	1	1	1	3
Laborers per Line	0.25	0.25	0.25	0.25	0.25	0.25
Line Utilization	0.6%	5.9%	17.8%	47.3%	59.2%	98.6%
Cycle Time (s)	0.66	0.66	0.66	0.66	0.66	0.66
Effective Total Machine Rate ($/hr)	$3,120.50	$1,422.02	$1,422.02	$1,422.02	$1,422.02	$1,422.02
Stainless Steel Rib Material Cost ($/kg)	$3.93	$3.93	$3.93	$3.93	$3.93	$3.93

Figure 163. Machine rate parameters for stainless steel rib formation

Annual Production Rate	1,000	10,000	30,000	80,000	100,000	500,000
Materials ($/stack)	$1	$1	$1	$1	$1	$1
Manufacturings ($/stack)	$63	$7	$2	$1	$1	$1
Toolings ($/stack)	$2	$2	$2	$2	$2	$2
Total Costs ($/stack)	$65	$9	$5	$3	$3	$3
Total Costs ($/kWnet)	$0.82	$0.11	$0.06	$0.04	$0.04	$0.03

Figure 164. Cost breakdown for stainless steel rib formation

Stack Formation

The plate frame membrane humidifier stack is assembled by "pick and place" robots. The following steps are used for assembly.

1. Repeated robotic steps for the number of pouches required in the stack (58 cell pouches for automotive system).
   a. Robot acquires and places pouch cell with flow field insert
   b. Apply silicone gasket/adhesive bead on three sealing lines
   c. Acquire and place three parallel SS rib spacers onto the sealing lines
   d. Apply additional silicone gasket/adhesive beads on three sealing lines on rib spacers

2. Compress stack in an assembly jig and hold for 24 hours in a humidified warm enclosure. (72 hours curing time would be required if left at room temperature.)
3. Use optical quality control system to detect membrane misalignment in stack.

The total capital cost of the pick and place robots and other equipment required for the system is $185,000. The cycle time is 9 seconds for each pouch (~9 min for an 80 cell pouch stack).

Figure 165 and Figure 166 show stack formation processing parameters. Cost results for stack formation process are in Figure 167.

Annual Production Rate	1,000	10,000	30,000	80,000	100,000	500,000
Equipment Lifetime (years)	15	15	15	15	15	15
Interest Rate	10%	10%	10%	10%	10%	10%
Corporate Income Tax Rate	40%	40%	40%	40%	40%	40%
Capital Recovery Factor	0.175	0.175	0.175	0.175	0.175	0.175
Equipment Installation Factor	1.4	1.4	1.4	1.4	1.4	1.4
Maintenance/Spare Parts (% of CC)	10%	10%	10%	10%	10%	10%
Miscellanous Expenses (% of CC)	7%	7%	7%	7%	7%	7%
Power Consumption (kW)	22	22	22	22	22	22

Figure 165. Stack formation process parameters

Annual Production Rate	1,000	10,000	30,000	80,000	100,000	500,000
Capital Cost ($/line)	$185,000	$185,000	$185,000	$185,000	$185,000	$185,000
Simultaneous Lines	1	1	1	3	3	14
Laborers per Line	0	0	0	0	0	0
Line Utilization	3%	27%	80%	71%	89%	96%
Cycle Time (s)	9	9	9	9	9	9
Effective Total Machine Rate ($/hr)	$865.28	$98.36	$41.55	$45.10	$38.71	$37.00
Silicon Adhesive Cost ($/kg)	$12.05	$12.05	$12.05	$12.05	$12.05	$12.05

Figure 166. Machine rate parameters for stack formation

Annual Production Rate	1,000	10,000	30,000	80,000	100,000	500,000
Materials ($/stack)	$2	$2	$2	$2	$2	$2
Manufacturings ($/stack)	$78	$9	$4	$4	$3	$3
Total Costs ($/stack)	$80	$11	$6	$6	$5	$5
Total Costs ($/kWnet)	$1.00	$0.14	$0.07	$0.08	$0.07	$0.07

Figure 167. Cost breakdown for stack formation

Formation of the Housing

The humidifier aluminum housing is formed using a 900 ton cold chamber die casting machine to form two separate parts (body and upper lid). Boothroyd Dewhurst Inc. (BDI) software was used for the cost estimate. The housing walls are 2.5mm thick and have approximate dimensions of 11cm tall by 11cm length and width. The volume is less than 5 liters and the mass of the housing about 0.65kg. Four bolts/nuts are used to connect the body to the lid with an elastomer O-ring for sealing. A CAD drawing of the complete housing is shown in Figure 168 along with the corresponding cost results are displayed in Figure 169.
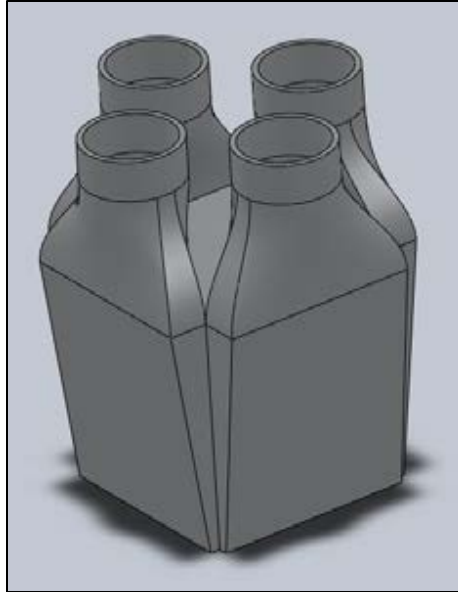
Figure 168. Process steps used in DFMA® analysis for humidifier cell pouch formation (Source: Johnson, William B. "Materials and Modules for Low-Cost, High Performance Fuel Cell Humidifiers," W.L. Gore & Associates, Inc., presentation at the 2012 DOE Hydrogen and Fuel Cell Program Annual Merit Review, Washington, DC, 17 May 2012.)

Annual Production Rate	1,000	10,000	30,000	80,000	100,000	500,000
Material ($/stack)	$4	$4	$4	$4	$4	$4
Manufacturing ($/stack)	$18	$4	$1	$1	$1	$1
Tooling ($/stack)	$31	$3	$2	$1	$1	$1
Total Cost ($/stack)	$52	$11	$8	$6	$6	$6
Total Cost ($/kWnet)	$0.65	$0.14	$0.10	$0.08	$0.07	$0.07

Figure 169. Cost breakdown for formation of the Housing

Assembly of the Composite Membrane and Flow Fields into the Housing

Complete manual assembly of the plate frame humidifier is performed at a custom work stand using the following sequence:

a. Acquire housing body and insert into fixture.
b. Acquire pouch stack and load stack into housing.
c. Acquire and insert gasket into housing body.
d. Acquire upper lid and place onto gasket/housing-body.
e. Acquire, insert and fasten 4 bolts/nuts.
f. Acquire finished housing and move to cart.
g. Weigh finished unit to detect missing/additional parts. (Quality control step.)

The cycle time is approximately 2 minutes per system. Figure 170 and Figure 171 show assembly process parameters. Cost results for assembly are shown in Figure 172.

Annual Production Rate	1,000	10,000	30,000	80,000	100,000	500,000
Equipment Lifetime (years)	10	10	10	10	10	10
Interest Rate	10%	10%	10%	10%	10%	10%
Corporate Income Tax Rate	40%	40%	40%	40%	40%	40%
Capital Recovery Factor	0.205	0.205	0.205	0.205	0.205	0.205
Equipment Installation Factor	1.4	1.4	1.4	1.4	1.4	1.4
Maintenance/Spare Parts (% of CC)	10%	10%	10%	10%	10%	10%
Miscellanous Expenses (% of CC)	7%	7%	7%	7%	7%	7%
Power Consumption (kW)	18	18	18	18	18	18

Figure 170. Assembly of the composite membrane and flow fields into the housing process parameters

Annual Production Rate	1,000	10,000	30,000	80,000	100,000	500,000
Assembly Method	Manual	Manual	Manual	Manual	Manual	Manual
Capital Cost ($/line)	$34,212	$34,212	$34,212	$34,212	$34,212	$34,212
Simultaneous Lines	1	1	1	1	1	5
Laborers per Line	1	1	1	1	1	1
Line Utilization	1.0%	9.9%	29.8%	79.4%	99.2%	99.2%
Index Time (min)	2	2	2	2	2	2
Effective Total Machine Rate ($/hr)	$429.56	$85.42	$59.83	$51.82	$50.86	$50.86

Figure 171. Machine rate parameters for assembly of the composite membrane and flow fields into the housing

Annual Production Rate	1,000	10,000	30,000	80,000	100,000	500,000
Manufacturings ($/stack)	$14	$3	$2	$2	$2	$2
Total Costs ($/stack)	$14	$3	$2	$2	$2	$2
Total Costs ($/kWnet)	$0.18	$0.04	$0.02	$0.02	$0.02	$0.00

Figure 172. Cost breakdown for assembly of the composite membrane and flow fields into the housing

Humidifier System Testing

A simple functionality test is completed for each completed humidifier system. It includes testing for air flow pressure drop and air leakage. These tests require an air compressor, gas manifolding, and a diagnostic measurement system. The steps considered in this testing process are:

a. Acquire unit and insert into fixture.
b. Connect 4 inlet and outlet air manifolds.
c. Sequentially flow gas (as appropriate) to test:
   - Pressure drop in primary flow (20 seconds)
   - Pressure drop in secondary flow (20 seconds)
   - Air leakage (primary to secondary) (20 seconds)
d. Disconnect inlet and outlet air manifolds.
e. Remove unit from fixture.

The estimated capital cost is:
- $30,000 for a 1-system test fixture (used at low production levels)
- $40,000 for a 3-system test fixture (used at high production levels)

The cycle time for testing is about 83 seconds per cycle.
- 83 seconds per system for a 1-system test fixture and 1 worker
- 23 seconds per system for a 3-system test fixture and 1 worker

Figure 173 and Figure 174 show humidifier system testing process parameters. Cost results are displayed in Figure 175.

Annual Production Rate	1,000	10,000	30,000	80,000	100,000	500,000
Equipment Lifetime (years)	15	15	15	15	15	15
Interest Rate	10%	10%	10%	10%	10%	10%
Corporate Income Tax Rate	40%	40%	40%	40%	40%	40%
Capital Recovery Factor	0.175	0.175	0.175	0.175	0.175	0.175
Equipment Installation Factor	1.4	1.4	1.4	1.4	1.4	1.4
Maintenance/Spare Parts (% of CC)	10%	10%	10%	10%	10%	10%
Miscellanous Expenses (% of CC)	7%	7%	7%	7%	7%	7%
Power Consumption (kW)	2	2	2	5	5	5

Figure 173. Humidifier system testing process parameters

Annual Production Rate	1,000	10,000	30,000	80,000	100,000	500,000
Capital Cost ($/line)	$30,000	$30,000	$30,000	$40,000	$40,000	$40,000
Simultaneous Lines	1	1	1	1	1	1
Laborers per Line	1	1	1	1	1	1
Line Utilization	0.7%	6.9%	20.6%	15.2%	19.0%	95.1%
Systems partially connected at any one time	1	1	1	3	3	3
Selected Effective Test time per System (min)	1.4	1.4	1.4	0.4	0.4	0.4
Effective Total Machine Rate ($/hr)	$492.07	$90.61	$60.75	$73.01	$67.62	$50.35

Figure 174. Machine rate parameters for humidifier system testing

Annual Production Rate	1,000	10,000	30,000	80,000	100,000	500,000
Manufacturings ($/stack)	$11	$2	$1	$0	$0	$0
Total Costs ($/stack)	$11	$2	$1	$0	$0	$0
Total Costs ($/kWnet)	$0.143	$0.026	$0.018	$0.006	$0.005	$0.004

Figure 175. Cost breakdown for humidifier system testing

8.2.2.3.2 Combined Cost Results for Plate Frame Membrane Humidifier

Cost results for the Gore plate frame membrane humidifier are summarized in Figure 176 at 500,000 systems per year and in Figure 177 for all manufacturing rates, with costs further subdivided into materials, manufacturing, tooling, markup, and total costs. The greatest cost drivers are the material costs, particularly for the membrane materials at $15.45/humidifier. Costs are strongly impacted by the quantity of membrane material needed for the humidifier. The largest processing cost for the humidifier

is the flow field fabrication due to the innate details of the flow field design which are deemed to require a (relatively) expensive etching process. Membrane and flow fields make up approximately 2/3[rds] of the total cost and materials are about half the total humidifier cost (at 500,000 systems per year), as seen in Figure 178.

		All at 500k systems per year				
Component Costs per Humidifier System		Materials	Manuf.	Tools	Markup	Total
Station 1: Membrane Fabrication	$/stack	$15.45	$2.64	$0.07	$4.54	$22.71
Station 2: Humidifier Etching (Flow Field Plates)	$/stack	$6.79	$5.24	$0.00	$0.00	$12.03
Station 3: Pouch Forming	$/stack	$0.20	$0.81	$0.03	$0.00	$1.04
Station 4: Stamp SS ribs	$/stack	$0.53	$0.63	$1.62	$0.00	$2.78
Station 5: Stack Forming	$/stack	$1.98	$3.33	$0.00	$0.00	$5.31
Station 6: Stack Housing	$/stack	$4.05	$0.50	$1.21	$0.00	$5.76
Station 7: Assembly of Stack into Housing	$/stack	$0.00	$1.70	$0.00	$0.00	$1.70
Station 8: System Test	$/stack	$0.00	$0.32	$0.00	$0.00	$0.32
Totals =		$29.00	$15.17	$2.93	$4.54	$51.64

Figure 176. Membrane humidifier system cost results: ~$110 at 500k systems/year

Annual Production Rate	1,000	10,000	30,000	80,000	100,000	500,000
Materials ($/stack)	$58	$46	$40	$38	$37	$29
Manufacturings ($/stack)	$872	$140	$52	$34	$29	$15
Toolings ($/stack)	$33	$5	$4	$3	$3	$3
Markups ($/stack)	$62	$30	$16	$12	$10	$5
Total Costs ($/stack)	$1,025	$221	$113	$87	$78	$52
Total Costs ($/kWnet)	$12.81	$2.76	$1.41	$1.09	$0.98	$0.65

Figure 177. Combined cost results for all plate frame humidifier processes.

Markup is typically applied to the sum of materials, manufacturing, and tooling to capture the real business costs associated with overhead, general administrative (G&A), scrap, R&D, and profit. Per previous DOE directive, markup is only applied to lower-tier suppliers and is NOT applied to the system assembler. A high degree of vertical integration for the overall auto fuel cell power system is assumed. (As discussed in more detail in Section 2.3, a lower level of vertical integration is assumed for the bus fuel cell system, therefore markup is applied to the humidifier.) For the plate frame membrane humidifier, markup is not applied to the auto humidifier assembler. However, markup is included in the costs of the ePTFE, PET, and composite humidifier membrane as those components are assumed to be manufactured by lower tier suppliers. (Markup on the manufacturing process for the composite membrane appears in the markup column in Figure 176.)
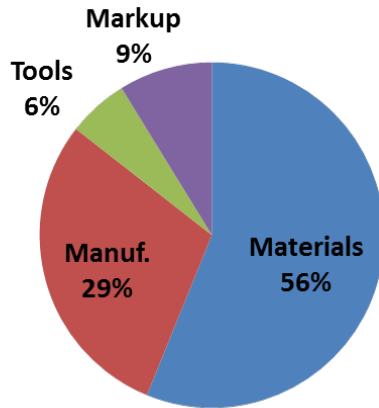
Figure 178. Humidifier membrane cost dominated by material cost at 500k systems/year

In cost analysis of fuel cell system components, it is beneficial to benchmark results with currently developed systems. Figure 179 compares SA's cost estimate to Gore's cost estimate and shows good agreement at medium and high production rates (for the same 2m^2 of membrane area). SA estimates are much higher than Gore's at low manufacturing rates due to poor utilization of expensive equipment (i.e. composite membrane fabrication). At low utilization of equipment, a business may decide to "job shop" or outsource the work to a company that has higher utilization of similar equipment. Such "job shopping" is not assumed for the humidifier in the 2016 analysis although as mentioned in Section 8.2.2.3.1, the production of membrane area is assumed to be five times more than what is used for 1,000 systems per year. This multiplier stems from the assumption that the membrane manufacturer would most likely supply to more than one customer and may have multiple industrial applications for this membrane.
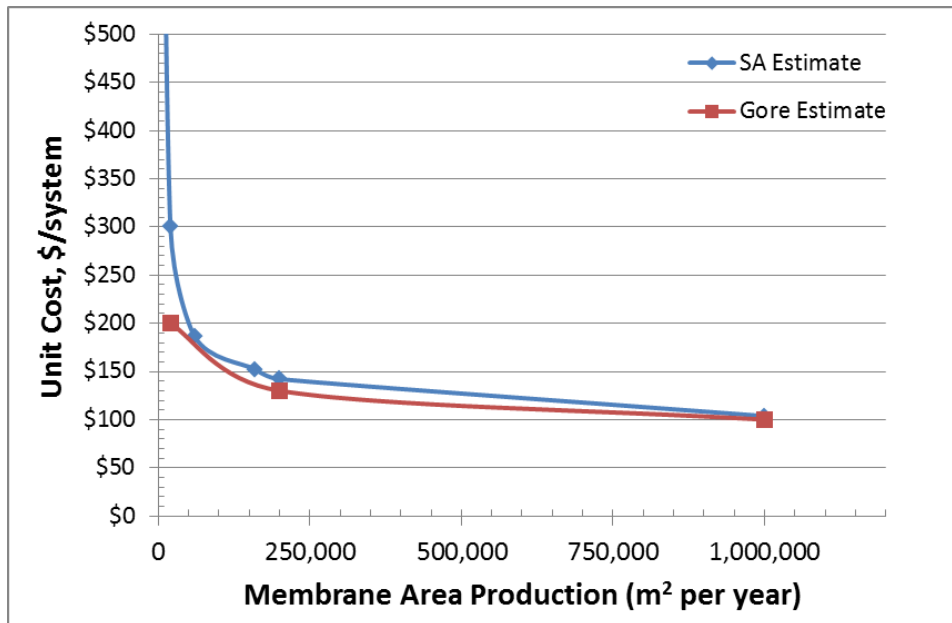
Figure 179. Comparison of Gore and SA cost estimates for the plate frame membrane humidifier (for 2m^2 membrane area).

In 2014, SA ran a sensitivity analysis of multiple parameters at 500,000 systems per year (and can be seen in SA's 2014 Update report).[106] The most important cost driver for the humidifier is the quantity of membrane material required. This indicates that between $0.5m^2$ and $2.6m^2$ of membrane area the plate frame humidifier would cost between \$35/system and \$131/system. The second most important cost driver is the price of the ePTFE material used in the membrane. Both the fuel cell stack MEA and humidifier manufactured costs are quite sensitive to the cost of ePTFE. While plate frame humidifier uncertainty is high (-68%/+19%), the overall humidifier cost is low compared to the total auto fuel cell power system cost.

In comparison to the tubular membrane humidifier previously used in the 2012 analysis, the 2016 plate frame humidifier is projected to be higher cost. However, in retrospect, the 2012 tubular membrane humidifier is now viewed as undersized for the 2012 flow conditions (even at $3.8m^2$ of membrane area) and thus a direct comparison of the two systems is not valid. In general, plate frame humidifiers will require less membrane area than tubular designs since their membranes may be thinner, (by virtue of being supported on ePTFE). However, the cost of the ePTFE support is a significant fraction of the total plate frame humidifier cost, and manufacturing (particularly of the etched plates) also adds considerably to cost (see Figure 180).

As shown by the sensitivity analysis, membrane area is an extremely important parameter in the determination of humidifier cost. Uncertainty exists related to the required membrane area. Consequently, an optimistic value of $0.5m^2$/system was included in the sensitivity analysis based on ANL modeling projections and a pessimistic value of $2.6m^2$ was included to reflect a large allowance for performance degradation. Further testing is required to confidently determine the membrane area requirement.

---

[106] "Mass Production Cost Estimation of Direct H_2 PEM Fuel Cell Systems for Transportation Applications: 2014 Update" Brian D. James, Jennie M. Moton & Whitney G. Colella, Strategic Analysis, Inc., January 2015.
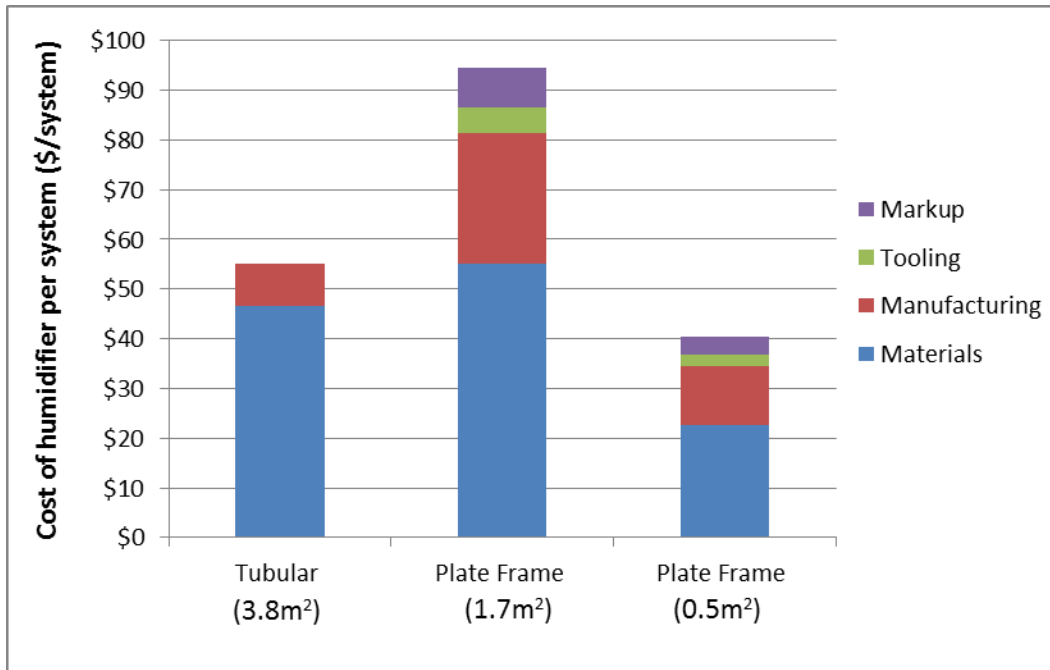
Figure 180. Graph showing the cost (at 500k sys/yr) comparison between a tubular membrane humidifier and two plate frame membrane humidifiers with different membrane area requirements.

8.2.3 Coolant Loops

The 2016 system has two coolant loops, a high-temperature loop to cool the fuel cell stacks and a low-temperature loop to cool electronic components. The low temperature loop is also used to cool the CEM motor and in the precooler (to cool the compressed intake air prior to going into the membrane humidifier).

8.2.3.1 High-Temperature Coolant Loop

Coolant Reservoir: The cost is based on a molded plastic water tank.

Coolant Pump: Small pumps to provide this flow are commercially available in large quantities at approximately $97 per pump at quantities of 1,000, dropping to $74 at high quantity.

Coolant DI Filter: The cost is based on a resin deionizer bed in a plastic housing.

Thermostat & Valve: The cost is based on standard automotive components.

Radiator: The heat dissipation requirements of the fuel cell system are similar to those of today's standard passenger cars. Consequently, costs for the high and low-temperature loop radiators are aligned with those of appropriately sized radiators used in contemporary automotive applications.

Radiator Fan: The cost is based on a standard automotive radiator fan and sized based on the cooling load.

Coolant Piping: Cost is based on 2" diameter rubber pipe from McMaster Carr and set at a constant $6.93/ft.

High-temperature coolant loop cost results are shown in Figure 181.

Annual Production Rate	1,000	10,000	30,000	80,000	100,000	500,000
Coolant Reservoir ($/system)	$13	$12	$11	$8	$8	$6
Coolant Pump ($/system)	$63	$63	$63	$63	$63	$63
Coolant DI Filter ($/system)	$81	$71	$65	$49	$45	$39
Thermostat & Valve ($/system)	$11	$9	$9	$6	$6	$5
Radiator ($/system)	$198	$188	$178	$169	$159	$149
Radiator Fan ($/system)	$89	$78	$68	$52	$50	$47
Coolant Piping ($/system)	$25	$24	$24	$23	$22	$20
Total Cost ($/system)	$480	$446	$417	$369	$352	$330
Total Cost ($/kW$_{net}$)	$6.00	$5.58	$5.21	$4.62	$4.40	$4.12

Figure 181. Cost breakdown for high-temperature coolant loop

8.2.3.2 Low-Temperature Coolant Loop

In the 2012 analysis, the low-temperature loop previously cooled components both within the fuel cell system (precooler, CEM motor) and the drive train system (main traction motor inverter (TIM) electronics). Consequently, the cost of the 2012 low-temperature coolant loop was apportioned between these systems and only the cost of the loop associated with the fuel cell system was tabulated in the fuel cell cost summary. Based on the expected duties of the components, 67% of the low-temperature coolant loop cost was attributable to the fuel cell system.

The low-temperature loop for the 2014-2016 analysis is modeled as a dedicated fuel cell system cooling loop and thus only cools components within the fuel cell system (precooler, CEM motor). Drive train components have been removed from the cooling loop: thus 100% of the coolant loop cost is charged to the fuel cell system. This change was made in order to simplify the analysis and to be in closer alignment with Argonne National Laboratory modeling methodology.

Coolant Reservoir: The cost is based on a molded plastic water tank.

Coolant Pump: The low and high-temperature loops require similar flow rates, so the same type of pump is used in each.

Thermostat & Valve: The cost is based on standard automotive components.

Radiator: As with the radiator for the high-temperature coolant loop, the exhaust loop uses a radiator similar to those used in conventional automotive applications. It does not need to be as large as the one for the coolant loop however, so it is scaled down in cost.

Radiator Fan: It is assumed that the radiators for the high and low-temperature loops are installed together such that the air flow exiting the low-temperature radiator immediately enters the high-temperature radiator, and as such, there is a single fan for both radiators, which is accounted for in the high-temperature coolant loop (Reason why radiator fan cost is $0 in Figure 182).

Coolant Piping: Assumed 2" diameter rubber pipe from McMaster Carr, at $6.93/ft.

Low-temperature coolant loop cost results are shown in Figure 182.

Annual Production Rate	1,000	10,000	30,000	80,000	100,000	500,000
Coolant Reservoir ($/system)	$2	$130	$130	$130	$130	$130
Coolant Pump ($/system)	$16	$2	$2	$2	$2	$2
Thermostat & Valve ($/system)	$4	$2,168	$2,168	$2,168	$2,168	$2,168
Radiator ($/system)	$43	$78	$68	$52	$50	$47
Radiator Fan ($/system)	$0	$0	$0	$0	$0	$0
Coolant Piping ($/system)	$5	$437	$437	$437	$437	$437
Total Cost ($/system)	$71	$68	$65	$61	$59	$56
Total Cost ($/kW$_{net}$)	$0.88	$142.14	$136.37	$128.80	$123.24	$117.18

Figure 182. Cost breakdown for low-temperature coolant loop

8.2.4 Fuel Loop

Per DOE system analysis guidelines, the hydrogen tank, the hydrogen pressure-relief device & regulator, hydrogen fueling receptacle, proportional valve, and pressure transducer are not included in the fuel cell power system cost analysis as they are considered part of the hydrogen storage system.

Inline Filter for Gas Purity Excursions: This filter ensures that any contaminants that may have gotten into the fuel lines do not damage the stack.

Flow Diverter Valve: The flow diverter valve routes hydrogen to either the low-flow or the high-flow ejector, depending on the pressure.

Over-Pressure Cut-Off (OPCO) Valve: The over-pressure cut-off valve is included as a safety precaution to prevent inadvertent stack pressurization from the high pressure (>5000psi) in the hydrogen storage tank.

Low-Flow and High-Flow Ejectors: Dual static ejectors are employed to re-circulate hydrogen from the anode exhaust to the anode inlet to achieve target flow rates and hence high stack performance. The ejectors operate on the Bernoulli Principle wherein high-pressure hydrogen gas from the fuel tank (>250 psi) flows through a converging-diverging nozzle to entrain lower-pressure anode exhaust gas. Two ejectors (high-flow and low-flow) are operated in parallel to achieve a wide turn-down range. The design of the ejectors is based on concepts from Graham Manufacturing and the patent literature (US Patent 5,441,821). The fabrication of each ejector consists of stainless steel investment casting of a two-part assembly, followed by machining, welding, and polishing. Ejectors with variable geometry are a possible design improvement for future systems. While ANL modeling suggests that a hydrogen recirculation blower is needed during very low part-power system operation to ensure proper gas flow, only the ejector system is included in the analysis.

Check Valves: The check valves ensure that no hydrogen may flow backwards from the ejectors

Purge Valve: The purge valve allows for periodic purging of the hydrogen in the fuel loop.

Hydrogen Piping: The hydrogen flow lines are modeled as 1/2" SS316 schedule 10 pipe and are priced between $90 and $100/system based on estimates provided by Ford.

Fuel loop cost breakdown is shown in Figure 183.

Annual Production Rate	1,000	10,000	30,000	80,000	100,000	500,000
Inline Filter for GPE ($/system)	$15	$15	$15	$15	$15	$15
Flow Diverter Valve ($/system)	$16	$16	$16	$16	$16	$16
Over-Pressure Cut-Off Valve ($/system)	$25	$22	$20	$15	$14	$12
Hydrogen High-Flow Ejector ($/system)	$51	$38	$36	$33	$31	$31
Hydrogen Low-Flow Ejector ($/system)	$44	$31	$29	$26	$25	$24
Check Valves ($/system)	$10	$10	$10	$10	$10	$10
Purge Valves ($/system)	$80	$70	$64	$48	$45	$38
Hydrogen Piping ($/system)	$106	$104	$103	$99	$96	$92
Total Cost ($/system)	$346	$306	$291	$261	$251	$238
Total Cost ($/kW$_{net}$)	$4.32	$0.41	$0.39	$0.35	$0.33	$0.32

Figure 183. Cost breakdown for fuel loop

8.2.5 System Controller

Conventional electronic engine controllers (EEC's) are assumed to control the fuel cell power system. These programmable circuit boards are currently mass-produced for all conventional gasoline engines and are readily adaptable for fuel cell use. Prototype fuel cell vehicles may use four or more controllers out of convenience, so that each subsystem is able to have a separate controller. However, even at 1,000 vehicles per year, the system will be refined enough to minimize controller use on the rationale of simplicity of cost and design. A single EEC is judged adequate for control and sensor leads to the power plant.

Controller cost is assessed by a bottom-up analysis of the system controller which breaks the controller into 17 input and output circuits, as listed in Figure 184.

For each input or output circuit, it is estimated that approximately 50 cents in electronic components (referencing catalog prices) would be needed. The costs of input and output connectors, an embedded controller, and the housing are also estimated by catalog pricing. A price quote forms the basis for the assumed dual-layer 6.5" x 4.5"circuit board. Assembly of 50 parts is based on robotic pick-and-place methods. A 10% cost contingency is added to cover any unforeseen cost increases.

Name	Signal
Inputs	
Air Mass Flow Sensor	Analog
H2 pressure Sensor (upstream of ejector)	Analog
H2 Pressure Sensor (stack inlet manifold)	Analog
Air Pressure sensor (after compressor)	Analog
Stack Voltage (DC bus)	Analog
Throttle Request	Analog
Current Sensors (drawn from motor)	Analog
Current Sensors (output from stack)	Analog
Singnal for Coolant Temperature	Analog
H2 Leak Detector 1	Digital
H2 Leak Detector 2	Digital
Outputs	
Singnal to TIM	Analog
Singnal to CEM	Analog
Singnal to Ejector 1	PWM
Singnal to Ejector 2	PWM
High voltage System Relay	Digital
Signal to Coolant Pump	PWM
Signal to H2 Purge Valve	Digital
Total Analog	11
Total Digital	4
Total PWM	3
Total Inputs/Outputs	**18**

Figure 184. System controller input & output requirements

Figure 185 and Figure 186 detail estimated system controller costs.

Component	Description	Cost at 500k systems/year	Cost Basis
Main Circuit Board	2 layer punnchboard	$8.01	$5.34 for single layer of 6.5"x4.5" punchboard, Q=500, Assume 25% discount for Q=500k
Input Connector	Wire Connector for inputs	$0.18	$0.23 each in Q=10k, reduced ~20% for Q=500k
Output Connector	Wire Connector for outputs	$0.20	$0.23 each in Q=10k, reduced ~20% for Q=500k
Embedded Controller	25 MHz, 25 channel microprocessor board	$32.50	Digi-Key Part no. 336-1489-ND, $50 @Q=1, assumed 35% reduction for Q=500k
MOSFETs (18 total, 1 each per I/O)	P-channel, 2W, 49MOhm @SA, 10V	$3.93	Digi-Key Part No. 785-1047-2-ND, $0.2352 @Q=3k, $0.2184@Q=12k
Misc. Board Elements	Capacitor, resistors, etc.	$4.50	Estimate based on $0.25 component for each input/output
Housing	Shielded plastic housing, watertight	$5.00	Estimate based on comparable shielded, electronic enclosures. Includes fasteners.
Assembly	Assembly of boards/housing	$5.83	Robotic Assembly of approx. 50 parts at 3.5 sec each, $2/min assembly cost
Contingency	10% of all components	$6.02	Standard DFMA additional cost to capture un-enumerated elements/activities.
Markup	25% of all components	$16.54	Manufacturer's Markup
Total		**$82.72**	

Figure 185. System controller component costs

Annual Production Rate	1,000	10,000	30,000	80,000	100,000	500,000
System Controller	$172	$152	$138	$103	$97	$83
Total Cost ($/system)	$172	$152	$138	$103	$97	$83
Total Cost ($/kW$_{net}$)	$2.15	$1.90	$1.72	$1.29	$1.21	$1.03

Figure 186. Cost breakdown for system controller

8.2.6 Sensors

Aside from the air mass flow sensor (which is book-kept as part of the air loop), there are three types of sensors in the fuel cell system: current sensors, voltage sensors, and hydrogen sensors. The basic sensor descriptions and their costs are listed in Figure 187 and Figure 188.

Component	Description	Cost at 500k systems/year	Cost Basis
Current Sensor (for stack current)	~400A, Hall Effect transducer	$10	Based on LEM Automotive Current Transducer HAH1BV S/06, 400A
Current Sensor (for CEM motor current)	~400A, Hall Effect transducer	$10	Based on LEM Automotive Current Transducer HAH1BV S/06, 400A
Voltage Sensor	225-335 V	$8	Rough estimate based on a small Hall Effect sensor in series with a resistor
H$_2$ Sensor (2 needed)	Sensor unit for 0 to 4 vol% H$_2$ concentrations in air in 2 seconds	$51.28 each (2 needed)	Fis (A Nissha Company) model FH2-HY04
Total		$130.57	

Figure 187. Sensor details

Annual Production Rate	1,000	10,000	30,000	80,000	100,000	500,000
Current Sensors ($/system)	$20	$20	$20	$20	$20	$20
Voltage Sensors ($/system)	$8	$8	$8	$8	$8	$8
Hydrogen Sensors ($/system)	$484	$262	$198	$156	$148	$103
Total Cost ($/system)	$512	$290	$226	$184	$176	$131
Total Cost ($/kW$_{net}$)	$6.40	$3.63	$2.83	$2.30	$2.20	$1.63

Figure 188. Cost breakdown for sensors

8.2.6.1 Current Sensors

The current sensors are located on the stack, and allow the system controller to monitor the current being produced.

8.2.6.2 Voltage Sensors

The voltage sensors are located on the stack, and allow the system controller to monitor the voltage being produced.

8.2.6.3 Hydrogen Sensors

The vehicle will require a hydrogen sensing system to guard against hydrogen leakage accumulation and fire. It is postulated that a declining number of hydrogen sensors will be used within the fuel cell power system as a function of time and as real-world safety data is accumulated. Consequently, it is estimated

that two sensors would initially be used in the engine compartment, eventually dropping to zero. Additional sensors may be necessary for the passenger compartment and the fuel storage subsystem but these are not in the defined boundary of our fuel cell power system assessment.

The hydrogen sensor system specified is from FiS (A Nissha Company), based on model FH2-HY04 technology used in the Toyota Mirai fuel cell system. According to a DOE-funded report by Lawrence Livermore National Laboratory,[107] the detection threshold for vehicular uses of H_2 sensors is 1% (10,000 ppm) H_2 with a response time of less than 1 min. Each FiS sensor unit can detect between 0 and 4 vol% H_2 in air in 2 seconds. The replacement schedule required for these sensors is 10 years without requirement for calibration.

Hydrogen sensors are currently quite expensive. 2010 discussion with Makel Engineering reveals that the specified hydrogen sensors are currently hand built and cost approximately $850 each. Jeffrey Stroh from Makel estimates that such units would cost approximately $100 each if mass-produced at 500,000 per year. With further technology and manufacturing improvements, including a move to integrated circuitry, he estimates that the unit cost could drop to only $20 per sensor. In 2015, discussions with NTM Sensors suggested a cost for a single sensor of $399, $299 for quantity 3, $199 for quantity 1,000, and $75 for quantity 1 million (projected cost target). In 2016, FiS provided a quotation for JPY 22,050 per detector ($220 USD/detector) at quantity 2,000, and JPY2500 ($35 USD) per sensor in 1 million unit orders (with availability at that manufacturing rate expected in the year 2020). Figure 189 lists the estimated hydrogen sensor costs that include additional connectors ($17-$24) needed to plug into the system power controller.

Annual Production Rate	1,000	10,000	30,000	80,000	100,000	500,000
Sensors per system	2	2	2	2	2	2
Sensor ($)	$242	$131	$99	$78	$74	$51
Total Cost ($/system)	$484	$262	$198	$156	$148	$103
Total Cost ($/kW$_{net}$)	$6.05	$3.28	$2.48	$1.95	$1.85	$1.28

Figure 189. Cost breakdown for hydrogen sensors

8.2.7   Miscellaneous BOP

The BOP components which do not fit into any of the other categories are listed here in the miscellaneous section.

Figure 190 shows the cost breakdown for these components.

---

[107] R.S. Glass, J. Milliken, K. Howden, R. Sullivan (Eds.), Sensor Needs and Requirements for Proton-Exchange Membrane Fuel Cell Systems and Direct-Injection Engines, 2000, pp. 7 – 15. DOE, UCRL-ID-137767.

Annual Production Rate	1,000	10,000	30,000	80,000	100,000	500,000
Belly Pan ($/system)	$63	$11	$7	$6	$6	$5
Mounting Frames ($/system)	$100	$64	$43	$33	$30	$30
Wiring ($/system)	$83	$75	$72	$70	$69	$67
Fasteners for Wiring & Piping ($/system)	$17	$15	$14	$14	$14	$13
Total Cost ($/system)	$263	$165	$136	$123	$119	$115
Total Cost ($/kW$_{net}$)	$3.28	$2.06	$1.70	$1.54	$1.48	$1.43

Figure 190. Cost breakdown for miscellaneous BOP components

8.2.7.1 *Belly Pan*

The belly pan is modeled as a 1 x 1.5 m shallow rectangular pan, bolted to the underside of the fuel cell system to protect it from weather and stone strikes.

The belly pan manufacturing process is modeled as a vacuum thermoforming process, in which thin polypropylene sheets are softened with heat and vacuum drawn onto the top of a one-sided mold. The capital cost of the vacuum thermoforming machine is approximately $300,000, and utilizes an optional automatic loading system, which costs another $200,000. If manual loading is selected, the process requires one laborer per line, instead of the 1/4 laborer facilitated by the automatic loading system. The analysis shows that the automatic system is only cost effective at the 500,000 systems per year production rate. Naturally, the loading option also changes the time per part; the vacuum time is 8 seconds per part, on top of which the insertion time adds another 11.2 seconds for the manual loading, or 2 seconds for the automatic method. The process parameters are shown in Figure 191, and the machine rate parameters are shown in Figure 192.

Annual Production Rate	1,000	10,000	30,000	80,000	100,000	500,000
Equipment Lifetime (years)	8	8	8	15	15	15
Interest Rate	10%	10%	10%	10%	10%	10%
Corporate Income Tax Rate	40%	40%	40%	40%	40%	40%
Capital Recovery Factor	0.229	0.229	0.229	0.175	0.175	0.175
Equipment Installation Factor	1.4	1.4	1.4	1.4	1.4	1.4
Maintenance/Spare Parts (% of CC)	5%	5%	5%	5%	5%	5%
Miscellanous Expenses (% of CC)	6%	6%	6%	6%	6%	6%
Power Consumption (kW)	30	30	30	35	35	40

Figure 191. Belly pan thermoforming process parameters

Annual Production Rate	1,000	10,000	30,000	80,000	100,000	500,000
Machine Selection	Vacuum Thermo-former #1	Vacuum Thermo-former #1	Vacuum Thermo-former #1	Vacuum Thermo-former #2	Vacuum Thermo-former #2	Vacuum Thermo-former #2
Assembly Type	Manual	Manual	Manual	Manual	Manual	Auto
Capital Cost ($/line)	$50,000	$50,000	$50,000	$250,000	$250,000	$655,717
Costs per Tooling Set ($)	$96,352	$96,352	$96,352	$96,352	$96,352	$96,352
Tooling Lifetime (years)	3	3	3	3	3	3
Cavities per platen	1	1	1	1	1	1
Total Cycle Time (s)	71.20	71.20	71.20	15.20	15.20	7.00
Simultaneous Lines	1	1	1	1	1	1
Laborers per Line	1	1	1	1	1	0.25
Line Utilization	0.6%	5.9%	17.7%	10.1%	12.6%	28.9%
Effective Total Machine Rate ($/hr)	$1,136.85	$156.88	$84.29	$310.80	$258.32	$253.68
Material Cost ($/kg)	$1.48	$1.48	$1.48	$1.48	$1.48	$1.48

Figure 192. Machine rate parameters for belly pan thermoforming process

Because of the extremely soft nature of the hot polypropylene and the low impact of the process, each mold (~$85,056) will easily last the entire lifetime of the thermoforming machine. However, belly pan designs are likely to change well before the forming machine wears out, so the mold's lifetime is set at three years. This means that the tooling costs are sufficiently low to ignore at all but the 1,000 systems per year level, where they account for almost 4% of the part cost. Figure 193 shows the cost breakdown.

Annual Production Rate	1,000	10,000	30,000	80,000	100,000	500,000
Material ($/system)	$4	$4	$4	$4	$4	$4
Manufacturing ($/system)	$22	$3	$2	$1	$1	$0
Tooling ($/system)	$36	$4	$1	$0	$0	$0
Total Cost ($/system)	$63	$11	$7	$6	$6	$5
Total Cost ($/kWnet)	$0.79	$0.14	$0.09	$0.08	$0.07	$0.06

Figure 193. Cost breakdown for belly pan

8.2.7.2 Mounting Frames

It is assumed that the fuel cell power system would be built as a subsystem, and then hoisted as an assembly into the automotive engine compartment. Consequently, the power system attaches to a mounting frame substructure to allow easy transport. These mounting frames are assumed to be contoured steel beams with various attachment points for power system components, facilitating attachment to the vehicle chassis. The cost is roughly estimated at $30 at 500,000 systems per year to $100 at 1,000 systems per year.

8.2.7.3 Wiring

Wiring costs include only wiring materials as wiring installation costs are covered under the system assembly calculations.

A conceptual fuel cell system wiring schematic (Figure 194) was created to determine where cables were needed and whether they were for transmission of data, power, or both. Cable types, detailed in Figure 195, are selected based on the maximum current required by each electrical component.

With the exception of the heavy-duty power cables attached to the current collectors, every cable is comprised of multiple wires. Each cable also requires a unique type of connector, of which two are needed for each cable.

It is assumed that the wires and connectors would be purchased rather than manufactured in-house, with high-volume pricing estimates obtained for the cable components from Waytek, Inc. Taking into account the required length of each cable, the number of wires per cable, and selecting the appropriate connectors, the component prices are applied to the wiring bill of materials and the total wiring cost is calculated for each system (seeFigure 196).
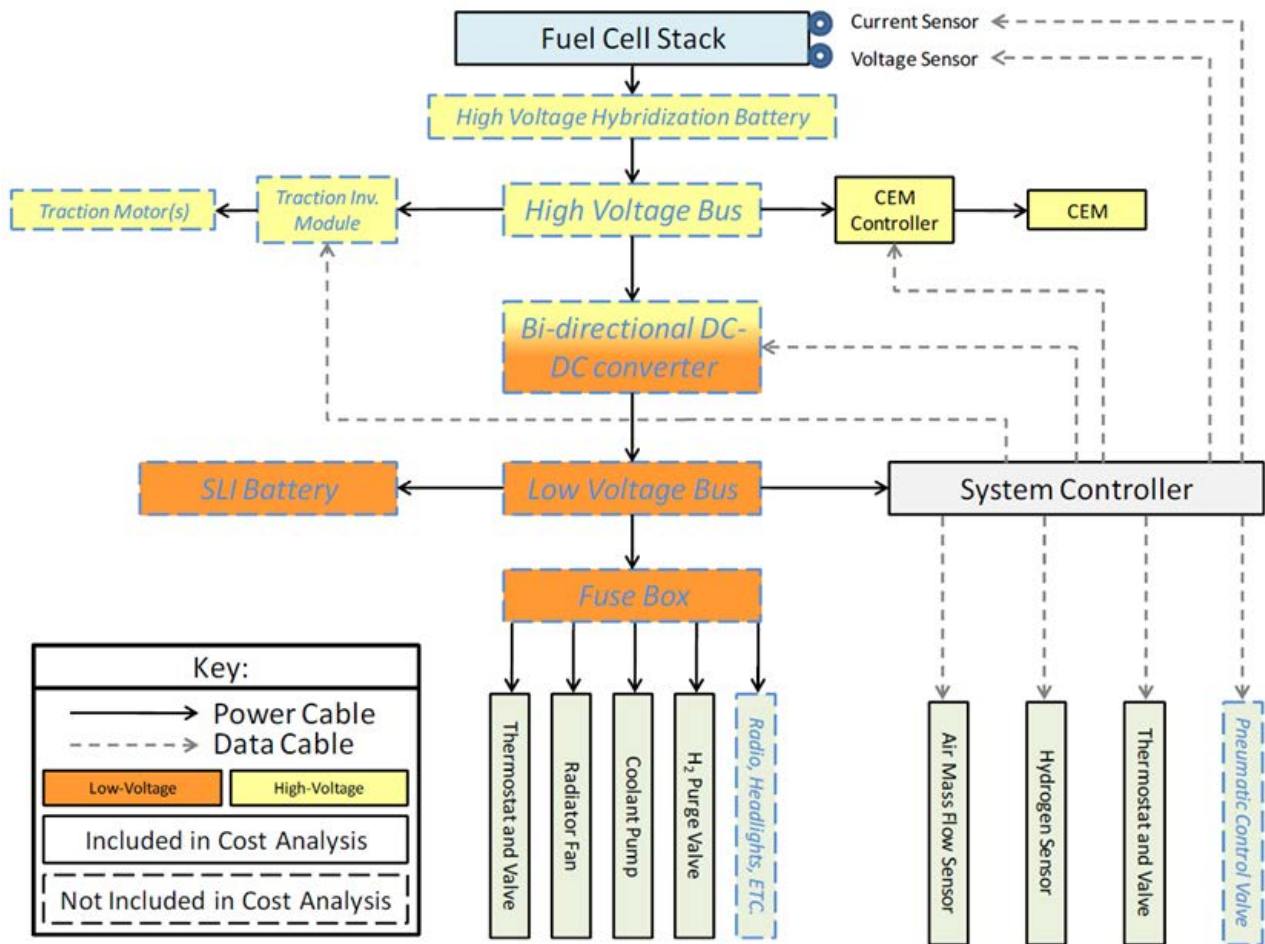
Figure 194. Fuel cell system wiring schematic

	Quantity	Length (m)
Cable Types		
Power Cable, OOOO Gauge	2	0.5
Power Cable, 6 Gauge	1	0.25
Power Cable, 7 Gauge	4	3.5
Power Cable, 12 Gauge	3	3
Power Cable, 16 Gauge	10	9
Totals	20	16.25

Figure 195. Wiring details

	1,000	10,000	30,000	80,000	100,000	500,000
Cables ($/system)	$29	$26	$25	$24	$24	$23
Connectors ($/System)	$54	$49	$46	$45	$45	$43
Total Cost ($/system)	$83	$75	$72	$70	$69	$67
Total Cost ($/kWnet)	$1.04	$0.94	$0.89	$0.87	$0.86	$0.83

Figure 196. Cost breakdown for wiring

8.2.7.4 Fasteners for Wiring & Piping

A detailed DFMA® analysis was not conducted for these components since the level of detailed required is well outside the bounds of this project. However, these components are necessary and, in aggregate, are of appreciable cost. Cost is estimated at 20% of the wiring and piping cost.

8.2.8 System Assembly

A detailed analysis of system assembly was not conducted since that would require detailed specification of all assembly steps including identification of all screws, clips, brackets, and a definition of specific component placement within the system. Such an analysis is beyond the scope of this project. Instead, an estimate of system assembly time is obtained by breaking the system down into five categories of assembly components (major, minor, piping, hoses, wiring), estimating the number of components within each category, and then postulating a time to assemble each of those components. Specific assumptions and total estimated assembly time for manual assembly are shown in Figure 197.

	Number of Components	Component Placement Time (seconds)	Component Fixation Time (seconds)	Component Totals (minutes)
Major Components (Stack, motors, pumps, vessels, etc.)	19	45	60	33.3
Minor Components (instruments, devices, etc.)	22	30	45	27.5
Piping				
# of pipe segments	5			
bends per segment	2			
time per bend	0			
pipe placement time	30			
# welds per pipe	2			
weld time	90			
# threaded ends per pipe	0			
threading time	0			
				17.5
Hoses	21	30	105	47.3
Wiring (manual)	23	41.8	66.7	41.6
System Basic Functionality Test				10.0
Total System Assembly Time				177.1

Figure 197. Single-station system assembly assumptions

Two types of system assembly methods are examined: single-station and assembly line. In single-station assembly approach, a single workstation is used to conduct assembly of the entire fuel cell power plant. Very little custom machinery is needed to assemble the system and components and subsystems are arrayed around the workstation for easy access. For 1,000 systems per year, only one such workstation is required. Assembly process parameters are listed in Figure 198.

Annual Production Rate	1,000	10,000	30,000	80,000	100,000	500,000
Assembly Method	Assembly Line	Assembly Line	Assembly Line	Assembly Line	Assembly Line	Assembly Line
Index Time (min)	104.55	83.64	83.64	83.64	83.64	83.64
Capital Cost ($/line)	$50,000	$100,000	$100,000	$100,000	$100,000	$100,000
Simultaneous Lines	1	1	2	5	6	27
Laborers per Line	10	10	10	10	10	10
Line Utilization	6.7%	53.2%	79.8%	85.1%	88.7%	98.5%
Effective Total Machine Rate ($/hr)	$663.94	$577.36	$567.74	$566.54	$565.82	$564.09
Cost per Stack ($)	$148	$103	$101	$101	$101	$101

Figure 198. System assembly process parameters

The assembly for all other annual production rates uses a ten-workstation assembly line configuration. Each fuel cell system flows through the assembly line sequentially. The line reduces the total cumulative time required for system assembly because workers at each workstation on the line have their tools and components closer at hand than they do under the single workstation approach, and because tool changes are minimized due to the higher repetitive nature of an assembly line. This method is

approximately 20% faster than the single-workstation approach, with an assembly line index time[108] of only 14.2 minutes. The system assembly cost is detailed in Figure 199.

Annual Production Rate	1,000	10,000	30,000	80,000	100,000	500,000
System Assembly & Testing ($/System)	$148	$103	$101	$101	$101	$101
Total Cost ($/system)	$148	$103	$101	$101	$101	$101
Total Cost ($/kWnet)	$1.85	$1.29	$1.27	$1.27	$1.26	$1.26

Figure 199. Cost breakdown for system assembly & testing

8.2.9 System Testing

A ten-minute system functionality and performance test is included in the system assembly process. Each stack has separately undergone multiple hours of testing as part of stack conditioning and thus there is high confidence in the stack performance. System testing is only needed to ensure that the peripheral systems are functioning properly and adequately supporting the stack. Typically, the only testing of gasoline engines contained within automobiles is a simple engine startup as the vehicles are driven off the assembly line. Corresponding, the fuel cell "engines" are only minimally tested for functionality. Cost for this system testing is reported under system assembly.

8.2.10 Cost Contingency

It is common practice in the automotive industry to include a 10% cost contingency to cover the cost of procedures or materials not already explicitly included in the analysis. This serves as a guard against an underestimation of cost which can derail a cost estimator's career within the automotive industry. However, no such cost contingency has been included in this cost analysis upon the request of the DOE.

---

[108] Assembly line index time is defined as the time interval each system spends at a given workstation.

9 Bus Fuel Cell Power System

In addition to the annual automotive fuel cell power system cost update, a 40' transit bus fuel cell power system is also analyzed for the 2016 cost report. The bus fuel cell system was cost analyzed for the first time in 2012, thus the 2016 analysis represents an annual update to last year's bus study. Primary differences between the 2015 bus and the 2016 bus include most all of the above-listed changes between the 2015 and 2016 auto technology systems, including updates to the bipolar plate forming and coating assumptions, laser welding parameters, and GDL cost. Bus operating conditions remain the same as in 2015.

The 2016 automotive and bus power plants are very similar in operation but possess key differences in:

- power level, operating pressure, and catalyst loading,
- manufacturing rate, and
- level of vertical integration.

Section 9.1 below details the key differences between auto and bus power systems. If no difference is documented in this section, then details of material selection, manufacturing processes, and system design are assumed not to differ from that of the automotive system.

9.1 Bus Power System Overview

9.1.1 Comparison with Automotive Power System

Figure 200 below is a basic comparison summary of the 2016 auto and bus systems. As shown, most stack mechanical construction and system design features are identical between the bus and automotive power plants. Primary system differences include:

- Use of two ~90 kW_{gross} fuel cell stacks to achieve a net system power of 160 kW_{net} (instead of one ~90 kW_{net} stack for an 80 kW_{net} power level as used in the automotive system)
- Higher cell platinum loading (0.5 $mgPt/cm^2$ instead of 0.134 $mgPt/cm^2$ as used in the automotive system)
- Differences in cell active area and number of active cells per stack
- Higher system voltage (reflecting two stacks electrically in series and the desire to keep current below 400 amps)
- Operation at 1.9 atm (instead of 2.5 atm as used in the automotive system)
- Use of a multi-lobe air compressor (based on an Eaton-style design) without an exhaust gas expander (instead of a centrifugal-compressor/radial-inflow-expander based on a Honeywell-style design as used in the automotive system)
- Reduced stack operating temperature (72 °C instead of 95 °C as used in the auto system)
- Increased size of balance of plant components to reflect higher system gross power

	2016 Auto Technology System	2016 Bus Technology System
Power Density (mW/cm^2)	749	739
Total Pt loading (mgPt/cm^2)	0.134	0.5
Net Power (kW$_{net}$)	80	160
Gross Power (kW$_{gross}$)	87.7	194.7
Cell Voltage (V)	0.659	0.659
Operating Pressure (atm)	2.5	1.9
Stack Temp. (Coolant Exit Temp) (°C)	94	72
Air Stoichiometry	1.4	1.8
Q/ΔT (kW/°C)	1.45	5.4
Active Cells	379	758
Membrane Material	Nafion on 17-micron ePTFE	Nafion on 20-micron ePTFE
Radiator/ Cooling System	Aluminum Radiator, Water/Glycol Coolant, DI Filter, Air Precooler	Aluminum Radiator, Water/Glycol Coolant, DI Filter, Air Precooler
Bipolar Plates	Stamped SS 316L with TreadStone Litecell™ Gen 2 Coating	Stamped SS 316L with TreadStone Litecell™ Gen2 Coating
Air Compression	Centrifugal Compressor, Radial-Inflow Expander	Eaton-Style Multi-Lobe Compressor, Without Expander
Gas Diffusion Layers	Carbon Paper Macroporous Layer with Microporous Layer	Carbon Paper Macroporous Layer with Microporous Layer
Catalyst & Application	Slot Die Coating of: Cath.: Dispersed 0.116 mgPt/cm^2 d-PtNi$_3$ on C Anode: Dispersed 0.0182mgPt/cm^2 Pt on C	Slot Die Coating of: Cath.: Dispersed 0.4 mgPt/cm^2 Pt on C Anode: Dispersed 0.1mgPt/cm^2 Pt on C
Air Humidification	Plate Frame Membrane Humidifier	Plate Frame Membrane Humidifier
Hydrogen Humidification	None	None
Exhaust Water Recovery	None	None
MEA Containment	Screen Printed Seal on MEA Sub-gaskets, GDL hot pressed to CCM	Screen Printed Seal on MEA Sub-gaskets, GDL hot pressed to CCM
Coolant & End Gaskets	Laser Welded(Cooling)/ Screen-Printed Adhesive Resin (End)	Laser Welded (Cooling), Screen-Printed Adhesive Resin (End)
Freeze Protection	Drain Water at Shutdown	Drain Water at Shutdown
Hydrogen Sensors	2 for FC System[109]	3 for FC System[110]
End Plates/ Compression System	Composite Molded End Plates with Compression Bands	Composite Molded End Plates with Compression Bands
Stack Conditioning (hours)	2	2

Figure 200: Comparison table between 2016 auto and 2016 bus technology systems

9.1.2 Changes to Bus System Analysis since the 2015 Report

This report represents the fourth annual update of the 2012 SA bus fuel cell system cost analysis and updates the previous work to incorporate advances made over the course of 2016. These advances may

---

[109] There are a total of 4 hydrogen sensors on-board the FC vehicle: 2 under the hood in the power system (within cost estimate), 1 in the passenger cabin (not in cost estimate), and 1 in the fuel system (not in cost estimate).
[110] Additional sensor added to bus system due to larger fuel cell compartment.

include new technologies, improvements and corrections made in the cost analysis, and alterations of how the systems are likely to develop. This 2016 analysis closely matches the methodology and results formatting of the 2015 analysis.[111] Figure 201 lists changes made on the bus system for the 2016 analysis with combined cost increase of $8.21/kWnet at 1,000 systems per year. The two most significant changes in 2016 that resulted in the greatest cost impact are the updates to catalyst material and markup assumptions, re-evaluation of the bipolar plate stamping process, and the updated GDL cost. Similar catalyst material and markup changes as applied to the automotive system were applied to the bus. Changes to the coolant gasket laser welding assumptions increased the system cost by $1.07/kW$_{net}$ due to added welding length over the active area. The switch from TreadStone LiteCell^{TM} Gen1 to TreadStone LiteCell^{TM} Gen2 with different materials and processing, reduced membrane thickness (from 25 microns to 20 microns[112]), and changes to QC for slot die coating individually had little cost impact. The polarization and operating conditions were kept constant at 2015 levels as there has been no new performance data available for the bus system since the end of 2015.

Change	Reason	Change from previous value ($/kW)	Cost ($/kW) (@ 1k sys/yr)
2015 Final Cost Estimate		NA	$261.97
BPP	Bipolar Plate stamping assumption changes (press force increase from 1,000 to 1,800 tons, capital from $530k to $2M, tooling cost increase from $100k to $600k and increase in tool lifetime of 600k to 10M cycles).	$11.52	$273.49
BPP Coating	Updated Treadstone Coating to Generation 2 materials and process	($1.49)	$272.00
GDL	Changed to DFMA analysis of GDL and added 25% markup for profit	($1.63)	$270.38
Coolant Gasket Laser Welding	Added extra laser welding length over the active area of the BPPs, reduced laser welding speed, and increased the number of simultaneous weld heads per station.	$1.84	$272.22
Dispersed Catalyst Synthesis	Numerous updates to dispersed catalyst synthesis and catalyst material markup based on feedback from catalyst material supplier.	$2.90	$275.11
Minor Changes	Updated membrane thickness from 25 microns to 20 microns and minor changes to QC on slot die coating.	($3.51)	$271.60
2016 Value		$9.63	$271.60

Figure 201. Table of changes made between the 2015 and 2016 bus system analysis

9.2   Bus System Performance Parameters

The bus and automotive power systems function in nearly identical fashion but have different power levels, flow rates, and pressure levels. The following sections describe the sizing methodology and values for key parameters of the bus power system.

---

[111] "Mass Production Cost Estimation of Direct H$_2$ PEM Fuel Cell Systems for Transportation Applications: 2015 Update" Brian D. James, Jennie M. Huya-Kouadio & Cassidy Houchins, Strategic Analysis, Inc., December 2015.

[112] While both the 2015 and 2016 performance estimates were based on a 20 micron thick membrane, the cost impact of reducing from 25 microns to 20 microns was only applied to the 2016 analysis. This minor error in the 2015 analysis had only slight cost impact.

9.2.1 Power Level

To provide sufficient power, two 80 kW$_{net}$ stacks are used, for a total net electrical power of 160 kW. This power level was chosen as an intermediate point in existing bus FC power systems, which nominally range from 140 kW$_{net}$ to 190 kW$_{net}$ electrical. Modeling a system which is an even multiple of 80 kW has the additional advantage of allowing a comparison between a dedicated bus system and a pair of automotive systems.

9.2.2 Polarization Performance Basis

Stack performance within the bus system is based on Argonne National Laboratory modeling of dispersed platinum on carbon catalyst membrane electrode assembly (MEA) performance data. The polarization curve model used for the bus stacks is different from the automotive system with modification for different operating conditions, catalyst material, and catalyst loading (as discussed below). As understood by the authors, the main bus fuel cell power plant supplier is Ballard Power Systems. They use the same stack construction and MEA composition within their bus power system stacks as they do for their light-duty vehicle stacks. From 2012 to 2014, SA assumed the stack construction and MEA composition was the same in the auto as the bus. In 2015 and 2016, the stack construction is the same, but the MEA composition is different with an alternative catalyst material (dispersed Pt on C for the bus vs. dispersed d-PtNi$_3$ on C for the auto system).

Beginning-of-life (BOL) stack design conditions at peak power selected for the 2015/2016 bus power system are shown in Figure 202 compared to the 2012, 2013, and 2014 analysis values. No changes were made to the operating conditions or performance curves for the bus between 2013 and 2014, but changed from 2014 to 2015. No changes were made to the operating conditions or performance curves between 2015 and 2016.

	2012 Bus Analysis	2013 Bus Analysis	2014 Bus Analysis	2015/2016 Bus Analysis
Cell Voltage (volts/cell)	0.676	0.676	0.676	0.659
Current Density (mA/cm^2)	1,060	889	889	1,121
Power Density (mW/cm^2)	716	601	601	739
Stack Pressure (atm)	1.8	1.8	1.8	1.9
Stack Temperature (outlet coolant temperature)	74°C	74°C	74°C	72°C
Air Stoichiometry	1.5	2.1	2.1	1.8
Total Catalyst Loading (mg/cm^2)	0.4	0.4	0.4	0.5
Cells per System	739	739	740	758

Figure 202: Bus fuel cell power system stack operating parameters from 2012 to 2015/2016

Past discussions with Ballard[113] regarding their latest generation[114] (HD7) fuel cell stacks suggests an anticipated bus application design peak power operating point of ~0.69 volts/cell at ~1,100 mA/cm^2

---

[113] Personal communication, Peter Bach, Ballard Power Systems, October 2012.

yielding a power density of 759mW/cm^2 at a stack pressure of 1.8 atm and a ~0.4mgPt/cm^2 total catalyst loading. This operating point is very similar to the selected 2015/2016 bus design point and is primarily a consequence of the 2015/2016 polarization curve.

As seen in Figure 203, the selected bus power density is noted to be slightly lower than the design point chosen for the automotive systems (746 vs. 739 mW/cm^2) and consequently results in a correspondingly larger bus fuel cell stack.
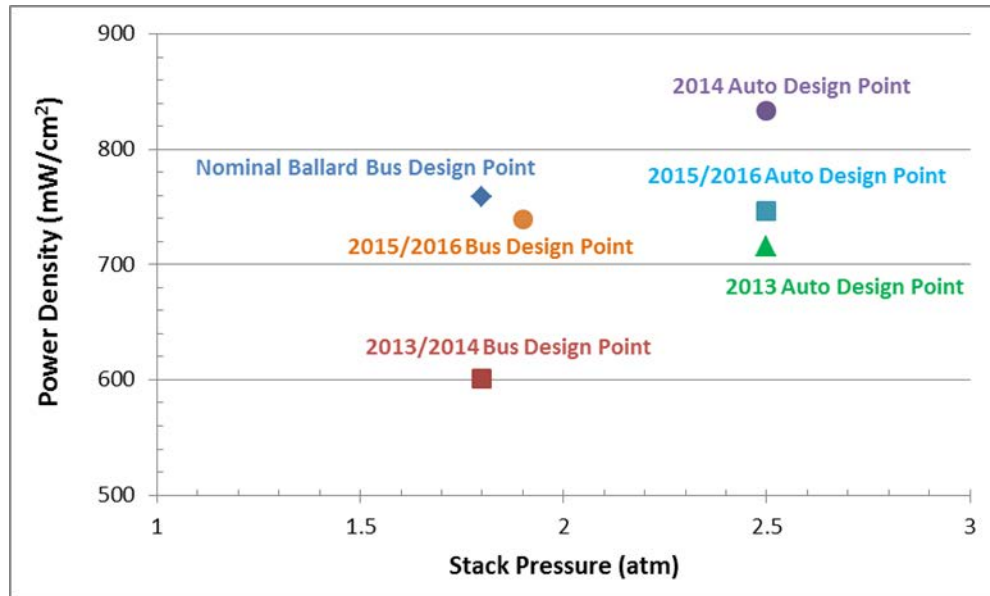
Figure 203: 2015/2016 Bus peak power design point: Based on 2015 ANL Modeling data, 0.5mgPt/cm^2 total catalyst loading, 1.8 air stoic, 0.659V/cell

9.2.3 Catalyst Loading

Catalyst loading is a key driver of system cost and significant effort on the part of fuel cell suppliers has gone towards its reduction. In general, bus applications are less cost-sensitive and have longer lifetime requirements than automotive systems. Consequently, bus fuel cell stacks are more likely to have high catalyst loading since there is a general correlation between platinum loading and stack durability[115]. Whereas past examination of the 3M NSTF cell performance as represented by ANL modeling results and discussions with 3M researchers revealed that increases in catalyst cathode loading past

---

[114] Ballard FCvelocity® HD6 stacks are currently used in Ballard bus fleets. The HD7 stack is the next generation stack, has been extensively tested at Ballard, and is expected to be used in both automotive and bus vehicle power systems future years.

[115] Many factors affect stack lifetime and degradation rate. But to the extent that degradation is caused by platinum catalyst poisoning, reduction in surface area, and/or reduced utilization, high catalyst loading tends to correlate with longer lifetime.

~0.2mgPt/cm^2 result in declining polarization performance due to a catalyst crowding[116] effect, such an effect is not expected for dispersed Pt on C catalyst systems. Consequently, for the bus application, catalyst loading is set at 0.5 mgPt/cm^2 total loading (nominally 0.4mgPt/cm^2 on the cathode and 0.1mgPt/cm^2 on the anode) to achieve a balance of performance, durability, and cost based on ANL system modeling. This level of catalyst loading is also approximately consistent with the levels used in Ballard fuel cell stacks.

9.2.4 Catalyst Ink

The catalyst layer is formed by applying a catalyst ink to the membrane as described in the next section. The catalyst ink is based on a slurry of platinum, Vulcan XC-72 carbon powder, and ~4% wt ionomer solution, with an aqueous methanol solution for a solvent. The platinum is dispersed on the carbon powder via a precipitation method. The overall catalyst ink preparation process used in the DFMA® model is described in Figure 204. For a full description of CPA formulation and the assumptions used for the Pt donor reactant, see Section 8.1.3.2.
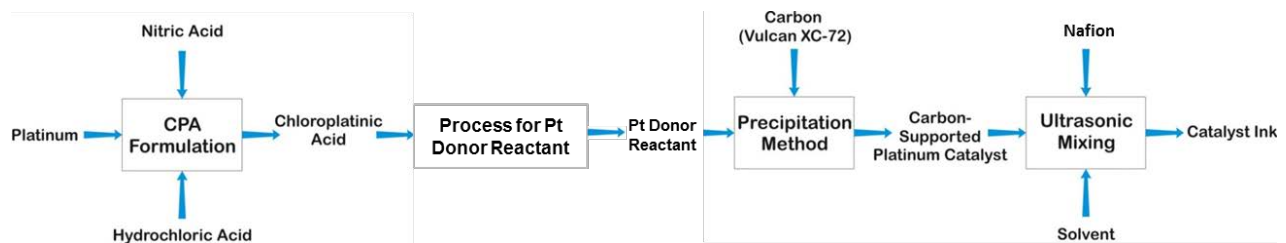
Figure 204. Catalyst ink preparation

In 2016, feedback from catalyst suppliers prompted a few changes to markups associated with Pt and various safety/security aspects of a catalyst manufacturing facility. See Section 6.2.2 for a detailed description of markup applied to the auto catalyst (assumed to be similar, if not the same for the bus system).

9.2.5 Parasitic Load Requirements

In 2015, the parasitic loads were updated for the bus system to bring them in alignment with ANL modeling results. The most significant change to the parasitic loads was the electrical power for the high temperature coolant loop radiator fan which increased from 0.9 kW to 8.26kW. The previous 0.9 kW power estimate was based on the automotive system and scaled with system net power. The radiator fan power is now based on ANL's fan power of 4.3 kW for an 83 kW$_{net}$ bus system and is scaled to the 160kWnet bus system. This significant radiator fan power difference between automotive and bus systems is thought to be due to the lower operating temperature of the bus, the diminished use of ram air for the bus fuel cell due to fuel cell placement near the rear of the vehicle, and higher pressure drop through the bus radiator system due to radiator placement and size. The same component efficiencies

---

[116] The term "catalyst crowding" is meant to represent the situation where the catalyst layer on the substrate whiskers of the NSTF catalyst layer becomes so thick that it blocks gas flow or otherwise adversely affects performance.

are used in the bus as in the automotive application: 45% fan efficiency, 90% fan motor efficiency, and 95% DC-DC converter efficiency. Other parasitic load requirements are listed below in Figure 205.

Parasitic Load (kW)	2014 Value	2015/2016 Value
Air Compressor Shaft Power	24.05	23.74
Air Compressor/Motor Input Required (gross)	25.31	24.99
High-Temperature Coolant Loop Pump	1.1	1.15
High-Temperature Coolant Loop Radiator Fan	0.9	8.26
Low-Temperature Coolant Loop Pump	0.12	0.11
Other (Controller, Instruments, etc.)	0.2	0.2
Total Parasitic Loads	**27.63**	**34.71**

Figure 205. Table of parasitic loads for the 2014 and 2015/2016 Bus systems

9.2.6 Operating Pressure

As previously stated, the two main fuel cell bus power plant developers are Ballard Power Systems and UTC Power/US Hybrid.[117] Recent Ballard buses, using their FCvelocity® HD6 fuel cell stacks, typically operating at a stack pressure of ~1.8 atm (at rated power) and do not employ an exhaust gas expander. Recent UTC Power fuel cell bus power plants, using their porous carbon bipolar plates, typically operate near ambient pressure. The UTC Power porous carbon plates allow water management within the cell (both humidification and product water removal) and are a key element of their ability to achieve high polarization performance at low pressure. The porous carbon bipolar plate construction has not been cost-modeled under this effort and it would be inappropriate to postulate the combination of stamped metal bipolar plate construction with performance of platinum on carbon catalyst MEA at near ambient pressure.[118] Consequently, ambient pressure operation is not selected for bus application cost modeling at this time, although it could be considered in future analysis tasks.

A stack pressure of 1.9 atm is selected as the bus system baseline operating stack pressure at rated power to reflect ANL's 2015/2016 optimized performance model. An exhaust gas expander is not used as there is a limited power available from the expansion of gas at this moderate pressure. This operating point of 1.9 atm without expander is in contrast to the optimized automotive system operating conditions of 2.5 atm with expander. A system level cost optimization (i.e. varying stack operating conditions to determine the combination of parameters leading to lowest system cost) was not conducted as polarization performance is not available at the higher catalyst loadings expected to be employed to ensure durability.

---

[117] In January 2014, UTC announced the execution of a global technology and patent licensing agreement with US Hybrid Corporation for the commercialization of UTC's Proton Exchange Membrane (PEM) fuel cell technologies for the medium and heavy duty commercial vehicle sectors.
[118] This combination is theoretically possible but experimental data is not readily available nor, to the author's knowledge, have NSTF catalyst MEA parameters been optimized for ambient pressure operation.

9.2.7   Stack Operating Temperature

In the 2012 bus analysis, design stack temperature[119] at rated (peak) power was determined by an ANL correlation with stack operating pressure and was set at 72 °C to be consistent with 1.9 atm. This was a significant reduction from the 95 °C temperature of the 2014-2016 automotive system at 2.5 atm. For the 2013/2014 analysis, ANL added temperature as an independent variable in their polarization model, thereby potentially allowing an optimization of operating temperature for lowest system cost. However, for a variety of non-polarization curve related reasons (as discussed below), bus fuel cell systems tend to operate at cooler temperatures. Thus rather than estimating stack performance on an optimal (high) temperature as determined by polarization data, it is more realistic to base performance on the temperature most likely to be experienced with the bus stacks. For this reason, a broader system level cost optimization is not conducted and the 72 °C stack temperature is retained for the 2016 analysis. Future analysis is planned to more fully explore the impact of bus stack temperature on performance and cost.

It is noted that Ballard reports their fuel cell bus stack temperatures at only 60 °C. The reasons for this are several-fold. First, the system may not typically operate at rated power for long enough times for stack temperature to rise to its nominal value. This is particularly true for a bus power plant for which, depending on the bus route, maximum power may be demanded only a low fraction of the time. Second, various stack and membrane failure mode mechanisms are associated with high temperature. Thus it may be desirable to deliberately limit stack peak temperature as a means to achieving the stack lifetime goal of >12,000 hours (this is less of a concern for auto applications with lower lifetime requirements). Thirdly, higher stack temperature reduces the size of the heat rejection temperature since it increases the temperature difference with the ambient air. For an automobile, volume and frontal area are at a premium under the hood. Minimizing the size of the radiator is important for the auto application but is less important for the bus application where radiators may be placed on the roof. Thus, there are several good reasons—and fewer disadvantages—in selecting a low operating temperature for the bus compared to the auto application.

9.2.8   Q/ΔT Radiator Constraint

A Q/ΔT radiator constraint of <1.45 kW/°C was applied to the automotive system for the first time in 2013. However, such a radiator constraint is not applied to the bus fuel cell system because 1) buses are larger vehicles and have generally larger frontal areas to accommodate radiators, and 2) an appropriate numerical Q/ΔT constraint is not obvious.[120] Additional analysis to determine the appropriate Q/ΔT constraint is needed before it can be imposed.

---

[119] For modeling purposes, stack operating temperature is defined as the stack exit coolant temperature. Modeling suggests approximately a 10°C temperature difference between coolant inlet and outlet temperatures and the cathode exhaust temperature to be approximately 5°C higher than coolant exit temperature.

[120] The automotive Q/ΔT constraint of <=1.45 kW/°C was set by DOE per suggestion of the Fuel Cell Technical Team (FCTT). Neither the DOE nor the FCTT has set a comparable constraint for the bus application.

9.2.9 Cell Active Area and System Voltage

Because the system consists of two stacks electrically in series, system voltage has been set to 500 V at design conditions.[121] This bus voltage represents a doubling relative to the automotive system and is necessary to maintain the total electrical current below 400 amps. These values are broadly consistent with the Ballard fuel cell bus voltage range[122] of 465 to 730 V. Specific cell and system parameters are detailed in Figure 206 for beginning-of-life (BOL) conditions.

Parameter	Value
Cell Voltage (BOL at rated power)	0.659 V/cell
System Voltage (BOL at rated power)	500 V
Number of Stacks	2
Active Cells per Stack	379
Total Cells per System	758
Active Area per Cell	348 cm^2
Stack Gross Power at Rated Power Conditions (BOL)	194.7 kW

Figure 206: Bus stack parameters

9.3 Eaton-style Multi-Lobe Air Compressor-Motor (CM) Unit

9.3.1 Design and Operational Overview

An Eaton-style twin vortex, Roots-type air compressor such as that currently used in Ballard fuel cell buses is used for the 2016 bus cost analysis. A complete DFMA® analysis of the Eaton-style air compressor was conducted in 2013. Cost is projected at $5,680 for a compressor unit at 1,000 units per year. The baseline compressor is SA's interpretation of a unit using Eaton technology and is modeled on Eaton's R340 supercharger (part of Eaton's Twin Vortices Series (TVS)) and Eaton's DOE program.[123]

The 2013 bus compressor-motor system efficiency was based on the DOE MYRD&D 2011 status values for an 80kW automotive compressor, motor, and motor controller, as seen in Figure 207. For the 2014 - 2016 baseline values, SA uses Eaton's 2014 projected minimum bus compressor efficiency and Eaton's motor/motor-controller combined efficiency. The change in efficiencies from 2013 to 2014 was significant and resulted in a larger motor (due to lower compressor efficiency and motor scaling with shaft power). This increased the total cost of the bus fuel cell system by about $5/kW$_{net}$ at 1,000 systems per year. Since 2013, SA's compressor unit does not include an exhaust gas expander as expanders are not typically utilized by deployed fuel cell buses. However, Eaton projects a >=59% expander efficiency on a future, advanced design compressor/expander/motor integrated unit. Future SA analysis may consider the combined compressor/expander for the bus system, but for 2016, the baseline bus system does not include an expander.

---

[121] For purposed of the system cost analysis, design conditions correlate to rated maximum power at beginning of life.

[122] Ballard FCvelocity®-HD6 Spec Sheet. http://www.ballard.com/fuel-cell-products/fc-velocity-hd6.aspx Accessed 9 October 2012.

[123] Eaton/DOE Contract Number DE-EE0005665.

Parameter	2013 Bus Values	2014 Bus Values	2015/2016 Bus Values	2014 Eaton Projected Bus Values
Compression Ratio at Design Point	1.96	1.96	1.96	1.96
Air Flow Rate at Design Point	732 kg/hr (203 g/s)	750 kg/hr (208 g/s)	685 kg/hr (190g/s)	662 kg/hr (184 g/s)
Compression Efficiency[124] at Design Point	71%	58%	58%	>58%
Expander Efficiency[125] at Design Point	Not used	Not used	Not Used	>59%
Combined Motor and Motor Controller Efficiency[126]	80%	95%	95%	>95%

Figure 207: Details of the baseline bus roots (twin vortices) air compressor.

9.3.2 Compressor Manufacturing Process

The compressor-motor unit modeled as part of the bus DFMA® analysis consists of several components including the motor, motor controller, compressor rotors, drive shafts, couplings, bearings, housing, and other components. A schematic of the SA conceptual design used for the cost analysis (derived from Eaton R340 supercharger design) is shown in Figure 208. The motor shaft is attached to a torsional coupling that fits onto one of the compressor drive shafts with multiple dowels for alignment. Two timing gears drive the second compressor shaft at the same rotation speed as the electric motor. Each shaft has a key slot where the rotor slides on and attaches. Each rotor-shaft assembly has both ball bearings and needle bearings that hold it in place against a bearing plate and the compressor housing. Shaft seals are required so as to isolate any oil within the gear housing and to maintain pressure within the compressor. A complete list of the compressor-motor unit components is shown in Figure 209 along with selected material, type of manufacturing process used in the analysis, dimensions, quantity, and mass.

Within the DFMA® model, compressor-motor system parameters are adjusted to match requirements from the fuel cell system. Thus as stack efficiency and gross power change, the compressor-motor system is resized to the altered air flow requirement, dimensions (rotors, compressor wheel, motor size), and power level (of motor and controller). Compressor-motor system cost is correspondingly updated.

Costs of the compressor-motor system components were estimated by use of Boothroyd Dewhurst Inc. (BDI) software (housings), vendor cost quotes (electric motor and most small purchased items such as bearings, seals, nuts, etc.), or by DFMA® analysis (compressor rotors and timing drive gears).

---

[124] Compression efficiency is defined as adiabatic efficiency.
[125] Expander efficiency is defined as adiabatic efficiency.
[126] Combined efficiency is defined as the product of motor efficiency and motor controller efficiency.
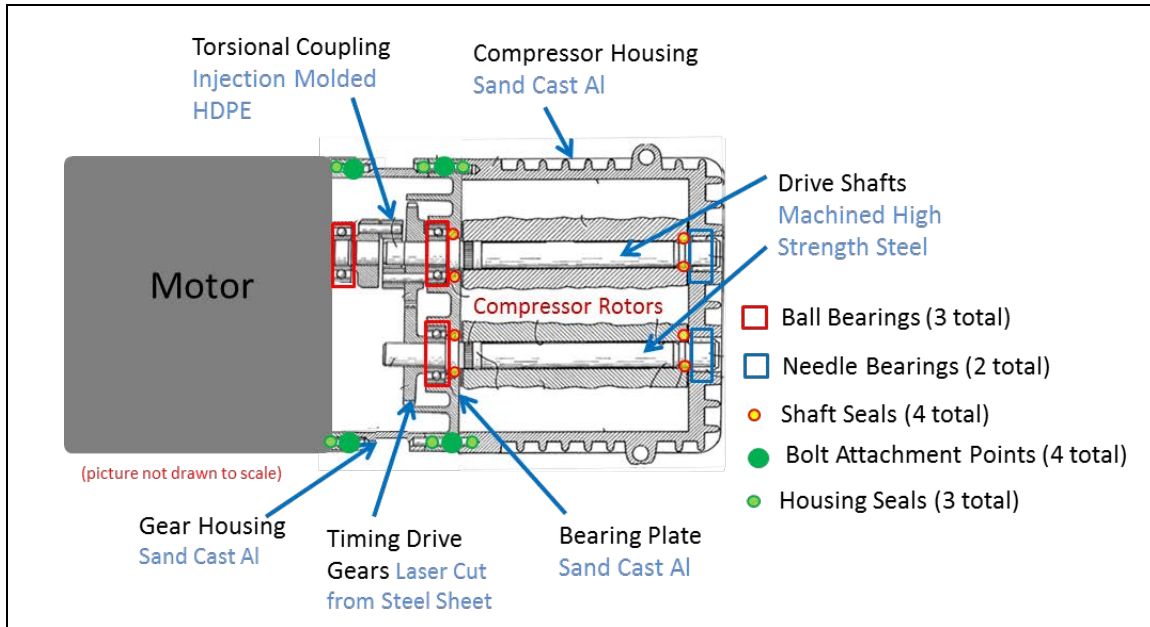
Figure 208. Schematic of cross-section of compressor-motor unit used in the DFMA® cost analysis (Source: Drawing derivation from US patent 4,828,467: Richard J. Brown, Marshall, Mich. "Supercharger and Rotor and Shaft Arrangement Therefor", Eaton Corporation, Cleveland, Ohio, May 9, 1989)

The compressor rotors were modeled as hot extrusions of aluminum 6061-T1. Aluminum billets are assumed to be fed to an aluminum extrusion machine, such as that shown in Figure 210, using a custom stainless steel die to add twist to the extruded rotor billet. Extrusion rates are estimated at approximately 3 cm/sec[127] plus 30 seconds setup time (total 0.62min/rotor). At this extrusion rate and for only 1,000 systems per year, the machinery is highly underutilized. Consequently, the rotors are assumed to be fabricated by a vendor who can pool orders to more highly utilize machinery and thereby lower fabrication cost. A 30% markup is added to the projected vendor costs to reflect G&A, scrap, R&D, and profit and thereby translate the vendor cost into a sales price to the compressor manufacturer/assembler. Cost for extra precision machinery and quality control using a conjugate pair measuring machine[128] is included in the cost.

---

[127] Khalifa, N. B., Tekkaya, A.E., "Newest Developments on the Manufacture of Helical Profiles by Hot Extrusion", Journal of Manufacturing Science and Engineering, ASME, December 2011, Vol 133, 061010-1 to 8.

[128] "Inspection of Screw Compressor Rotors for the Prediction of Performance, Reliability, and Noise" International Compressor Engineering Conference at Purdue University, School of Mechanical Engineering, July 12-15,2004. http://docs.lib.purdue.edu/cgi/viewcontent.cgi?article=2691&context=icec

Summary of Components for SA Compressor/Motor Unit for Bus (Based on Eaton Design)							Annual Production Rate (systems/year)	
							200	1,000
	Material	**Manufacturing Method**	**Qty/sys**	**Dimensions**	**kg/part**	**kg/sys**	**$/system**	
Compressor Components								
Compressor Rotor	6061-T1 Aluminum	Extrusion w/twist	2	21cm x 15cm Max OD	4.68	9.36	$143.77	$134.20
Compressor Housing	6061 Aluminum	Permanent Mold	1	26cm x 17cm x 22cm x 1cm (aver. Thickness)	2.33	2.33	$997.72	$223.79
Compressor Bearing Plate	6061-T1 Aluminum	Permanent Mold	1	17cm (width) x 22cm (height) x 1cm (aver. Thickness)	0.43	0.43	$329.84	$69.48
Compressor Shaft Seals	O-ring seal, polymer	Purchased	4	1.9cm (ID), 5cm (OD)	0.005	0.02	$11.17	$10.92
Timing Drive Gears (compressor: steel)	Stainless Steel	Laser cut from sheet	2	8.76 cm max OD, 1cm thick	0.435	0.869	$33.65	$32.91
Total						**13.00**	**$1,516.14**	**$471.32**
Other Components								
Housing/Motor Seals	O-ring seal, PET	Injection molded	3	17cm x 22cm x 0.2cm (diameter round X-section)	0.07	0.21	$93.51	$20.38
Housing Screws	SS 316	Purchased	4		0.005	0.02	$2.23	$2.18
Front Bearing	steel ball bearings, self lubricated	Purchased	3	5cm (diameter), 1.9cm (ID)	0.322	0.966	$9.05	$8.85
Rear Bearing	steel needle bearings, self lubricated	Purchased	2	5cm (diameter), 1.9cm (ID)	0.322	0.644	$8.71	$8.52
Rotor Drive Shafts	High carbon Steel Alloy	Rod, machined	2	1.9cm (diameter) x 23cm (length)	0.769	1.538	$20.24	$18.99
Torsionally Flexed Coupling	Fiberglass filled HDPE	Injection molded	1	3cm max OD, 1cm thick	0.004	0.004	$37.02	$9.24
Coupling Dowels	Steel	Rod, machined	3	0.25cm diameter, 3cm length	0.001	0.003	$1.73	$1.70
Gear Housing/Motor End Plates	6061-T1 Aluminum	Sand casting	1	17cm x 22cm (height) x 7cm (length) x 1cm (aver. Thickness)	1.08	1.08	$59.09	$24.10
Contingency (5% of total cost to account of any missing parts or erros in cost assumptions)							$396.28	$270.50
Assembly							$11.55	$11.16
Total						**4.47**	**$639.42**	**$375.62**
Motor Components								
Motor		Purchased	1		est 30	est 30	$4,094.85	$2,949.94
Motor Shaft Seal	formed seal	Purchased	1		0.01	0.01	$3.49	$3.41
Total						**30.01**	**$4,098.34**	**$2,953.36**
Subtotal Without Motor Controller								**$3,800.30**
Motor Controller Components								
Controller		Purchased	1		2.00	2.00	$2,067.94	$1,880.20
Total						**2.00**	**$2,067.94**	**$1,880.20**
Total Cost for 160kW Bus Fuel Cell System (including assembly and markup*)						**> 50**	**$8,321.83**	**$5,680.50**

*Each cost per system includes either a manufacturer markup (25% @ 1ksys/yr and 29% at 200sys/yr) or a pass-through markup (18%@1ksys/yr and 20%@200 sys/yr)

Figure 209. List of components for compressor, motor, and motor controller unit for the bus DFMA® analysis.

The timing drive gears are laser cut from a stainless steel sheet 1cm thick. The assumed laser cutting speed is approximately 0.6 cm per second (generously slower to account for intricate details in the driving gear geometry). The drive shafts for the compressor are made of a high carbon steel material and machined with a precision surface finish.

Figure 210. Medium hot extrusion press (HEP-112/72)[129]

The motor used in the analysis is considered to be a purchased component. Estimates obtained by Eaton through their DOE program suggest the cost of the motor for an automotive system to be ~$340 at 10,000 systems per year, $190 at 200,000 systems per year, and $160 at 500,000 systems per year. Cost of the compressor-motor drive motor for the bus system was scaled with air compressor motor shaft power and adjusted for lower manufacturing rates. The projected cost for the motor is shown in Figure 211 and is the most expensive component in the system other than the motor controller. The motor controller is about 40% the cost of the compressor-motor bus unit. The DFMA® analysis of the motor controller was completed in the previous 2012 bus analysis and re-used for the 2013 to 2015 analyses, after scaling for controller input power. The motor controller was also adjusted for lower manufacturing rates. Motor controller costs can also be viewed in Figure 211.

---

[129] Image from http://www.hydrononline.com/machines/hep-medium.htm

2016 Bus Compressor/Motor System Cost					
Annual Production Rate	systems/year	**200**	**400**	**800**	**1,000**
Compressor/Motor Components					
Compressor Rotor	$/sys	$143.77	$138.00	$135.15	$134.20
Compressor Housing	$/sys	$997.72	$512.57	$271.74	$223.79
Compressor Bearing Plate	$/sys	$329.84	$166.61	$85.59	$69.48
Compressor Shaft Seals	$/sys	$11.17	$11.06	$10.96	$10.92
Compressor Timing Drive Gears	$/sys	$33.65	$33.33	$33.02	$32.91
Housing/Motor Seals	$/sys	$93.51	$47.66	$24.19	$20.38
Housing Screws	$/sys	$2.23	$2.21	$2.19	$2.18
Front Bearing	$/sys	$9.05	$8.96	$8.87	$8.85
Rear Bearing	$/sys	$8.71	$8.63	$8.55	$8.52
Rotor Drive Shaft	$/sys	$20.24	$19.53	$19.09	$18.99
Torsionally Flexed Coupling	$/sys	$37.02	$19.62	$10.97	$9.24
Coupling Dowels	$/sys	$1.73	$1.72	$1.70	$1.70
Gear Housing/Motor end plates	$/sys	$59.09	$38.06	$26.41	$24.10
Contingency (5% of total)	$/sys	$396.28	$328.23	$282.30	$270.50
Assembly	$/sys	$11.55	$11.38	$11.21	$11.16
Motor	$/sys	$4,094.85	$3,555.70	$3,087.26	$2,949.94
Motor Shaft Seals	$/sys	$3.49	$3.46	$3.42	$3.41
Controller	$/sys	$2,067.94	$1,986.09	$1,905.75	$1,880.20
Total Eaton CEM Cost With Markup	**$/sys**	**$8,321.83**	**$6,892.82**	**$5,928.39**	**$5,680.50**
Total CEM Cost (Net)	**$/kWnet**	**$52.01**	**$43.08**	**$37.05**	**$35.50**
Total CEM Cost (Gross)	**$/kWgross**	**$42.74**	**$35.40**	**$30.45**	**$29.17**

Figure 211. Cost breakdown for bus compressor-motor unit

Figure 212 compares the cost of the Honeywell-style centrifugal compressor with that of the 2015 bus analysis Eaton-style compressor system. The Eaton-style system is observed to be appreciably more expensive, owing primarily to an increased motor cost. While real differences in type of motor exist (Honeywell uses a high rpm permanent magnet motor whereas Eaton uses a much lower rpm permanent magnet motor), the motor cost difference may be significantly influenced by differences in costing methodology between the two estimates: quote based vs. DFMA® analysis. The Eaton-style motor cost was based on quotations for automotive size motors at high manufacturing rates (10,000 to 500,000 sys/yr), with a curve fit extrapolation used to predict cost of the automotive size motors at lower manufacturing rates (200-1,000 sys/yr). This projected cost was then scaled with power to reflect the cost of a bus size unit. In contrast, the Honeywell-style motor cost was based on a detailed DFMA® analysis. The same markup percentages were applied to both the Honeywell and Eaton-style compressor systems for the bus so as to allow a fair comparison. However, the authors feel that the resulting motor cost may not accurately represent a motor used in the Eaton-style compressor-motor system and that using a curve fit extrapolation at such low production volumes (200-800 systems per year) does not accurately represent the cost. SA plans to re-evaluate more cost effective manufacturing processes at low volumes, particularly for the motor and motor controller in the future. In 2016, a detailed DFMA® analysis was conducted for a hydrogen recirculation pump motor as a side study (based on the H_2 pump for the Toyota Mirai). SA plans to continue studying various types and sizes of motors to understand the main cost drivers. For 2016, motor controller cost was held constant for the Honeywell-style and Eaton-style systems, which may not be a valid assumption given the disparate compressor speeds (165,000

rpm for the Honeywell-style unit vs. 24,000 rpm for the Eaton-style unit). There were no changes between the 2015 and 2016 bus CEM analyses.
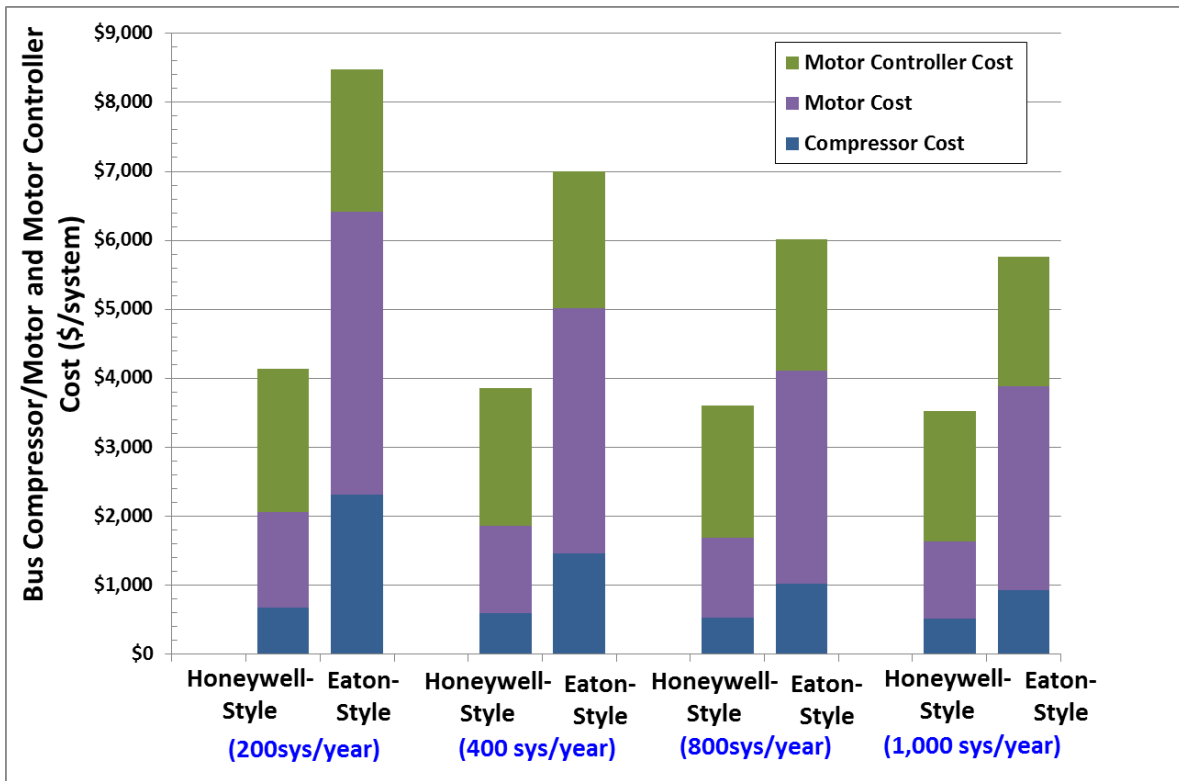
Figure 212. Comparison of cost for Honeywell-style design and the Eaton-style Compressor-Motor for a bus

9.4 Bus System Balance of Plant Components

To accommodate the increased flows and power level of a two-stack 160 kW$_{net}$ system, many balance of plant (BOP) components had to be revised. In some cases, the previous automotive DFMA®-style analysis of the balance of plant component automatically adjusted in response to the system design change. In other cases, new quotes were obtained, part scaling was included, or individual parts were increased in number (e.g. some parts are used on each of the two stacks). The changes to BOP components to reflect a bus system are summarized in Figure 213.

Balance of Plant Item	Bus System Change
CEM & Motor Controller	DFMA® analysis scaled to new flow and pressure ratio parameters, but switched to design without Expander
Air Mass Flow Sensor	New quote obtained for higher mass flow of bus system
Air Temperature Sensor	No change
Air Filter & Housing	New quote obtained for higher mass flow of bus system
Air Ducting	Piping and tubing diameters increased by a factor of 1.5 to adjust for higher mass flow of bus system
Air Precooler	DFMA® analysis scaled to new mass flow and temperature parameters.
Demister	Area size scaled by ratio of bus to automotive air flows
Membrane Air Humidifier	DFMA® analysis scaled to new gas mass flow and temperature parameters
HTL Coolant Reservoir	New quote obtained for larger expected coolant liquid volume of bus system
HTL Coolant Pump	New quote obtained for larger expected coolant flow of bus system
HTL Coolant DI Filter	Size scaled by factor of 2 to correspond to higher expected coolant flow rates of bus system
HTL Thermostat & Valve	New quote obtained for larger flow rate and pipe diameter of bus system
HTL Radiator	DFMA® analysis scaled to new heat rejection and temperature parameters of bus system
HTL Radiator Fan	New quote obtained corresponding to larger fan diameter and air flow rate parameters of bus system
HTL Coolant piping	Piping and tubing diameters increased by a factor of 1.5 to adjust for higher coolant flow of bus system
LTL Coolant Reservoir	New quote obtained for larger expected coolant liquid volume of bus system
LTL Coolant Pump	New quote obtained for larger expected coolant flow of bus system
LTL Thermostat & Valve	New quote obtained for larger flow rate and pipe diameter of bus system
LTL Radiator	DFMA® analysis scaled to new heat rejection and temperature parameters of bus system
LTL Radiator Fan	New quote obtained corresponding to larger fan diameter and air flow rate parameters of bus system
LTL Coolant Piping	Piping and tubing diameters increased by a factor of 1.5 to adjust for higher coolant flow of bus system
Inline Filter for Gas Purity Excursions	Size scaled by factor of 2 to correlate to increased hydrogen flow rate of bus system
Flow Diverter Valve	Quantity doubled to reflect use of two stacks in bus system
Over-Pressure Cut-Off Valve	Quantity doubled to reflect use of two stacks in bus system
Hydrogen High-Flow Ejector	Quantity doubled to reflect use of two stacks in bus system
Hydrogen Low-Flow Ejector	Quantity doubled to reflect use of two stacks in bus system
Check Valves	Quantity doubled to reflect use of two stacks in bus system
Hydrogen Purge Valve	Quantity doubled to reflect use of two stacks in bus system
Hydrogen Piping	Piping and tubing diameters increased by a factor of 1.5 to adjust

	for higher hydrogen flow of bus system
System Controller	Quantity doubled to reflect increased control/sensors data channels in bus system
Current Sensors	Quantity doubled to reflect use of two stacks in bus system
Voltage Sensors	Quantity doubled to reflect use of two stacks in bus system
Hydrogen Sensors	One additional sensor added to fuel cell compartment to reflect much larger volume of bus fuel cell system
Belly Pan	Excluded from bus system since a dedicated, enclosed engine compartment is expected to be used
Mounting Frames	Size increased to reflect use of two stacks and larger BOP component in bus system
Wiring	Cost doubled to reflect use of two stacks in bus system
Wiring Fasteners	Cost doubled to reflect use of two stacks in bus system

Figure 213: Explanation of BOP component scaling for bus power plant

10 Capital Equipment Cost

Figure 214 and Figure 215 display the tabulation of manufacturing/assembly processing steps along with the capital cost of each corresponding process train.[130] Multiple process trains are usually required to achieve very high manufacturing rates. The total capital cost (process train capital cost multiplied by the number of process trains) is also tabulated and shows that bipolar plate coating is the highest capital cost process of the stack. This tabulation is meant to give an approximate cost of the uninstalled capital required for automotive stack and BOP production at 500,000 vehicles per year. Some steps are not included in the tabulation as they modeled as purchased components and thus their equipment cost is not estimated. Furthermore, the capital equipment estimates do not include installation, buildings, or support infrastructure and thus should not be used as an estimate of total capital needed for power plant fabrication. None the less, some insight may be obtained from this partial tabulation.

Stack Manufacturing Machinery Capital Costs at 500,000 sys/yr			
Step	Capital Cost per Process Train	Number of Process Trains	Total Capital Cost
Bipolar Plate Stamping	$2,119,298	110	$233,122,759
BPP Coating Step 1	*$1,764,868*	34	$60,005,500.45
BPP Coating Step 2	*$927,161*	26	$24,106,182.86
BPP Coating	$2,941,433	25	$84,111,683
Membrane Production	$35,000,000	1	$35,000,000
Dispered Slot Die Coating	Proprietary	4	Proprietary
CCM Acid Wash	$907,000	11	$9,977,000
GDL	Purchased Comp.		Not Incl.
MEA Gasketing-Subgaskets	$2,958,600	3	$8,875,800
MEA Cutting and Slitting	$469,136	2	$938,272
MEA Gasketing - Screen Printed Co	$1,458,755	17	$24,798,842
Coolant Gaskets (Laser Welding)	$1,031,444	34	$35,069,092
End Gaskets (Screen Printing)	$392,735	1	$392,735
End Plates	$536,676	3	$1,610,027
Current Collectors	$166,443	1	$166,443
Stack Assembly	$821,339	52	$42,709,638
Stack Housing	$655,717	1	$655,717
Stack Conditioning	$670,905	22	$14,759,911
Stack Total			**$482,210,920**

* Bipolar plate coating is based on a vendor-proprietary manufacturing method that consists of multiple sub-process trains. The process train quantity listed is an average of the constituent sub-trains.

---

[130] A process train is a grouping of related manufacturing or assembly equipment, typically connected by the continuous flow of parts on a conveyor belt. For instance, the bipolar plate stamping process train consists of a sheet metal uncoiling unit, a tensioner, a 4-stage progressive stamping die, and a re-coil unit.

Figure 214. Automotive stack manufacturing machinery capital costs at 500,000 systems per year

Balance of Plant Manufacturing Machinery Capital Costs at 500,000 sys/yr			
Step	**Capital Cost per Process Train**	**Number of Process Trains**	**Total Capital Cost**
Membrane Air Humidifier	5,543,850	4	$8,815,798
Belly Pan	655,717	1	$655,717
Ejectors	*[Not Calculated]*	*N/A*	*[Not Calculated]*
Stack Insulation Housing	655,717	1	$655,717
Air Precooler	*[Not Calculated]*	*N/A*	*[Not Calculated]*
Demister	288,522	1	$288,522
CEM	*[Not Calculated]*	*N/A*	*[Not Calculated]*
(Partial) BOP Total	*Does not include processes with un-calculated capital costs* →		**$10,415,754**
* The membrane air humidifier involves an aluminum casting step which is not included in the capital equipment tabulation.			

Figure 215. Automotive balance of plant manufacturing machinery capital costs at 500,000 systems per year

11 Quality Control Procedures

Although quality control (QC) is listed under individual component sections above, the authors felt it beneficial to the reader to have all QC systems summarized in one section to compare/contrast diagnostic techniques. The QC systems were last updated in 2015 to reflect further review and analysis by QC expert Mike Ulsh of NREL. Overall, a more rigorous definition of the quality control systems was established. The general approach for defining the new QC systems was to:

1. Postulate the required resolution for defect identification.
2. Specify equipment needed to achieve desired resolution at specified line speed.
3. Incorporate automatic adjustment (within the model) for web width processing that varies with production volume.
4. Identify and define QC equipment changes for low volume production processes.

When low volume processing assumptions changed, SA requested the expertise of NREL to identify changes required for the updated process. While under review, NREL suggested additional changes for high volume processes as well. A detailed table of changes between 2014 and 2015/2016 and low volume (1,000 systems per year) and high volume (500k systems per year) is shown in Figure 216

Part Tested	2013/2014 Diagnostic System	2015 Diagnostic System (Low Volume)	2015 Diagnostic System (High Volume)	Comment on Change from 2014 to 2015	Detection Resolution	Total QC Cost	Fault/Parameters Tested
Membrane	XRF OR Optical Diagnostic System - QC - PROPRIETARY	Optical Detection System (ODS)	Optical Detection System (ODS)	Changed from XRF to ODS System at low and high volume	20 micron	$205k (per line 1k and 500k sys/yr)	Visual inspection to locate pinholes in ionomer, discolorations that would indicate thickness variation
Dispersed (slot die coating) Catalyst	IR/DC QC System ($210k)	IR/DC QC System + XRF QC System	IR/DC QC System + XRF QC System	While IRDC gives full width uniformity, added XRF QC System can detect loading/thickness of electrode layers. XRF is most widely used today.	2,000 microns	1k sys/yr: = $1.028M 500k sys/yr: = $1.123M	IRDC gives full width uniformity, XRF loading/thickness rastoring across web width.
Gasketed MEA (Subgasket)	Optical Detection System (ODS) (commercial system from Keyence)	Optical Detection System (ODS) (commercial system from Keyence) mounted above single stacked cell or on arm of robot.	Optical Detection System (ODS) (commercial system from Keyence)	At 1k sys/yr, ODS is mounted above the single stacked sub-gasketed cell or on the arm of the robot. Any conveyor system was removed. At high volume, adjusted cost increased number of cells across the width of web.	0.6mm	(1k sys/yr) $50k (no conveyor system required) (500k sys/yr): $210k	Misalignment of subgasket and membrane. Folds, bends, tears, scratches in subgasket or membrane.
Bipolar Plate	NIST Non-Contact Laser Triangulation Probe, Optical Detection System (commercial system from Keyence)	NIST Non-Contact Laser Triangulation Probe ($70.6k)	NIST Non-Contact Laser Triangulation Probe, Optical Detection System (commercial system from Keyence) ($100.6k)	No change at high volume. At low volume, update to not include ODS system. BPP stacking by worker can simultaneously inspect part so no ODS system needed.	~30 micron over 3 scan lines (one side of plate, 3 probes, single pass), 0.6 mm for Optical Camera (entire plate, one side)	(1k sys/yr): $70.6k (no optical system) (500k sys/yr): $100k	Triangulation: flow field depth, plate flatness. Optical System: general dimensions, completeness of manifold apertures.
MEA (after cutting/slitting)	XRF (point measurement only)	NA	Optical Detection System (ODS) (commercial system from Keyence)	Previously used XRF does not detect cracks and delamination, however ODS is able to detect this.	0.6mm	(1k sys/yr): NA (500k sys/yr): $210k	Thickness, cracks, delamination, misalignment of cutting/slitting.
Air Humidifier Membrane Station B (inspection of ePTFE web)	Optical Detection System	Optical Detection System	Optical Detection System	Set of line cameras to optically detect pinholes or other anomolies of top surface of ePTFE/ionmer membrane. Higher anomaly detection size and also adapt calculation to account for various web widths.	100 micron	(1k sys/yr): $36.5k (30cm web width - 1 line camera) (500k sys/yr): $92k (1 m web width - 4 line cameras)	Visual inspection to locate pinholes in ionomer, discolorations that would indicate thickness variation or other problems.

Figure 216. Summary of changes for quality control systems used in stack and membrane humidifier manufacture.

12 Automotive Simplified Cost Model Function

A simplified cost model to estimate the total automotive power system cost at 500,000 systems/year production rate is shown in Figure 217. The simplified model splits the total system cost into five subcategories (stack cost, thermal management cost, humidification management cost, air management cost, fuel management cost, and balance of plant cost) and generates a scaling equation for each one. The scaling equations for individual cost components are based on key system parameters for that component that are likely to be known to analysts conducting a general study. The curves are generated by regression analysis of data generated by successive runs of the full DFMA®-style cost model over many variations of the chosen parameters. The simplified model allows a quick and convenient method to estimate system cost at off-baseline conditions.

C_{system} = Total System Cost = C_{stack} + $C_{thermal}$ + C_{Humid} + C_{air} + C_{Fuel} + C_{BOP}

C_{stack} = **Total Fuel Cell Stack Cost**

100 Volt, Cstack = 1.9732 x 10^{-4} x ((0.17281 x A + 771.74) x L x PC) + (0.01070 x A) + 114.93

150 Volt, Cstack = 1.9732 x 10^{-4} x ((0.17281 x A + 771.74) x L x PC) + (0.01005 x A) + 165.84

200 Volt, Cstack = 1.9732 x 10^{-4} x ((0.17281 x A + 771.74) x L x PC) + (0.00987 x A) + 185.98

250 Volt, Cstack = 1.9732 x 10^{-4} x ((0.17281 x A + 771.74) x L x PC) + (0.00916 x A) + 290.78

300 Volt, Cstack = 1.9732 x 10^{-4} x ((0.17281 x A + 771.74) x L x PC) + (0.00901 x A) + 338.27

Where: A = Total active area of the stack (cm^2)

L = Pt Loading (mg/cm^2)   **Baseline Stack Cost: $2,199**

PC = Platinum cost ($/troy ounce)

$C_{thermal}$ = **Thermal Management System Cost**

= [100.11449 x (Q_{HT}/ΔT_{HT}) + 180.82]

+ [-0.95516x (Q_{LT} / ΔT_{LT})^2 + 107.61229 x (Q_{LT} / ΔT_{LT}) - 2.41233 x P^2 + 22.31666 x P -2.46100 x P x (Q_{LT}/ΔT_{LT}) - 17.87]

Where: Q_{HT}= Radiator Duty (kW$_{thermal}$) of High Temperature Loop

Q_{LT} = Radiator Duty (kW$_{thermal}$) of Low Temperature Loop

ΔT_{HT} = Difference between coolant outlet temperature from fuel cell stack and ambient temperature (°C)

ΔT_{LT} = Difference between coolant outlet temperature from air precooler and ambient temperature (°C)

P = Stack Operating Pressure (atm)

*High Temperature Loop includes: coolant reservoir, coolant pump, coolant DI filter, coolant piping, thermostat & valve, radiator fan, and radiator.

*Low Temperature Loop includes: coolant reservoir, coolant pump, coolant piping, thermostat & valve, and radiator.

Baseline Thermal Management System Cost: $402

C_{Humid} = **Humidification Management System Cost**

= (-1.77747 x A^2 + 52.83440 x A + 13.27) + (491.76862 x (Q/ΔT) - 1.46)

Where: A = Humidifier Membrane Area (m^2)

Q = Heat Duty for Precooler (kW)

ΔT = Delta Temp. (compr. exit air minus coolant temperature into air precooler)(°C)

*Includes Air Precooler and Membrane Humidifier.

Baseline Humidification Management System Cost: $83

C_{air} = **Air Management System Cost**

= 487.04 + (12.99860 x P) + (0.58524 x P x MF)

Where: P = Air Peak Pressure (atm)

MF = Max Air Mass Flow Out of Compressor (kg/hr)

*Includes demister, compressor, expander, motor, motor controller, air mass flow sensor, air/stack inlet manifold, air temperature sensor, air filter and housing, and air ducting.

Baseline Air Management System Cost: $897

C_{Fuel} = **Fuel Management System Cost**

= (3801.97 x BP^3 − 2967.73 x BP^2 + 1573.1 x BP − 87.81) + 237.59

Where: BP = blower power (kW)

*Includes valves, ejectors, hydrogen inlet and outlet of stack manifolds, piping, and recirculation blower. Baseline system does not include blower, therefore the Fuel Management System is a constant $238.

Baseline Fuel Management System Cost: $238

C_{BOP} = **Additional Balance of Plant Cost**

Where: C_{BOP} = $428.89

*Includes system controllers, sensors, and miscellaneous components.

Baseline Additional BOP Cost: $429

Figure 217: Simplified automotive cost model at 500,000 systems per year production rate

Because the simplified cost model equations are based upon regression analysis, there is an input parameter range outside of which the resulting cost estimates are not guaranteed to be accurate. The ranges for each parameter in each sub-equation are given in Figure 218 below.

Validity Range for Stack Cost				
Parameter	Min Value	Baseline Value	Max Value	Units
System Power	60	80	120	kW$_{net}$
Stack Voltage	100	250	300	V
L	0.1	0.134	0.8	mg/cm^2
A	88,987	117,060	177,086	cm^2
PC	800	1,500	2,000	$/troy ounce
Validity Range for Thermal Management System				
Parameter	Min Value	Baseline Value	Max Value	Units
ΔT_{HT}	38	54	70	°C
ΔT_{LT}	25	25	70	°C
Q_{HT}	57	81	120	kW
Q_{LT}	1.8	9	18	kW
P	1.5	2.5	3.0	atm
Validity Range for Humidification Management System				
Parameter	Min Value	Baseline Value	Max Value	Units
A	0.3	0.74	4	m^2
Q	2	6.78	15	kW
ΔT	22	98	132	°C
Validity Range for Air Management System				
Parameter	Min Value	Baseline Value	Max Value	Units
P	1.65	2.57	3.15	atm
MF	184	245	544	kg/hr
Validity Range for Fuel Management System				
Parameter	Min Value	Baseline Value	Max Value	Units
BP	0.2	0	0.3	kW

Figure 218: Range of validity for simplified cost model parameters

As a check on the accuracy of the simplified regression model, the results of the full DFMA® model are compared to the calculations from the simplified model for the parameter of system net power. These results are displayed in Figure 219 indicating very good agreement between the two models within the range of validity.
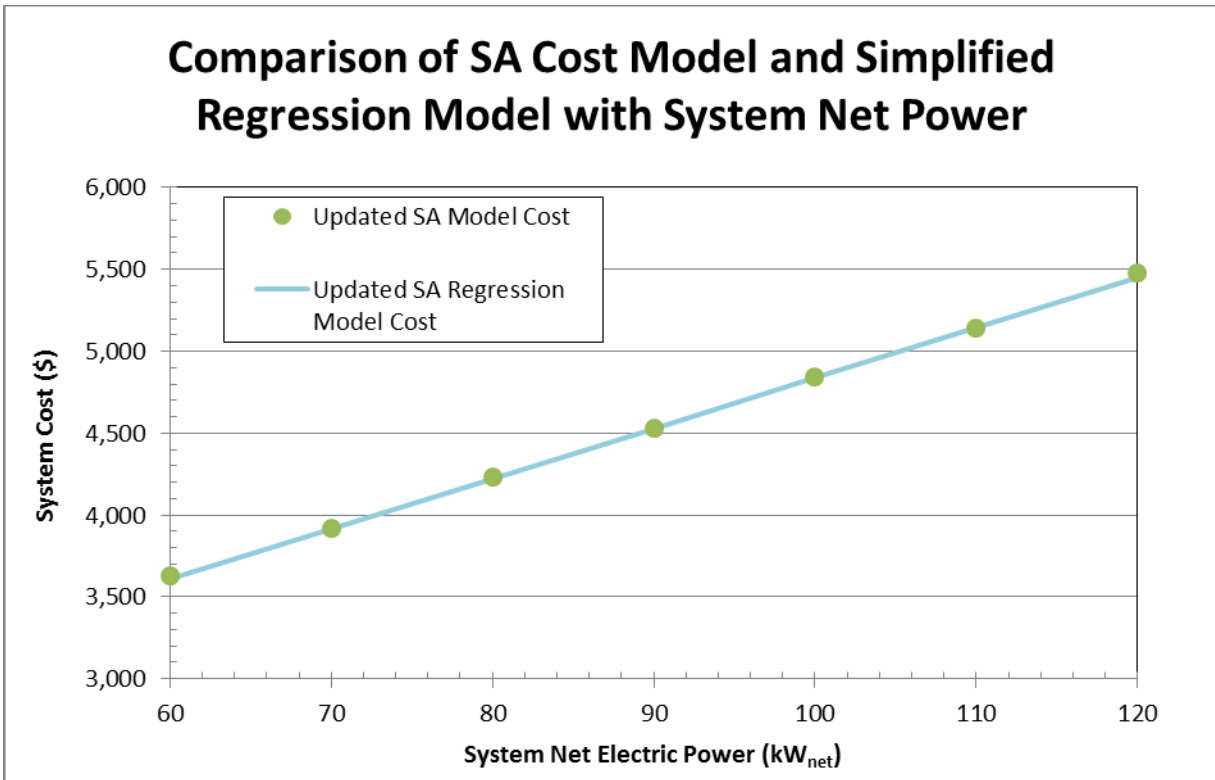
Figure 219: Comparison of SA cost model with simplified cost model at 500,000 systems per year.

13 Life Cycle Analysis (LCA)

Up-front cost per kW, while a useful metric and the primary focus of this report, is not the sole determining factor in market worthiness of a power system. Total life cycle cost is an equally important consideration that takes into account the initial purchase price, cost of fuel used over the lifetime of the system, system decommissioning costs and recycle credits, and operating and maintenance expenses, all discounted to the present value using a discounted cash flow methodology. By comparing life cycle costs, it is possible to determine whether an inexpensive but inefficient system (low initial capital cost but high operating and fuel expenses) or an expensive but efficient system (high initial capital cost but low operating and fuel expenses) is a better financial value to the customer over the entire system lifetime.

13.1 Platinum Recycling Cost

Since cost of the catalyst platinum within the fuel cell stacks represents a significant fraction of total system cost, particular attention is paid to recovering the Pt at the end of stack life. Two basic approaches are possible for allocating Pt cost:

- An ownership paradigm wherein the consumer buys the Pt contained within the stacks of the fuel cell vehicle, and thus the Pt has a value to the vehicle owner at the end of stack life. (This is the paradigm used in the baseline cost analysis and in the LCA.)
- A renting paradigm, wherein a precious metal dealer (such as Johnson-Matthey or the vehicle manufacturer) owns the Pt in the stacks, the Pt purchase price is not charged to the vehicle owner at the time of purchase, and the value of the Pt at the end of stack life accrues to the precious metal dealer (not to the vehicle owner). (This paradigm is not used in the baseline analysis or LCA but may be considered in future years.)

The ownership paradigm will now be more fully explored.

The life cycle cost analysis under the ownership paradigm is based upon adapting existing vehicular catalytic converter recycling parameters to expectations for a fuel cell system.[131,132] Based on analysis of platinum recycling conducted by Mike Ulsh at the National Renewable Energy Laboratory, total platinum loss during operation and recovery is estimated at:

- a 1% loss during operational life,
- 5% loss during recycling handling, and
- 2%-9% loss during the recycling process itself.[133,134]

---

[131] "The impact of widespread deployment of fuel cell vehicles on platinum demand and price," Yongling Sun, et. al. International Journal of Hydrogen Energy 36 (2011).

[132] "Evaluation of a platinum leasing program for fuel cell vehicles," Matthew A. Kromer et. al., International Journal of Hydrogen Energy 34 (2009).

[133] L. Shore, "Platinum Group Metal Recycling Technology Development," BASF Catalysts LLC final project report to DOE under subcontract number DE-FC36-03GO13104, 2009.

[134] "The impact of widespread deployment of fuel cell vehicles on platinum demand and price," Yongling Sun, et. al. International Journal of Hydrogen Energy 36 (2011).

Ten percent (10%) is chosen as the Pt loss baseline value while the low (8%) and high (15%) end are represented in the sensitivity analysis below. The cost of recycling[135] is expected to range between $75 and $90 per troy ounce of recovered platinum. However, this is only the cost incurred by running the actual recycle process. In addition, there are supply chain costs as the capturer or salvager collecting the unit desires to be paid. Based on current catalyst converter practice, the salvager expects to be paid by the recycler about 70%-75% of the total value of recycled platinum[136] with the remaining Pt value going to the recycle as payment for the recycle process. Whether this comparatively high fraction of Pt value would continue to accrue to the supply chain salvager for fuel cell stack platinum is unclear. If it does, the owner of the fuel cell automobile effectively gets no value from the recycled Pt, just as, in general, a person selling an internal combustion vehicle for scrap does not separately receive payment for the catalytic converter. However, as the value of Pt in the fuel cell may be greater than that of a catalytic converter, the paradigm may be different in the future. Consequently, as a baseline for the LCC analysis, the salvager is estimated to receive 35% (half the value received for catalytic converters) of the value of the recovered Pt less recycling cost. A sensitivity analysis is conducted for cases where the salvager captures only 10% and 75% of the recovered value. Finally, due to platinum market price volatility, it is unlikely that Pt price will be exactly the same at system purchase as it is 10 years later at time of recycle. Consequently, for purposes of the baseline LCC analysis, the price of platinum is held constant at the purchase price used for the catalyst within a new vehicle ($1,500 / tr. oz.), and sensitivity analysis is conducted for a future[137] higher Pt price ($2100/tr. oz. at end of life).

To further explore these assumptions, additional conversations were held with precious metal suppliers. The current methodology for recovery of Pt was described as consisting of the following steps:

1) Agreement between refiner and supplier of the expected total Pt in the sample
2) Assay of contaminants within the sample
3) Assessment of a "deleterious elements" charge
4) Imposition of a Retention charge (typically 2-3%)
5) Imposition of a Refining charge (typically 1-2%)

This would appear to place the recycling charge within the 2-9% range as projected above, thereby broadly confirming the analysis assumptions. However, further clarification of terms and values is needed and will be pursued in future analyses.

---

[135] Ibid.

[136] Ibid.

[137] Platinum price is considered more likely to increase in the future rather than decrease. Consequently, the future price of Pt is based on the current Pt market price (~$1500/tr. oz) plus a $60/tr. oz. per year increase, resulting in a $2100/tr. oz. price after 10 years.

13.2 Automotive Life Cycle Analysis Assumptions and Results

The auto life cycle analysis (LCA) of life cycle cost analysis (LCCA[138]) for this report assumes a set of driving conditions and platinum recycling costs to compute the total present value cost of ownership for the lifetime of the vehicle. These assumptions are summarized in the figure below.

Auto Life Cycle Cost Assumption	Value
Sales markup	25% of calculated system cost
Discount rate	10%
System lifetime	10 years
Distance driven annually	12,000 miles
System efficiency at rated power	48% (calculated by model)
Fuel economy	62.6 mpgge[139]
Hydrogen to gasoline lower heating value ratio	1.011 kgH$_2$/gal gasoline
Fuel cost	$5 / kg H$_2$
Total Pt loss during system lifetime and the Pt recovery process	10%
Market Pt price at end of system lifetime	$1,500 / tr. oz.
Cost of Pt recovery	$80 / tr. oz.
% of final salvaged Pt value charged by salvager	35%

Figure 220. Auto life cycle cost assumptions

Under these assumptions, a basic set of cost results is calculated and displayed in Figure 221. Note that these results for the automotive system, whereas the results for the bus system appear in the next section; bus drive cycle and use patterns are vastly different from the average personal vehicle.

	2016 Auto System Life Cycle Costs					
Annual Production Rate	**1,000**	**10,000**	**30,000**	**80,000**	**130,000**	**500,000**
System Cost	$17,236	$7,456	$5,715	$4,858	$4,686	$4,232
System Price (After Markup)	$21,545	$9,320	$7,143	$6,073	$5,857	$5,289
Annual Fuel Cost	$969	$969	$969	$969	$969	$969
Lifecycle Fuel Cost	$5,954	$5,954	$5,954	$5,954	$5,954	$5,954
Net Present Value of Recoverable Pt in System at End of System Lifetime	$249	$249	$249	$249	$249	$249
Final Pt Net Present Value Recovered	$162	$162	$162	$162	$162	$162
Total Lifecycle Cost	$27,338	$15,113	$12,936	$11,865	$11,649	$11,082
Total Lifecycle Cost ($/mile)	**$0.228**	**$0.126**	**$0.108**	**$0.099**	**$0.097**	**$0.09235**

Figure 221: Auto LCC results for the baseline assumptions

The variation of life cycle cost with system efficiency was studied in order to examine the trade-offs between low efficiency (higher operating costs but lower initial capital costs) and high efficiency (lower operating costs but higher initial capital costs) systems. Figure 222 shows the polarization curve with system efficiency at rated power.

---

[138] The abbreviations LCA and LCCA are both used within the analysis community.
[139] Calculated from system efficiency at rated power based on formula derived from ANL modeling results: Fuel economy = 0.0028x^3 - 0.3272X^2+12.993X - 116.45, where x = system efficiency at rated power.
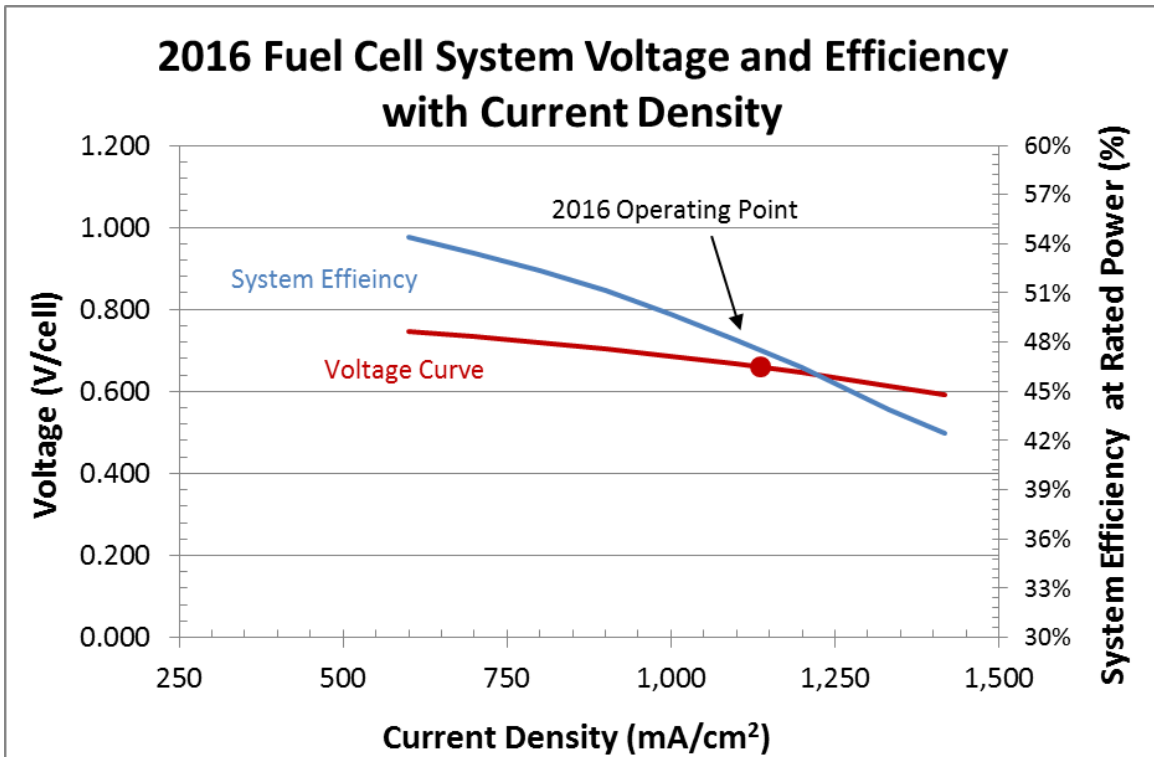
Figure 222: Auto polarization curves for efficiency sensitivity analysis

With this relationship, it is possible to calculate the variation in life cycle cost contributors over a range of efficiencies. These results are shown below. Figure 223 displays the results for the total life cycle cost as well as its component costs on an absolute scale. Note that the total life cycle cost (i.e. the present value of the 10 year expenses of the power system) is expressed as a $/mile value for easy comparison with internal combustion engine vehicle life cycle analyses. Figure 224 shows a zoomed-in look at the total cost, indicating a minimum total life cycle cost at the baseline system value of 48% system efficiency (corresponding to 52% fuel cell stack efficiency and cell voltage of 0.659 V/cell). However, the range of LCC cost variation over the range of system efficiencies examined is quite small, indicating that LCC is generally insensitive to system efficiency.
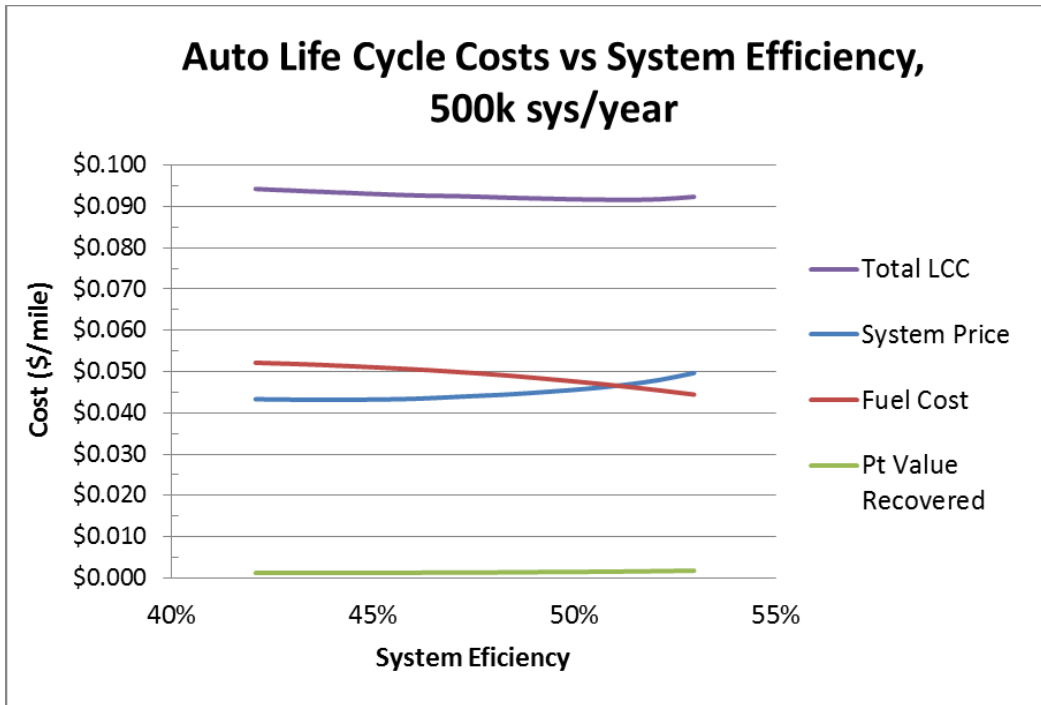
Figure 223: Auto life cycle cost components vs. fuel cell efficiency for 500k automobile systems/ year
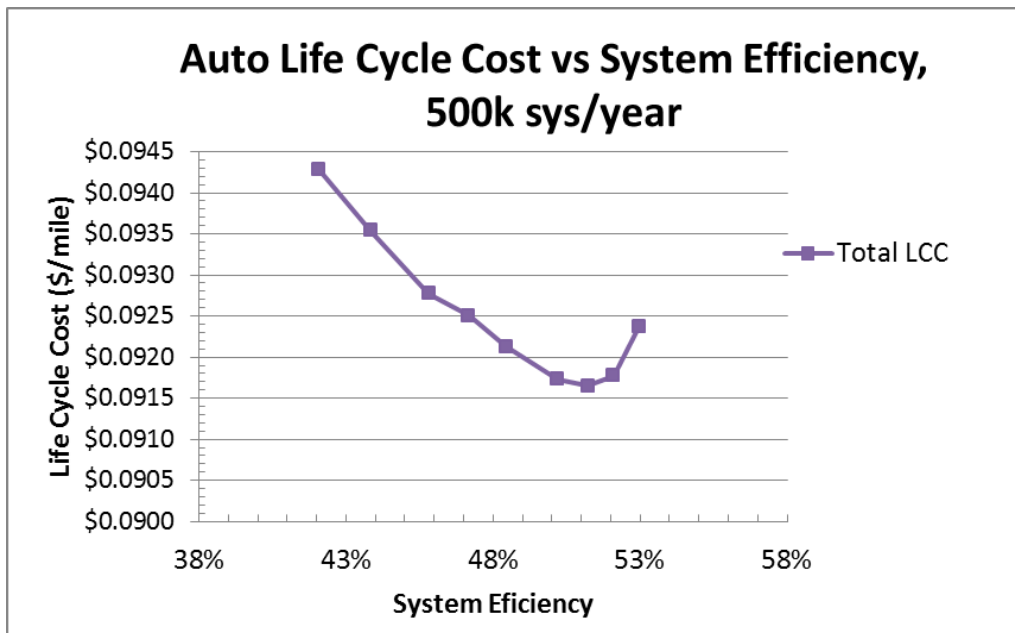
Figure 224: Auto life cycle cost vs. fuel cell efficiency for 500k automobile systems/year

In addition to the efficiency analysis, a simple sensitivity study was conducted on the parameters governing the platinum recycle, to determine the magnitude of the effect platinum recycling has on the life cycle cost. Figure 225 below displays the total life cycle cost in $ per mile as a function of platinum price during the year of the recycle for three scenarios: the baseline case where the salvager captures 35% of the value of recovered platinum and two sensitivity cases where the salvager captures 10% of the value at the low end and 75% of the value at the high end.

205
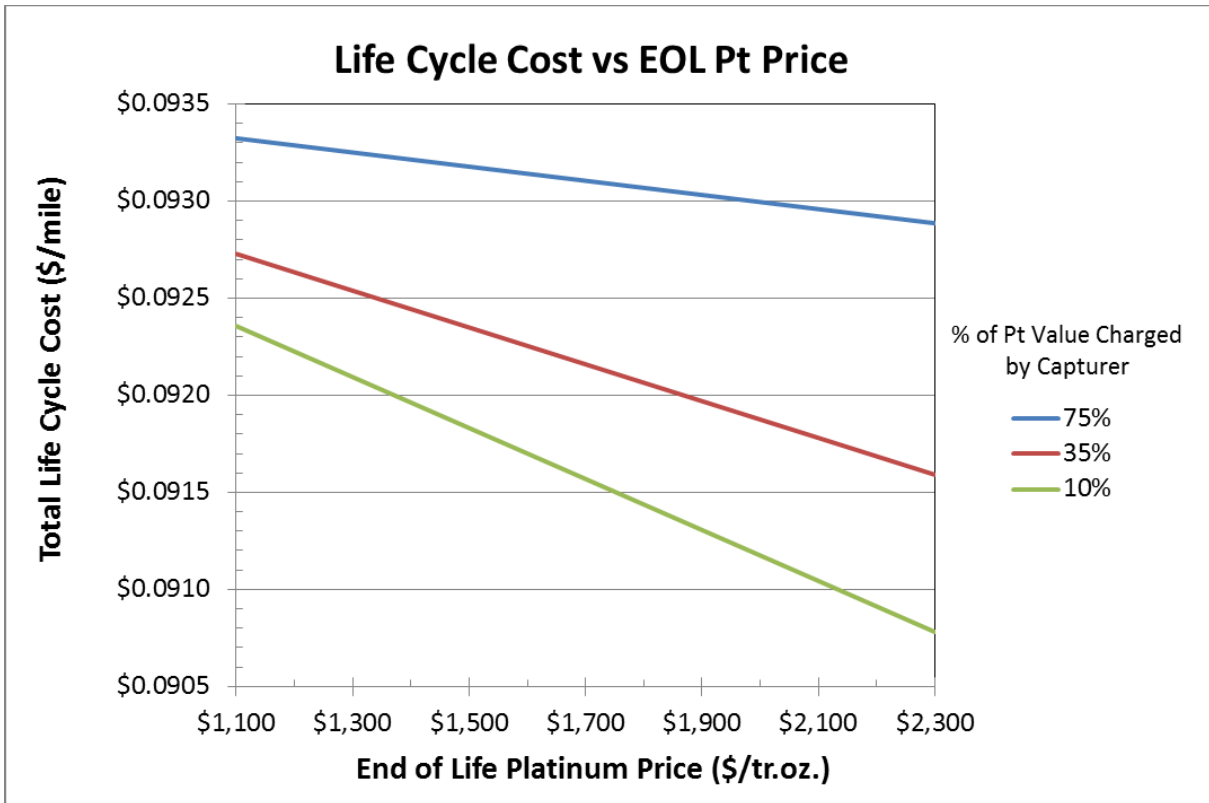
Figure 225: Auto life cycle cost vs. end of life platinum price (at 500k system/year)

Additional parameters were explored and are displayed as a tornado chart in Figure 226 and Figure 227. These results indicate that platinum recycle parameters do not have a large effect on the overall life cycle cost (~1%).

Life Cycle Cost ($/mile), 500,000 systems/year				
Parameter	Units	Low Value of Variable	Base Value	High Value of
Salvage Value Charged	%	10%	35%	75%
Pt Price at Recovery	$/tr.oz.	$1,100	$1,500	$2,100
Total Pt Loss	%	8%	10%	15%
Cost of Recovery	$	$70	$80	$90
2016 Auto System LLC ($/mile)			**$0.09235**	

Figure 226: Auto life cycle cost tornado chart parameters
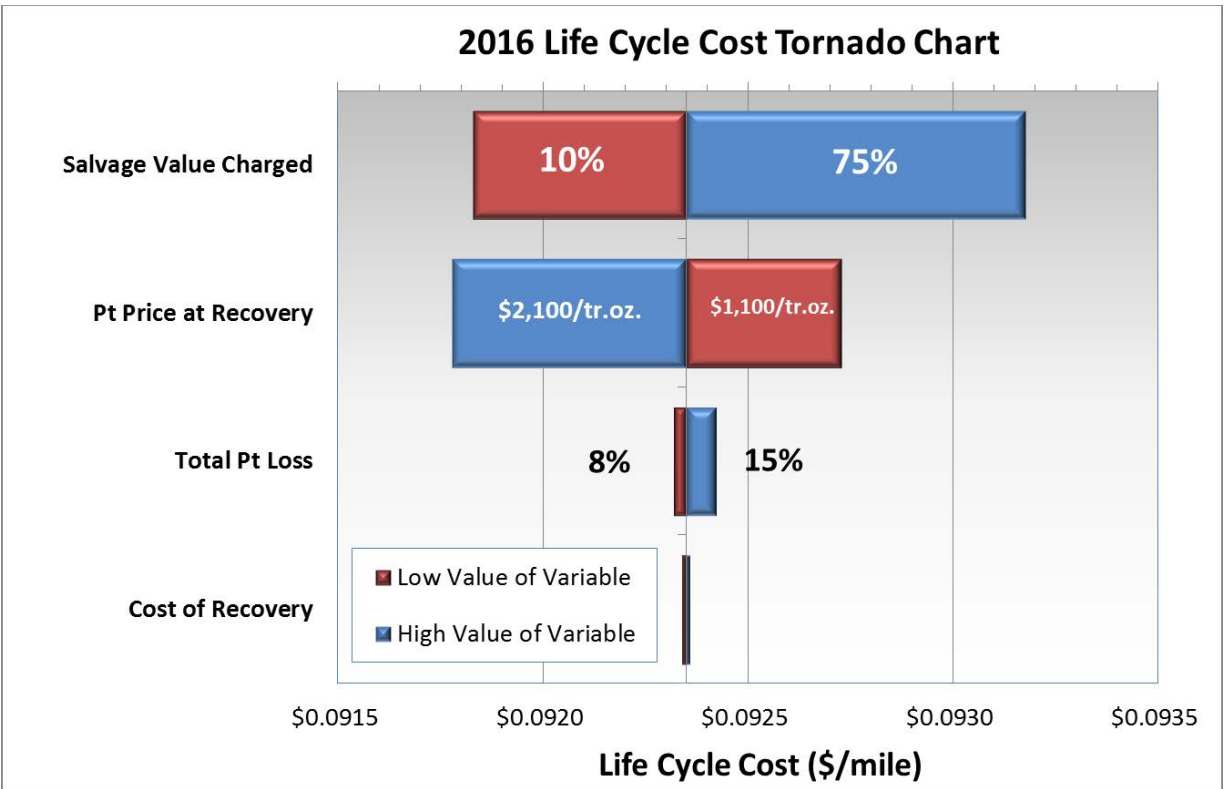
Figure 227: Auto life cycle cost tornado chart (at 500k systems/year)

13.3 Bus Life Cycle Cost Analysis Assumptions and Results

In collaboration with ANL and Aalto University, Strategic Analysis Inc. (SA) conducted a bus life cycle cost (LCC) analysis using performance modeling data (built from experimental results) to determine fuel consumption over a drive cycle. Fuel consumption was provided to SA by ANL/Aalto and used to construct the LCC model. ANL modeled bus system performance for two types of air compressor designs for this study (1) roots air compressor-only, and (2) roots air compressor/expander/motor (CEM). Aalto University used the FCS operating conditions within Autonomie vehicle simulation software to obtain the energy requirements for each system at various drive cycles (Braunschweig (BRN) and Berkeley Line 51B (L51B)). [140,141] The modeling results for the roots compressor-only had the lowest fuel consumption (kgH$_2$/100 km) and highest efficiency between the two types of drive cycles.

Literature review of three main reports was conducted to compare, and in some cases reference, fuel cell and diesel system cost, lifetime, maintenance cost, warranty, markup, and life cycle cost. [142, 143, 144]

---

[140] Autonomie is a Matlab$^{©}$- based vehicle simulation software used for automotive control-systems analysis. http://www.autonomie.net/expertise/Autonomie.html

[141] Lajunen, A., Lipman, T., "Lifecycle cost assessment and carbon dioxide emissions of diesel, natural gas, hybrid electric, fuel cell hybrid and electric transit buses", *Energy*, March 2016.

[142] Eudy, L., Post, M., Gikakis, C., "Fuel Cell Buses in U.S. Transit Fleets: Current Status 2015", National Renewable Energy Laboratory Report in collaboration with the Federal Transit Administration, December 2015.

The NREL report provided near current (2015) bus performance status for comparison to DOE targets. The Federal Transit Administration (FTA) report contained detailed diesel bus costs and replacement schedules.

As summarized in Figure 228, the SA DFMA® reported bus fuel cell system baseline costs are lower than the NEXTHY LIGHTS report costs. The projected range in fuel cell system cost provided in the NEXTHY LIGHTS report for > 100 to 500 buses per year (<€954 - €1,094/kW (in 2010 €) for ~20,000 hour warranty and including cooling system) for 2015 and beyond is equivalent to $1,335 to $1,532/kW.[145] In comparison, the SA DFMA® fuel cell system cost estimates are between $392 and $309/kW for 200 and 400 systems per year. However, the NEXTHY LIGHTS report notes that issuance of warranties for longer than one year can increase the cost 40%. The DFMA® analysis does not take into account the cost to extend the lifetime of the fuel cell stack other than increased Pt loading for durability. Thus an additional 40% markup for warranty could be reasonably applied to the DFMA® estimate. Including such a warranty markup increases the SA projected fuel cell system cost to $527 and $415/kW, bringing it closer to, but still below, the NEXTHY LIGHTS estimate. Additionally, one significant cost difference between the reported cost and the DFMA® baseline cost is the fuel cell cooling system cost; this area may need to be re-evaluated for the baseline bus system.

	NEXTHY Report	SA DFMA® Report
Production Rate	>100 to 500 per year	200 and 400 per year
Fuel Cell System Cost	<€954 - €1,094/kW (in 2010 €) $1,335 – $1,532/kW	$392/kW and $309/kW
Warranty	20,000 hours	None included in base price
Comments		Est. cost with 40% markup for warranty: $527 and $415/kW

Figure 228: Comparison of NEXTHY and SA DFMA® Cost Projections

A breakdown in the DFMA® fuel cell bus costs at 200, 400, 800, and 1,000 systems per year production is listed in Figure 229, and shows a majority of the cost (82-86%) coming from non-fuel cell system or hydrogen storage components. The largest cost of the system is the chassis and body of the bus ($248,000/system), quite close to the documented $300,000 for total diesel bus costs. SA believes the chassis, body, and additional parts (seats, windows, breaks, bumpers) should be the same for both FC buses and diesel buses unless there are additional safety components specifically for hydrogen fuel cell buses not mentioned in the reference reports.

The assumptions SA made for the bus LCC analysis were derived from multiple sources such as SA's previous automotive LCC analysis, discussions with ANL and Aalto University, and the reports mentioned above. Parameter values are shown in Figure 230.

---

[143] Zaetta, R., Madden, B., "Hydrogen Fuel Cell Technology State of the Art Review", Version 3.1, NEXT**HY** LIGHTS report by Element Energy, co-financed by fund from European commission under FCH-JU-2008-1 Grant Agreement Number 245133, December 2010.
[144] Federal Transit Administration report, "Useful Life of Transit Buses and Vans", Report No. FTA VA-26-7229-07.1, April 2007.
[145] Based on US$1.4/€ exchange rate in 2010.

	SA's Fuel Cell Bus Cost Breakdown ($/system)			
FC Bus Production Volume	200 sys/yr	400 sys/yr	800 sys/yr	1,000 sys/yr
FC Stack[146]	$84,385	$66,393	$51,629	$48,982
FC BOP[146]	$25,395	$21,910	$19,552	$18,940
H2 Storage (tanks & BOP)[147]	$47,890	$47,890	$47,890	$47,890
Battery System Price[148]	$10,170	$10,170	$10,170	$10,170
Chassis and Body[148]	$248,500	$248,500	$248,500	$248,500
Power Electronics and Electric Motors[148]	$148,400	$148,400	$148,400	$148,400
Additional Bus Parts (seats, windows, breaks, bumpers)[149]	$105,090	$105,090	$105,090	$105,090
Labor for Drivetrain Integration[148]	$60,200	$60,200	$60,200	$60,200
OEM Investment Costs (Markup of 26%)[148, 150]	$189,986	$184,367	$179,888	$179,035
Total FC Bus Price	$920,017	$892,920	$871,318	$867,207

Figure 229. Table showing breakdown of capital cost used in LCC analysis

Bus LCC Parameter	Value @ 1ksys/yr	Assumption Basis
Bus Operational Time	4,000 hrs/yr	Based on roughly 12hrs/day, 7 days/week
Bus Service Life	12 years	Based on DOE Target and FTA lifetime for diesel transit buses[144]
Annual Distance	BRN: 56k miles L51B: 34k miles	Based on drive cycle miles per hr provided by Aalto University
Discount Rate	5.25%	Middle value of two reported values (3.5% & 7%)[143,144]
Maintenance Cost	$0.54/mile	NREL report: $0.06/mile for scheduled; $0.48/mile for unscheduled maintenance [151]
Fuel Cost	$5/kg	Based on previous SA automotive LCC analysis
FC Stack Operating Hrs	25,000 hrs	Based on DOE ultimate target[152]
Fuel Cell Air Humidifier Lifetime	5,000 hrs	Based on Gore/dPoint report on plate frame membrane humidifier
Other Bus Replacement Costs	$128k/life	Total diesel bus replacements would be $210k. Excluding diesel engine parts and fuel parts equates to $128k.[149]
Fuel Economy	BRN:6.98 mpgde L51B:5.37mpgde	Based on Analysis performed by Aalto University using Autonomie model. [140,140]

Figure 230. Bus LCC parameter assumptions

---

[146] SA DFMA^{TM} analysis results inclusive of fuel cell system supplier markup, hybrid system integrator markup, 16% bus company markup (derived from New Flyer 14% gross margin), and 40% markup for ~20,000 hr fuel cell system warranty.

[147] Based on $766/kgH$_2$ for automotive pressure vessel system at 1,000 tanks per year, 40 kgH$_2$ per bus systems, additional 56% markup added for warranty and profit. In comparison, NEXTHY LIGHTS reported 700-800€/kgH$_2$ for storage system.

[148] Based on $900/kWh for a 11.3kWh battery.

[149] Values obtained from the Federal Transit Administration report: "Useful Life of Transit Buses and Vans"

[150] From NEXT**HY** LIGHTS report: includes risk premium, non-recurring engineering costs, and additional labor cost required to manufacture a novel product.

[151] Eudy, L., Post, M., "American Fuel Cell Bus Report Evaluation: Second Report", National Renewable Energy Laboratory, September 2015.

[152] Fuel Cell Technologies Office Multi-year Research, Development, and Demonstration Plan, Section 3.4 Fuel Cell, 2016.

Results from the bus LCC model do not show an appreciable difference between air compressor types, but there is a large impact due to the assumed annual distance driven by the type of drive cycle. As seen in Figure 231 the LCC ranges from $2.40/mile to $3.50/mile depending on the drive cycle. In comparison to diesel bus LCCs for the same bus route, the FC bus LCC is 30% higher for the BRN line and almost 95% higher for the L51B line due to the substantially higher balance of bus cost (made up of power electronics, electric motor, and bus chassis and body).
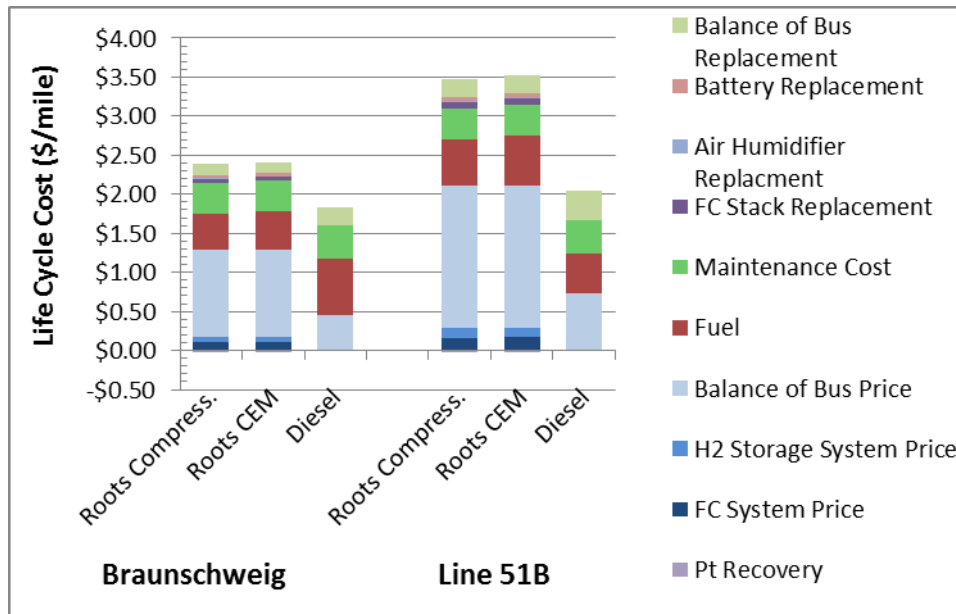
Figure 231. Lifecycle cost graph comparing three FC system design types for two drive cycles at 1,000 systems per year, and a comparison to diesel bus LCC.

In review of this analysis, Leslie Eudy from the National Renewable Energy Laboratory (NREL) made a few observations that may impact the interpretation of this study.

1) Durability: Many of the fuel cell buses under NREL's study have been in operation since 2010 or 2011 and are now experiencing reduced fuel economy due to durability or changes in drive cycle. Over a one year period, an average 15% reduction in fuel economy (from 7 down to 6 miles per diesel gallon equivalent (MPDGE)) was observed.[153] This change in durability is used within a sensitivity study for the bus LCC, seen in the parameter list (Figure 232) and Tornado chart in Figure 233.

2) Maintenance Cost: With any new drive train in buses, the system usually includes some warranty or extra cost for the power system to cover expensive part replacements and high labor costs for maintenance performed by the power system manufacturer. An initial warranty, covering 3-5 years) was provided by the bus company for most of the fuel cell buses under NREL's study. An additional extended warranty was arranged to cover 3 more years (although not all parts from all sub-systems are covered). When the industry develops a better supply chain for parts and the technology improves enough to reduce the amount of maintenance

---

[153] Eudy, L., Post, M., Gikakis, C., "Fuel Cell Buses in U.S. Transit Fleets: Current Status 2015", National Renewable Energy Laboratory Report in collaboration with the Federal Transit Administration, December 2015.

required by the power system manufacturer, maintenance costs will likely come down (as has been seen with diesel hybrids buses[154]). To assess this uncertainty in future maintenance cost, this parameter is added to the parameter list in Figure 232 and the Tornado chart in Figure 233.

Yearly operation time (or distance the bus traveled over a year) and maintenance cost are the two most significant parameters for bus life cycle cost ($/mile).

Bus Life Cycle Cost ($/mile) Parameters, 1,000 systems/year				
Parameter	Units	Low Value of Variable	Base Value	High Value of Variable
Operation Time in a year	hrs	2,400	4,000	6,720
Maintenance Cost	$/mile	$0.39	$0.54	$1.33
Discount Rate	%	3.5%	5.25%	7%
Fuel Cost	$/kg	$4	$5	$6
Fuel Economy	miles/(diesel gallon equiv.)	6	7	7
Total Markup on FC System	%	36%	56%	76%
Pt Price at Recovery	$/tr.oz.	$1,100	$1,500	$2,100
Total Pt Loss	%	8%	10%	15%
Cost of Recovery	$	$80	$160	$240
2016 Bus System LLC ($/mile)			$2.38	

Figure 232. Bus life cycle cost sensitivity parameters for Tornado chart (BRN drive cycle using system with roots compressor)

---

[154] Private discussions with Leslie Eudy at NREL suggest that diesel hybrid buses experienced a similar high maintenance cost when diesel hybrid buses were first implemented into the field. After some time for the technology to mature, these maintenance costs came down.
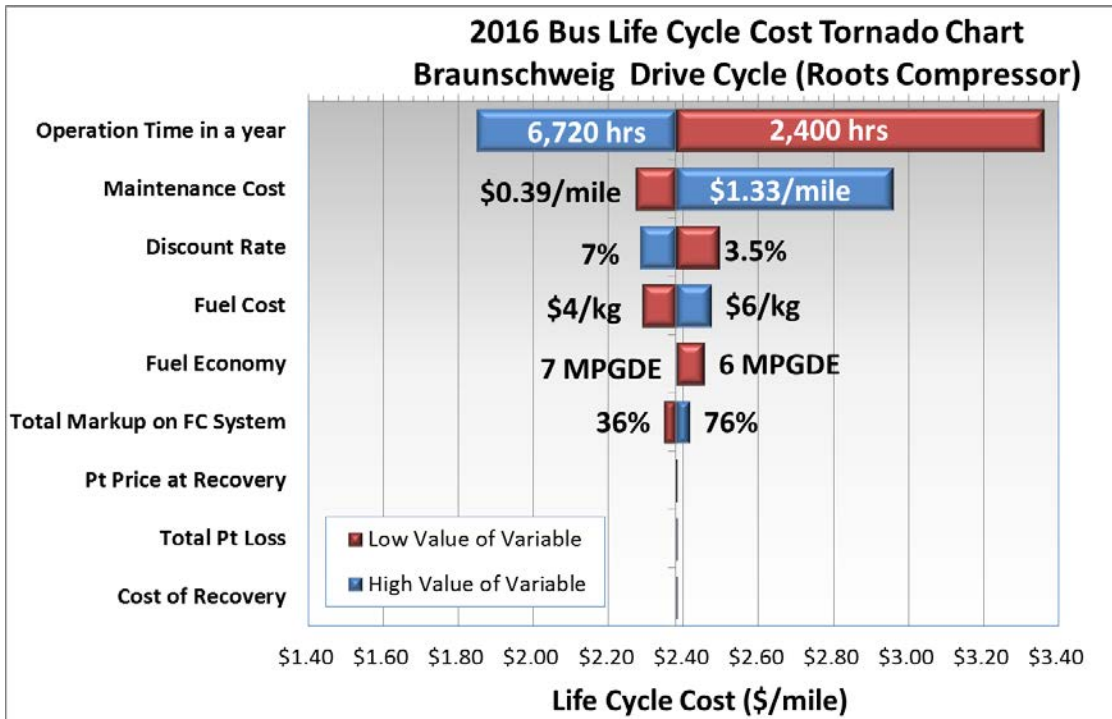
Figure 233. Bus life cycle cost Tornado chart for BRN drive cycle using system with roots compressor.

Potential LCC reduction can be achieved from reduced maintenance cost, increased miles per gallon diesel equivalent, and reduction in capital cost of the bus. A waterfall chart in Figure 234 depicts the magnitude of LCC reduction corresponding to achievement of a series of DOE ultimate targets. The waterfall is based on the BRN bus route at 400 systems per year production and shows achievement of eventual LCC parity with a diesel bus.
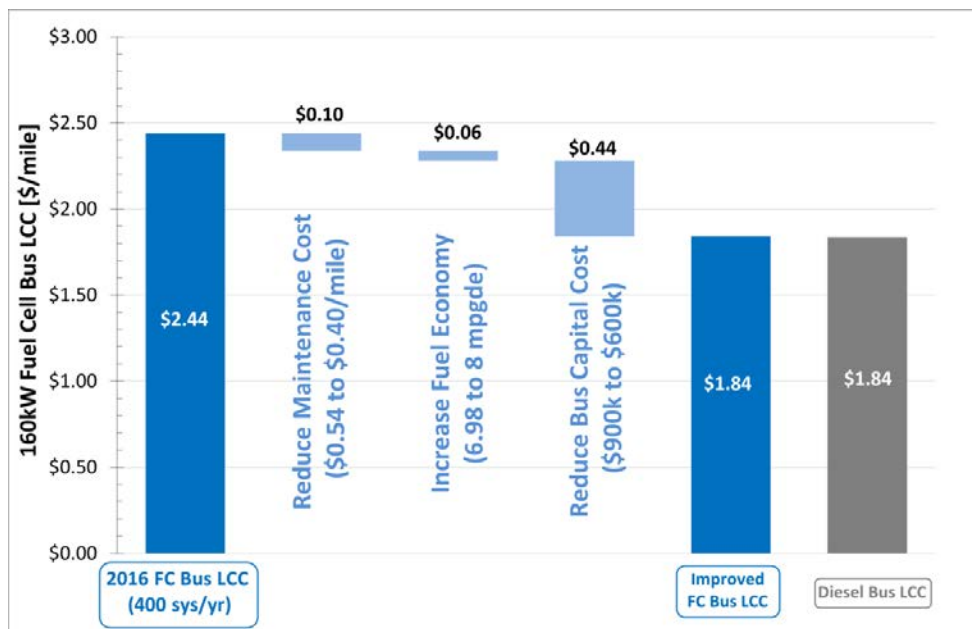
Figure 234. Waterfall chart showing potential LCC reduction using DOE ultimate target values[152].
Values in chart are for FC bus costs at 400 systems per year production using BRN bus route.

14 Sensitivity Studies

A series of tornado and Monte Carlo sensitivity analyses were conducted to determine key parameters and assess avenues to further reduce cost.

14.1 Single Variable Analysis

14.1.1 Single Variable Automotive Analysis

A single variable analysis was performed to evaluate which parameters have the largest effect on system cost. Figure 235 shows the parameter ranges used to develop the tornado chart, while Figure 236 displays the results of the analysis.

2016 Auto Sensitivity Ranges (500,000 sys/year)				
Parameter	Units	Min Param. Value	Base Value	Max Param. Value
Pt Loading	mgPt/cm^2	0.125	0.134	0.300
Power Density	mW/cm^2	637	749	1123.5
Air Loop Cost (including CEM)	$/system	$558	$891	$1,167
Bipolar Plate Cost	$/kW$_{net}$	$3.00	$8.17	$10.00
GDL Cost	$/m^2	$3.00	$6.44	$16.00
Air Stoichiometry		1.4	1.4	2.0
Hydrogen Recirculation System Cost	$/system	$158.48	$237.59	$356.39
Active to Total Area Ratio		0.55	0.625	0.80
Q/ΔT Constraint	kW/°C	1.35	1.45	1.55
ePTFE Cost	$/m2	$3.00	$6.00	$10.20
Ionomer Cost	$/kg	$53.14	$88.57	$177.14
Membrane Humidifier Cost	$/system	$38.73	$51.64	$77.46
Bipolar Plate Welding Speed	m/min	2.5	7.5	15.0
2016 Auto System Cost ($/kWnet)			$52.89	

Figure 235: 2016 automotive results tornado chart parameter values

As shown in Figure 236, variations in operating condition parameters power density and platinum loading have the most capacity to affect system cost. For the case of power density, this affects the size and performance of the entire system, trickling down into cost changes in many components. Platinum loading's large effect is attributable to the very high price of platinum relative to the quantities used in the system. Bipolar plate and GDL costs have moved up to the 3rd and 4th largest impacts to the fuel cell system. For both components, the range in projected cost is based on 2016 reported costs at high volume. Air loop cost range takes into account the air compressor cost range,[155] efficiencies for the air

---

[155] CEM cost multiplier: Low end is 33% reduction of calculated cost to get a min value of $500/system from DOE targets. High end is 20% increase of calculated cost.

compressor, expander, and motor controller,[156] and balance of air compressor cost range.[157] Note that while resizing of the compressor and stack to reflect a different air flow rate (range in stoichiometric rates) is included in the system cost impact, the impact on power density is not.
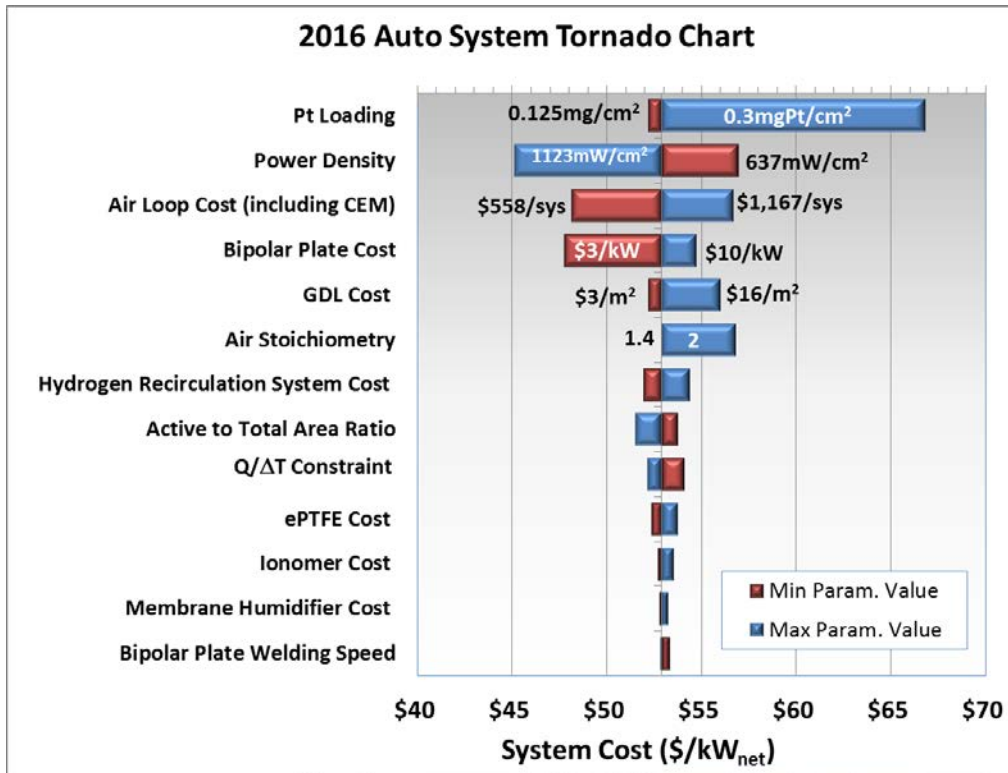
Figure 236: 2016 Auto results tornado chart

14.1.2 Automotive Analysis at a Pt price of $1100/troy ounce

To aid in comparisons to other previous cost studies, the automotive system was also evaluated with a platinum price of $1,100/troy ounce (instead of the baseline value of $1,500/troy ounce). All other parameters remain the same. Results are shown in Figure 237.

---

[156] Efficiencies: 0.97 factor on efficiency for min values and max value is DOE target: Compressor Effic.: 69% min (71% baseline) to 75% max; Expander Effic.: 71% min (73% baseline) to 80% max; Motor/Controller Effic.: 78% min (80% baseline) to 90% max.
[157] Balance of Air Compressor Cost: 2/3 of value at min, 1.5 factor at max.

		2016 Automotive System					
Annual Production Rate	systems/year	1,000	10,000	30,000	80,000	100,000	500,000
System Net Electric Power (Output)	**kWnet**	80	80	80	80	80	80
System Gross Electric Power (Output)	**kWgross**	88	88	88	88	88	88
Component Cost/System							
Fuel Cell Stacks	**$/system**	$12,032	$4,036	$2,864	$2,353	$2,271	$1,977
Balance of Plant	**$/system**	$4,833	$3,094	$2,527	$2,181	$2,092	$1,932
System Assembly & Testing	**$/system**	$148	$103	$101	$101	$101	$101
Total System Cost	**$/system**	$17,013	$7,233	$5,492	$4,636	$4,463	$4,009
Total System Cost	**$/kWnet**	$212.67	$90.42	$68.65	$57.95	$55.79	$50.12
Cost/kWgross	**$/kWgross**	$194.05	$82.50	$62.64	$52.88	$50.91	$45.73

Figure 237: Detailed system cost for the 2016 automotive technology system with a Pt price of $1,100/troy ounce

14.1.3 Single Variable Bus Analysis

A single variable Tornado Chart analysis of the bus system was also conducted. Assumptions are shown in Figure 238 and result in Figure 239.

As with the automotive system, power density and platinum loading have the largest potential to vary system cost. Unlike the automotive system, however, there is also a large cost variation potential to be found in GDL cost variations. This is because at lower manufacturing rate, the cost of manufactured component items is high and subject to large changes in cost relative to components manufactured at high volume, as in the automotive case.

2016 Bus System Cost ($/kWnet), 1,000 sys/year				
Parameter	Units	Low Value	Base Value	High Value
Pt Loading	mgPt/cm^2	0.25	**0.5**	1
Power Density	mW/cm^2	517	**739**	1012
GDL Cost	$/m^2	$47.27	**$64.76**	$84.19
Bipolar Plate & Coating Cost Factor		1	**1**	2
Air Stoichiometry		1.5	**1.8**	2.1
Compressor / Motor & Motor Controller Efficiencies	%	56%/92%	**58%/95%**	75%/95%
ePTFE Cost Multiplier		0.667	**1.00**	2.20
Air Compressor Cost Factor		0.8	**1**	1.2
Ionomer Cost	$/kg	$48.39	**$219.95**	$538.88
Hydrogen Recirculation System Cost	$/system	$594.20	**$891.26**	$1,782.52
Membrane Humidifier Cost	$/system	$324.92	**$649.83**	$1,299.66
Active to Total Area Ratio		0.55	**0.625**	0.8
Balance of Air Compressor Cost	$/system	$341.88	**$512.79**	$1,025.57
Membrane Thickness	µm	15	**20.0**	25.4
2016 Bus System Cost			**$271.60**	

Figure 238: 2016 Bus result tornado chart parameter values
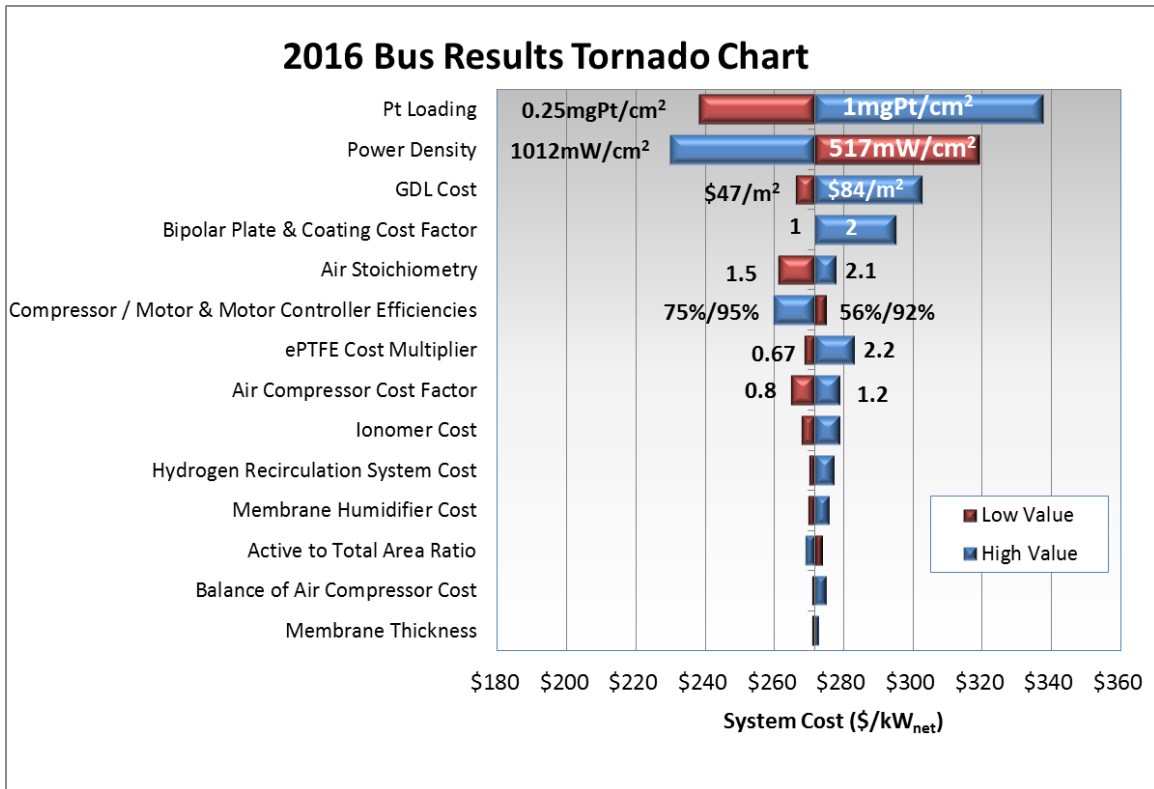
Figure 239: 2016 Bus results tornado chart

14.2 Monte Carlo Analysis

In order to evaluate the bounds for the likely variation in final results, a Monte Carlo analysis was conducted for both the automotive and bus results. With these results, it is possible to examine the probability of various model outcomes based upon assumed probability distribution functions (PDFs) for selected inputs. For all inputs, triangular distributions were chosen with a minimum, maximum, and most likely value. The most likely value is the result used in the baseline cost analysis, while the maximum and minimum were chosen with the input of the Fuel Cell Tech Team to reflect likely real-world bounds for 2016. The 2016 limits are quite similar to those from 2015, with no major deviations.

14.2.1 Monte Carlo Automotive Analysis

Assumptions and results for the Monte Carlo analysis of the automotive system are shown in Figure 240. In previous years, the Monte Carlo analysis was conducted solely for 500,000 systems per year. In 2014 the Monte Carlo analysis was expanded to all manufacturing rates. The lower and upper limits for the Monte Carlo analysis are presented as multipliers (or percentages) on each parameter's most likely value (eg. lower bound = 50% of the likeliest value, upper bound = 150% of the likeliest value). While these limits were initially conceived solely for application at 500,000 systems per year, upon consideration they were judged to be reasonably applied to all manufacturing rates.

The numerical bounds for the Monte Carlo Results for manufacturing rate of 500,000 systems per year are shown in Figure 241. Results are shown graphically in Figure 242. Further results of automotive stack, BOP, and total system cost are shown in Section 5.1.

Monte Carlo analysis indicates that the middle 90% probability range of cost is between $47.49/kW$_{net}$ and $63.37/kW$_{net}$ for the automotive system at 500,000 systems per year.

2016 Auto Technology Monte Carlo Analysis				
Parameter	Unit	Minimum Value	Likeliest Value	Maximum Value
Power Density	mW/cm2	637	**749**	1123.5
Pt Loading	mgPt/cm2	0.125	**0.134**	0.3
Ionomer Cost Multiplier		0.6	**1**	2
GDL Cost		0.55	**1**	2.91
Bipolar Plate Welding Speed	m/min	2.5	**7.5**	15
Air Stoichiometry		1.4	**1.4**	2
Membrane Humidifier Cost Multiplier		0.75	**1**	1.5
Compressor Effic. Multiplier		0.97	**1**	1.06
Expander Effic. Multiplier		0.97	**1**	1.10
Motor/Controller Effic.Multiplier		0.97	**1**	1.125
Air Compressor Cost Multiplier		0.7067	**1**	1.2
Balance of Air Compressor Cost Multiplier		0.667	**1**	1.5
Hydrogen Recirculation System Cost Multiplier		0.667	**1**	1.5
EPTFE Cost Multiplier		0.5	**1**	1.7
Active to Total Area Ratio		0.55	**0.625**	0.8
Bipolar Plate Cost Multiplier		0.367	1	1.224

Figure 240. Parameter values used in Monte Carlo analysis for all manufacturing rates.

2016 Auto Technology Monte Carlo Analysis, 500k sys/year				
Parameter	Unit	Minimum Value	Likeliest Value	Maximum Value
Power Density	mW/cm^2	637	**749**	1123.5
Pt Loading	mgPt/cm^2	0.125	**0.134**	0.3
Ionomer Cost	$/kg	$53.14	**$88.57**	$177.14
GDL Cost	$/m^2 of GDL	$3.00	**$5.50**	$16.00
Bipolar Plate Welding Speed	m/min	2.5	**7.5**	15
Air Stoichiometry		1.4	**1.4**	2
Membrane Humidifier Cost	$/system	$38.73	**$51.64**	$77.46
Compressor Effic.	%	69%	**71%**	75%
Expander Effic.	%	71%	**73%**	80%
Motor/Controller Effic.	%	78%	**80%**	90%
Air Compressor Cost		$500.00	**$707.56**	$849.07
Balance of Air Compressor Cost	$/system	$122.06	**$183.00**	$274.49
Hydrogen Recirculation System Cost	$/system	$158.48	**$237.59**	$356.39
EPTFE Cost	$/m^2 of EPTFE	$3.00	**$6.00**	$10.20
Active to Total Area Ratio		0.55	**0.625**	0.8
Bipolar Plate Cost	$/kWnet	$3.00	**$8.17**	$10.00

Figure 241: 2016 automotive Monte Carlo analysis bounds at 500,000 systems per year
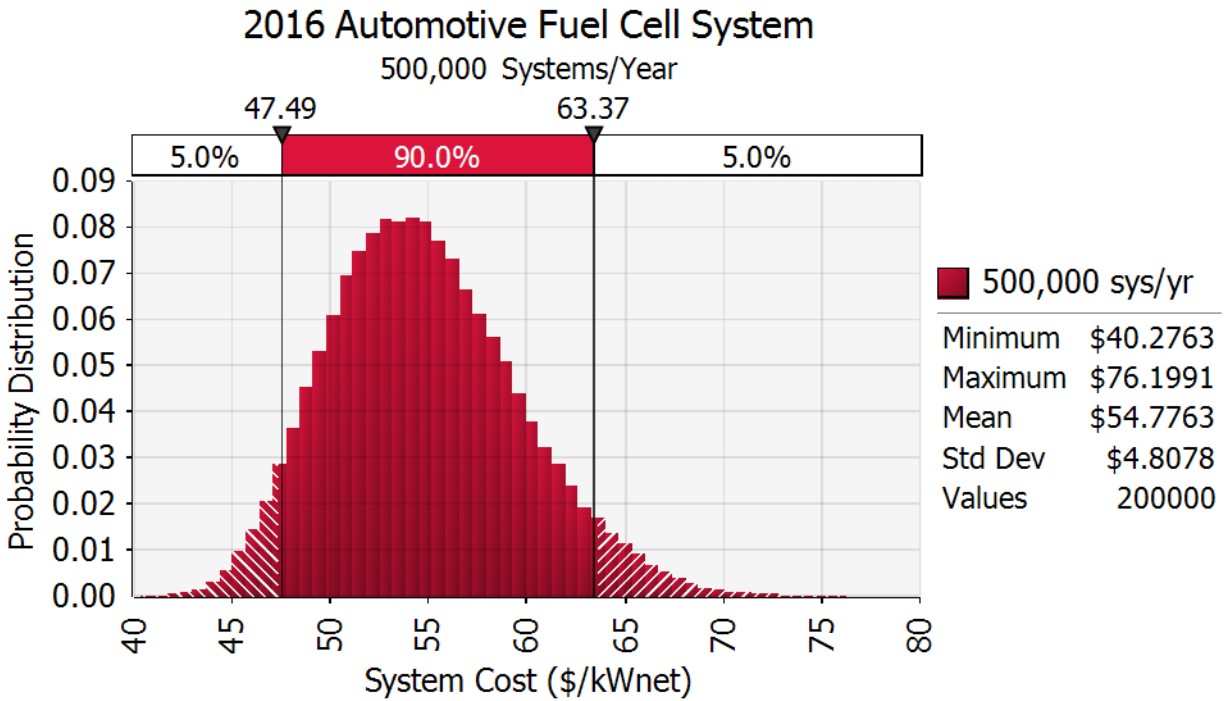
Figure 242: 2016 automotive Monte Carlo analysis results at 500k systems per year

14.2.2 Monte Carlo Bus Analysis

Similar to the auto sensitivity analysis, Monte Carlo analysis was also conducted for all manufacturing rates of the bus cost study (200, 400, 800, and 1,000 systems per year). The same multiplication factors for the parameters were used at all manufacturing rates. The range in cost for the bus stack, BOP, and total system cost are detailed in Section 5.2. Assumptions and results for the Monte Carlo analysis of the bus system are shown in Figure 243 and the graph at a manufacturing rate of 1,000 systems per year appears in Figure 244.

Monte Carlo analysis indicates that the middle 90% probability range of cost is between $239.33/kW$_{net}$ and $343.64/kW$_{net}$ for the bus system at 1,000 systems per year.

2016 Bus Technology Monte Carlo Sensitivity Analysis				
Parameter	**Unit**	**Minimum Value**	**Likeliest Value**	**Maximum Value**
Power Density	**mW/cm2**	517	**739**	1012
Pt Loading	**mgPt/cm2**	0.25	**0.5**	1
Ionomer Cost Multiplier		0.22	**1.00**	2.45
Ionomer Cost (@ 1ksys/yr)	$/kg	$48.39	$219.95	$538.88
GDL Cost Multiplier		0.73	**1.00**	1.30
GDL Cost (@ 1ksys/yr)	$/m2	$47.27	$64.76	$84.19
Bipolar Plate & Coating Cost Multiplier		1	**1**	2
Bipolar Plate Cost (1k sys/yr)	**$/kWnet**	$23.03	**$23.03**	$46.06
Membrane Humidifier Cost Multiplier		0.5	**1.00**	2
Membrane Humidifier Cost (@ 1ksys/yr)	$/system	$324.92	$649.83	$1,299.66
Compressor Effic. Multiplier		0.97	**1.00**	1.29
Compressor Effic	%	56%	58%	75%
Motor/Controller Effic.Multiplier		0.97	**1.00**	1.00
Motor/Controller Effic	%	92%	95%	95%
Air Compressor Cost Multiplier		0.8	**1.00**	1.2
Air compressor Cost	**$/system**	$4,544	**$5,681**	$6,817
Balance of Air Compressor Cost Multiplier		0.6667	**1.00**	2
Balance of Air Compressor Cost (@ 1ksys/yr)	$/system	$341.88	$512.79	$1,025.58
Hydrogen Recirculation System Cost Multiplier		0.6667	**1.00**	2
Hydrogen Recirculation System Cost (@ 1ksys/yr)	$/system	$594.20	$891.26	$1,782.52
EPTFE Cost Multiplier		0.667	**1.00**	2.20
EPTFE Cost (@ 1ksys/yr)	**$/m2**	$9.67	$14.49	$31.89
Membrane Thickness	**μm**	15	**20.0**	25.4
Active to Total Area Ratio		0.55	**0.625**	0.80

Figure 243: 2016 bus Monte Carlo analysis bounds. Cost multipliers listed were applied to all manufacturing rates. Most of the individual costs are specified for the 1,000 systems per year manufacturing rate.
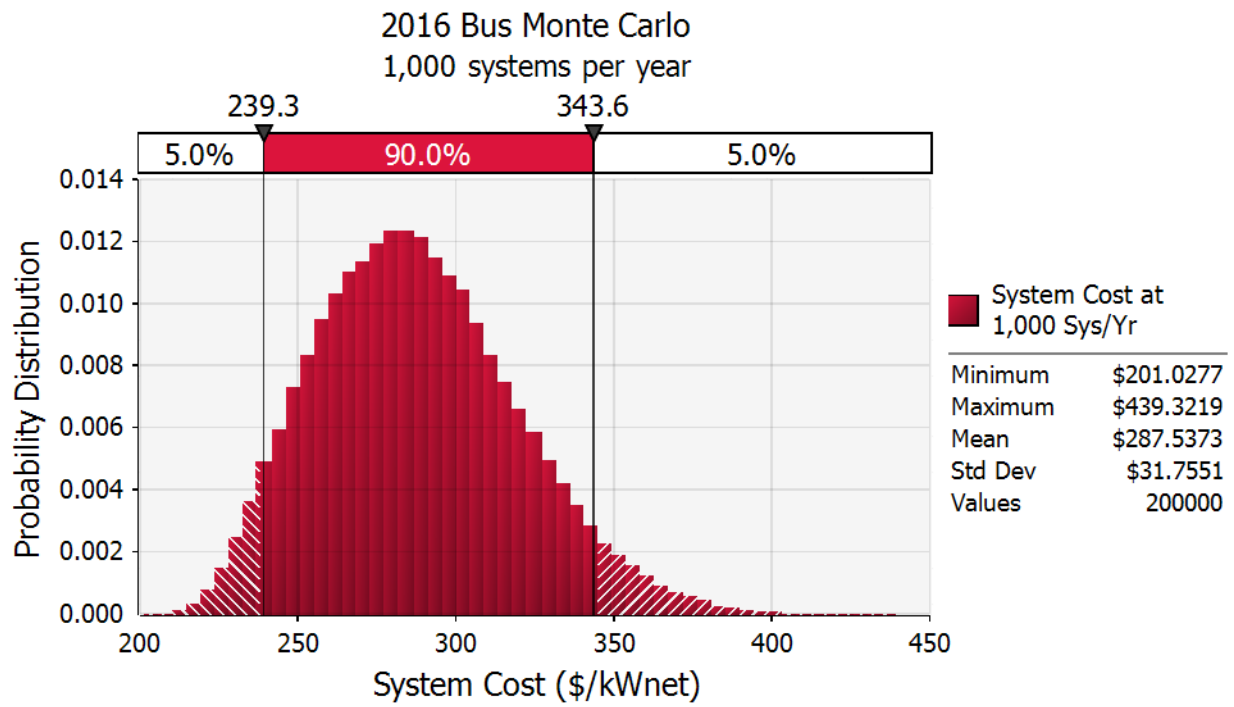
Figure 244: 2016 bus Monte Carlo analysis results

14.2.3 Extension of Monte Carlo Sensitivity

Monte Carlo multi-variable sensitivity analyses are updated each analysis year, however prior to 2014 the analysis has always focused on highlighting results for the highest manufacturing volumes (500,000 systems per year for the auto system and 1,000 systems per year for the bus system).

The 2014 analysis extended the Monte Carlo sensitivities to all manufacturing rates so that cost results may be shown as both a nominal value and a range of most likely values. Figure 245 graphs the range in cost for the 2016 automotive system at all manufacturing rates based on Monte Carlo analysis. The range in cost for the automotive system generally decreases as manufacturing volume increases. Additionally, Monte Carlo results are reported for the stack and total BOP cost categories. These results are shown in Section 5.1. As in previous years, the range of cost correlates with the middle 90% of results from the Monte Carlo analysis. The summation of the stack and BOP low value costs do not exactly numerically equal the low value for total system cost. Similarly, the summation of the stack and BOP high value costs do not equal the high value for total system cost.
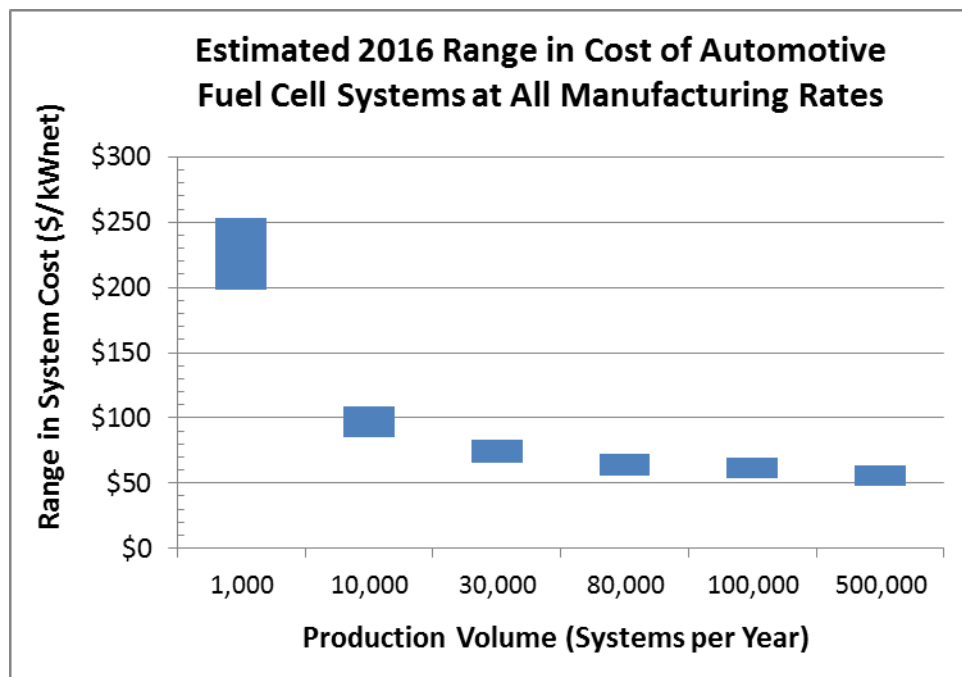
Figure 245. Middle 90% range is 2016 automotive fuel cell cost based on Monte Carlo results at all production rates.

15 Future System Cost Projection to $40/kW_{net}$

In a previous SA study in 2006, automotive fuel cell system costs were projected for 2010 and 2015 technology. In 2016, an alternate approach is used to project a potential pathway to lower automotive fuel cell system cost: target values are applied to significant cost-driving components/parameters and the resulting system cost assessed. An example pathway to $40/kW_{net}$ (at 500,000 systems per year) is shown in the form of a waterfall chart, with each step corresponding to a system cost parameter improvement. At the left end of the waterfall chart is the 80 kW_{net} 2016 baseline system cost ($53/kW_{net}$). By varying the input values in the DFMA® model for power density, Pt content, air CEM cost, and bipolar plate (BPP) cost, the combined improvements result in $40/kW_{net}$ DOE 2020 cost target. The target values used in this waterfall chart are taken from the Fuel Cell Technical Team U.S. Drive 2013 Roadmap.[158] The most significant steps in reducing cost are the system power density (delta $6/kW_{net}$, based on an increase from 749 to 1,000 mW/cm^2) and the BPP cost reduction (delta $4/kW_{net}$, based on a decrease from $8.17 to $3/kWnet). Additional performance or component cost parameters will need to be improved to meet or beat the ultimate DOE system cost target of $30/kW_{net}$.
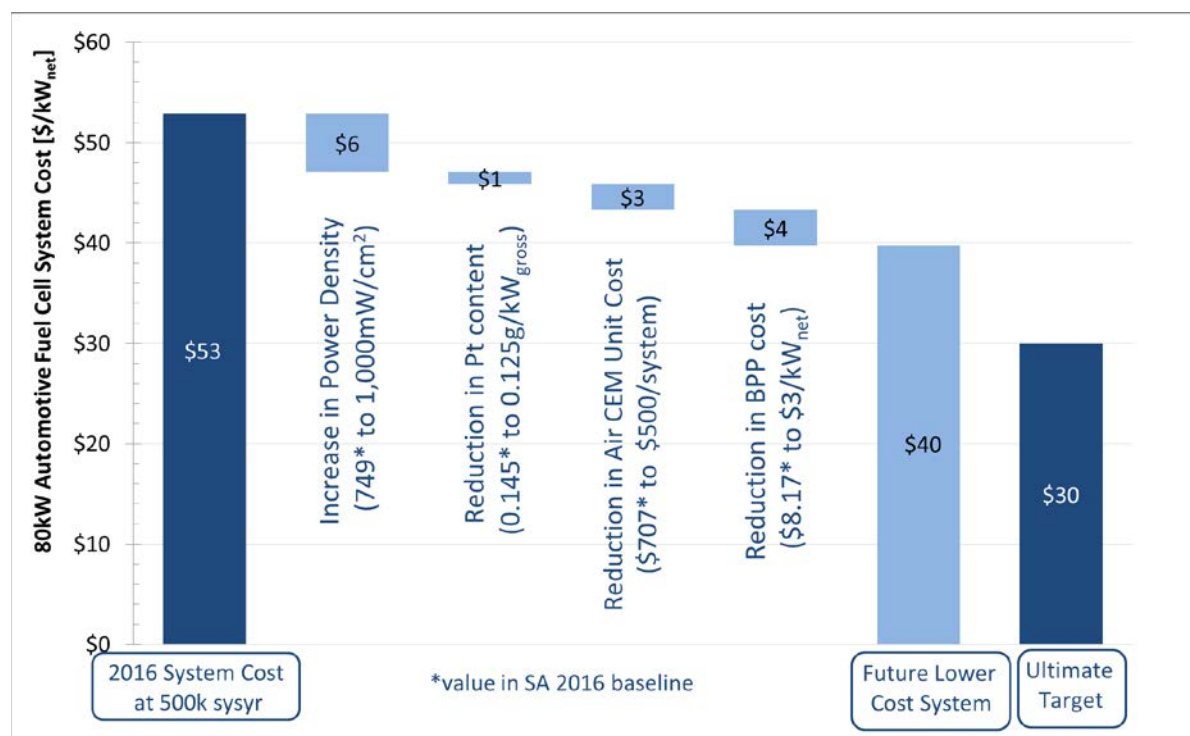
Figure 246. Waterfall chart for projection of automotive fuel cell system cost down to $40/kW_{net}$, and DOE ultimate target $30/kW_{net}$

---

[158] http://energy.gov/sites/prod/files/2014/02/f8/fctt_roadmap_june2013.pdf

16 SA Recommendations for Future Study

Analysis of the automotive and bus fuel cell systems over the past year has shed light on technology and cost shortfalls in achievement of the DOE cost targets. The following is a top level list of recommendations for further research.

Bipolar Plates

- Plate Forming: Despite the ability to produce bipolar plates at fast rates in progressive stamping presses (a few seconds per plate), the rates are not fast enough for the millions of plates needed per year. High numbers of parallel forming lines would be required, leading to infeasible factory setups and difficult quality control issues. Faster bipolar plate forming systems are needed.
- Plate Coating: There is no clearly identified pathway to a low cost, high volume-feasible bipolar plate coating (for corrosion resistance and electrical contact improvement).
- Laser welding: (to seal and create a cooling cell between the plates)
    - Laser welding lengths need to be minimized to achieve low cost. Systems with low effective welding cycle times need to be demonstrated.
    - High rate, low cost, alternates to laser welding should be explored.
    - Clamping of the BPPs to ensure plate contact while welding is identified as a key parameter for welding success. Additional research is needed for optimization.
- Material: Metal plates (as opposed to graphite, Grafoil, or composite materials) appear to be preferred for automotive applications. Alternate alloys with both lower cost and inherent anti-corrosion properties should be explored.

Membranes

- Increased power density remains the number one pathway to reduced system cost.
- Ionomer costs at high production rates remain uncertain.
- While ePTFE has proven to be an effective membrane support, its cost is high. Fabrication (at production level) and performance assessment of alternate supports (such as the Giner DSM) should be conducted.

Catalysts

- Non-Pt based catalysts: Pt-based catalysts have been demonstrated to be most cost effective. To achieve competitiveness, non-Pt catalysts need to substantially improve their power density.
- Pt Usage: Substantial strides have been achieved in reducing Pt usage (and improving kW/gPt). Nonetheless, Pt cost is one of the largest cost elements within the fuel cell system. Efforts to further reduce Pt while maintaining performance and durability should continue.
- Catalyst Synthesis: Synthesis is complicated but appears to be relatively inexpensive (excluding Pt cost), particularly at high rate production. It appears to be a favorable tradeoff to exchange synthesis complexity (possibly higher cost) for high polarization performance.

- **Durability:** Catalyst (and membrane) durability has not been explicitly factored in the cost analyses. However, it is clear that durability improvements are needed to meet minimum customer requirements.

Gas Diffusion Layers

- There is a wide distribution in GDL costs seemingly due to a combination of production scale, material wastage, and GDL company markup. More investigation is warranted to better understand these cost drivers.

Manufacturing Research

- Numerous components can be produced in quantities suitable for 1,000 vehicle systems per year but require manufacturing process development to achieve 100k vehicles per year production capability. They require not only a high-confidence market demand (to allow confidence in capital investment) but also substantial R&D dollars to develop the high-speed production systems.

17 Key Progress in the 2016 Automotive and Bus Analyses

This section summarizes key progress for both the automotive and bus power systems analyses.

80 kW$_{e\ net}$ light-duty automotive fuel cell power systems:

- The 2015 DFMA®-style cost analysis was updated to reflect changes/improvements achieved in 2016.
- Performance is based on updated 2016 stack polarization projections provided by ANL (based on the latest single cell test data for Johnson-Matthey dispersed binary de-alloyed PtNi$_3$ on carbon cathode catalyst, with CCM acid washing).
- The 2016 system is optimized for low cost, and the resulting design point (at rated power) is shown in Figure 247. These optimized operating conditions differ from the 2014 and 2015 optimization conditions.

	2014 Design Point	2015 Design Point	2016 Design Point
Cell voltage	0.672 volts/cell	0.661 volts/cell	0.661 volts/cell
Power density	834 mW/cm^2	746 mW/cm^2	749 mW/cm^2
Pressure	2.5 atm	2.5 atm	2.5 atm
Total catalyst loading	0.153 mgPt/cm^2	0.142 mgPt/cm^2	0.134 mgPt/cm^2
Stack Temp. (Coolant Exit Temp)	95°C	95°C	94°C
Cathode Air Stoichiometry	2	1.5	1.4

Figure 247. Design point comparison between 2014, 2015, and 2016.

- Other significant changes for 2016 include:
  - Improvements made to the analysis of the dispersed catalyst synthesis process
  - Re-evaluation of bipolar plate stamping process parameters based on manufacturer feedback to reflect a requirement for substantially higher press force that had been previously modeled
  - Laser welding processing assumptions based on manufacturer feedback to reflect length of weld, laser welding speed, and the number of weld heads simultaneously welded to increase productivity
  - GDL DFMA® analysis based on Avcarb's process including a markup to reflect GDL purchase from a supplier
  - Use of TreadStone LiteCell™ Gen2 bipolar plate coating using lower cost materials and simplified processing compared to TreadStone LiteCell™ Gen1.
  - Switching from NTM hydrogen sensor to FiS model FH2-HY04 hydrogen detector used in the Toyota Mirai.

- Several analyses were performed to explore alternate manufacturing procedures or types of system components (but were not incorporated into the baseline cost analysis):
  - DFMA® analysis of Borit Hydrogate bipolar plate stamping technology (and a comparison to conventional progressive stamping as used in the baseline)
  - DFMA® analysis of amorphous carbon bipolar plate coating (as an alternative to the TreadStone coating)
  - Benchmarking against Toyota Mirai fuel cell system at 1,000 systems per year

- The estimated fuel cell system cost for automobiles is $52.89/kW$_{net}$ at 500,000 systems per year and represents the "2016 Update" to previous annual estimates. (This value does not include the cost of hydrogen storage or the electric drive train.)
- A Monte Carlo analysis indicates that the automotive fuel cell system cost is likely to be between $47.49/kW$_{net}$ and $63.37/kW$_{net}$, with 90% probability.
- The 2016 automotive system balance of plant components represent approximately 49% of the overall system cost at a production rate of 500,000 systems per year.

160 kW$_{net}$ bus fuel cell power systems:

- Primary differences between the bus and automotive power systems include:
  - system power (160 kW$_{net}$ vs. 80 kW$_{net}$),
  - number of stacks (two vs. one),
  - operating pressure (1.9 atm vs. 2.5 atm),
  - catalyst loading (0.5 mgPt/cm^2 vs. 0.134 mgPt/cm^2),
  - type of air compressor (twin vortex vs. centrifugal).
  - use of an exhaust gas expander (no expander vs. expander), and

- Stack performance is based on a stack polarization model provided by Argonne National Laboratory in 2015 based on a total Pt loading of 0.5 mgPt/cm^2 and dispersed Pt on carbon catalyst within the MEAs.
- Power density, voltage, pressure, and catalyst loading of the selected system design point are roughly consistent with the actual operating conditions of Ballard fuel cell buses currently in service.

	Approximate Ballard Bus Design Point	2013 Bus Design Point	2014 Bus Design Point	2015/2016 Bus Design Point
Cell voltage	~0.69 volts/cell	0.676 volts/cell	0.676 volts/cell	0.659 volts/cell
Power density	~759 mW/cm^2	601 mW/cm^2	601 mW/cm^2	739 mW/cm^2
Pressure	~1.8 atm	1.8 atm	1.8 atm	1.9 atm
Total catalyst loading	~0.4 mgPt/cm^2	0.4 mgPt/cm^2	0.4 mgPt/cm^2	0.5 mgPt/cm^2
Stack Temperature	~60°C	74°C	74°C	72°C
Cathode Air Stoichiometry	1.5-2.0	1.5	1.5	1.8

Figure 248. Design Point Comparison for FC Bus between Ballard Bus, 2013, 2014, and 2015/2016 analysis

- Changes between 2015 and 2016 bus analyses include:
  - all of the 2016 automotive updates (adjustment to catalyst synthesis, bipolar plate forming process assumptions, laser welding, GDL cost, and switch from TreadStone LiteCell^{TM} Gen1 to Gen 2),
- The system schematics and stack construction are nearly identical between the bus and automobile systems.
- The final 2016 bus cost is projected to be $271.60/kW$_{net}$ at 1,000 systems per year.
- A Monte Carlo analysis indicates that the bus fuel cell system cost is likely to be between $239.33/kW$_{net}$ and $343.64/kW$_{net}$, with 90% probability.
- The 2016 bus system balance of plant represented only 30% of the overall system cost at a production rate of 1,000 systems per year.
- Because bus systems are expected to be produced at much lower rates than auto systems (1,000/year vs. 500,000/year), bus system costs are much more sensitive to component cost variations (eg. GDL, bipolar plate manufacturing, coating costs). Reducing the uncertainty in component costs will improve the accuracy of the bus system cost.

18 Appendix A: 2016 Transit Bus Cost Results

18.1 Fuel Cell Stack Materials, Manufacturing, and Assembly Cost Results

18.1.1 Bipolar Plates

Annual Production Rate	200	400	800	1,000
Manufacture or Job Shop	Job Shop	Job Shop	Job Shop	Manufactured
Job Shop Line Utilization (%)	46%	55%	72%	0%
Job Shop Total Machine Rate ($/min)	$13.86	$11.77	$9.11	$14.46
Manufactured Line Utilization (%)	9%	18%	35%	44%
Manufactured Total Machine Rate ($/min)	$53.03	$26.84	$13.74	$11.12
Line Utilization Used (%)	46%	55%	72%	44%
Total Machine Rate Used ($/min)	$13.86	$11.77	$9.11	$11.12

Annual Production Rate	200	400	800	1,000
Material ($/stack)	$326	$326	$326	$326
Manufacturing ($/stack)	$612	$519	$402	$491
Tooling ($/stack)	$110	$55	$55	$66
Secondary Operations: Coating ($/stack)	$286	$271	$246	$235
Markup ($/stack)	$539	$460	$393	$758
Total Cost ($/stack)	$1,873	$1,632	$1,422	$1,876
Total Cost ($/kWnet)	$23.41	$20.39	$17.78	$23.45

18.1.1.1 Alloy Selection and Corrosion Concerns

Annual Production Rate	200	400	800	1,000
Material ($/stack)	$23	$23	$23	$23
Manufacturing ($/stack)	$268	$257	$235	$223
Total Cost ($/stack)	$291	$280	$258	$246
Total Cost ($/kWnet)	$3.64	$3.50	$3.22	$3.07

18.1.2 Membrane

Annual Production Rate	200	400	800	1,000
Material ($/m^2)	$48	$42	$38	$36
Manufacturing ($/m^2)	$259	$167	$108	$94
Markup ($/m^2)	$124	$82	$56	$49
Total Cost ($/m^2 (total))	$430	$291	$201	$179
Total Cost ($/stack)	$9,563.16	$6,475.40	$4,467.17	$3,980.05
Total Cost ($/kWnet)	$119.54	$80.94	$55.84	$49.75

18.1.3 Pt on Carbon Catalyst

18.1.3.1 Catalyst Synthesis Cost

Annual Production Rate	200	400	800	1,000
Manufacture or Job Shop	Job Shop	Job Shop	Job Shop	Job Shop
Job Shop Line Utilization (%)	60%	47%	90%	57%
Job Shop Total Machine Rate ($/min)	$1.03	$1.18	$0.86	$1.06
Manufactured Line Utilization (%)	23%	47%	90%	57%
Manufactured Total Machine Rate ($/min)	$1.42	$0.91	$0.66	$0.82
Line Utilization Used (%)	60%	47%	90%	57%
Total Machine Rate Used ($/min)	$1.03	$1.18	$0.86	$1.06

Annual Production Rate	200	400	800	1,000
Pt cost ($/system)	$7,039	$7,039	$7,012	$7,012
Material (exluding Pt) ($/system)	$495	$291	$185	$129
Total Material ($/system)	$7,534	$7,330	$7,197	$7,142
Manufacturing ($/system)	$269	$292	$202	$248
Markup ($/system)	$5,351	$4,374	$3,633	$3,322
Total Cost ($/system)	$13,154	$11,996	$11,032	$10,712
Total Cost ($/kWnet)	$82	$75	$69	$67
Total Cost/kgCatalyst(net)	$18,651	$17,009	$15,643	$15,189

18.1.3.2 Catalyst Application: Slot Die Coating

Annual Production Rate	200	400	800	1,000
Manufacture or Job Shop	Job Shop	Job Shop	Job Shop	Job Shop
Job Shop Line Utilization (%)	38%	39%	40%	41%
Job Shop Total Machine Rate ($/min)	$13.21	$12.96	$12.52	$12.31
Manufactured Line Utilization (%)	1%	2%	3%	4%
Manufactured Total Machine Rate ($/min)	$449.09	$224.97	$116.44	$93.32
Line Utilization Used (%)	38%	39%	40%	41%
Total Machine Rate Used ($/min)	$13.21	$12.96	$12.52	$12.31

Annual Production Rate	200	400	800	1,000
Materials ($/stack)	$36	$32	$28	$27
Manufacturing ($/stack)	$93	$90	$82	$80
Markup ($/stack)	$52	$48	$42	$41
Total Cost ($/stack)	$182	$169	$153	$148
Total Cost ($/kWnet)	$2.27	$2.12	$1.91	$1.85

18.1.4 Gas Diffusion Layer

Annual Production Rate	200	400	800	1,000
GDL Cost ($/stack)	$4,272	$2,970	$2,065	$1,837
Markup ($/stack)	$3,374	$2,196	$1,430	$1,246
Total Cost ($/stack)	$6,641	$5,340	$3,406	$2,952
Total Cost ($/kWnet)	$83.01	$66.75	$42.58	$36.90

18.1.5 MEA Sub-Gaskets Total

Annual Production Rate	200	400	800	1,000
Material ($/stack)	$84	$84	$84	$84
Manufacturing ($/stack)	$237	$207	$191	$168
Tooling (Kapton Web) ($/stack)	$121	$71	$45	$38
Cost/Stack	$179	$142	$161	$142
Total Cost ($/stack)	$621	$503	$481	$432
Total Cost ($/kWnet)	$3.88	$3.15	$3.01	$2.70

18.1.5.1 Sub-Gasket Formation

Annual Production Rate	200	400	800	1,000
Manufacture or Job Shop	Job Shop	Job Shop	Job Shop	Job Shop
Job Shop Line Utilization (%)	39%	41%	45%	47%
Job Shop Total Machine Rate ($/min)	$8.18	$7.87	$7.36	$7.14
Manufactured Line Utilization (%)	2%	4%	8%	10%
Manufactured Total Machine Rate ($/min)	$83.66	$43.74	$23.26	$19.08
Line Utilization Used (%)	39%	41%	45%	47%
Total Machine Rate Used ($/min)	$8.18	$7.87	$7.36	$7.14

Annual Production Rate	200	400	800	1,000
Material ($/stack)	$70	$70	$70	$70
Manufacturing ($/stack)	$91	$86	$78	$75
Tooling (Kapton Web) ($/stack)	$121	$71	$45	$38
Markup ($/stack)	$114	$89	$74	$69
Total Cost ($/stack)	$397	$316	$268	$252
Total Cost ($/kWnet)	$4.96	$3.95	$3.35	$3.16

18.1.5.2 Sub-Gasket Adhesive Application (screen-printing)

Annual Production Rate	200	400	800	1,000
Manufacture or Job Shop	Job Shop	Job Shop	Manufactured	Manufactured
Job Shop Line Utilization (%)	49%	62%	49%	61%
Job Shop Total Machine Rate ($/min)	$2.36	$1.96	$2.36	$1.96
Manufactured Line Utilization (%)	12%	25%	49%	61%
Manufactured Total Machine Rate ($/min)	$6.46	$3.37	$1.82	$1.51
Line Utilization Used (%)	49%	62%	49%	61%
Total Machine Rate Used ($/min)	$2.36	$1.96	$1.82	$1.51

Annual Production Rate	200	400	800	1,000
Material ($/stack)	$13	$13	$13	$13
Manufacturing ($/stack)	$146	$121	$113	$93
Markup ($/stack)	$64	$53	$87	$73
Total Cost ($/stack)	$224	$188	$213	$179
Total Cost ($/kWnet)	$2.80	$2.35	$2.67	$2.24

18.1.6 Hot Pressing GDL to Catalyst Coated Membrane

Annual Production Rate	200	400	800	1,000
Capital Cost ($/Line)	$1,501,443	$1,501,443	$1,501,443	$1,501,443
Simultaneous Lines	1	1	1	1
Laborers per Line	0.25	0.25	0.25	0.25
Line Utilization (%)	10%	20%	40%	50%
Total Cycle Time (seconds)	95	95	95	95
Manufacture or Job Shop	Job Shop	Job Shop	Manufactured	Manufactured
Job Shop Line Utilization (%)	47%	57%	40%	50%
Job Shop Total Machine Rate ($/min)	$1.29	$1.11	$1.46	$1.22
Manufactured Line Utilization (%)	10%	20%	40%	50%
Manufactured Total Machine Rate ($/min)	$3.85	$2.03	$1.12	$0.94
Line Utilization Used (%)	47%	57%	40%	50%
Total Machine Rate Used ($/min)	$1.29	$1.11	$1.12	$0.94

Annual Production Rate	200	400	800	1,000
Manufacturing ($/stack)	$66	$57	$57	$48
Tooling ($/stack)	$1.87	$0.94	$0.47	$0.37
Markup ($/stack)	$53	$43	$40	$33
Total Cost ($/stack)	$121	$100	$97	$81
Total Cost ($/kWnet)	$1.51	$1.25	$1.22	$1.01

18.1.7 Cutting, and Slitting

Annual Production Rate	200	400	800	1,000
Manufacture or Job Shop	Job Shop	Job Shop	Job Shop	Job Shop
Job Shop Line Utilization (%)	37%	38%	38%	39%
Job Shop Total Machine Rate ($/min)	$2.52	$2.50	$2.47	$2.45
Manufactured Line Utilization (%)	0.3%	0.7%	1.3%	1.6%
Manufactured Total Machine Rate ($/min)	$193.58	$99.03	$50.64	$40.81
Line Utilization Used (%)	37%	38%	38%	39%
Total Machine Rate Used ($/min)	$2.52	$2.50	$2.47	$2.45

Annual Production Rate	200	400	800	1,000
Manufacturing ($/stack)	$4	$4	$4	$4
Tooling ($/stack)	$6	$6	$6	$6
Markup ($/stack)	$4	$4	$4	$4
Total Cost ($/stack)	$14	$14	$13	$13
Total Cost ($/kWnet)	$0.18	$0.17	$0.17	$0.17

18.1.8 End Plates

Annual Production Rate	200	400	800	1,000
Manufacture or Job Shop	Job Shop	Job Shop	Job Shop	Job Shop
Job Shop Line Utilization (%)	38%	39%	41%	42%
Job Shop Total Machine Rate ($/min)	$2.41	$2.36	$2.27	$2.23
Manufactured Line Utilization (%)	1%	2%	4%	5%
Manufactured Total Machine Rate ($/min)	$53.14	$26.78	$13.60	$10.97
Line Utilization Used (%)	38%	39%	41%	42%
Total Machine Rate Used ($/min)	$2.41	$2.36	$2.27	$2.23

Annual Production Rate	200	400	800	1,000
Material ($/stack)	$103	$97	$92	$91
Manufacturing ($/stack)	$13	$12	$12	$12
Tooling ($/stack)	$4	$2	$1	$1
Markup ($/stack)	$48	$44	$40	$39
Total Cost ($/stack)	$168	$156	$145	$142
Total Cost ($/kWnet)	$2.10	$1.95	$1.82	$1.78

18.1.9   Current Collectors

Annual Production Rate	200	400	800	1,000
Manufacture or Job Shop	Job Shop	Job Shop	Job Shop	Job Shop
Job Shop Line Utilization (%)	37%	37%	37%	37%
Job Shop Total Machine Rate ($/min)	$2.18	$2.18	$2.18	$2.18
Manufactured Line Utilization (%)	0%	0%	0%	0%
Manufactured Total Machine Rate ($/min)	$1,199.35	$694.70	$347.74	$287.40
Line Utilization Used (%)	37%	37%	37%	37%
Total Machine Rate Used ($/min)	$2.18	$2.18	$2.18	$2.18

Annual Production Rate	200	400	800	1,000
Material ($/stack)	$8	$8	$8	$8
Manufacturing ($/stack)	$0	$0	$0	$0
Tooling ($/stack)	$0	$0	$0	$0
Secondary Operation ($/stack)	$1	$1	$1	$1
Markup ($/stack)	$4	$4	$3	$3
Total Cost ($/stack)	$13	$13	$12	$12
Total Cost ($/kWnet)	$0.16	$0.16	$0.15	$0.15

18.1.10   Coolant Gaskets/Laser-welding

Annual Production Rate	200	400	800	1,000
Manufacture or Job Shop	Job Shop	Job Shop	Manufactured	Manufactured
Job Shop Line Utilization (%)	50%	64%	53%	67%
Job Shop Total Machine Rate ($/min)	$5.11	$4.10	$4.84	$3.93
Manufactured Line Utilization (%)	13%	27%	53%	67%
Manufactured Total Machine Rate ($/min)	$14.31	$7.25	$3.73	$3.02
Line Utilization Used (%)	50%	64%	53%	67%
Total Machine Rate Used ($/min)	$5.11	$4.10	$3.73	$3.02

Annual Production Rate	200	400	800	1,000
Material ($/stack)	$0	$0	$0	$0
Manufacturing ($/stack)	$343	$275	$250	$203
Tooling ($/stack)	$0	$0	$0	$0
Markup ($/stack)	$139	$108	$173	$138
Total Cost ($/stack)	$482	$383	$423	$340
Total Cost ($/kWnet)	$6.02	$4.79	$5.29	$4.25

18.1.11 End Gaskets

Annual Production Rate	200	400	800	1,000
Manufacture or Job Shop	Job Shop	Job Shop	Job Shop	Job Shop
Job Shop Line Utilization (%)	37%	37%	37%	37%
Job Shop Total Machine Rate ($/min)	$3.02	$3.02	$3.01	$3.00
Manufactured Line Utilization (%)	0.1%	0.1%	0.3%	0.3%
Manufactured Total Machine Rate ($/min)	$1,176.68	$588.53	$294.40	$235.57
Line Utilization Used (%)	37%	37%	37%	37%
Total Machine Rate Used ($/min)	$3.02	$3.02	$3.01	$3.00

Annual Production Rate	200	400	800	1,000
Material ($/stack)	$0	$0	$0	$0
Manufacturing ($/stack)	$1	$1	$1	$1
Markup ($/stack)	$0	$0	$0	$0
Total Cost ($/stack)	$2	$1	$1	$1
Total Cost ($/kWnet)	$0.02	$0.02	$0.02	$0.02

18.1.12 Stack Assembly

Annual Production Rate	200	400	800	1,000
Manufacture or Job Shop	Manufactured	Manufactured	Manufactured	Manufactured
Job Shop Line Utilization (%)	57%	39%	78%	98%
Job Shop Total Machine Rate ($/min)	$1.30	$1.22	$1.05	$1.03
Manufactured Line Utilization (%)	20%	39%	78%	98%
Manufactured Total Machine Rate ($/min)	$0.90	$0.83	$0.80	$0.79
Line Utilization Used (%)	20%	39%	78%	98%
Total Machine Rate Used ($/min)	$0.90	$0.83	$0.80	$0.79

Annual Production Rate	200	400	800	1,000
Compression Bands ($/stack)	$0	$0	$0	$0
Assembly ($/stack)	$88	$82	$78	$78
Markup ($/stack)	$70	$60	$54	$53
Total Cost ($/stack)	$158	$142	$132	$130
Total Cost ($/kWnet)	$1.97	$1.77	$1.66	$1.63

18.1.13 Stack Housing

Annual Production Rate	200	400	800	1,000
Manufacture or Job Shop	Job Shop	Job Shop	Job Shop	Job Shop
Job Shop Line Utilization (%)	37%	37%	38%	38%
Job Shop Total Machine Rate ($/min)	$1.41	$1.41	$1.41	$1.41
Manufactured Line Utilization (%)	0%	0%	1%	1%
Manufactured Total Machine Rate ($/min)	$46.17	$23.49	$12.14	$9.87
Line Utilization Used (%)	37%	37%	38%	38%
Total Machine Rate Used ($/min)	$1.41	$1.41	$1.41	$1.41

Annual Production Rate	200	400	800	1,000
Material ($/stack)	$11	$11	$11	$11
Manufacturing ($/stack)	$3	$3	$3	$3
Tooling ($/stack)	$181	$91	$45	$36
Markup ($/stack)	$79	$41	$23	$19
Total Cost ($/stack)	$275	$146	$83	$70
Total Cost ($/kWnet)	$1.72	$0.91	$0.52	$0.44

18.1.14 Stack Conditioning and Testing

Annual Production Rate	200	400	800	1,000
Capital Cost ($/line)		Proprietary		
Simultaneous Lines	1	1	2	2
Laborers per Line	0.1	0.1	0.1	0.1
Test Duration (hrs/stack)	2	2	2	2
Line Utilization Used (%)	14%	28%	28%	35%
Total Machine Rate Used ($/min)	$1.35	$0.72	$0.72	$0.60

Annual Production Rate	200	400	800	1,000
Conditioning/Testing ($/stack)	$162	$87	$87	$71
Markup ($/stack)	$128	$64	$60	$48
Total Cost ($/stack)	$290	$151	$146	$120
Total Cost ($/kWnet)	$3.62	$1.88	$1.83	$1.50

18.2 2016 Transit Bus Balance of Plant (BOP) Cost Results

18.2.1 Air Loop

Annual Production Rate	200	400	800	1,000
Filter and Housing ($/system)	$75	$75	$74	$74
Compressor, Expander & Motor ($/system)	$8,322	$6,893	$5,928	$5,681
Mass Flow Sensor ($/system)	$102	$101	$100	$100
Air Ducting ($/system)	$197	$194	$190	$189
Air Temperature Sensor ($/system)	$11	$10	$10	$10
Markup on Purchased Components ($/system)	$156	$149	$143	$141
Total Cost ($/system)	$8,863	$7,421	$6,445	$6,193
Total Cost ($/kW$_{net}$)	$55.39	$46.38	$40.28	$38.71

18.2.2 Humidifier & Water Recovery Loop

Annual Production Rate	200	400	800	1,000
Air Precooler ($/system)	$162	$157	$153	$152
Demister ($/system)	$101	$75	$61	$58
Membrane Air Humidifier ($/system)	$1,017	$811	$682	$650
Total Cost ($/system)	$1,279	$1,044	$896	$859
Total Cost ($/kW$_{net}$)	$7.99	$6.52	$5.60	$5.37

18.2.2.1 Air Precooler

Annual Production Rate	200	400	800	1,000
Material ($/system)	$45	$45	$45	$45
Manufacturing ($/system)	$45	$45	$45	$45
Markup ($/system)	$71	$67	$63	$61
Total Cost ($/system)	$162	$157	$153	$152
Total Cost ($/kWnet)	$1.01	$0.98	$0.96	$0.95

18.2.2.2 Demister

Annual Production Rate	200	400	800	1,000
Manufacture or Job Shop	Job Shop	Job Shop	Job Shop	Job Shop
Job Shop Line Utilization (%)	37%	37%	37%	37%
Job Shop Total Machine Rate ($/min)	$3.09	$3.09	$3.09	$3.09
Manufactured Line Utilization (%)	0.07%	0.08%	0.11%	0.12%
Manufactured Total Machine Rate ($/min)	$819.46	$705.18	$551.46	$497.28
Line Utilization Used (%)	37%	37%	37%	37%
Total Machine Rate Used ($/min)	$3.09	$3.09	$3.09	$3.09

Annual Production Rate	200	400	800	1,000
Material ($/system)	$40	$38	$36	$35
Manufacturing ($/system)	$2	$1	$1	$1
Tooling ($/system)	$29	$15	$7	$6
Markup ($/system)	$29	$21	$17	$16
Total Cost ($/system)	$101	$75	$61	$58
Total Cost ($/kWnet)	$0.63	$0.47	$0.38	$0.36

18.2.2.3 Membrane Humidifier

18.2.2.3.1 Membrane Humidifier Manufacturing Process
Station 1: Fabrication of Composite Humidifier Membranes

Annual Production Rate	200	400	800	1,000
Manufacture or Job Shop	Job Shop	Job Shop	Job Shop	Job Shop
Job Shop Line Utilization (%)	37%	37%	37%	37%
Job Shop Total Machine Rate ($/min)	$22.96	$22.65	$22.30	$22.17
Manufactured Line Utilization (%)	0.1%	0.1%	0.3%	0.3%
Manufactured Total Machine Rate ($/min)	$7,675.15	$3,939.86	$2,022.63	$1,631.97
Line Utilization Used (%)	37.1%	37.1%	37.3%	37.3%
Total Machine Rate Used ($/min)	$22.96	$22.65	$22.30	$22.17

Annual Production Rate	200	400	800	1,000
Material ($/stack)	$255	$232	$211	$204
Manufacturing ($/stack)	$122	$69	$42	$36
Tooling ($/stack)	$0	$0	$0	$0
Markup ($/stack)	$150	$115	$93	$88
Total Cost ($/stack)	$527	$417	$346	$328
Total Cost ($/kWnet)	$3.29	$2.61	$2.16	$2.05

Station 2: Fabrication of Etched Stainless Steel Flow Fields

Annual Production Rate	200	400	800	1,000
Manufacture or Job Shop	Job Shop	Job Shop	Job Shop	Job Shop
Job Shop Line Utilization (%)	38%	38%	39%	39%
Job Shop Total Machine Rate ($/min)	$11.69	$11.60	$11.43	$11.35
Manufactured Line Utilization (%)	1%	1%	2%	2%
Manufactured Total Machine Rate ($/min)	$374.95	$189.45	$96.71	$78.80
Line Utilization Used (%)	38%	38%	39%	39%
Total Machine Rate Used ($/min)	$11.69	$11.60	$11.43	$11.35

Annual Production Rate	200	400	800	1,000
Material ($/stack)	$37	$37	$37	$37
Manufacturing ($/stack)	$63	$63	$62	$61
Markup ($/stack)	$40	$38	$37	$36
Total Cost ($/stack)	$140	$138	$135	$134
Total Cost ($/kWnet)	$0.88	$0.86	$0.85	$0.84

Station 3: Pouch Formation

Annual Production Rate	200	400	800	1,000
Manufacture or Job Shop	Job Shop	Job Shop	Job Shop	Job Shop
Job Shop Line Utilization (%)	37%	38%	38%	38%
Job Shop Total Machine Rate ($/min)	$3.25	$3.23	$3.19	$3.16
Manufactured Line Utilization (%)	0%	1%	1%	1%
Manufactured Total Machine Rate ($/min)	$289.15	$144.77	$72.54	$58.09
Line Utilization Used (%)	37%	38%	38%	38%
Total Machine Rate Used ($/min)	$3.25	$3.23	$3.19	$3.16

Annual Production Rate	200	400	800	1,000
Material ($/stack)	$1	$1	$1	$1
Manufacturing ($/stack)	$10	$10	$9	$9
Tooling ($/stack)	$0	$0	$0	$0
Markup ($/stack)	$4	$4	$4	$4
Total Cost ($/stack)	$15	$15	$15	$15
Total Cost ($/kWnet)	$0.10	$0.09	$0.09	$0.09

Station 4: Stainless Steel Rib Formation

Annual Production Rate	200	400	800	1,000
Manufacture or Job Shop	Job Shop	Job Shop	Job Shop	Job Shop
Job Shop Line Utilization (%)	38%	38%	40%	40%
Job Shop Total Machine Rate ($/min)	$1.35	$1.33	$1.30	$1.28
Manufactured Line Utilization (%)	1%	1%	3%	3%
Manufactured Total Machine Rate ($/min)	$47.87	$24.18	$12.23	$9.84
Line Utilization Used (%)	38%	38%	40%	40%
Total Machine Rate Used ($/min)	$1.35	$1.33	$1.30	$1.28

Annual Production Rate	200	400	800	1,000
Material ($/stack)	$3	$3	$3	$3
Manufacturing ($/stack)	$9	$9	$8	$8
Tooling ($/stack)	$10	$9	$9	$9
Markup ($/system)	$9	$8	$8	$7
Total Cost ($/stack)	$30	$28	$28	$28
Total Cost ($/kWnet)	$0.19	$0.18	$0.17	$0.17

Station 5: Stack Formation

Annual Production Rate	200	400	800	1,000
Manufacture or Job Shop	Job Shop	Job Shop	Job Shop	Job Shop
Job Shop Line Utilization (%)	40%	43%	49%	52%
Job Shop Total Machine Rate ($/min)	$1.52	$1.44	$1.30	$1.24
Manufactured Line Utilization (%)	3%	6%	12%	15%
Manufactured Total Machine Rate ($/min)	$13.26	$6.74	$3.48	$2.83
Line Utilization Used (%)	40%	43%	49%	52%
Total Machine Rate Used ($/min)	$1.52	$1.44	$1.30	$1.24

Annual Production Rate	200	400	800	1,000
Material ($/stack)	$11	$11	$11	$11
Manufacturing ($/stack)	$45	$42	$38	$37
Markup ($/system)	$22	$20	$18	$17
Total Cost ($/stack)	$77	$73	$67	$64
Total Cost ($/kWnet)	$0.48	$0.46	$0.42	$0.40

Station 6: Formation of the Housing

Annual Production Rate	200	400	800	1,000
Material ($/stack)	$13	$13	$13	$13
Manufacturing ($/stack)	$48	$28	$17	$15
Tooling ($/stack)	$97	$56	$33	$27
Markup ($/system)	$63	$37	$23	$20
Total Cost ($/stack)	$220	$133	$86	$75
Total Cost ($/kWnet)	$1.38	$0.83	$0.53	$0.47

Station 7: Assembly of the Composite Membrane and Flow Fields into the Housing

Annual Production Rate	200	400	800	1,000
Manufacture or Job Shop	Job Shop	Job Shop	Job Shop	Job Shop
Job Shop Line Utilization (%)	37%	37%	38%	38%
Job Shop Total Machine Rate ($/min)	$1.24	$1.24	$1.24	$1.24
Manufactured Line Utilization (%)	0%	0%	1%	1%
Manufactured Total Machine Rate ($/min)	$32.68	$16.73	$8.76	$7.16
Line Utilization Used (%)	37%	37%	38%	38%
Total Machine Rate Used ($/min)	$1.24	$1.24	$1.24	$1.24

Annual Production Rate	200	400	800	1,000
Manufacturing ($/stack)	$2	$2	$2	$2
Markup ($/system)	$1	$1	$1	$1
Total Cost ($/stack)	$3	$3	$3	$3
Total Cost ($/kWnet)	$0.02	$0.02	$0.02	$0.02

Station 8: Humidifier System Testing

Annual Production Rate	200	400	800	1,000
Manufacture or Job Shop	Job Shop	Job Shop	Job Shop	Job Shop
Job Shop Line Utilization (%)	37%	38%	38%	38%
Job Shop Total Machine Rate ($/min)	$1.17	$1.17	$1.17	$1.17
Manufactured Line Utilization (%)	0%	1%	1%	1%
Manufactured Total Machine Rate ($/min)	$19.36	$10.06	$5.41	$4.48
Line Utilization Used (%)	37%	38%	38%	38%
Total Machine Rate Used ($/min)	$1.17	$1.17	$1.17	$1.17

Annual Production Rate	200	400	800	1,000
Manufacturing ($/stack)	$2	$2	$2	$2
Markup ($/system)	$1	$1	$1	$1
Total Cost ($/stack)	$2	$2	$2	$2
Total Cost ($/kWnet)	$0.03	$0.03	$0.03	$0.03

18.2.2.3.2 Combined Cost Results for Plate Frame Membrane Humidifier

Annual Production Rate	200	400	800	1,000
Material ($/stack)	$319	$296	$275	$268
Manufacturings ($/stack)	$301	$224	$181	$171
Tooling ($/stack)	$108	$66	$42	$37
Markup ($/stack)	$288	$224	$184	$174
Total Cost ($/stack)	$1,016	$810	$682	$650
Total Cost ($/kWnet)	$12.70	$10.13	$8.53	$8.12

18.2.3 Coolant Loops

18.2.3.1 High-Temperature Coolant Loop

Annual Production Rate	200	400	800	1,000
Coolant Reservoir ($/system)	$16	$16	$16	$16
Coolant Pump ($/system)	$141	$139	$136	$136
Coolant DI Filter ($/system)	$174	$167	$161	$158
Thermostat & Valve ($/system)	$20	$20	$20	$20
Radiator ($/system)	$785	$764	$744	$737
Radiator Fan ($/system)	$134	$132	$130	$129
Coolant Piping ($/system)	$109	$107	$105	$104
Markup ($/system)	$557	$528	$502	$493
Total Cost ($/system)	$1,935	$1,873	$1,813	$1,794
Total Cost ($/kW$_{net}$)	$12.10	$11.71	$11.33	$11.21

18.2.3.2 Low-Temperature Coolant Loop

Annual Production Rate	200	400	800	1,000
Coolant Reservoir ($/system)	$2	$2	$2	$2
Coolant Pump ($/system)	$35	$34	$34	$34
Thermostat & Valve ($/system)	$8	$8	$8	$8
Radiator ($/system)	$99	$97	$94	$93
Radiator Fan ($/system)	$0	$0	$0	$0
Coolant Piping ($/system)	$14	$14	$13	$13
Markup ($/system)	$64	$61	$58	$57
Total Cost ($/system)	$222	$216	$209	$207
Total Cost ($/kW$_{net}$)	$1.39	$1.35	$1.31	$1.30

18.2.4 Fuel Loop

Annual Production Rate	200	400	800	1,000
Inline Filter for GPE ($/system)	$27	$26	$25	$25
Flow Diverter Valve ($/system)	$31	$31	$31	$31
Over-Pressure Cut-Off Valve ($/system)	$54	$52	$50	$49
Hydrogen High-Flow Ejector ($/system)	$118	$110	$103	$101
Hydrogen Low-Flow Ejector ($/system)	$103	$96	$88	$86
Check Valves ($/system)	$20	$20	$20	$20
Purge Valves ($/system)	$171	$164	$157	$155
Hydrogen Piping ($/system)	$186	$183	$180	$179
Markup ($/system)	$287	$268	$250	$245
Total Cost ($/system)	$997	$950	$905	$891
Total Cost ($/kW$_{net}$)	$6.23	$5.94	$5.66	$5.57

18.2.5 System Controller

Annual Production Rate	200	400	800	1,000
System Controller	$201	$197	$194	$193
Markup ($/system)	$81	$78	$74	$73
Total Cost ($/system)	$283	$275	$268	$266
Total Cost ($/kW$_{net}$)	$1.77	$1.72	$1.67	$1.66

18.2.6 Sensors

Annual Production Rate	200	400	800	1,000
Current Sensors ($/system)	$40	$40	$40	$40
Voltage Sensors ($/system)	$16	$16	$16	$16
Hydrogen Sensors ($/system)	$719	$656	$599	$581
Markup ($/system)	$313	$280	$250	$242
Total Cost ($/system)	$1,087	$992	$905	$879
Total Cost ($/kW$_{net}$)	$6.80	$6.20	$5.66	$5.50

18.2.6.1 Hydrogen Sensors

Annual Production Rate	200	400	800	1,000
Sensors per system	3	3	3	3
Sensor ($)	$240	$219	$200	$194
Total Cost ($/system)	$719	$656	$599	$581
Total Cost ($/kW$_{net}$)	$4.49	$4.10	$3.74	$3.63

18.2.7 Miscellaneous BOP

Annual Production Rate	200	400	800	1,000
Belly Pan ($/system)	$263	$135	$71	$58
Mounting Frames ($/system)	$249	$239	$230	$227
Wiring ($/system)	$237	$232	$227	$225
Fasteners for Wiring & Piping ($/system)	$47	$46	$45	$45
Markup ($/system)	$322	$256	$219	$211
Total Cost ($/system)	$1,118	$909	$792	$766
Total Cost ($/kW$_{net}$)	$6.99	$5.68	$4.95	$4.79

18.2.7.1 Belly Pan

Annual Production Rate	200	400	800	1,000
Manufacture or Job Shop	Job Shop	Job Shop	Job Shop	Job Shop
Job Shop Line Utilization (%)	37%	37%	37%	38%
Job Shop Total Machine Rate ($/min)	$1.42	$1.41	$1.41	$1.41
Manufactured Line Utilization (%)	0.1%	0.2%	0.5%	0.6%
Manufactured Total Machine Rate ($/min)	$91.54	$46.17	$23.49	$18.95
Line Utilization Used (%)	37.1%	37.2%	37.5%	37.6%
Total Machine Rate Used ($/min)	$1.42	$1.41	$1.41	$1.41

Annual Production Rate	30,000	80,000	100,000	500,000
Material ($/system)	$4	$4	$4	$4
Manufacturing ($/system)	$2	$2	$2	$2
Tooling ($/system)	$181	$91	$45	$36
Markup ($/system)	$76	$38	$20	$16
Total Cost ($/system)	$263	$135	$71	$58
Total Cost ($/kWnet)	$1.64	$0.84	$0.44	$0.36

18.2.7.2 Wiring

Annual Production Rate	200	400	800	1,000
Cables ($/system)	$79	$77	$75	$75
Connectors ($/System)	$159	$155	$152	$151
Total Cost ($/system)	$237	$232	$227	$225
Total Cost ($/kWnet)	$1.48	$1.45	$1.42	$1.41

18.2.8 System Assembly

Annual Production Rate	200	400	800	1,000
Assembly Method	Assembly Line	Assembly Line	Assembly Line	Assembly Line
Index Time (min)	111	111	111	111
Capital Cost ($/line)	$50,000	$50,000	$50,000	$50,000
Simultaneous Lines	1	1	1	1
Laborers per Line	12	12	12	12
Cost per Stack ($)	$231.90	$169.28	$137.44	$130.86
Line Utilization Used (%)	1%	3%	6%	7%
Total Machine Rate Used ($/min)	$18.23	$13.69	$11.42	$10.97

Annual Production Rate	200	400	800	1,000
System Assembly & Testing ($/System)	$259	$195	$162	$156
Markup ($/system)	$205	$144	$112	$106
Total Cost ($/system)	$464	$339	$275	$262
Total Cost ($/kWnet)	$2.90	$2.12	$1.72	$1.64